Multifunctional surfaces for implants in bone contact applications

Doctoral Dissertation
UniTo-PoliTo Doctoral Program in Bioengineering and Medical-Surgical sciences
(30th Cycle)

Multifunctional surfaces for implants in bone contact applications

By

Martina Cazzola

******

Supervisors:
Prof. Enrica Vernè, Supervisor
Prof. Silvia Spriano, Co-Supervisor
Dr. Sara Ferraris, Co-Supervisor

Politecnico di Torino
2017

Declaration

I hereby declare that, the contents and organization of this dissertation constitute my own original work and does not compromise in any way the rights of third parties, including those relating to the security of personal data.

Martina Cazzola

2017

* This dissertation is presented in partial fulfillment of the requirements for **Ph.D. degree** in the Graduate School of Politecnico di Torino (ScuDo).

Acknowledgment

At the end of this journey I would like to thank all the people who have been by my side along the way.

Firstly, I would like to thank my tutors Prof. Enrica Vernè, Prof. Silvia Spriano and Dr. Sara Ferraris for their support to my Ph.D research, for sharing with me their knowledge and for motivating me. Without their help all this work would not have been possible.

My sincere gratitude also goes to all the people who have collaborated at this research work. My sincere thanks to Prof. Enrico Prenesti and Dr. Ingrid Corazzari of the chemistry department of the Università degli Studi di Torino, To Prof. Lia Rimondini, Dr. Andrea Cochis, Dr. Barbara Azzimonti and Ms. Rita Sorrentino from The Department of Health Sciences of The Università del Piemonte Orientale, To Prof Giuliana Banche and Dr. Valeria Allizont from the Department of Public Health and Pediatrics, Microbiology Division of the Univerità degli Studi di Torino, To Prof. Cinzia Margherita Bertea from the Plant Physiology Unit, Department Life Sciences and Systems Biology of the Università degli Studi di Torino, To Prof. Aleksandra Czyrska-Filemonowicz and Dr. Grzegorz Cempura from the International Centre of Electron Microscopy for Materials Science & Faculty of Metals Engineering and Industrial Computer Science from the AGH University of Science and Technology and thanks to Prof. Giuseppe Pezzotti from the Ceramic Physics Laboratory of the Kyoto Institute of Technology. All of these people have made their knowledge, skills and instrumentation available to make this work possible.

Thank you to Cri, Vero, Gian, Dlp, Ale and the mansarda's girls, Fabiana, Giulia, Dome and all my colleagues because I've bothered you a lot, but you did not kill me and thanks for all the beers.

Thanks to Cri, Sara, Cla, Catalù, Andre, Fra, Fra B. and all my university friends for sharing all these years with me supporting and motivating me.

Thanks to Ele, Sara, Paola and Marti because we have known each other for so long and we have shared so many things. I never tell you before, but I love you.

Last but not least, I would like to thanks my family; my parents, my brother, my grandparents and my uncle for supporting me every days of my life.

If I forgot someone it's because I'm a mess with these things, but I'm really grateful to all of you.

Martina

Abstract

The idea behind this thesis is the use of natural molecules to confer to the surface of biomaterials for bone contact applications multifunctional properties by means of functionalization. Natural molecules can be extracted from plants or food waste and wine industries, in order to obtain molecules with high added value, but low cost; local sources are preferred in order to valorize the territory, for examples Barbera grapes and *Mentha Piperita* of Pancalieri in the case of Piedmont. Polyphenols and essential oils are natural extracts from these types of sources and they have antitumoral, anti-inflammatory, antioxidant and osteoinductive properties and they are also reductive agents useful for the *in situ* reduction of silver nanoparticles in order to confer antibacterial properties to the surfaces. The substrates used for functionalization were a surface chemical treated bioactive titanium alloy and a silica based bioactive glass. Different functionalization protocols were studied and improved. The procedures of functionalization were tailored for each molecule and both substrates by varying pH, medium, solute concentration and time of functionalization in order to maximize the amount of molecules grafted to the surface and minimize any effect of degradation of the molecules. After functionalization, the samples were physically and chemically characterized and tested *in vitro* with bacterial and cellular assays. The presence and the activity of the natural molecules on the surface after functionalization was confirmed by means of Fourier Transform Infrared Spectroscopy, X-ray photoelectron spectroscopy, spectroscopic measurements with the Folin&Ciocalteu method, Gaschromatographic analysis and Fluorescence microscope analysis. The cellular tests highlighted the selective actions of polyphenols with tumoral and healthy cells showing cytotoxicity effects on tumoral cells and protective effects against RONS on healthy cells.

Bioactivity tests of apatite precipitation *in vitro* in Simulated Body Fluid and of cellular mineralization show the ability of polyphenols to improve mineralization process. They influence the deposition kinetic of hydroxyapatite deposition kinetic and the formation of different apatite structure depending on the type of polyphenol used for the functionalization. Functionalization with *Mentha* essential oil shows the reduction of the bacterial adhesion on the treated surfaces tested with *Staphylococcus Aureus* and the same result was found for the surfaces with the silver nanoparticles. In both cases, it is evidenced that it is challenging to find a proper balance between an effective antibacterial action (bactericide or bacteriostatic) and cytocompatibility.

Silver nanoparticles were in situ reduced on the surface of chemically-treated titanium alloy by means of the use of polyphenols as natural reducing agents in order to confer antibacterial activity to the surface. The presence, distribution and shape of the silver nanoparticles were investigated with Field Emission Scanning Electron Microscopy equipped with energy dispersive spectroscopy, as well as Transmission electron microscopy with selected area electron diffraction patterns. The nanoparticles are under the 10 nm and well dispersed on all the surface of the samples.

According to the results, surface functionalization of biomaterials is a promising strategy in order to combine the properties of biomolecules with those of surfaces and also to obtain is situ synthesis of antibacterial nanoparticles.

Contents

List of Figures

contact with CT(H2)_Ad+Ag(0.001M)_T2 samples while no toxic effects were notice for the bare CT(H2) ones. Bars represents means and standard deviations.

List of Tables

Introduction

This thesis concerns the development and characterization of osteointegrable multifunctional surfaces by means of the procedure of functionalization. Biomolecules with multifunctional properties were used for the surface functionalization of biomaterials or for the in situ reduction of silver nanoparticles. Chapter 1 introduces to the main requirements of surfaces for implants in bone contact applications of which this work aims to answer. The subsequent chapters are designed as self-contained with a bibliographic part, the explanation of the experimental part, the exposition of the results and the conclusions.

Chapter 2 deals with the surface functionalization of two bioactive materials with polyphenols. Protocols for the functionalization were developed and tailored for each surface and the main properties conferred by polyphenols such as antioxidant, osteostimulating and antitumoral effects were investigated.

Chapter 3 deals with surface functionalization or coating of bioactive titanium alloy with essential oils which is without precedent in literature. Protocols for the surface coating or functionalization were developed and the antibacterial effect as well as cytocompatibility was tested.

Chapter 4 deals with the in situ reduction, with the use of polyphenols as reducing agents, of silver nanoparticles for antibacterial purpose on the osteointegrable oxide layer of a treated titanium alloy. The silver nanoparticles distributing and the silver release were investigated in order to tailor the antibacterial effects.

In the end, the general conclusions of all the work and the possible outcomes and future plans are exposed.

Chapter 1

Introduction to critical aspects concerning surface characteristics of bone contact implants

1.1 Introduction

The joint replacements are increasing over the years. For example, prosthetic junction surgeries were increased by 2.7% in 2013 in Italy with respect to previous years, reaching 170000 joint surgeries, 97000 of which were hip replacements, 65000 knee replacements, 6000 shoulder replacements and 2000 other joint substitutions [1]. The prosthesis request is destined to grow with progressive aging of population and considering the prosthetic improvements in terms of duration, which allows to implant in even younger patient.

Dental implants are definitely more numerous and it is difficult to have a precise number of implants per year in Italy, but they are unquestionably in continuous increase.

A biomaterial in contact with bone tissue requires several surface characterizations in order to be suitable. Both for orthopedic devices and dental implants, one of the main goals is to obtain a biocompatible and osteointegrable implant. Starting from biocompatible or bioactive materials, the surface finishing and the eventual functionalization play a fundamental role in the development of bone tissue around the implant, avoiding excessive inflammation and formation of

fibrous tissue. Another important characteristic is the ability of implants to avoid bacterial contamination which could lead to prosthetic failure and pain for the patients. Implants in critical situations, such as patients with poor bone quality or implants after tumoral resections, other characteristics like osteostimulating behavior, antioxidants effects and antitumoral effects are interesting added values. In this chapter, the main issues involving osteointegration and antibacterial aspects and their relationship with biomaterials' surface structure and chemistry will be introduced in order to give an overview of the main problems which the development of multifunctional surfaces, which are the topic of this thesis, want to face off.

1.2 Osteointegration

Osteointegration is defined as "the direct anchorage of an implant by the formation of bony tissue around the implant without the growth of fibrous tissue at the bone–implant interface" while a material could be defined osteostimulant when it is able to stimulate undifferentiated and pluripotent cells to develop into bone forming cells[2] (Figure 1.1).

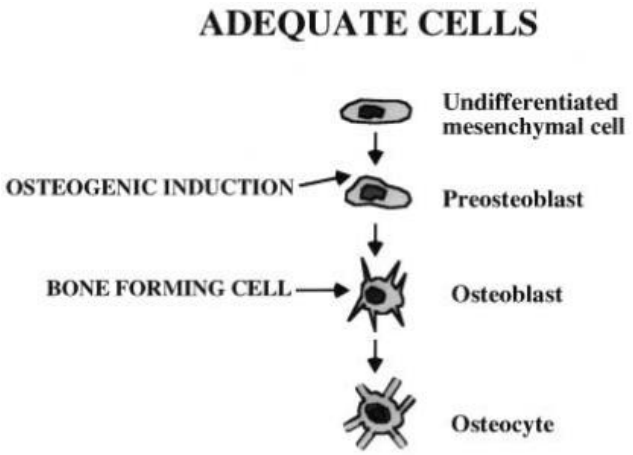

Figure 1.1: bone cells differentiation due to osteoinductive stimuli[2].

The recruitment and differentiation of undifferentiated cells are biological mechanisms which occur normally for fracture healing and implants incorporation. A good osteointegrable material (for cementless implants) has to be able to not delay this process, but preferably to facilitate it with osteoinductive stimulation [2].

Starting from biocompatible materials, the design and chemistry of implants' surfaces are among the main factors influencing osteointegration. The first reaction of the body after implanting of a biomaterial is an acute inflammation with the activation of nonspecific immune system. After the contact with bone, the biomaterials are reached by blood protein and interstitial fluid which are adsorbed before the interaction with cells. This protein layer guides the inflammation process and the subsequent reaction of the tissue, for this reason the interaction of the surface chemistry with the protein is fundamental for osteointegration [3]. The protein adhesion is followed by the formation of a fibrin clot acting as scaffold for the migration of blood-derived cells and mesenchymal stem cells to the implant surface. If the surface is suitable for osteointegration, the undifferentiated cells turns into bone cells with subsequent osteoid formation and mineralization [4], [5]. The mesenchymal cells and osteoblasts migrate to the implants since day one, creating a non-collagenous matrix layer binding minerals. This is a calcified afibrillar layer rich of calcium, osteopontin, phosphorus and bone protein. After the formation of this first layer, cells are able to organize themselves in new trabecular bone and/ or lamellar bone [6]. The different steps of osteointegration are reported in Figure 1.2.

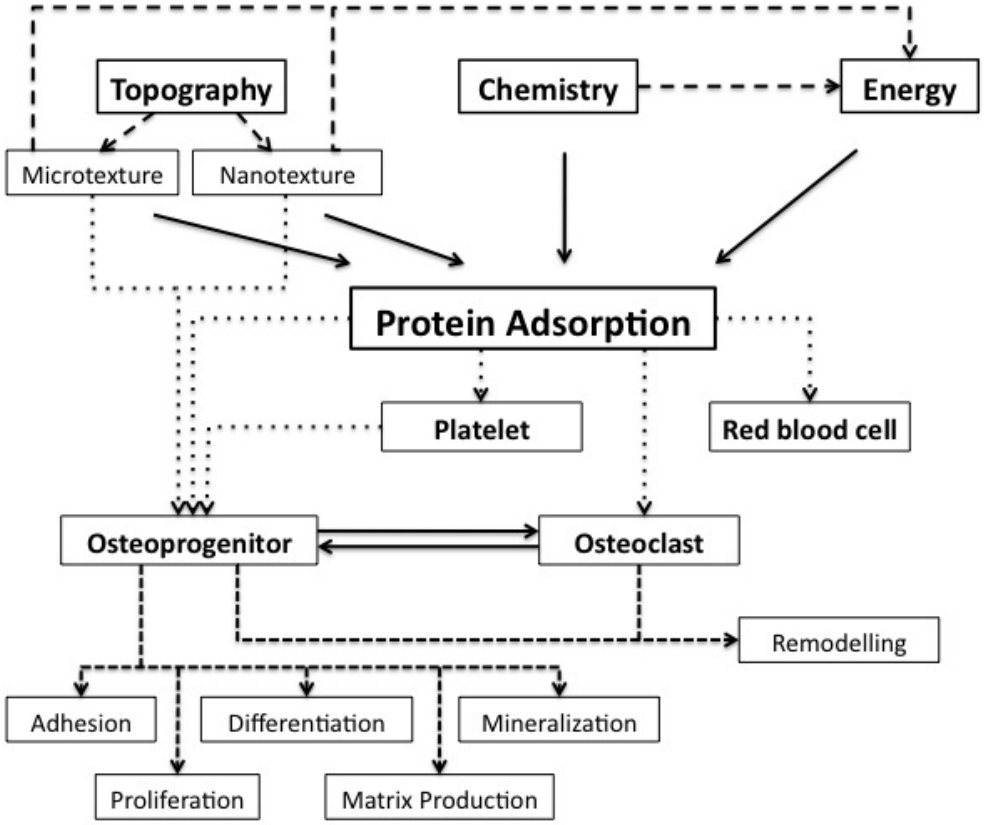

Figure 1.2: Scheme of the steps involved in osteointegration[7].

1.2.1 Surfaces modifications to enhance osteointegrability

Several attempts of surface design, in terms of finishing and chemistry, were performed in order to improve implants osteointegration. The main ways followed are those of topographic modification and of coating.

The topographical texture of implants surfaces has an important role on tissue response. Textured surfaces have a greater surface area for tissue integration compared with smooth implants and porous surface finishing can also allow ingrowth of bone. The topography of the implants surface has been investigated for many years both in dental and orthopedic field. Tailoring the surface texture of the implants allows the modulation of cell response and stimulates osteointegration [8].

Surface with complex topography and simultaneous presence of micro, sub micro and nano roughness promotes osteointegration (Figure 1.3).

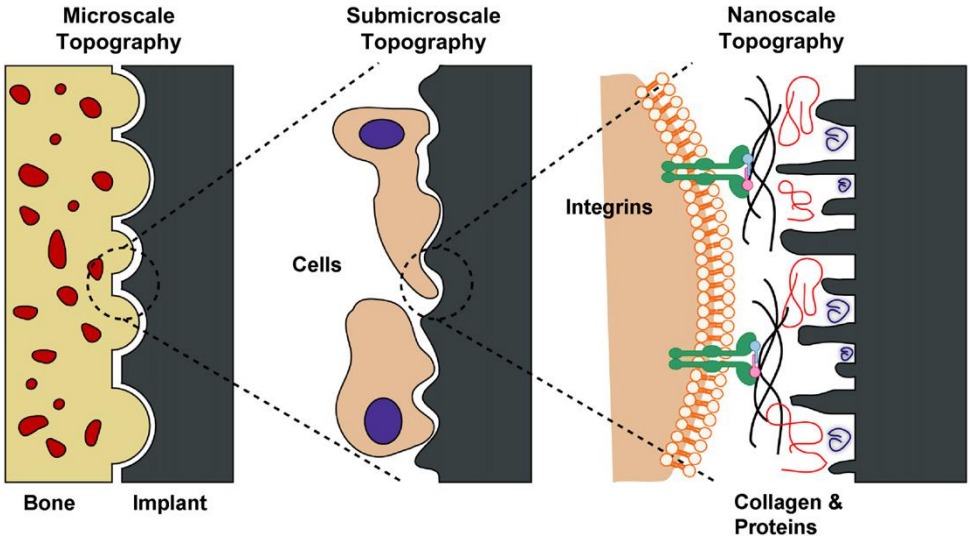

Figure 1.3:scheme of the interaction between bone and implant at micro, submicro and nano scale[9].

Micro and submicron roughness with size comparable with resorption pits and cells dimensions enhance osteoblast differentiation and local factor release increasing the osteointegration of the implant. Nanoscale roughness with size in the magnitude of protein and cell membrane receptors dimensions could also act in cell adhesion, proliferation and spreading, but some studies reports no osteoblast differentiation and proliferation in presence only of nano roughness without micro roughness. These results suggests that the best topographic bone stimulation for osteointegration derives from the combination of multiscale roughness [9]–[11].

The ideal size of submicro and micro roughness which gives better osteointegration is around 0.4-2 μm because it is a good compromise between bone-implants interlocking, high osteoblasts adhesion and proliferation rates and increased number of focal adhesion points, avoiding side effects like the increase of ion release and weakening of the implants [12], [13]. Several approaches were developed in order to introduce the appropriate micro and nano roughness on titanium osteointegrable implants and are listed below [12]:

- Titanium plasma spray
- Grit blasting
- Sand blasting
- Acid etching
- Anodization

In order to confer nano roughness overlapped to microroughness surfaces, the most common combination of treatment used is sand blasting + acid etching, but other method investigated over years are reported in Table 1.1.

Table 1.1: techniques for the creation of nanofeatures on titanium substrates [5].

Methods	**Characteristics**
Self-assembly of monolayers	The exposed functional end group could be a molecule with different functions (an osteoinductive or cell adhesive molecule).
Physical approaches Compaction of nanoparticles	Conserves the chemistry of the surface among different topographies. Not readily applied over implant surfaces
Ion beam deposition	Can impart nanofeatures to the surface based on the material used
Chemical methods Acid etching	Combined with other methods (sandblasting and/or peroxidation) can impart nanofeatures to the surface and remove contaminants.
Peroxydation	Produces a titania gel layer. Both chemical and topography changes are imparted.
Alkali treatment (NaOH)	Produces a sodium titanate gel layer allowing hydroxyapatite deposition. Both chemical and topography changes are imparted.
Anodization	Can impart nanofeatures to the surface creating a new oxide layer (based on the material used).
Nanoparticles deposition Sol–gel (colloidal particle adsorption)	Creates a thin-film of controlled chemical characteristics. Atomic-scale interactions display strong physical interactions
Discrete crystalline deposition	Superimposes a nanoscale surface topographical complexity on the surface.
Lithography and contact printing technique	Many different shapes and materials can be applied over the surface. Approaches are labor intensive and require considerable development prior to clinical translation and application on implant surface.

Regarding coatings, many attempts were performed. The mineral component of bone is mainly carbonated hydroxyapatite (HAp) and coating the surface implants with this compound can improve osteointegration. The techniques of application of HAp on titanium substrates include sputtering, pulse laser deposition and layer-by- layer deposition. Critical aspects of this type of coating are the possible

decrease of the fatigue properties and the resorption of the HAp layer in dental implants with implant mobilization [4]. Increase of osteointegrability can also be obtained with an electrodeposited calcium phosphate coating [12], [14]. Buscemi and Hench suggested the use of bioactive glass for implants coating to create a stable bone-to-implant fixation with chemical reaction which occurs at the interface with bioactive glass[15].

Bisphosphonate have been used to enhance osteointegration and the positive effects of zoledronic acid coating in canine implant model and of alexandronate and HAp to improve bone-implant coating were observed, but long term observation and tailoring of the dosage are requested in order to better understand the effect of this functionalization. Also biomolecules such as collagen, chondroitin sulfate, specific peptides and glycosaminoglycans were used in order to improve osteointegration, however the main issue is the instability of this biomolecules in vivo[4]. Bone morphogenic protein (BMP-2) were used to improve the rate of osteointegration in people with poor bone quality, but in these cases the principal problems are the high costs of the molecule and the potential development of tumor [16].

1.3 Infections

The total rate or infection after joint replacement is around 1% with an increase up to 3% in patients with osteoarthritis. Despite of the low incidence rate, joint bacterial infections are a severe complication which can lead to implant removal, generating high costs and relevant problems for the patients. The cost of the prosthetic joint infections was $566 millions only in 2009 and it is in constant rise with the increase of the surgical joint replacements. The highest incidence of infections (70% of total joint infections) occurs during the first two years from the surgery [17]–[19].

Prosthetic joint infection can be classified on the basis of the route of infection or on the basis of the onset of symptoms after implantation.

According to the route of infection they are defined as:

- Perioperative: presence of the bacteria into the surgical side
- Hematogeneous: bacterial reach the site of infection through blood or lymphatic system
- Contiguous: bacterial spread from an adjacent site of infection

According to onset of symptoms after the implantation they are defined as:

- Early infections : within 3 months after the surgery

- Delayed infections: within 3 and 24 months from the surgery
- Late infections: after 24 months from the surgery[20] .

Regarding dental field, perimplantitis is defined as "an inflammatory process affecting the tissues around an osseointegrated implant in function, resulting in loss of supporting bone" (Figure 1.4). This inflammation could leads to the implants failure and the worldwide reported data of its incidence varies between 5% and 63.4%. This large variable range of incidence is due to the different design of the studies with different population and risk of incidence. Despite of the variability of the data, perimplantitis is a serious problem for dental implants because the risks of infections is high also after many years of implantation [21], [22].

Figure 1.4: perimplantitis with bone resorption[23].

The main bacteria responsible for joint prosthetic infections are *Staphylococcus aureus* and *Staphylococcus epidermis* [24] ,while the most common bacteria related to perimplantitis are *Prevotella intermedia, Porphyromonas gingivalis, Aggregatibacter actinomycetemcomitans, Bacterioides forsythus, Treponema denticola, Prevotella nigrescens*, *Peptostreptococcus micros*, and *Fusobacterium nucleatum* [25].

The bacterial contamination starts with the adhesion to the implant surface of few bacteria cells. After adhesion, they start to proliferate and to produce extracellular matrix (biofilm) as shown in Figure 1.5. Once reached the mature state, some bacteria are able to leave the biofilm in planktonic state and infect new sites [26]. The biofilm formation makes bacteria resistant to antibacterial treatment [24]. For this reason, the period before the firm attachment, phenotypic change and biofilm formation is the window of opportunity for many antibacterial strategies [27].

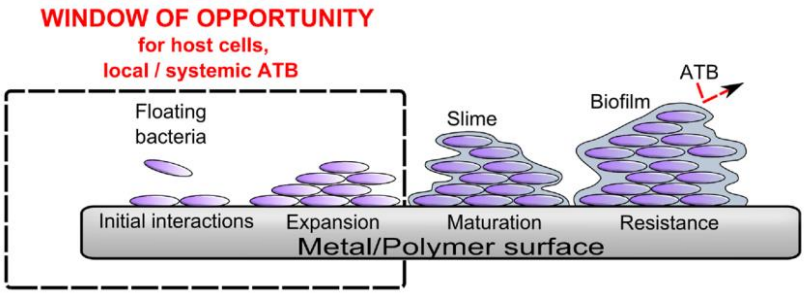

Figure 1.5: scheme of implant infection and biofilm formation [27].

1.3.1 Surface modifications in order to avoid bacterial infections

The bacterial adhesion to the surface is influenced by several variables reported in Table 1.2.

Table 1.2: variables related to bacterial adhesion to biomaterials [28].

Variables influencing bacterial adhesion and colonisation on biomaterial surfaces	
Surface morphometry	Macroporosity
	Microporosity
	Micro-roughness
	Nano-roughness
Physico-chemical properties	Surface energy
	Hydrophylicity/superhydrophylicity
	Hydrophobicity/superhydrophobicity
	Hydrophobic functional groups
	Polar functional groups
	Charged functional groups
	Functional groups with specific activities
	Degree of hydration
Environmental conditions	Electrolytes
	pH
	Temperature
	Host proteins/host adhesins
	Shear rate/fluid viscosity
	Fluid flow rate
Pathogen	Gram-positive/Gram-negative
	Genus/Species
	Bacterial shape
	Surface energy
	Strain type and specific set of expressed adhesins

The strategies studied in order to avoid surface bacterial contamination or to confer an active antibacterial ability to the implant surfaces themselves are

numerous and the main studies, with the relative issues, are reported below in Table 1.3.

Table 1.3: classification of the principal strategies studied to protect implant from bacterial contamination[29] .

Strategy	**Features**	**Examples**	**Development stage**	**Main issues**
Passive surface finishing	Prevention of bacterial adhesion	- Hydrophilic surface -Super-Hydrophobic surface -Anti-adhesive polymer -Nano-patterned surface -Albumin -Hydrogels -Biosurfactants	Preclinical	-Limited antibacterial and antibiofilm activity -Possible interferences with osteointegration -Unknown long term effects -Regulatory issues
Active surface finishing/ Modifications	Inorganic	Silver ions and nanoparticles	Market	-Incomplete implant coating -Questionable long term toxicity -Limited large scale application -Costs
		Other metals (copper, zinc, titanium dioxide, etc.)	preclinical	-Questionable long term toxicity -Regulatory issues
		Non-metal: Iodine	Clinical	-Incomplete implant coating -Questionable long term toxicity -Challenging large-scale application -Regulatory issues
		Other non-metal ions (selenium, graphene, etc.)	Preclinical	-Poorly studied compounds -Coating

				resistance to press-fit insertion -Questionable long term toxicity -Challenging large-scale application -Regulatory issues
	Organic	Coated/ linked antibiotics	Market	-Unique application to nail coating -Long-term effects on osteointegration -Single antibiotic (gentamicin)
		Covalently linked antibiotics	Preclinical	-Incomplete implant coating -Questionable long-term toxicity -Challenging large-scale application -Regulatory issues
		Antimicrobial peptides	Preclinical	-No data of in vivo or clinical effects
		Cytokines	Preclinical	-Coating resistance to press-fit insertion
		Enzymes and biofilm disrupting agents	Preclinical	-Questionable long term toxicity
		Chitosan Derivatives	Preclinical	-Challenging large scale application
	Synthetic	Non-antibiotics antimicrobial compounds	Preclinical	-Regulatory issues

Peri-operative antibacterial local carriers or coatings	Not-biodegradable	Antibiotic-loaded polymethylmethacrylate	Market	-Resistance and small-colony variants induction -No antibiofilm effect -incomplete implant coating -May not be used for cementless implants
	Biodegradable	Antibiotic-loaded bone grafts and substitutes	Market	-Limited availability -Not proven efficacy as implant coating Cost -Regulatory issues
		Fast-resorbable hydrogel	Market	-Early clinical use and results

1.4 Multifunctional surfaces

In the last years, multifunctional coatings or functionalizations, which are the topic of this thesis, has been explored [30]–[35]. The idea is to develop surfaces combining multiple functional activities such as osteointegrability and antibacterial effects.

Other effects such as anti-inflammatory, antioxidant and antitumoral activities are useful properties mostly in critical case such as prosthetic implants or bone filling with biomaterials after bone resection due to tumor removal. Many strategies are under investigation combining principally strategies for bone osteointegration and antibacterial effects, for example some attempts were performed with ECM protein functionalization of the surface [4].

The plant kingdom, with their multifunctional molecules and protective strategies, provides an important source of inspiration for multifunctional surfaces [36], [37]. Indeed, plants derived biomolecules, such as polyphenols and molecules of essential oils, are the main molecules used in this work of thesis for functionalization of biomaterial in order to obtain multifunctional surfaces.

The substrates chosen for the study are a silica based bioactive glass named CEL2[38] and a titanium alloy (Ti6Al4V) modified with a patented chemical treatment to impart bioactivity [39]. These two surfaces are osteointegrable, but functionalization allows to increase osteointegrability and addition of other properties like antibacterial, antioxidant and antitumoral effects. The main characteristics and the methods of preparation of the glass and metallic substrates will be explained in the next chapter.

References:

[1]"http://www.iss.it/binary/riap2/cont/2015_Presentazione_del_2_Report_Tabloid_Ortopedia_7_2015.pdf (12/11/2017, 11:15 am)."

[2] T. Albrektsson and C. Johansson, "Osteoinduction, osteoconduction and osseointegration," *Eur. Spine J.*, vol. 10, pp. S96–S101, 2001.

[3] R. Jimbo, M. Ivarsson, A. Koskela, Y.-T. Sul, and C. B. Johansson, "Protein Adsorption to Surface Chemistry and Crystal Structure Modification of Titanium Surfaces," *J. Oral Maxillofac. Res.*, vol. 1, no. 3, pp. 1–9, 2010.

[4] S. F. Badylak, *Host responce to biomaterials*. 2015.

[5] G. Mendonça, D. B. S. Mendonça, F. J. L. Aragão, and L. F. Cooper, "Advancing dental implant surface technology - From micron- to nanotopography," *Biomaterials*, vol. 29, no. 28, pp. 3822–3835, 2008.

[6] A. F. Mavrogenis, R. Dimitriou, J. Parvizi, and G. C. Babis, "Biology of implant osseointegration," *J. Musculoskelet. Neuronal Interact.*, vol. 9, no. 2, pp. 61–71, 2009.

[7] M. Ramazanoglu and and Y. Oshida, "Osseointegration and Bioscience of Implant Surfaces - Current Concepts at Bone-Implant Interface," in *Implant Dentistry - A Rapidly Evolving Practice*, 2011, pp. 57–82.

[8] R. Krishna Alla, K. Ginjupalli, N. Upadhya, M. Shammas, R. Krishna Ravi, and R. Sekhar, "Surface roughness of implants: A review," *Trends Biomater. Artif. Organs*, vol. 25, no. 3, pp. 112–118, 2011.

[9] R. A. Gittens *et al.*, "The effects of combined micron-/submicron-scale surface roughness and nanoscale features on cell proliferation and differentiation," *Biomaterials*, vol. 32, no. 13, pp. 3395–3403, 2011.

[10] R. A. Gittens *et al.*, "Differential responses of osteoblast lineage cells to nanotopographically-modified, microroughened titanium-aluminum-vanadium alloy surfaces," *Biomaterials*, vol. 33, no. 35, pp. 8986–8994, 2012.

[11] R. A. Gittens *et al.*, "The roles of titanium surface micro/nanotopography

and wettability on the differential response of human osteoblast lineage cells," *Acta Biomater.*, vol. 9, no. 4, pp. 6268–6277, 2013.
[12] L. Le Guéhennec, A. Soueidan, P. Layrolle, and Y. Amouriq, "Surface treatments of titanium dental implants for rapid osseointegration," *Dent. Mater.*, vol. 23, no. 7, pp. 844–854, 2007.
[13] M. B. Rosa, T. Albrektsson, C. E. Francischone, H. O. Schwartz Filho, and A. Wennerberg, "The influence of surface treatment on the implant roughness pattern," *J. Appl. Oral Sci.*, vol. 20, no. 5, pp. 550–555, 2012.
[14] M. Geetha, A. K. Singh, R. Asokamani, and A. K. Gogia, "Ti based biomaterials, the ultimate choice for orthopaedic implants - A review," *Prog. Mater. Sci.*, vol. 54, no. 3, pp. 397–425, 2009.
[15] J. L. T. Albrektsson, P. -I. Branemark, H. -A. Hansson, "Osseointegrated titanium implants: Requirements for ensuring a long-lasting, direct bone-to-implant anchorage in man," *Acta Orthop. Scand.*, vol. 52, pp. 155–170, 1981.
[16] A. Sachse *et al.*, "Osteointegration of hydroxyapatite-titanium implants coated with nonglycosylated recombinant human bone morphogenetic protein-2 (BMP-2) in aged sheep," *Bone*, vol. 37, no. 5, pp. 699–710, 2005.
[17] J. M. Schierholz and J. Beuth, "Implant infections: A haven for opportunistic bacteria," *J. Hosp. Infect.*, vol. 49, no. 2, pp. 87–93, 2001.
[18] A. J. Tande and R. Patel, "Prosthetic joint infection," *Clin. Microbiol. Rev.*, vol. 27, no. 2, pp. 302–345, 2014.
[19] D. Peres, I. Neves, F. Vieira, and I. Devesa, "Prosthesis infections after orthopedic joint replacement: the possible role of bacterial biofilms," *Acta Med. Port.*, vol. 5, no. e14, pp. 67–72, 2013.
[20] M. Ribeiro, F. J. Monteiro, and M. P. Ferraz, "Infection of orthopedic implants with emphasis on bacterial adhesion process and techniques used in studying bacterial-material interactions," *Biomatter*, vol. 2, no. 4, pp. 176–194, 2012.
[21] A. D. Pye, D. E. A. Lockhart, M. P. Dawson, C. A. Murray, and A. J. Smith, "A review of dental implants and infection," *J. Hosp. Infect.*, vol. 72, no. 2, pp. 104–110, 2009.
[22] R. Smeets, A. Henningsen, O. Jung, M. Heiland, C. Hammächer, and J. M. Stein, "Definition, etiology, prevention and treatment of peri-implantitis – a review," *Head Face Med.*, vol. 10, no. 1, p. 34, 2014.
[23] "http://www.miltonkeynesdentalimplants.com/perimplantitis/ (14/12/2017, 05:09 pm)."
[24] C. R. Arciola, D. Campoccia, G. D. Ehrlich, and L. Montanaro, "Biofilm-based Healthcare-associated Infections," *Adv. Exp. Med. Biol.*, vol. 830, pp. 29–46, 2015.
[25] J. Prathapachandran and N. Suresh, "Management of peri-implantitis," *Dent. Res. J. (Isfahan).*, vol. 9, no. 5, pp. 516–521, 2017.
[26] M. Katsikogianni and Y. F. Missirlis, "Concise review of mechanisms of bacterial adhesion to biomaterials and of techniques used in estimating

bacteria-material interactions - True Open Access," *MEu. rKopatesaink oCgeiallnsn ain adn dM Ya.tFe.r iMaliss*, vol. 8, no. August, pp. 37–57, 2004.
[27] Q. M. Anthony G. Gristina, Paul T. Naylor, "Infections from biomaterials and implants: a race for the surface," *Med. Prog. Technol.*, vol. 14, pp. 205–224, 1989.
[28] D. Campoccia, L. Montanaro, and C. R. Arciola, "A review of the biomaterials technologies for infection-resistant surfaces," *Biomaterials*, vol. 34, no. 34, pp. 8533–8554, 2013.
[29] C. L. Romanò, S. Scarponi, E. Gallazzi, D. Romanò, and L. Drago, "Antibacterial coating of implants in orthopaedics and trauma: a classification proposal in an evolving panorama," *J. Orthop. Surg. Res.*, vol. 10, no. 1, p. 157, 2015.
[30] B. Kasemo and J. Gold, "Implant surfaces and interface processes.," *Adv. Dent. Res.*, vol. 13, no. v, pp. 8–20, 1999.
[31] H. Lee, S. M. Dellatore, W. M. Miller, and P. B. Messersmith, "Mussel-Inspired Surface Chemistry for Multifunctional Coatings," *Science (80-.).*, vol. 318, no. 5849, pp. 426–430, 2007.
[32] M. Morra, C. Cassinelli, G. Cascardo, D. Bollati, and R. Rodriguez Y Baena, "Multifunctional implant surfaces: Surface characterization and bone response to acid-etched Ti implants surface-modified by fibrillar collagen I," *J. Biomed. Mater. Res. - Part A*, vol. 94, no. 1, pp. 271–279, 2010.
[33] U. Brohede, J. Forsgren, S. Roos, A. Mihranyan, H. Engqvist, and M. Strømme, "Multifunctional implant coatings providing possibilities for fast antibiotics loading with subsequent slow release," *J. Mater. Sci. Mater. Med.*, vol. 20, no. 9, pp. 1859–1867, 2009.
[34] S. B. Reeder, H. H. Hu, C. B. Sirlin, L. I. Group, and S. Diego, *Multifunctional Coatings to Simultaneously Promote Osteintegration and Prevent Infection of Orthopaedic Implants*, vol. 36, no. 5. 2016.
[35] D. V. Shtansky *et al.*, "Multifunctional biocompatible nanostructured coatings for load-bearing implants," *Surf. Coatings Technol.*, vol. 201, no. 7 SPEC. ISS., pp. 4111–4118, 2006.
[36] J. S. Lee *et al.*, "Plant Flavonoid-Mediated Multifunctional Surface Modification Chemistry: Catechin Coating for Enhanced Osteogenesis of Human Stem Cells," *Chem. Mater.*, vol. 29, no. 10, pp. 4375–4384, 2017.
[37] K. Koch, B. Bhushan, and W. Barthlott, "Multifunctional surface structures of plants: An inspiration for biomimetics," *Prog. Mater. Sci.*, vol. 54, no. 2, pp. 137–178, 2009.
[38] C. Vitale-Brovarone, E. Verné, L. Robiglio, G. Martinasso, R. A. Canuto, and G. Muzio, "Biocompatible glass-ceramic materials for bone substitution," *J. Mater. Sci. Mater. Med.*, vol. 19, no. 1, pp. 471–478, 2008.
[39] "S.Spriano et al., European Patent 2214732."

Chapter 2

Polyphenols

2.1Introduction

Polyphenols are natural biomolecules product by the secondary metabolism of plants and they are involved in the defense of the plants against external aggression. They defend plant from UV irradiation and attacks of pathogens and predator.
They are employed in the production of cosmetics, paper, colorants, and also for tinning skins, but they also can have beneficial effect on human health.
It is well known in the scientific community but also in the public knowledge that a daily intake of vegetables and fruits, rich in polyphenols can give health benefits.
Polyphenols have antitumor, antibacterial, ossteoinductive, angiogenetic, anti-inflammatory and antioxidant properties[1], [2].
Unfortunately stability and bioavailability of these molecules is a critical point. They are also sensible to light, temperature and pH[3] and because of these characteristics a great amount of the polyphenols intake with the diet are degraded during the digestion or expelled trough the urine[4].
For these reason the administration of the polyphenols using an inorganic carrier is a promising idea to improve the action of the polyphenols for our purpose.
Titanium alloy Ti6Al4V and bioactive glasses are biomaterials widely used in contact with bone and are good candidates for the development of protocols of functionalization of biomaterials with polyphenols.

This chapter includes bibliographic content, like the structure and the different properties of polyphenols and the functionalization of bioactive glass and bioactive titanium alloy with gallic acid, as model molecule for polyphenols, and natural extracts from green tea and red grapes/pomaces. Part of this chapter is included in two published manuscripts(M. Cazzola et al. "Bioactive glass coupling with natural polyphenols: Surface modification, bioactivity and anti-oxidant ability", 2017, Applied surface science and M. Cazzola et al. "Bioactive glasses functionalized with polyphenols: in vitro interactions with healthy and cancerous osteoblast cells", 2017, Journal of Materials Science) and in two submitted manuscripts (M. Cazzola et al., "Grafting of gallic acid onto a bioactive Ti6Al4V alloy: a physico-chemical characterization", 2017 submitted to the journal Progress in Natural Science: Material Internationals and M. Cazzola et al., "Green tea polyphenols coupled with a bioactive titanium alloy surface: in vitro characterization of osteoinductive behavior through a KUSA A1 cell study", 2017, submitted to the journal Materials Science and Engineering :C).

2.2 Classification and chemical structure of polyphenols

Polyphenols are chemical compounds located in every organs of plants.
They are present in large amount in fruits, vegetable, leaves and their derivate and they are fundamental for taste, color and nutritional properties[2].
These group of substances is extremely variable and complex and they range from simple phenolic molecule to big polymerized compounds with molecular weight greater than 30000 Da[5].The number of polyphenols known is still in growth and more than 8000 molecules have been identified so far. They are often correlated with mono or polysaccharides, linked to other phenolic groups, ammines and lipids. According to the number of phenol rings that they contain and the chemical structure that bind a ring to another, polyphenols are classified into four principal classes: phenolic acids, flavonoids, stilbenes and lignans. These classes and relatives under classifications as reported in Figure 2.1 [6],[7] .

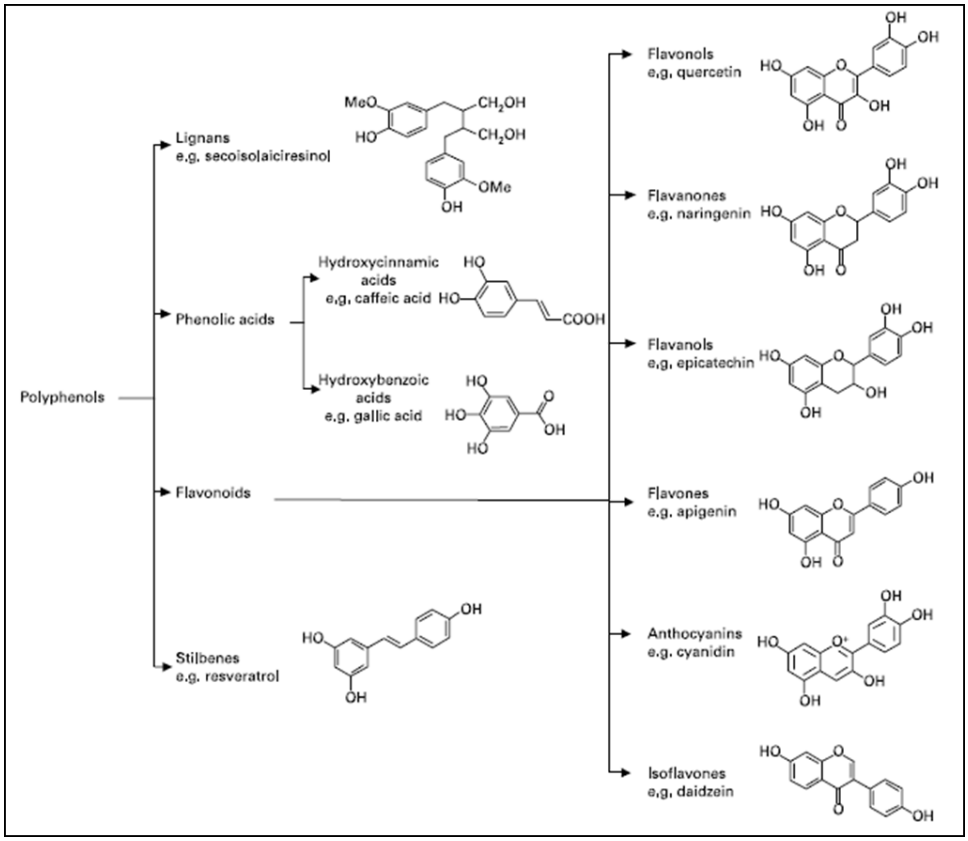

Figure 2.1: Classification of polyphenols in Food [8].

Lignans derive from the dimerization of two phenilprophane units. They are located in woody stems and in seeds, they play a role as insect deterrents and could have medical properties. Their most important source for human diet are flax seeds [9].

Stilbenes are present in the human diet and one of the most representative is resveratrol that is produced by plants in response of external attacks and it is present in grape and berries [6]. This polyphenol has anticarcinogenic effect and this will be discussed more extensively afterwards [10].

Phenolic acids are abundant in plants and are divided into 2 classes: Hydroxycinnamic acids derivatives of cinnamic acid and Hydroxybenzoic acid derivatives of benzoic acid based on the C1-C6 and C3-C6 backbone[2], [11].

One of the more simple and known phenolic acid is gallic acid or 3,4,5-trihydroxicbenzoic acid that is abundant in fruits, tea and wine. After the extraction it has the form of a yellowish crystal and it influences several physiologic pathways. They have indeed anti-inflammatory and antitumor effects[12].

Flavonoids have low molecular weight and they have fifteen carbon atoms with the configuration C6-C3-C6.
The structure reported in Figure 2.2 essentially consist of 2 aromatic rings, A e B, joined by a 3-carbon bridge usually in the C Heterocyclic form [13].

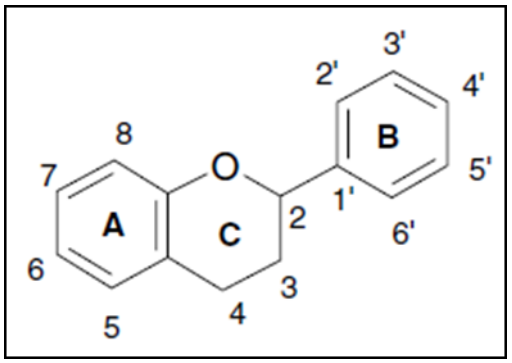

Figure 2.2: general structure of flavonoids [13].

The division of flavonoids in several classes is mainly the results of the variation in the substitution pattern of ring C. Flavonoids are classified in 6 big classes: flavonols, flavanones, flavanols, flavones, anthocyanins and isoflavones.
Flavonols are the most diffused flavonoids in the human diet and the most representative are quercetin and kaempferol. They are abundant in onions, curly kale, broccoli and blueberries.
Flavanones have a 3-carbon chain saturated and an oxygen atom in the C4 and they are also generally glycosylated by a disaccharide in C7. They are present in citrus, tomatoes and aromatic plant such as mint.
Flavanols exist in two forms, the monomer form named catechins and the polymer form named of proanthocyanidins.
Catechins are present in green tea, chocolate, red wine and fruits.
The proanthocyanidins are polymers of catechins that are bound together with links between C4 and C8 or C6 and they are also known as condensed tannins. They are responsible of the astringent character of certain fruits and of the bitterness of chocolate because of their ability of complex with salivary proteins.
Flavones are less diffused than the other flavonoids end they are present in appreciable amount in food only in parsley and celery [10],[14],[15].
Isoflavones have a structure similar to estrogens and they could be found in nature both in the native or conjugated form.
Anthocyanidins are the basic structure of anthocyanins and they have the ring A bound to heterocyclic ring C containing oxygen which is also bonded by a carbon-carbon bond to the aromatic ring B.

Anthocyanins are the glycosylated form of anthocyanidins and they are present in all plant tissues. They could appear with different colors (red, purple or blue) depending on pH[6].

2.2.1 Composition and structure of red grape polyphenols

Grape and grape products are rich of polyphenols that are related to important health benefits and their concentration depends of the variety, the growing area, the state of ripeness.
Wine is one of the main sources of polyphenols in human diet [16].
The polyphenols in grape berries are mainly in skin, stems and seeds.
Grape pomace is the by-product of wine industry and is mainly constituted by skins, seeds and stems and is about 20-25% of the weight of the grape used for the production of the wine. For the waste of wine production is possible to extract polyphenols because about 70% of grape polyphenols remain in the
pomace and the recycling of wastes from agro-food and winemaking industries is rising attention [17]–[20].
The polyphenols average concentration is around 2178, 374, 351, and 23 mg/g GAE (gallic acid equivalent) in seeds, skins, leaves and flesh respectively. The principal components are proanthocyanidins, anthocyanins, flavonols, flavanols, resveratrol and phenolic acids. The anthocyanins are responsible of red grape color. White grape do not contain this kind of polyphenols. In the red grape the anthocyanins and the flavonoids are the two most abundant compounds and (+)-catechin is the most representative [21][22].
The phenolic compound present in the different part of grape and in red wine are reported in Table 2.1.

Table 2.1: polyphenol compounds in grape and red wine [21].

Resource	Phenolic compounds
seed	gallic acid, (+)-catechin, epicatechin, dimeric procyanidin, proanthocyanidins
skin	Proanthocyanidins, ellagic acid, myricetin, quercetin, kaempferol, trans-resveratrol
leaf	myricetin, ellagic acid, kaempferol, quercetin, gallic acid
stem	rutin, quercetin 3-O-glucuronide, trans-resveratrol, astilbin
raisin	hydroxycinnamic acid, hydroxymethylfurfural
red wine	malvidin-3-glucoside, peonidin-3-glucoside, cyanidin-3-glucoside, petunidin-3-glucoside, catechin, quercetin, resveratrol, hydroxycinnamic acid

Skin contains a greater amount of phenolic acids than seeds, but a lower amount of catechins and proanthocyanidins.

The principal phenols on seeds are flavan-3-ols like catechin, epicatechin, and epicatechin-3-o-gallate monomers and their polymers. Furthermore flavan-3-ols easily polymerize into condensed tannins [17].

Epicatechin is the most abundant extension unit in grape tannins and tannins are amphipathic molecules having both hydrophobic aromatic rings and hydrophilic hydroxyl groups allowing them to bind simultaneously at several sites on the surface of the other molecules[23]. In grape and wine are present several hydroxybenzoic acids such parahydroxybenzoic, protocatechic, vanillic, gallic, and syringic acids. Gallic acid is the most important compounds because it is the precursor of the hydrolysable tannins. The Hydroxycinnamic acids, para-coumaric, caffeic, ferulic and sinapic acids, are some of the most reported compound in literature for grape and wine[24]. Resveratrol, 3,5,4′-trihydroxystilbene (Figure 2.3), is a stilbene present in grapes and in certain type of red wine can reach up to 14 mg/l. It is produced by plants in response to external attacks and it has anti-inflammatory, antioxidant and antitumor properties [25]–[27].

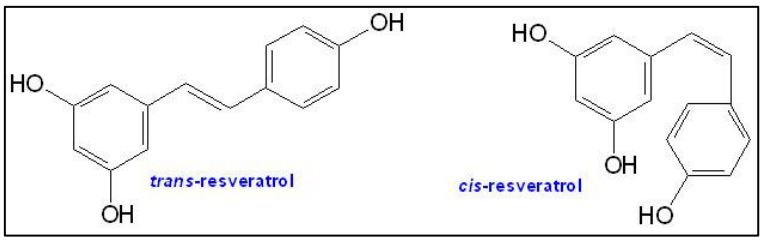

Figure 2.3: Structure of resveratrol [28].

2.2.2 Composition and structure of green tea leaves polyphenols

Tea started to be consumed in china over 5000 years ago and is today largely drunk all over the word [29]. It is a beverage obtained by the soaking in hot water of the leaves of *Camelia Sinensis* and all the types of tea (black, green and white) come from the leaves of the same botanic source and it depends on the processing of the raw material. The leaves of *Camelia Sinensis* are rich in extractable polyphenols and even more in specific of flavan-3-ols, commonly named catechins, which constitute 30% of the weight of the leaves [30], [31]. Polyphenols are present in green tea with the percentage of 10%-15% while are only around 5% in the black tea.

For the production of the white tea the leaves are harvested before they are fully open and the buds are still covered with white hairs. This tea undergoes the least amount of processing and maintains the maximum amount of polyphenols, however it is really expensive and produced only in China. Black tea is produced with the tender shoots of *Camelia Sinensis* and the enzyme polyphenols oxidase is left to act to obtain fully fermented leaves rich of caffeine, theaflanins and thearubigins. Theaflanins are responsible for the astringency and thearubigins contribute to the color of the tea, while caffeine is responsible of the stimulatory effect. Theaflanins are produced by the oxidase dimerization of simple and gallo-cathechins catalyzed by the enzyme polyphenol oxidase.

In order to obtain green tea, the leaves are heated with rolling after the harvest to inactivate the enzyme polyphenol oxidase.

This tea contains flavonols up to 4% [30] (e.g.: rutin, quercetin, kaempferol, caffeine, phenolic acid, theanine, flavor compounds and leucoanthocyanins). The mayor phenolic compounds are catechins such as (–)–epigallocatechin- 3-gallate (EGCG), (–)–epigallocatechin (EGC), (–)–epicatechin-3-gallate (ECG), and (–)–epicatechin (EC) [32]. The components of green and black tea are reported in table 2.2.

Table 2.2 : components of black and green tea[33].

	occurence (% dry weight)		
	green tea	black tea	structure
Catechins	**30-42**	**10-12**	
epigallocatechin gallate	11		**B** (-)2,3-cis R1=OH R2=**A**
epicatechin gallate	2		**B** (-)2,3-cis R1=H R2=**A**
gallocatechin gallate			**B** (+)2,3-trans R1=OH R2=**A**
epicatechin	2		**B** (-)2,3-cis R1=R2=H
epigallocatechin	10		**B** (-)2,3-cis R1=OH R2=H
gallocatechin			**B** (+)2,3-trans R1=OH R2=H
catechin			**B** (+)2,3-trans R1=R2=H
Teaflavin		**3-6**	
theaflavin-3-gallate			**C** R1=OH R2=OH
theaflavin-3'-gallate			**C** R1=**A** R2=OH
theaflavin-3,3'-digallate			**C** R1=OH R2=**A**
Thearubigens		**12-18**	**C** R1=**A** R2=**A**
Theogallin	**2-3**		
Proanthoocyanidin			
Flavonols	**5-10**	**6-8**	
quercetin			**D** R1=OH R2=H R3=OH
kaempferol			**D** R1=R2=H R3=OH
rutin			**D** R1=OH R2=H R3=O-rutinose
Methylxanthines	**7-9**	**8-11**	
caffeine	3-5		**E** R1=R2=CH_3
theobromine	0.1		**E** R1=H R_2=CH_3
theophylline	0.02		**E** R= CH_3 R2=H
Amino acids			
theanine	4-6		**F**
Organic acids			
caffeic acid			
quinic acid	2		
gallic acid			
Volatiles			
linalool			
delta-cardinene			
geraniol			
nerolidol			
alpha-terpineol			
cis-jasmone			
indole			
beta-ionone			
1-octanal			
indole-3-carbinol			
beta-caryophyllene			

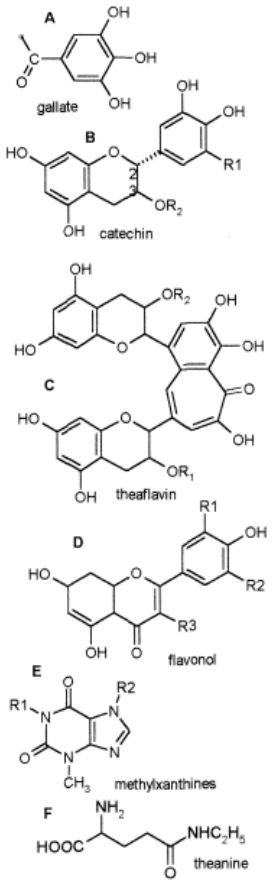

EGCG has eight free –OH groups that confer to this polyphenol antioxidant activity [34]. This molecules is also known to have cardioprotective, vasculoprotective, antitumoral and antidiabetic effects [35]–[37].

2.3 Properties of polyphenols

Polyphenols play a crucial role in the protection of plants. They are involved in the defense against UV light, bacterial attack (antibacterial effect), attacks of parasites, and they also have a role in the interaction between plants and the other living organism [38], [39]. The presence of the phenol group is the principal responsible of the effect of the polyphenols in the plants health. Phenol groups also have beneficial effects on other organisms interacting with different biological molecules as shown in Figure 2.4.

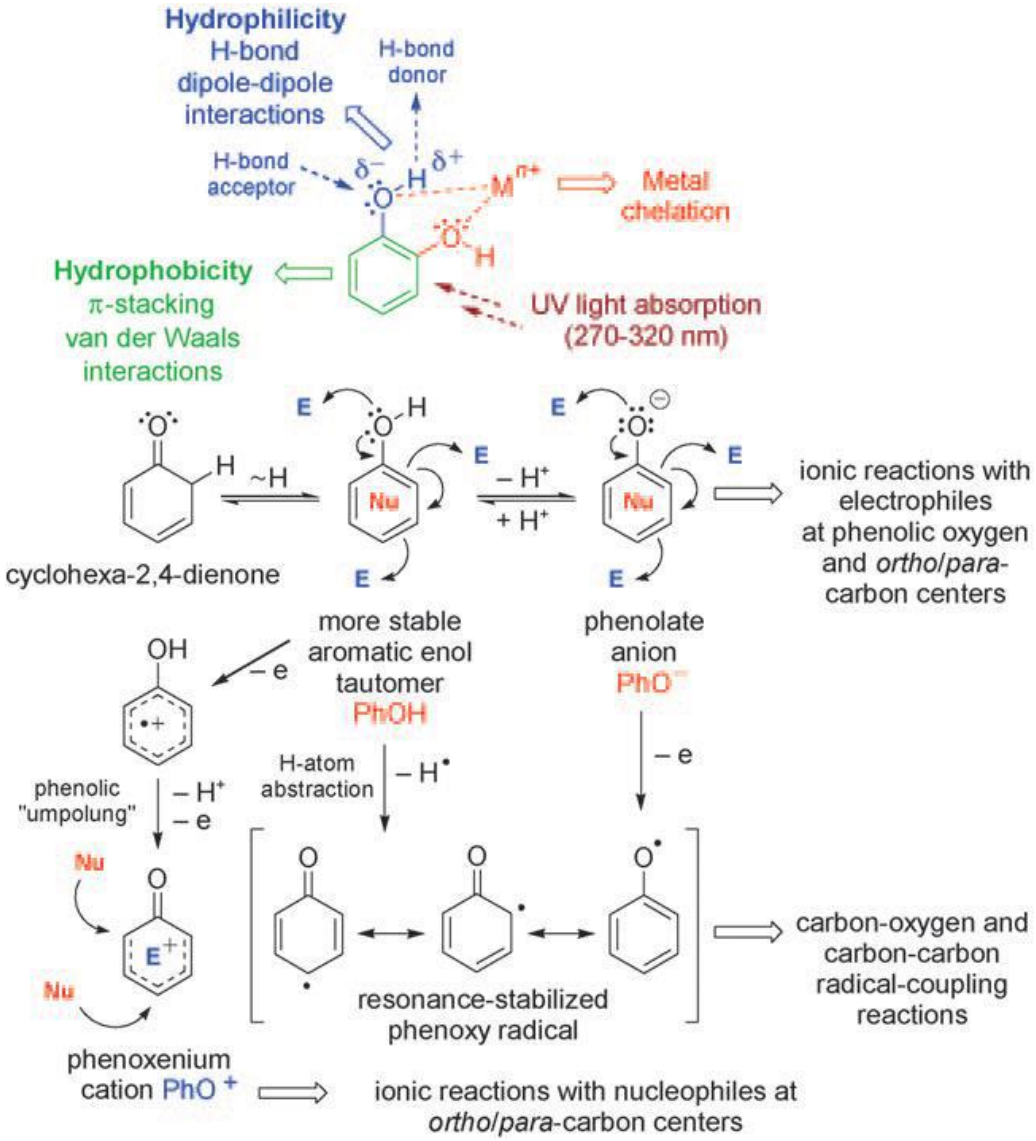

Figure 2.4: Reactions linked to the presence of the phenolic functional group [40].

Polyphenols have antibacterial, antioxidant, antitumoral, proapoptotic, vasculoprotective effects and they have also positive effects in the bone health.

2.3.1 Antitumoral properties

Polyphenols are involved in several tumoral cell processes acting as chemoprotective and proapoptotic agents. It was theorized that they could have 6 different way of actions against tumoral cells[41]:

- induction of cell apoptosis
- anti-inflammatory effect
- antiproliferative effect
- arrest of the cellular cycle
- inhibition of metastasis
- antioxidant effect against the damage of the DNA of healthy cells

S. Patrudu et al.[42] studied the effects of various non mutagenic polyphenols against the mutagenic effects of Benzidine (human bladder carcinogen). Benzidine causes lipid peroxidation and production of oxygen free radical. The presence of polyphenols inhibits the lipid peroxidation induced by Benzidine and also reduces the one induced by iron. They suppose that polyphenols reduce the oxidase mutagenicity trough inhibition effects enzymes such as cytochrome P-450.

S. Kunt et al. [43] investigated the effects of more than 30 flavonoids against colon rectal cancer cells (CaCo-2) and all the tested biomolecules showed antiproliferative activity without cytotoxicity effects on the co-cultures HT-29 intestinal epithelial cells[44].

Polyphenols inhibit also the metastatic process with molecular actions in the signaling pathways involved in tumoral cells proliferation and migration[45], and the protein target and the signaling pathways are resumed in Figure 2.5.

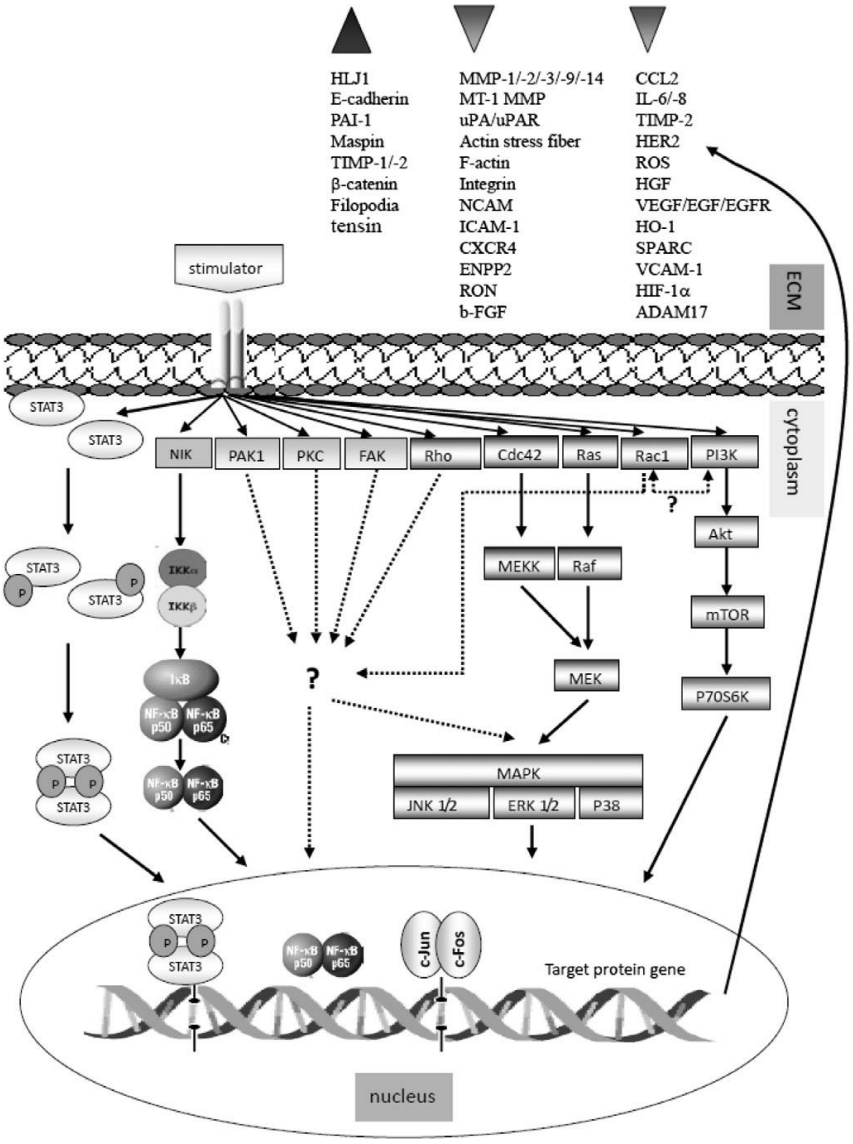

Figure 2.5: signal pathways and proteins involved in inhibition of metastasis by phenolic compounds. "?" mean unknown regulation, ▲ upregulation and ▼ downregulation [45].

Anthocyanins and extracts rich of anthocyanin have anti proliferative effect against several cancer cell types *in vitro* and this is due to the ability of this kind of polyphenols to block different stage of cell cycle acting on proteins that regulate it such as Cyclin A and cyclin D1. Some investigation have also compared the action of anthocyanins on tumoral cells vs normal cells highlighting a selectivity action on cancer cells[46].

Gallic acid is one of the polyphenols with the simplest structure, well present in plant and fruits and it was widely studied in literature[47].
It has effect on inhibition of cancer cells line through the modulation of genes involved in the cell cycle.
NF-κB and Akt signaling pathway were inhibited by the action of gallic acid with the activity of COS, GSH and ribonucleotide reductase.
Gallic acid prevent also the process of carcinogenesis by mean of the activation of ATM kinase signaling pathway and the mentioned pathway is resumed in Figure 2.6[12].

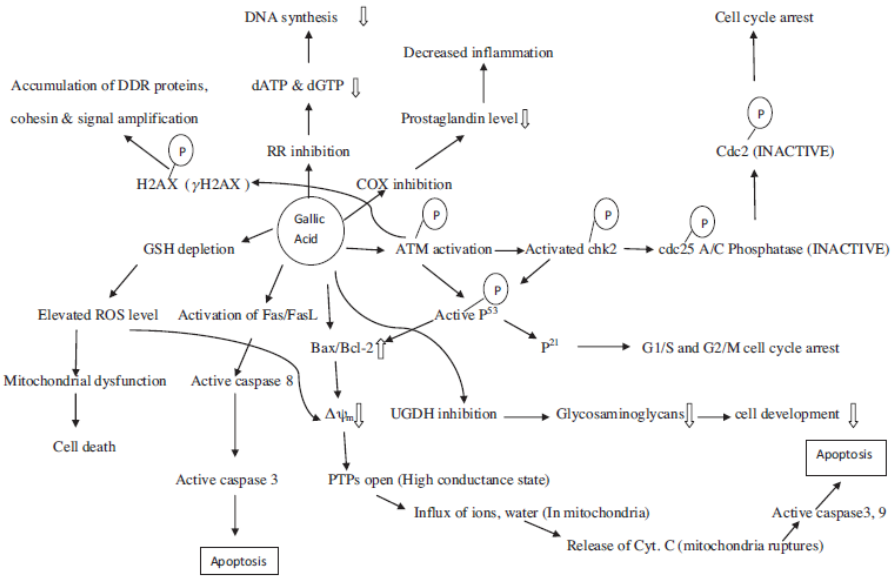

Figure 2.6: effects of gallic acid in the pathway involved in the genesis of tumor [12].

Another polyphenols that was extensively investigated in literature was resveratrol (3,5,4'-triidrossi-trans-stilbene).
It blocks the carcinogenesis by inhibition of Phase I enzymes, improves the antioxidant capacity, arrests cell proliferation by regulating cell cycle, induces apoptosis on damaged cells, blocks neovascularization and angiogenesis of cancer tissues, suppresses the invasion of metastasis and sensitizes tumor cells at the chemotherapy induced apoptosis[25], [48]–[51].
The polyphenolic extracts of grape and wine had antitumoral effects and the results obtained for different polyphenols present in these extracts are reported in table 2.3.

Table 2.3:antitumoral activities of polyphenols from grapes[52].

Phenols	Subject	Effects
proanthocyanidins	mouse mammary carcinoma cell line	inhibited breast cancer metastasis
anthocyanin	rat liver clone 9 cells	activated antioxidant response element upstream of genes
	colon cancer cell lines (HT-29 and Caco-2)	induced 2–4 times increase in DNA fragmentation
	vascular tumor biology	repaired and protected genomic DNA integrity and retard blood vessel growth in some tumors
procyanidin, catechin or gallic acid	mice spleen cells	inhibited DNA damage induced by hydrogen peroxide
catechin	human breast cancer cell line	decreased cell viability and proliferation at 30 and 60 µg/mL
procyanidins		decreased cell viability and proliferation at 30, but not 60 µg/mL
flavone	human colon carcinoma HT-29 cells	reduced cell proliferation with an EC50 value of 54.8 ± 1.3 µmol/L, induced differentiation and apoptosis
flavonoid	HT-29 cells	more effectively induced apoptosis than antitumor agent camptothecin
resveratrol	prostate cancer cell lines	induced apoptotic and antiproliferative effects at ≥ 15 µmol/L and above 24 hours
	human mammary epithelial cells	inhibited cyclooxygenase-2 transcription

They can inhibit the activity of matrix metalloproteinases-2 and -9 with antiproliferative effect on colon cancer cells CaCo-2 and they also inhibit DNA adduct in rat model and DNA synthesis in breast cancer cells.
The principal cell target of cell regulation apoptosis against which act polyphenols is phosphatidylinositol3-kinase–Ak mitogen-activated protein kinase survival pathways reducing transcription and improving degradation[52].
Green tea polyphenols has been shown to have antitumor effect on several cancer cell lines as reported in table 2.4.

Table 2.4: Green tea effect on several tumor line [53].

S. No	Green tea/ constituents	Cancer type	Remedial effects
1	EGCG	Tumor	Apoptosis rate increased by increasing EGCG
2	Green tea	Liver, lung and colon cancer	Relative lower risk was observed for liver, lung and colon cancer, lower repetition rate (16.7%) for breast cancer
3	GTE and green tea polyphenols	Tumor cell (A427/human lungs)	Anchorage independent development, decaffeinated and GTE revealed reduced inhibition. Green tea polyphenols inhibition was significant (74%–92%)
4	Green tea	Stomach and gastric cancer	Stomach and gastric cancer goes to decreased level in smoking persons and alcoholic drinkers
5	EGCG	Transformed cells	More induced apoptosis and anticancer effect in transformed cells as compared to normal
6	EGCG	Leukemic cancerous cells	Reduction in ornithine decarboxylase (50%) and remedial potential
7	Green tea	Metastatic prostate carcinoma	Low therapeutic effect can be seen, 2%
8	Green tea	Epithelial ovarian cancer	Reduction in epithelial ovarian cancer hazard rates
9	Green tea	Prostate cancer	Decline risk of prostate cancer with duration, quantity and frequency amplification of green tea utilization
10	EGCG	LNCaP (A type of human prostate carcinoma cell)	Chemo-therapeutic drugs and EGCG mixture have remedial effects against prostate cancer
11	Green tea catechins	Prostate cancer	Cancer growth inhibition
12	Green tea	Prostate cancer	Advance prostate cancer reduced risk
13	Green tea	Breast cancer	Declined breast cancer risk with high consumption of green tea
14	EGCG	Human breast cancer cells	Inhibition of breast cancer proliferation
15	Green tea	Leukemia cells	Reduction in adult leukemia risk with green tea consumption
16	Green tea	Lung cancer	Lung cancer reduced risk
17	Green tea	A549 tumor cells	Cell motility was modulated by GTE induced lamin A/C and annexin. These contribute to the anticancer activity of green tea.
18	EGCG polyphenol	Leukemia cancerous cells	EGCG polyphenol has low relative cell proliferation of leukemia cancerous cell
19	Green tea, ascorbic acid, arginine, lysine, proline	Tumor cells	Reduction in diversity and growth of tumor
20	EGCG	Quercetin LNCaP cell	EGCG and quercetin LNCaP cell proliferation inhibition with 40 µmol/L EGCG 10 µmol/L quercetin, 48 h compared with 60% inhibition
21	Methanolic extract of *Gracilaria tenuispitata*	Tumor cells	Maximum reduction in tumor volume by higher dose of (MEGT 400 mg)
22	Green tea	Human cervical cancer cells	Methanol extract of green tea has cytotoxic towards human HeLa and potent anticancer compound with an IC_{50} of 111.9 g/mL inducing growth inhibition in the human cervical cancer cells
23	EGCG, paclitaxel and docetaxel combinations	Human head, neck, lung, breast, prostate, liver and stomach cancer cells	Synergistic increase in anticancer activity with decline in tumor (70.3%)
24	EGCG and synergistic	Human lung cancer cells	Anticancer activity of EGCG and synergistic hardware related work is a striking up-regulation of two genes, growth arrest and DNA damage-inducible gene 153 induced and p21, 12 times as and 3 PC-9 cells in the floor.
25	Jasmine green tea and catechins	Human cancer cells	Jasmine green tea has the most synergistic effects with catechins. It increases the scavenging effect

The principal actor of the anticancer effects from the green tea is the EGCG ((–)–epigallocatechin-3-gallate). It binds to carcinogens, induces Phase II enzymes and inhibits the formation of heterocyclic amine. Other relevant molecular mechanism are the catechins-mediated induction of apoptosis, the cell cycle arrest, the inhibition of transcription factors NF-kB and AP-1 and the reduction of c-jun mRNA expression and of protein tyrosine kinase activity[32]. B.B Hafeez et al. [54] studied the effect of green tea polyphenols on osteosarcoma cells Saos-2 and highlighted the induction of apoptosis mediated via activation of captase and inhibition of NF-κB[55]. EGCG also suppresses in murine model osteosarcoma cell growth with the upregulation of miR-1[56].

2.3.2 Antioxidant properties

The production of radicals by aerobes is constantly modulated by synthesizing antioxidants. A balance in the production of radicals is fundamental to allow them to perform useful function but avoid oxidative damage of tissues that is involved in the development of several diseases [57].
A loss of electrons or a gain of oxygen is defined as oxidation. Antioxidant inhibits the oxidative damage which occurs when radicals chemically interact with cell DNA and lipids stealing their electrons in order to become stable [58].
In Figure 2.7 are reported the correlation between tissue damage and oxidative stress.

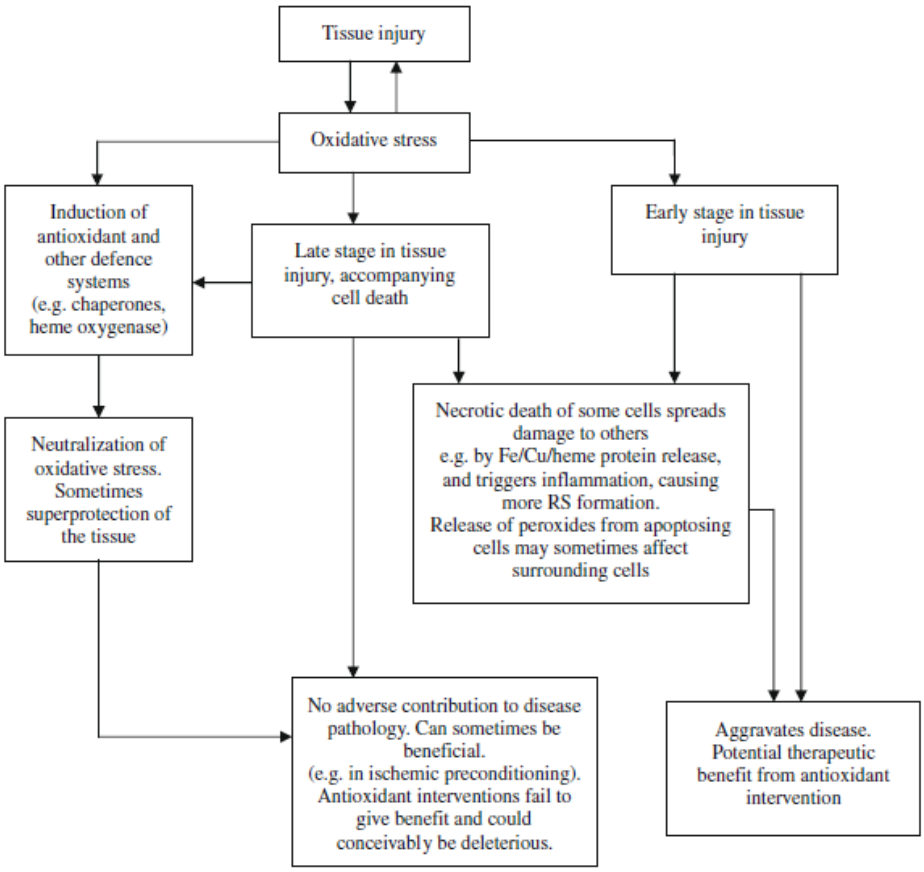

Figure 2.7: correlation between tissue damage and oxidative stress[58].

Polyphenols are great antioxidants[59] against free radicals induced by external factors or metabolism. An excess of radicals can damage nucleic acid, proteins, lipids and causes cell membrane peroxidation upregulating inflammatory mediators. Polyphenols acts as primary antioxidant in three principal ways reported in Figure 2.8.

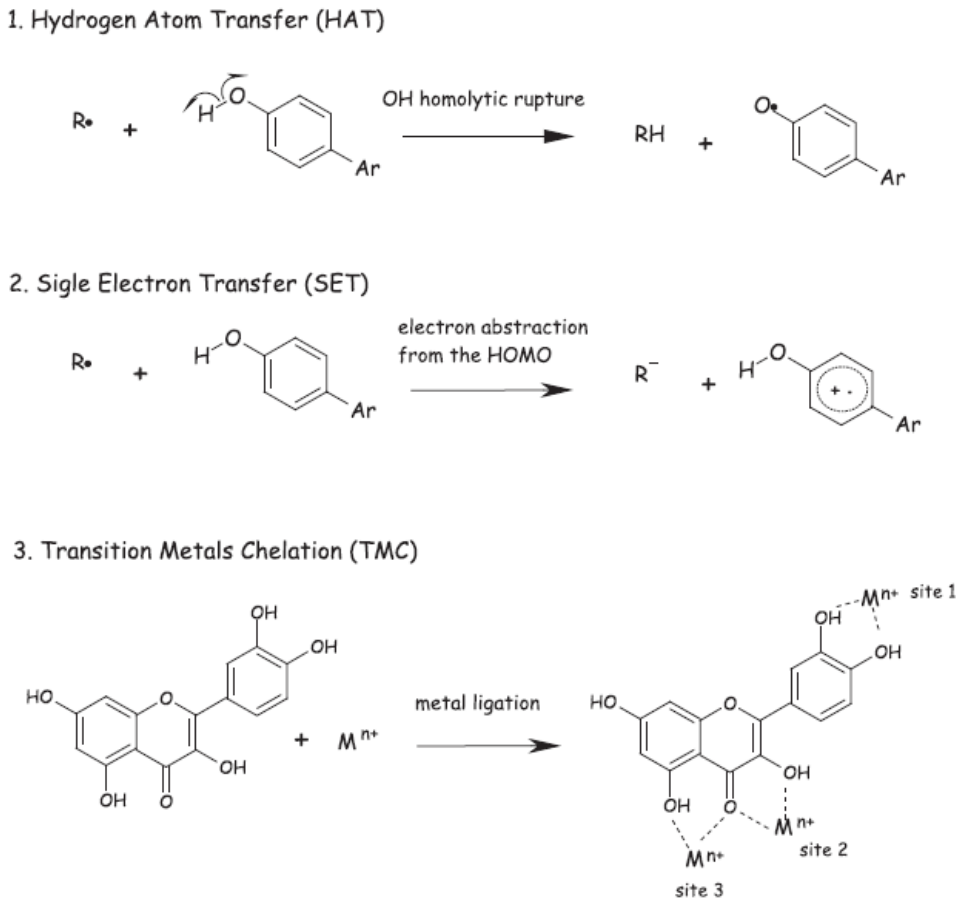

Figure 2.8: way of action of the polyphenols as antioxidant[60].

The first mechanism of action is the hydrogen atom transfer (HAT). In this mechanism the antioxidant ArOH reacts with the radical R with the transfer to it of a hydrogen atom by the homolytic rupture of the O-H group.

$ArOH + R\bullet \rightarrow ArO^{+}\bullet + RH^{-}$

The second mechanism involve the single electron transfer (SET) that consist in the donation of an electron to R• obtaining less reactive radical species.

$ArOH + R\bullet \rightarrow ArOH^{+}\bullet + R^{-}$

The third antioxidant mechanism is due to the chelation of transition metal ions by polyphenols leading to stable compounds. Chelating metal ions polyphenols inhibits the generation of oxygen radical species[60].
These three pathways are the main process leading to the polyphenol antioxidant properties. However secondary ways of actions are known. They can [61]:

- activate antioxidant enzymes
- reduce α-tocopheryl radicals
- inhibit oxidases
- mitigate oxidative stress caused by nitric oxide
- increase uric acid levels
- increase antioxidant properties of low molecular antioxidants.

Gallic acid is able to scavenge radicals, to regulate the pathway of oxygen radical species generation and to reduce the peroxidation of the cellular membrane [62]. This polyphenol is also able to chelate iron (II) and iron(III) ions [63], [64].
Polyphenols from red grape inhibit peroxidation of LDL- cholesterol reducing the incidence of cardiovascular problems [20]. Resveratrol, that is present in red grape, has hydrogen peroxide scavenging activity, superoxide anion radical scavenging activity, and metal ions chelating activity[65].
The polyphenols of green tea (mainly catechins) are active against oxidation and they are able to scavenge reactive oxygen species and chelate iron ions[66], [67].

2.3.3 Antibacterial properties

Several studies have investigated the antibacterial activity of polyphenols.
Flavonoids, tannins, vanillic, caffeic, gallic, syringic and ρ-hydroxy benzoic acid are able to inhibit the growth of *E.Coli, klebsiella pneumonie* at concentration $300mgl^{-1}$ and all these polyphenols except for syringic acids are able to complete inhibit the growth of *B. cereus* at 500 mgl^{-1} [68].
Phenolic extracts of tea inhibit the growth of *Vibrio cholerae, Salmonella typhi, Campilobacter jejuni, Campilobactercoli, Helicobacter pylori, Shigella, Salmonella,Clostridium, Pseudomonas, Candida, Mycoplasma and Cryptococcus* and are more effective against Gram-positive bacteria [33][69].
Polyphenols from Chinese green tea are also been tested with success against *Escherichia coli, Salmonella, Listeria monocytogenes, Staphylococcus aureus*,

and a diarrhoea food-poisoning pathogen *Bacillus Cereus* with the highest activity against *Staphylococcus Aureus* and the lowest against *Escherichia coli*.
Single polyphenols extracted from tea were also tested: epicatechin gallate (ECG), epigallocatechin gallate (EGCG), epicatechin (EC). ECG and EGCG were the most effective, particularly EGCG against *S. aureus* [70].
In vitro studies highlighted the ability of polyphenols to reduce dental plaque accumulation and the grow of *the Staphylococci* improving oral hygiene[71] and also extract of grape seeds has inhibitory effects on the oral anaerobe bacteria[72].
Gallic acid, tannic acid, quercetin end polyphenols from natural source has also inhibitory effects against *Staphylococco Mutans*[73].
The effect of gallic acid and catechins was studied on *Helicobacter Pyroli* and the gallic acid showed at the same dose a stronger activity than catechins[74] .
Concerning flavonoids, remarkable activity has been reported on different bacterial strain: *Staphylococcus aureus*, *Lactobacillus acidophilus, Actinomyces naeslundii, Prevotella oralis, Prevotella melaninogenica, Porphyromonas gingivalis,* and *Fusobacterium nucleatum*[75]. A list of the flavonoids and their effects on different bacteria are reported in Table 2.5:

Table 2.5: Antimicrobial activity (halo test) of some flavonoids against bacteria. (-) means no antimicrobial activity, (w) weak antibacterial activity, (+) inhibition zone 2-3 mm, (++) inhibition zone 4-5 mm, (+++) inhibition zone 6-9 mm, (++++) inhibition zone >9mm [75].

Phenolic compounds (mg/l)		*Serratia marcescens*	*Proteus mirabilis*	*Escherichia coli*	*Klebsiella pneumoniae*	*Flavobacterium* sp.	Mean of inhibition zone
Rutin	1	w	–	w	–	–	0.4
	10	+	–	w	–	–	0.6
	25	+	–	+	–	–	0.8
	50	+	–	++	–	–	1.2
	100	+	–	++	–	–	1.2
	500	+	–	++	–	–	1.2
	1000	+	–	++	–	–	1.2
Quercetin	2	+	–	–	–	–	0.4
	10	+	+	–	–	–	0.6
	25	++	+	+	+	–	2.0
	50	++	+	++	++	–	2.8
	100	++	++	++	+++	–	3.4
	500	+++	++	++	+++	–	3.8
	1000	+++	++	+++	+++	–	4.2
Catechin	10	w	–	w	–	–	0.4
	50	w	–	+	–	–	0.6
	100	+	–	+	–	–	0.8
	200	+	–	+	–	–	0.8
	500	+	+	+	–	–	1.2
	1000	++	+++	++	–	–	2.8
Control (+) chloramphenicol 1000 mg/l		++++	++++	++++	++++	++++	
Mean of inhibition zone		2.5	1.3	2.6	1.2	–	

The relation between the antibacterial activities and the structure of flavonoids (figure 2.9) has been investigated.

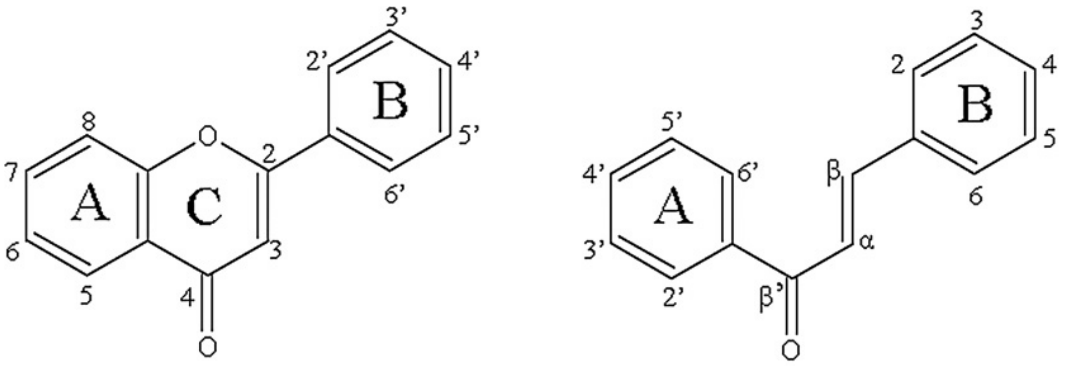

Figure 2.9: skeleton structure of flavonoids with evidenced A, B and C rings[76].

It is possible to separately discuss the structure of the action of chalcones (open chain flavonoids) and of the other flavonoids.

For chalcones, the hydroxylation in position 2' of the A ring is important for antibacterial activity, but also the hydroxylation in other positions of the A ring improves the effect.
Substitutions with acetoxylation or metoxylation at position 2' and fluorination at position 3' and 5' decrease the antibacterial activity. The antibacterial effects are instead improved by lipophilic substituents trifluoromethyl or bromo in position 3 of ring B.
For the other flavonoids the presence of an O- acyl or an O-alkylamino chain in the position 7 of ring A improves the antibacterial effect and the activity is also improved by the presence of a lipophilic group in position 6 or 8.
bromo- and chloro- groups in positions 2', 3', and 4' on ring B improved the activity.
For ring C, the activity is improved by hydroxylation at position 3[76].
The effects of some non-flavonoids polyphenols against different bacteria are reported in Table 2.6.

Table 2.6: Antimicrobial activity halo test) of some non-flavonoids against bacteria. (-) means no antimicrobial activity, (w) weak antibacterial activity, (+) inhibition zone 2-3 mm, (++) inhibition zone 4-5 mm, (+++) inhibition zone 6-9 mm, (++++) inhibition zone >9mm [75].

Phenolic compounds (mg/l)		*Escherichia coli* ATCC 35218	*Escherichia coli* ATCC 25922	*Pseudomonas aeruginosa* ATCC 27853	*Staphylococcus aureus* ATCC 29213	*Staphylococcus aureus* ATCC 25923	Mean of inhibition zone
Gallic acid	5	w	–	–	–	–	0.2
	10	w	–	–	–	–	0.2
	25	w	w	–	–	–	0.4
	50	w	w	w	–	–	0.6
	100	w	w	w	–	–	0.6
	200	+	w	w	w	–	1.0
	500	+	+	+	+	–	1.6
	1000	+	+	+	+	–	2.0
Vanillic acid	5	–	–	–	–	–	–
	10	–	–	–	–	–	–
	25	–	–	–	–	–	–
	50	–	–	–	–	–	–
	100	w	–	–	–	–	0.2
	200	w	w	–	–	–	0.4
	500	+	w	–	–	–	0.6
	1000	+	w	–	–	–	0.6
Protocatechuic acid	5	–	–	–	–	–	–
	10	–	–	–	–	–	–
	25	–	–	–	–	–	–
	50	–	–	–	–	–	–
	100		w	–	–	–	0.2
	200	w	w	–	–	–	0.4
	500	+	w	w	–	–	0.8
	1000	+	+	w	–	–	1.0
Caffeic acid	1	+	–	–	–	–	0.4
	5	+	w	–	–	–	0.6
	20	+	w	–	–	–	0.6
	50	+	w	–	w	–	1.0
	100	+	+	w	+	–	1.6
	500	++	+	+	+	–	2.4
Control (+) chloramphenicol 1000 mg/l		++++	++++	++++	++++	++++	
Mean of inhibition zone		1.3	0.8	0.4	0.4	–	

2.3.4 Effects on bone health

Some studies have investigated the effect of tea consumption in bone health. In particular green tea seemed to improve bone density and reduce the risk of fracture. This effect could be correlated with the decrease of oxidative stress, the upregulation of the antioxidant enzymes and the downregulation of proinflammatory mediators. Oxidative stress plays a crucial role in the osteoblastic and osteoclastic cells regulation.

Osteoblasts are the cells that form the bone, they are located on the surface of the bone which produces cytokines such as nuclear factor κB (NF-κB), fundamental for osteoblasts differentiation and actions. Osteoclasts are the cells devoted to bone resorption formatting resorption lacuna by means of the recreation of

protons, protease and superoxide. The imbalance between bone resorption and deposition is the central point of metabolic bone disorder (egg. Osteoporosis).
Oxidative stress is a central factor leading to bone loss with an increase of osteoblast and osteocyte apoptosis.
Green tea, rich in polyphenols, has antioxidant properties and can reduce oxidative stress related to bone resorption[77]. The polyphenols of tea seemed to reduce also the bone reduction due to estrogen deficiency[78], [79].
Resveratrol was studied for the repair of critical bone defects and the retention of implants and it seemed to be effective through the up-regulation of important gene correlated to osteogenic markers[80].
It also inhibits osteoclast differentiation of murine osteoclast progenitors RAW 264.7 by means ROS production inhibition [81].
Quercetin used for the functionalization of synthetic hydroxyapatite enhances the differentiation and proliferation of human osteoblast-like cells MG63 while it reduces the differentiation of osteoclast precursors 2T-110 in co-culture[82].

2.3.5 Bioavailability and stability

Polyphenols are sensible to high pH and temperature, so the evaluation of their stability is a crucial point. Natural polyphenols extracts and single polyphenol are subjected to variation in their structure at different pH and this becomes visible with a clear change in the color of the solutions containing these molecules. For examples, malvidin, an anthocyanin present in red wine, is red at pH1, transparent at pH 4-5, purple at pH 6-7, yellow at pH 7-8 and dark blue at pH 8-10.
At pH around 12 the polyphenols hydrolyze in chalcones. This sensitivity to pH has to be considered in the preparation of food in order to maintain the antioxidant and antitumoral properties of these molecules.
All the polyphenols are able to maintain their properties stable in pH between 1 and 8, indeed not all the polyphenols have the same sensitivity to the change of pH. Gallic acid is more sensitive to pH change than catechins. This is due to the single phenol ring present in gallic acid compared with the multiple phenolic rings in the structure of catechins. Sensitivity of pH is also time dependent: the longer is the polyphenols exposition to alkaline pH the greater is the degradation[3].
Polyphenols are also sensible to UV degradation and high temperature. When a polyphenol-containing aqueous solution was exposed to UV-C light for 3 hours 40% of vanillic acid, 50% of gallic acid and 83% of catechins were removed. In

solution of mixed natural polyphenols from vegetable extracts the reduction was between 15% and 30%.
Studies to investigate the stability of the polyphenols at different temperatures were also performed and catechins are the most sensitive with a rate of degradation of 20% at 60°C and 80°C and 32% at 100°C. Gallic acid and valinic acid are more stable with a rate of degradation of 15% at 60°C, 25% at 80°C and 30% at 100°C[83]–[85]. These aspects have to been considered for the choice of a method of extraction. The effect on human health of the polyphenols taken with the diet is correlated with the amount of their amount consumed but also with their bioavailability after the digestion. Polyphenols released from food matrix can potentially be absorbed from gut wall and it was estimated that 48% of the extractable polyphenols become bioavailable in the small intestine, while 42% in the colon. Around 10% of polyphenols remain not extracted from food matrix after the whole digestive process[4], [10].
Some studies suggest that the digestion of polyphenols can modify their biological properties [86], [87].

2.4 Functionalization with polyphenols

To overcome the problem of stability and bioavailability, the coupling of polyphenols with biomaterials seems to be a promising way for the *in loco* administration of these molecules.
Polyphenols show increasing interest in the scientific community.
In order to investigate the presence in literature of works involving polyphenols a search was performed in PubMed with the following keywords:
Polyphenol, quercetin, rutin, resveratrol, gallic acid, flavonoid, anthocyanin of anthocyanidins and tannin.
Searching the general word polyphenols and the main studied single polyphenols in the title or abstract of articles between 01/01/1970 and the 31/12/2016, 61116 articles were found.
The number of manuscripts concerning the arguments is exponentially growing over the years with a peak in 2016 as reported in figure 2.10.

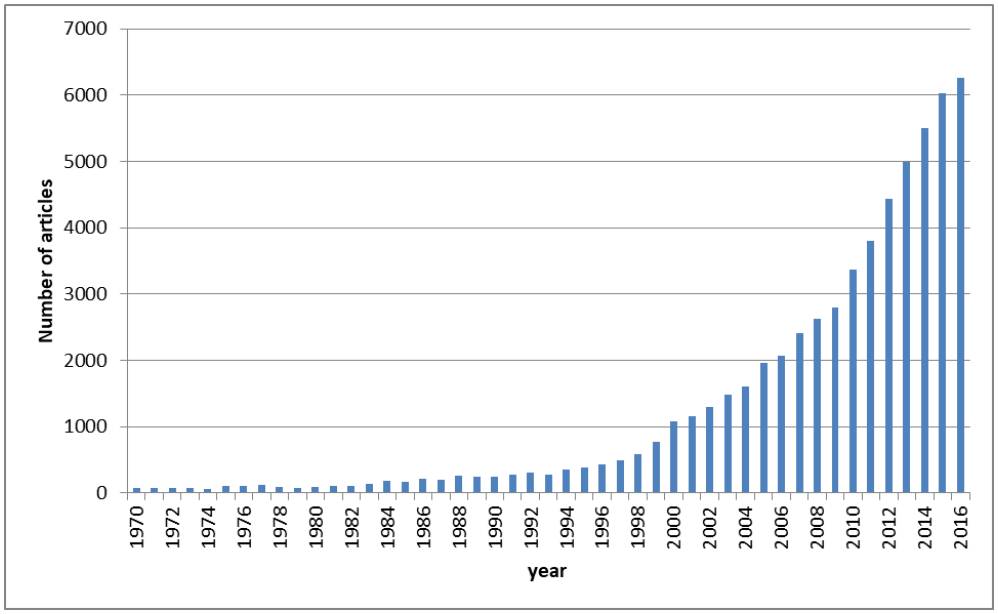

Figure 2.10: number of articles for years from 01/01/1970 to 31/12/2016 found on PubMed with the keywords polyphenol, quercetin, rutin, resveratrol, gallic acid, flavonoid, anthocyanin of anthocyanidins and tannin.

Despite of this growing interest only few attempts of coupling polyphenols with materials are present in literature and in Figure 2.11 are reported the distribution of the articles over years performing a research with the following keywords: Polyphenol, quercetin, rutin, resveratrol, gallic acid, flavonoid, anthocyanin of anthocyanidins, tannin, biomaterial, glass, titanium, polymer.

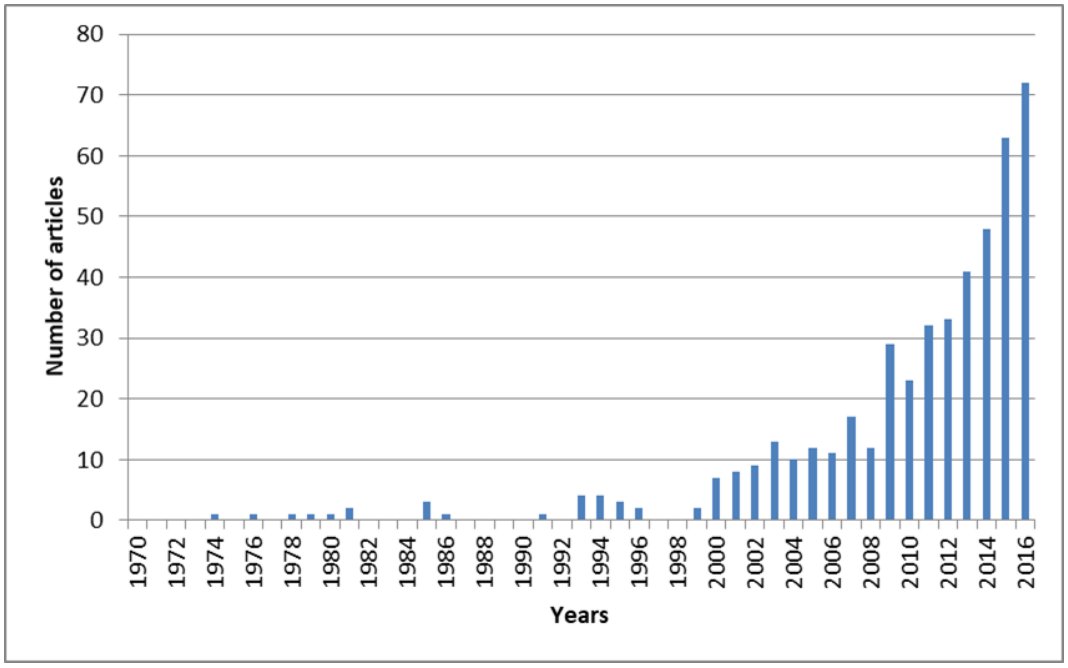

Figure 2.11: number of articles for years from 01/01/1970 to 31/12/2016 found on PubMed with the keywords polyphenol, quercetin, rutin, resveratrol, gallic acid, flavonoid, anthocyanin of anthocyanidins, tannin, biomaterial, glass, titanium, polymer.

Some of these works are here summarized. Chitosan fibers were functionalized by mean of the tyrosine kinase enzyme with flavonoids for antibacterial and antioxidant purpose[88] and chitosan was functionalized with caffeic acid, gallic acid, tannic acid and quercetin by means of laccase enzyme for the same purpose[89], [90]. Chitosan film was used for the encapsulation of *Zataria multiflora Boiss* and grape seeds extract in order to maintain their antioxidant activity[91] and caffeic acid was used in the polymerization of chitosan film for food packaging to reduce the degradation in aqueous acid media[92].
Microspheres of chitosan were used for the encapsulation of thyme polyphenols for the modulation of the release in the digestive system[93] and a polymer chitosan-alginate was used for the encapsulation of extract of raspberry leaves, hawthorn, ivy, nettle and olive leaves preserving the antioxidant ability[94].
Nanosponges of β-cyclodextrins were used for the encapsulation of rutin and chlorogenuc acid from apples[95] and magnetic nanoparticles were decorated with benzoic acid, caffeic acid, coumaric acid, ferulic acid and syringe acid from vegetal origin using PEG (Polyethylene glycol) as linker[96].

Rutin was coupled with silica mesoporous nanoparticles by means of adsorption[97] and the polyphenols of green tea were coupled to carbon nanotubes[98].
Nanoparticles of rare earth oxides were functionalized with quercetin by covalent bond obtained with silane[99]. Sphere of calcium pectate were coupled with resveratrol in order to enhance the release of this molecules in the gut[100] and resveratrol was also coupled with gold nanoparticles as carrier for tumor treatment[101].
Resveratrol was bonded to polycaprolactone in order to improve the in vivo regeneration and mineralization of bone[102] and for the same purpose PCL/collagen copolymer was functionalized still with resveratrol[103].
Polyurethane membranes were used for the physical encapsulation of curcumin for a good adhesion of fibroblasts and preserve the antibacterial, antioxidant and anti-inflammatory activity[104].
Nanocomposites of polymethylmethacrylate and TiO_2 nanoparticles were functionalized with Gallic acid esters[105] and calcium hydrogenophospate was functionalized with *Gusuibu* molecules conferring osteoinductive properties to the bioceramic[106].
Silver nanoparticles were obtained using extracts from plants as reducing and stabilizing agents[107] and Polysulfone, Polycarbonate, Titanium Dioxide, Stainless Steel, Polytetrafluoroethylene were coated with natural polyphenols and pyrogallol for antibacterial purpose[108].
Titanium was coated with a hydroxyapatite/silver/ lignin coating still for antibacterial purpose[109] and fibers of zein were used for the encapsulation of gallic acid for the same scope[110].
Titanium oxides was also functionalized with quercetin[111]and rhamnogalacturonan-Is (RG-Is) isolated from potatoes and apples[112].
For the support, during the healing of fractures a bone substitute with biphasic phosphate calcium, chitosan and casein with coriander extract was developed[113].
Natural polyphenols and gallic acid were also coupled with bioactive glasses and bioactive ferrimagnetic glass-ceramics[114]–[116].

2.5 Materials and methods

2.5.1 Polyphenols extraction

The biomolecules employed for the functionalization of the samples were gallic acid (3, 4, 5-Trihydroxybenzoic acid, GA, 97.5–102.5% titration, G7384, Sigma-Aldrich), as a model molecule, and polyphenols extracted from red grape skins or pomace and green tea leaves.
The green tea leaves (Longjing) were imported from Hangzhou(China) and the red grape skins and pomace were obtained from red grape (Barbera) provided by two small-scale producers in the north of Italy (vineyard situated in Vaglio Serra, Asti, Piedmont, Italy). The natural sources were dried in oven at 60°C for 36 h and grinded into powder in a ceramic mortar, then preserved in the dark under vacuum.
A conventional solvent extraction was employed[117] with a water ethanol solution 20:80 ratio.
The solid-liquid ratio employed for tea and pomace was 1:50 while for the red grape skins was 1:20 because of the major amount of bounded sugars that made the polyphenols less extractable [115], [116].
The solid part was put in a glass bottle covered with aluminum in order to avoid UV degradation, then covered with the alcoholic extraction solution and shacked for 1h at 60°C in a thermostatic bath.
The extraction solution was separated from the solid part by filtering and then placed into an incubator at 37°C until total ethanol solution evaporation.
Finally, the extracts were collected and suspended in double distilled water and freeze dried (Figure 2.12).

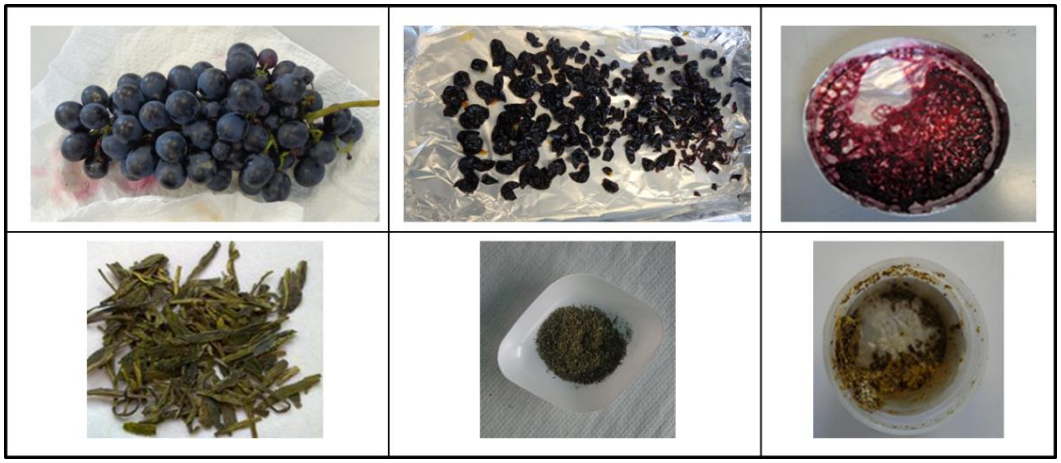

Figure 2.12: steps of the extraction of polyphenols from red grape skins and green tea leaves. Raw materials, fresh grape and dried tea leaves are shown in the first column, the second column shows dried grape skins and ground tea and the third column are shows the lyophilized extracts.

The extracts are named from now on with acronym reported in Table 2.7:

Table 2.7: acronym and description of the solution.

Solution acronym	**Solution description**
GA	Gallic acid
GPH	Red grape skins polyphenols
PPH	Red grape pomace polyphenols
TPH	Green Tea leaves polyphenols

2.5.2 Glass preparation

CEL2 [118]–[120] is a silica based bioactive glass of the system SiO_2-P_2O_5-CaO-MgO-Na_2O-K_2O developed at Politecnico of Torino.
The composition is reported in table 2.8.

Table 2.8: glass composition.

Oxides	Composition (%mol)	Composition (%wt)
SiO_2	45	43,77
CaO	26	23,61
P_2O_5	3	6,91
K_2O	4	6,10
Na_2O	15	15,08
MgO	7	4,54

The glass was obtained with melt and quenching method.
The used reagents with the relative molecular weight and the oxides of which they are precursors are reported in table 2.9.

Table 2.9: glass reagents.

Reagents	SiO_2	$Ca_3(PO_4)_2$	$CaCO_3$	$C_4H_2Mg_5O_{14}*5H_2O$	Na_2CO_3	K_2CO_3
Molecular weight (g/mol)	60,000	310,180	1000,009	485,650	106,000	138,200
Oxides	SiO_2	$P2O_5$+CaO	CaO	MgO	Na_2O	K_2O

For 100 g of CEL2 the amount or necessary reagents are reported in table 2.10:

Table 2.10: amount of each reagent necessary for 100 g of CEL2.

Reagent	SiO_2	$Ca_3(PO_4)_2$	$CaCO_3$	$C_4H_2Mg_5O_{14}*5H_2O$	Na_2CO_3	K_2CO_3
Weight (g)	43,77	15,09	27,55	11,02	25,78	8,97

The reagents were mixed and put in a platinum crucible with a platinum cover in order to avoid contaminations.
The crucible was put in an oven (Carbolite 1800) with a climb ramp of 10°C/min until 1500°C. Reached 1500°C the cover was removed and the crucible remains for 1h at 1500°C.

At the end of the melting procedure, two different ways of quenching were used in order to obtain glass bulk (quenching on plate) or a frit useful for obtaining powder (quenching in water).
For the preparation of massive samples the glass was cast on a brass plate with supports of the same material, previously cleaned with nitric acid 25% in water, in order to obtain bars (Figure2.13).

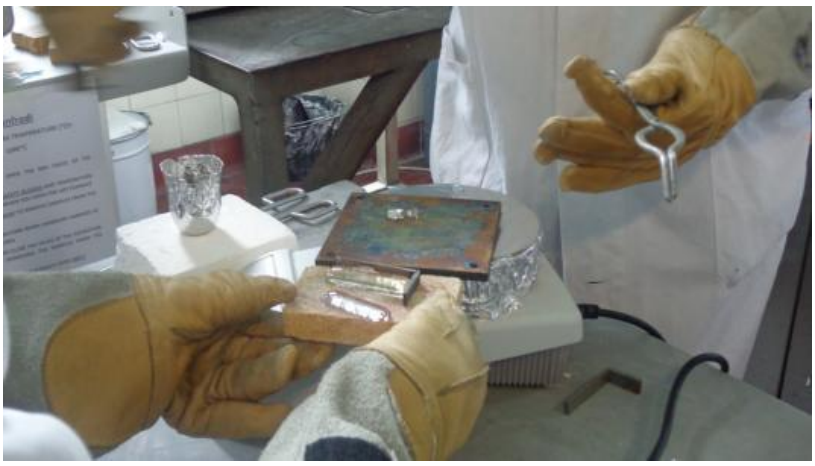

Figure 2.13: quenching on plate.

After the casting the bars were annealed at 500°C for 12 h to reduce internal stress[118] and then cooled to room temperature.
Once cooled, the bars were cut into 2 mm thick slices with an automatic cutter (Struers Accutom 5) with a diamond blade.
Both the sides of each slice were polished with an abrasive SiC paper 120 grit. After this first polishing performed in order to made the faces coplanar, one side was chosen for the functionalization and the second one was marked with a X using a diamond pen.
The side chosen for the functionalization was again polished with abrasive paper up to 4000 grit.
The samples obtained with this method are named from now on CEL2 (Figure 2.14).

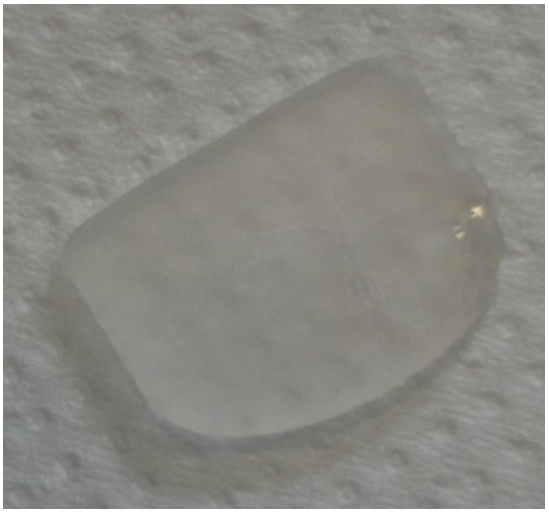

Figure 2.14: CEL2 bulk sample.

For the preparation of the powder samples, the glass was cooled in water.
The frit was put in a zirconia jar with spheres of the same materials in a grinder and then grinded at 250 rpm.
After the grinding the powder was sieved with a sieve with 20 μm mesh in order to obtain a uniform granulometry.
The samples obtained with this method are named from now on CEL2 pow (Figure 2.15).

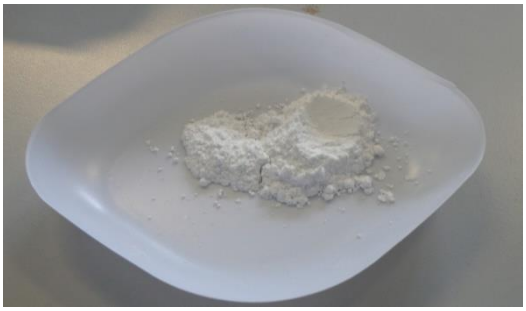

Figure 2.15: CEL2 powder sample.

2.5.3 Glass functionalization

The first step of the functionalization consist in the activation of the surface of the glass with a protocol previously developed by the research group[116].
Bulk slices or the powder were washed in acetone in an ultrasonic bath.
After 5 minutes the acetone was removed and the samples were washed 3 times in ultrapure water per 5 minutes in an ultrasonic bath.
The wash with acetone and water allows to remove impurity from the surface of the glass and to expose hydroxyl groups useful for the functionalization (Figure 2.16).

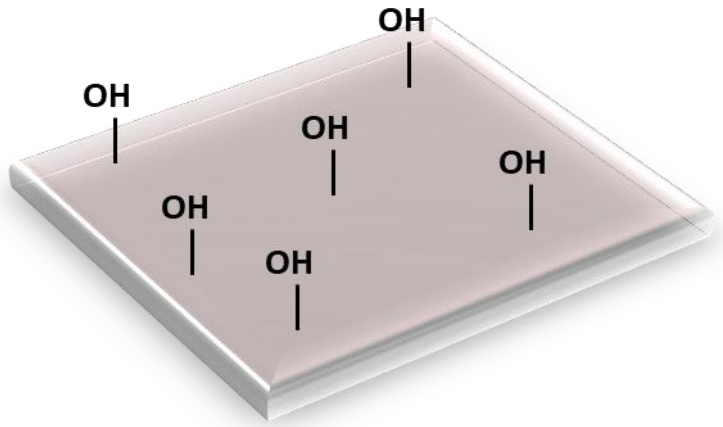

Figure2.16: drawing of hydroxylated bioactive glass.

After washing steps the samples were dried in a hood under laminar flow.
The samples of glass washed were named CEL2 washed and CEL2 pow washed.
For the functionalization, each bulk samples, was put in a holder covered with aluminum, in order to avoid UV degradation with the surface to be functionalized upward.
For the powder each samples consists of 100 mg of CEL2 powder and was put in a holder covered with aluminum.
The protocol of functionalization was developed by the research group in previous work[115], [116] and improved during this thesis.
The polyphenols used for the functionalization were GA, GPH and TPH.
The stock solutions of functionalization were obtained with an appropriate amount of polyphenols in double distilled water.

The concentration was 1mg/ml for gallic acid and tea polyphenols and 5 mg/ml for grape skins polyphenols because of the minor amount of the polyphenols in this extracts that are rich of sugars. The GPH concentration was chosen on the bases of trial and error experiments and previous treatments with other organic molecules.
The stock solutions were prepared as follow:

- GA solution: 200 ml ultrapure water+ 200 mg GA
- TPH solution: 200 ml ultrapure water+ 200 mg TPH
- GPH solution: 200 ml ultrapure water+ 1 g GPH

The water and the polyphenols were put in a bottle covered with aluminum and stirred with magnetic stirrer for at least 1h (Figure 2.17).

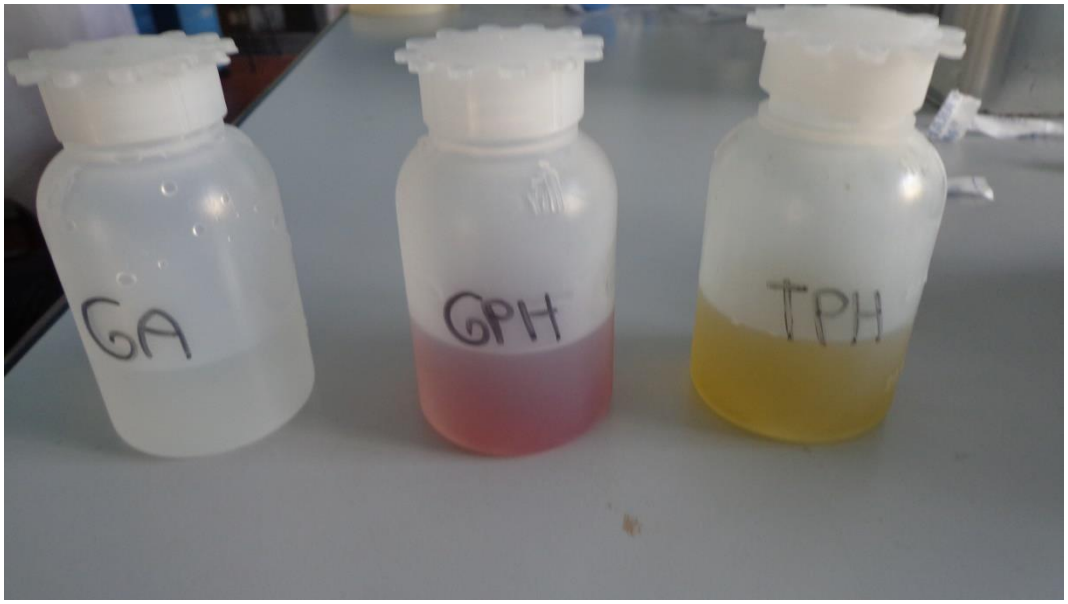

Figure 2.17: stock solutions of the polyphenols.

For the functionalization of the samples 5 ml of the functionalization solutions was put on the holder containing each sample and incubated at 37°C for 3 h.
The time was chosen in order to maximize the amount of molecules bonded and minimize the release of ions by the glass in the base of a previous work[121].
After the functionalization the samples were washed two times in double distilled water, dried under laminar flow and preserved in the dark. A scheme of glass functionalization is reported in Figure 2.18.

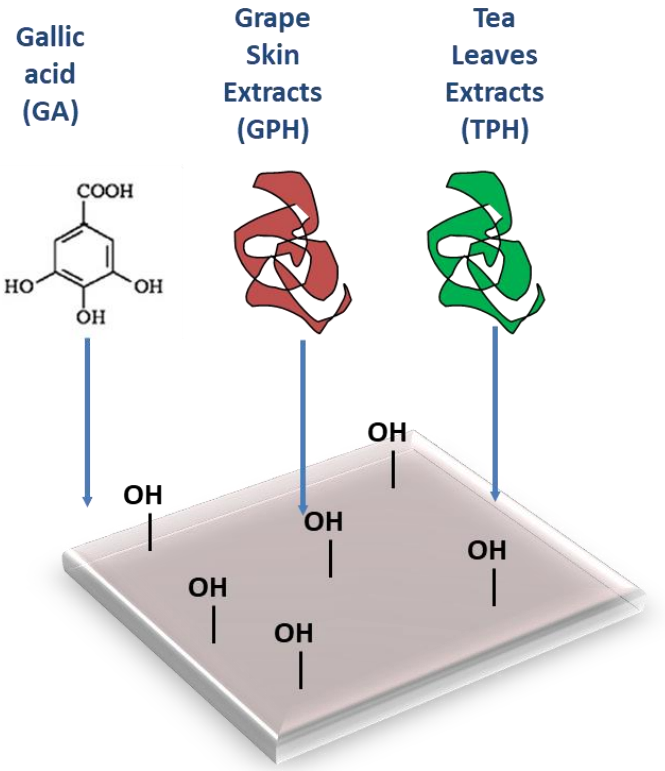

Figure 2.18: drawing of functionalized CEL2 glass.

From now on the functionalized samples were named as reported in Table 2.11.

Table 2.11: acronyms of the samples.

Sample acronym	**Sample description**
CEL2+GA	CEL2 bulk functionalized with gallic acid
CEL2+GPH	CEL2 bulk functionalized with polyphenols of red grape skins
CEL2+TPH	CEL2 bulk functionalized with polyphenols of green tea leaves
CEL2 pow+GA	CEL2 powder functionalized with gallic acid
CEL2 pow+GPH	CEL2 powder functionalized with polyphenols of red grape skins
CEL2 pow+TPH	CEL2 powder functionalized with polyphenols of green tea leaves

2.5.4 Titanium alloy preparation

The samples utilized were Ti6Al4V (ASTM B348, Gr5, Titanium Consulting and Trading). The samples were cut into slices with thickness of 2 mm from cylindrical bars (10 mm diameter) with an automatic cutter (Struers Accutom 5).
After the cutting the samples were signed with a letter on one side and polished on the opposite one with abrasive SiC papers (up to 4000).
The polished samples were washed in acetone for 5 minutes in an ultrasonic bath and then ultrasonically washed twice for 10 minutes in ultrapure water.
After the washing the samples were dried at room temperature under laminar flow (Figure 2.19).

Figure 2.19: Ti6Al4V sample.

2.5.5 Titanium alloy functionalization

In order to make the titanium alloy samples bioactive and functionalizable, they were treated with a patented chemical treatment developed by the research group[122], [123].
This treatment consists in acid etching with diluted hydrofluoric acid and controlled reoxydation in hydrogen peroxide. The surface obtained has a specific pattern at the nanometric and micrometric scale suitable for good adhesion and natural differentiation of osteoblast and rich of hydroxyl groups suitable for functionalization with biomolecules (Figure 2.20)

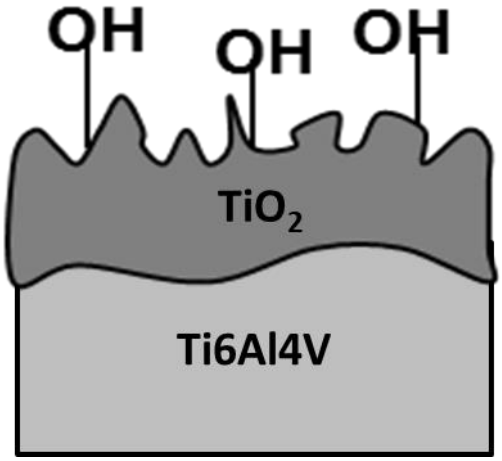

Figure 2.20: drawing of hydroxylated surface of the bioactive titanium alloy.

In order to improve the reactivity of the –OH groups, the samples were exposed for 1h to UV irradiation. The samples treated with the chemical treatment and irradiated with UV are named from now on CT (chemically-treated).
The biomolecule employed for functionalization were GA, TPH and PPH.
The stock solutions for functionalization were prepared with two different concentrations: 1 mg/ ml and 2 mg/ ml. The solutions with the model molecules gallic acid were prepared in 3 different media (ultrapure water, Phosphate Buffered Saline – PBS and Simulated Body Fluid – SBF) in order to find the best one for the titanium alloy functionalization, then functionalization with natural polyphenols were performed only with the medium chosen that was SBF .
PBS was prepared dissolving 1 tab (2g, PBS, Sigma-Aldrich, P4417) in 200 ml of ultrapure water and SBF was prepared in according with the protocol developed by Kokubo[124].
The solutions for functionalization were prepared as follow:

- WATER+GA_1: 200 ml of ultrapure water + 200 mg of gallic acid
- WATER+GA_2: 200 ml of ultrapure water + 400 mg of gallic acid
- SBF+GA_1: 200 ml of SBF+ 200 mg of gallic acid
- SBF+GA_2: 200 ml of SBF + 400 mg of gallic acid
- PBS+GA_1: 200 ml of PBS+ 200 mg of gallic acid
- PBS+GA_2: 200 ml of PBS + 400 mg of gallic acid
- SBF+TPH_1: 200 ml of SBF+ 200 mg of polyphenols of green tea leaves
- SBF+TPH_2: 200 ml of SBF + 400 mg of polyphenols of green tea leaves
- SBF+PPH_1: 200 ml of SBF+ 200 mg of polyphenols of red grape pomace

- SBF+PPH_2: 200 ml of SBF+ 400 mg of polyphenols of red grape pomace

The medium and the polyphenols were put in a bottle covered with aluminum and stirred with a magnetic stirrer for at least 1h.
After the above described chemical treatment and UV irradiation each samples (CT) were put in a holder cover with aluminum foil in order to avoid UV degradation and incubated at 37°C in 5 ml of the functionalization solution.
Two different time of incubation, 3h and 8 h, derived from literature and previous works[108], [121], [125], were performed in order to minimize the process time and maximize the amount of molecules bound to the surface.
After functionalization the samples were washed two times in ultrapure water in order to remove unbounded molecules, dried under laminar flow at room temperature and preserved in the dark.
The acronyms of the source solutions and of the samples are reported in table 2.12.

Table 2.12: Acronyms and a brief description of the source solutions and of the functionalized samples.

Sample acronym	**Sample description**
WATER+GA_1	Solution 1 mg/ml of Gallic acid in ultrapure water
WATER+GA_2	Solution 2 mg/ml of Gallic acid in ultrapure water
SBF+GA_1	Solution 1 mg/ml of Gallic acid in SBF
SBF+GA_2	Solution 2 mg/ml of Gallic acid in SBF
PBS+GA_1	Solution 1 mg/ml of Gallic acid in PBS
PBS+GA_2	Solution 2 mg/ml of Gallic acid in PBS
SBF+TPH_1	Solution 1 mg/ml of green tea polyphenols in SBF
SBF+TPH_2	Solution 2 mg/ml of green tea polyphenols in SBF
SBF+PPH_1	Solution 1 mg/ml of red grape pomace polyphenols in SBF
SBF+PPH_2	Solution 2 mg/ml of red grape pomace polyphenols in SBF
CT	Ti6Al4v sample chemical treated and UV irradiated
CT_W+GA_1	CT sample functionalized with solution 1 mg/ml of Gallic acid in ultrapure water
CT_ W+GA _2	CT sample functionalized with solution 2 mg/ml of Gallic acid in ultrapure water
CT_SBF+GA_1	CT sample functionalized with solution 1 mg/ml of Gallic acid in SBF
CT_ SBF+GA _2	CT sample functionalized with solution 2 mg/ml of Gallic acid in SBF

CT_PBS+GA_1	CT sample functionalized with solution 1 mg/ml of Gallic acid in PBS
CT_ PBS+GA _2	CT sample functionalized with solution 2 mg/ml of Gallic acid in PBS
CT_ SBF+TPH _1	CT sample functionalized with solution 1 mg/ml of TPH in SBF
CT_ SBF+TPH _2	CT sample functionalized with solution 2 mg/ml of TPH in SBF
CT_ SBF+PPH _1	CT sample functionalized with solution 1 mg/ml of GPH in SBF
CT_ SBF+PPH _2	CT sample functionalized with solution 2 mg/ml of GPH in SBF

2.5.6 Macroscopic observations and pH evaluation

For the glass samples, the change in the color is a signal of a successful functionalization and the color of the samples before and after the functionalization was observed. The color is also an important parameter for the solution of functionalization and was observed before and after functionalization in the uptake solution. Because of the sensitivity of polyphenols to the increase of pH, it was measured with a portable pHmetre before and after functionalization in order to optimize reactivity of the molecules with respect to the surface, while avoiding degradation.

2.5.7 Biomolecules detection

The presence and the activity of the polyphenols in the solution used for the functionalization were investigated by means of photometric analyses with Folin&Ciocalteu method. On the samples in addition of the spectrophotometric measurements, X-ray Photoelectron Spectroscopy analysis (XPS) was also performed. The photometric analysis (CARY 500 Varian) at 760 nm was performed on the source solution (before and after functionalization) and on the functionalized samples with the Folin&Ciocalteu method. This test measures the redox reactivity of phenolic polyphenols and the result is the amount of active molecule in the solution or on the surfaces. As far as the solutions are concerned, a quote of 2 ml of the solution was mixed with 6 ml of ultrapure water and with

0.5 ml of the Folin&Ciocalteu reagent (Folin&Ciocalteu phenol reagent, Sigma-Aldrich). After three minutes, 1.5 ml of 20% (w/V) Na_2CO_3 solution was added and, after 2 h, the measurement was carried out at 760 nm[126](Figure 2.21).

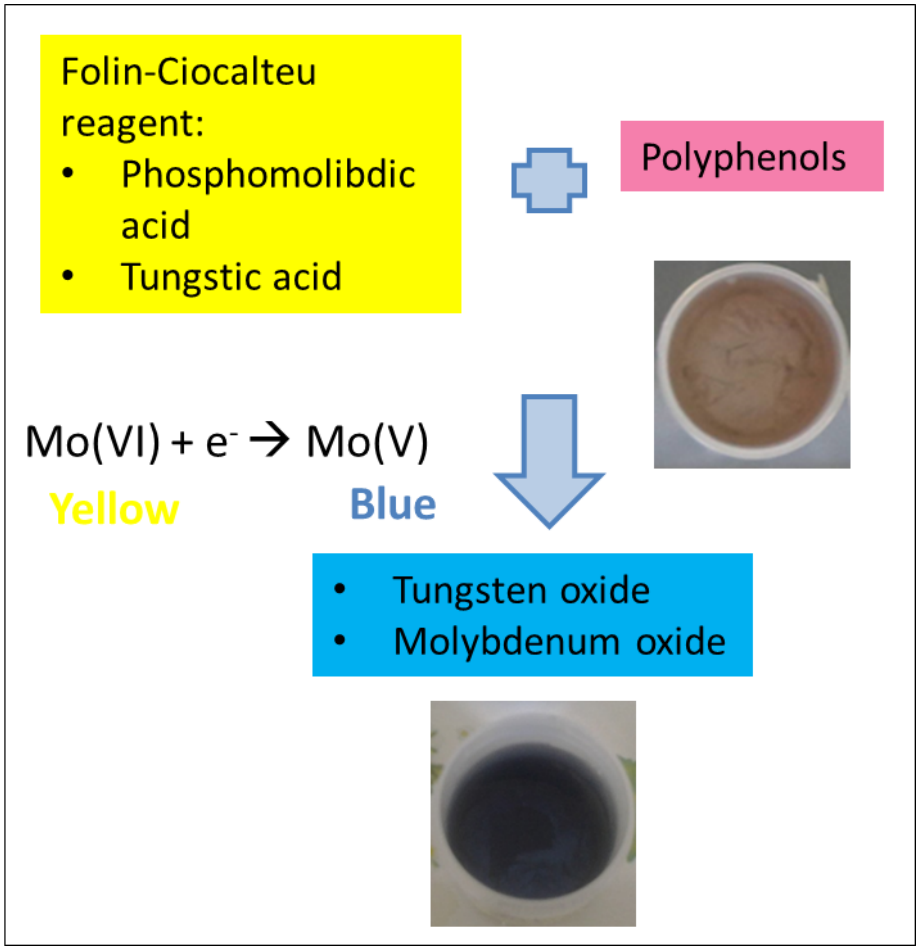

Figure 2.21: scheme of the Folin&Ciocalteu reaction.

A modified Folin&Ciocalteu method was utilized for the quantification of polyphenols on the surface of the functionalized samples. The samples were put in 8 ml of ultrapure water with 0.5 ml of Folin&Ciocalteu reagent. After 3 minutes, a quote of 1.5 ml of 20% (w/V) Na_2CO_3 solution was added and the measurement was carried out after 2 h at 760 nm[115], [116], [125] . In order to quantify the polyphenols concentration, a standard calibration curve was obtained by using solutions with different concentration of GA (namely, 0.0025, 0.005, 0.01, 0.02, 0.03 and 0.04 mg/ml) as described in[116] .This curve reported in figure 2.22 allows to determine the concentration of GA [mg/ml] trough the fitting equation

derived from the treatment of the dataset (y = 21.715x - 0.0088) and it has a good linear relationship and a good coefficient of correlation (R^2 = 0.9999).
The measurements are based on the assumption that all the polyphenols react as gallic acid in the redox Folin&Ciocalteu reaction and for this reason it is possible to define their concentration as "gallic acid equivalents".

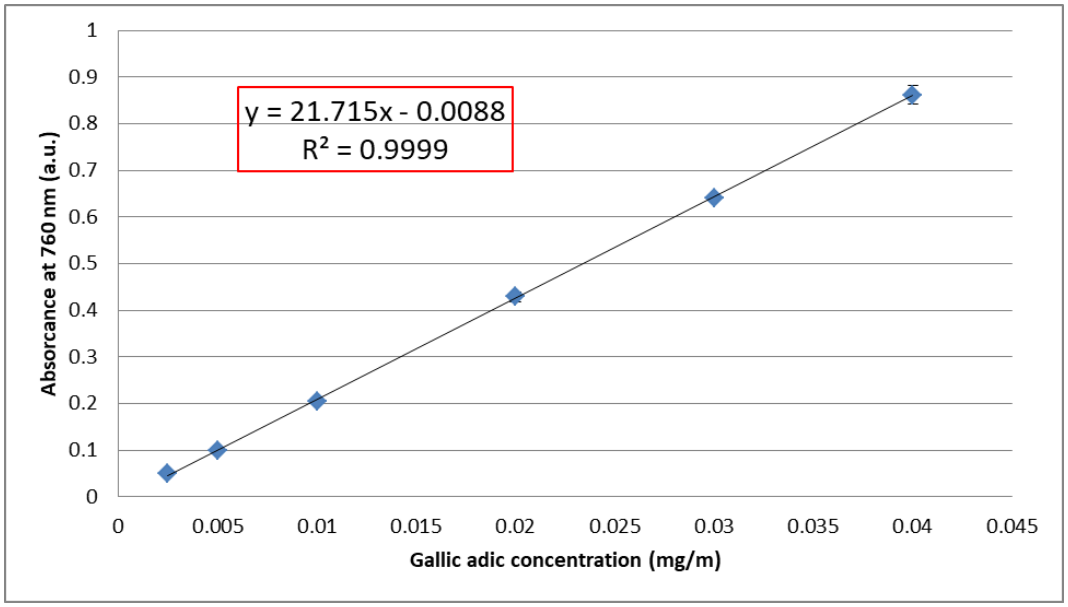

Figure 2.22: calibration curve.

This analysis was performed in triplicate on each source solution and on each type of functionalized sample. Statistical analysis of the data obtained by Folin&Ciocalteu method was performed trough ANOVA one way tests.
XPS analysis (XPS, PHI 5000 VERSAPROBE, PHYSICAL ELECTRONICS) were performed in order to determine the chemical composition of the samples surface before and after the functionalization and to identify the chemical groups exposed. For this analysis both survey spectra and high resolution spectra of carbon and oxygen regions were performed.
The presence of the polyphenols on the surfaces was also checked by fluorescence microscope (Leica DM5500 B, Leica Microsystems, IL, USA) exploiting the autofluorescence of the polyphenols [127].

2.5.8 Contact angle measurements

Surface wettability was evaluated by means of measurements of the contact angle with the sessile drop methods before and after the functionalization on bulk samples. Each sample was put on the support of the machine (Kruss DSA 100) in front of the camera with the treated side upward and a drop of 5 µl of ultrapure water was deposited with a micropipette on the surface. The images were acquired with the camera and elaborated by the software obtaining the value of the contact angle. The measures were performed in triplicate.

2.5.9 Zeta potential electrokinetic measurements

Measurements of the z potential were performed on the samples before and after functionalization by means of an electrokinetic analyzer (SurPASS, Anton Paar) equipped with an adjustable gap cell. For each measurement a couple of samples were inserted in the cell with the treated surfaces one facing the other. The distance between the two surfaces (gap) is adjusted to at about 100 µm and the flow of an electrolyte is forced through it. The flow of a fluid on the surface of a material causes the motion of the counterions that compensate the surface charge in the direction of the flow. The charge separation causes an electrical potential difference called streaming potential. This phenomenon is used for the determination of the zeta potential of solid surfaces. The zeta potential of the surface was analyzed in function of pH in a 0.001M KCl electrolyte solution varying the pH with the addition of 0.05 M HCl or 0.05 M NaOH trough the automatic titration unit of the instrument according with the standard procedure[128] .
For monitoring the reactivity of CEl2 glass bare and functionalized in SBF, measure of the zeta potential in SBF were performed. The solution of measurement was prepared by adding drop by drop SBF to ultrapure water up to pH 7.4 and conductivity close to 15 mS/m. No pH titration was performed but the measurement was repeated for 20 cycles (70 minutes) in order to monitor the early stage of the surface reactions exposed to physiological fluids.

2.5.10 In vitro apatite forming ability tests

The bioactive behavior of the samples was investigated before and after the functionalization by soaking in SBF. Two samples for each type were placed in a holder covered with aluminum and covered with 25 ml of SBF according with the protocol developed by Kokubo and Takadama[129]. Samples in SBF were incubated at 37°C until different timepoints: 1, 3, 7 and 14 days for the glass samples and 14 and 28 days for titanium samples because of their slower reactivity.
The solution refresh was made every 3 days in order to maintain the pH and ion concentration in the physiological range mimicking the physiological turnover of body fluids. After the soaking the samples were washed with ultrapure water and dried at room temperature.
The deposition of hydroxyapatite on the surfaces was investigated by means of Field Emission Scanning Electron Microscopy equipped with Energy Dispersive Spectroscopy (FESEM-EDS SUPRATM 40, Zeiss and Merlin Gemini Zeiss).
In the case of the samples of CEL2 pow Fourier Transform Infrared Spectroscopy analysis (FTIR, Alpha, Bruker Optics, Ettlingen, Germany) were also performed on pellets of the samples obtained with KBr.

2.5.11 Evaluation of the free radical scavenging activity by means of Electron Paramagnetic Resonance

The free radical scavenging activity of glass powder samples bare or functionalized was evaluated by means of Electron Paramagnetic Resonance (EPR)/spin trapping technique after UV photolysis of H_2O_2[130]–[132].
15 mg of the samples were put in a quartz cuvette with 100 µl of ultrapure water, then, under magnetic stirring 100 µl of saline buffer 0.5M, 200 µl of DMPO 0.17 M (5,5-Dimethyl-1-pyrroline-N-oxide) and 100 µl of H_2O_2 0.002M were added.
The suspension, under continuous stirring, was irradiated with UV by mean of a lamp with cut-off filter at 315 nm in order to induce the photolysis of H_2O_2 avoiding the photo-degradation of DMPO. After 5, 10 and 30 minutes of irradiation 50 µl of the suspension were collected with a capillary and the EPR spectrum was recorded with a X-band EPR spectrometer (Miniscope 100, Magnettech, Germany). The same experiment was carried out on positive control (blank solution without the glass powder).

The intensity of the characteristic signal obtained from the adduct DMPO-OH• (Figure 2.23) is proportional to the radical presence in the solution. The results of the EPR/spin trapping are provided as mean ±SD and analyzed by t-Student test. These tests were performed at the Università degli Studi di Torino, Department of Chemistry, Via Pietro Giuria 7, Torino 10125, Italy.

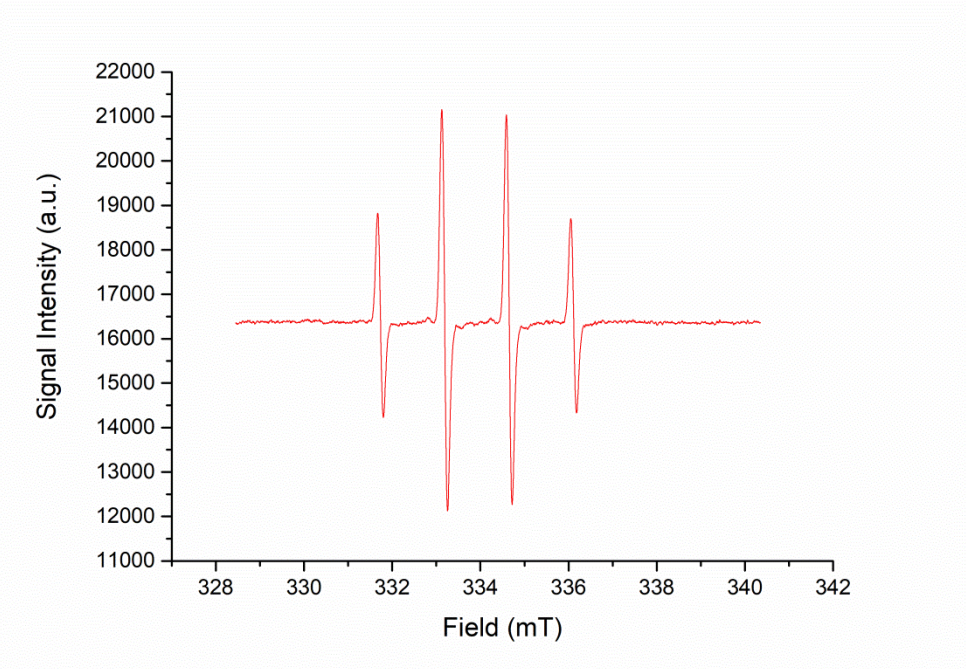

Figure 2.23: characteristic spectra of the adduct DMPO-OH•.

2.5.12 Cellular tests

In order to test the different effects of polyphenols grafted to the surface of biomaterials different tests were performed.
Bioactive glass are able to bind a great amount of polyphenols and it is possible to use them as bone filler after tumor resection and a study of the selectivity action of polyphenols with tumoral and healthy cells were performed on this samples by using human bone osteosarcoma cells U2OS and fetal human pre-osteoblasts hFOB. The bioactive surface of the titanium alloy was designed for osteointegration and the effects of polyphenols on this property were investigated cultivating mesenchymal stem cells Kusa A1 onto the surface of these functionalized samples.

Cells (U2OS and hFOB)

Human bone osteosarcoma cells U2OS (ATCC HTB-96) and human fetal pre-osteoblasts hFOB (hFOB 1.19, ATCC CRL-11372) were used for experiments as representative for tumor and non-tumor cells, respectively. U2OS cells were cultured in Dulbecco's Modified Eagle Medium (DMEM, Sigma) supplemented with 10% fetal bovine serum (FBS, SIGMA) and 1% antibiotics (penicillin/streptomycin) while hFOB were cultured in DMEM: Ham's F12 mixture (50:50, Sigma) supplemented with 10% foetal bovine serum,1% antibiotics and 0.3 mg/ml neomycin (G418 salt, Sigma). Cells were cultured at 37°C, 5% CO_2 until 80-90% confluence, detached with trypsin-EDTA solution (Sigma) and used for experiments.

- Direct cytotoxicity evaluation

Samples produced in clean conditions (CEL2 bare and functionalized) were collected into the wells of a 24 multiwell plate (Nunc Delta, Thermo Fisher Scientific) and cells (both U2OS and hFOB) were directly seeded onto each surface in a defined number (2x104 cells/specimens). After 1-3-7 days the cells viability was evaluated by the metabolic colorimetric assay (MTT, Sigma); briefly, at each time point cells were carefully washed with PBS and the MTT solution (2 mg/ml in fresh medium) was added to all specimens. Plate was incubated at 37°C, 5% CO_2 for 4 hours in the dark. Then, surnatans were gently removed and crystal formazans dissolved by 300 µl of dimethyl sulfoxyde (DMSO, Sigma).100 µl were then collected, spotted into a 96 multiwell (Nunc Delta, Thermo Fisher Scientific) plate and the optical density (o.d.) evaluated at 570nm by spectrophotometry (SpectraCount, Packard Bell). The o.d. of cells cultivated onto only-washed bioglasses was used as control and considered as 100% viability. Test specimens o.d. were normalized towards controls and expressed as percentage. Experiments were performed in triplicate.

- RONS evaluation

To quantify oxygen and nitrogen reactive species (RONS) generated from cells in response to the molecules bound on the samples, eitherU2OS or hFOB were cultured on CEL2 and CEL2+TPH samples as described for the direct culture. After 1, 2 and 3 day of culture, 100 µl of supernatants were collected from each well containing the samples, stirred for 5 min at 12,000 rpm and stored at -80°C.
RONS were evaluated by mean of OxiSelectTM In Vitro ROS/RNS Assay Kit (Cell Biolabs INC, San Diego, USA). 50 µl of surnatans were mixed with 50 µl of

Catalyst (1:250 in PBS) in each of the 96 well of a 96-black-bottom-well plate (Sigma) and stored for 5 minutes at room temperature.
100 µl of DCFH stabilized solution were added to each well. DCFH non-fluorescent probe rabidly oxidizable by ROS and RONS in the highly fluorescent molecules DCF.
The formation of DCF was investigated with a spectrophotometer (SpectraCount, Packard Bell) at 530 nm wavelength and the fluorescent unites (RFU) were converted in RONS concentration by means of a peroxide standard curve.

- Apoptosis and DNA damage evaluation

In order to understand the mechanism through which the biomolecules grafted to the surfaces lead to U2OS cells death by DNA damage, this cells were cultivated onto CEL2+TPH and CEL2 (control) glasses for 3 days as described for the direct cell test.
After 3 days, samples were collected, washed 3 times with PBS and fixed with ImmunoFix (BioOptica, Milan, Italy) for 5 min, at room temperature. Afterwards this procedure and after a carefully rinsing in PBS, the cells were permeabilized with Triton (0.5% in PBS) working at 0°C. Primary antibodies anti-53BP1 (Abcamab36823, Cambridge, UK, 1:800 in PBS containing 2% goat serum and 1% bovine serum albumin) and anti-cyclin B1 (Abcamab181593, Cambridge, UK, 1:250 in PBS containing 2% goat serum and 1% bovine serum albumin) were then added for 4 h at room temperature.
The samples were contained with a secondary antibody (AlexaFluo488, Immunological Science, Rome, Italy, 1:400 in PBS) and with 40,6-diamidino-2-phenylindole (DAPI; Sigma-Aldrich) in order to visualize the nuclei. The stained samples were analyzed with fluorescence microscope (Leica AF 6500; Leica Microsystems, Basel, Switzerland).
Statistical analyses on data were performed with the Statistical Package for the Social Sciences (SPSS v.20.0, IBM, Atlanta, GA, USA). Data were compared by ANOVA and by Sheffe's test for post hoc analysis in the case of independent samples and by Friedman's ANOVA followed by Conover's test, in the case of dependent samples. Two-sample comparisons were performed by mean of the Mann–Whitney U test. The significance level was set at $p<0.005$.

- Indirect cytotoxicity evaluation

Samples produced in clean conditions were collected into sterile 50 ml tubes and submerged with 10 ml of fresh medium each (10 ml medium / scaffold). Tubes were stored at 37°C, 5%CO_2 and after 1-2-3-5-7 days, 2 ml of supernatant was

collected from the tubes and used to cultivate cells previously seeded in a defined number (1x104 cells/well) into a new 48 wells plate. After 24 h cultured with supernatant, cells viability was evaluated by the MTT assay as previously described for the direct test. Cells cultured with fresh medium were used as control and considered as 100% viability; test specimens o.d. were normalized to the control and expressed as percentage. Experiments were performed in triplicate.

Culture and analysis with U2OS and hFOB cells were performed at the Università del Piemonte Orientale UPO, Department of Health Sciences, Via Solaroli 17, 28100 Novara, Italy

Cells (KUSA A1)

Two different cellular cultures were performed, one with a normal medium (NORM) and one with the addition of osteoinductive factors (OF). The culture was conducted on CT and CT_SBF+TPH_1.

In both the cultures, the cells used were KUSA A1, cultured for one week on the samples surfaces with two changes of medium.

The normal medium was composed by DMEM (D-glucose, L-glutamine, phenol red, and sodium pyruvate), 10%FBS (Fetal Bovine Serum) with SNP (sodium nitroprusside) (2%).

The culture with the osteoinductive factor was performed with 50 mg/mL of ascorbic acid, 10 mM b-glycerol phosphate, 100 mM hydrocortisone, 10% FBS added to 4.5 g/L of glucose DMEM.

After culture, the cells were fixed on the samples with 4% formaldehyde for FTIR, RAMAN and Laser microscope analysis.

For the Fluorescent microscopy, indeed, the protocol of immunostaining was applied after the culture. The disks were removed from the medium and washed twice in PBS , after they have been fixed with 4% formaldehyde (Incubated for 15min at room temperature) and washed again twice in PBS. Then, the primary antibody was added and incubated at room temperature for 30 minutes and at the end washed twice in PBS. Therefore, the staining solution containing mixed Hoechst33342, PI and DAPI as well as secondary antibody Goat anti IgG FITC conjugate was added and incubated for 30 minutes at room temperature in the dark. In the end, the samples were again washed twice in PBS and dried at room temperature. These cultures were performed to understand the effects of polyphenols on the differentiation of osteoblasts and the deposition of hydroxyapatite.

- Cell culture characterization

Fourier Transform Infrared Spectroscopy (FTIR JASCO 4000) analysis was performed on the surface of the samples CT and CT_SBF+TPH_1 after the two different types of culture in order to investigate the differentiation of the cells and the deposition of the hydroxyapatite in presence of polyphenols.

Raman analysis (T-64000, Horiba/Jobin-Yvon., Kyoto, Japan) was carried out in order to investigate the presence and the different degree of crystallinity of hydroxyapatite on the samples with and without the polyphenols.

Laser microscope (Laser Microscope 3D & Profile measurements, Keyence, VK-x200 series, Osaka, Japan) analysis was performed in order to investigate and quantify the growth of the extracellular matrix on the surface of the samples.

A map of all the samples was taken at 10x and an analysis of the surface was conducted on the single images. The data were analyzed with the software of the machine.

Fluorescence microscopy (FTIR JASCO 4000) analysis was performed in order to understand cell viability and osteocalcin production with or without polyphenols. The images were collected at 20x magnification using three different probes: Blue for cell nucleus (DAPI), Red for dead cells (PI) and Green for osteocalcin (Hoechst33342).

Culture and analysis with U2OS and hFOB cells were performed at the Kyoto Institute of Technology, Ceramic Physics Laboratory, Sakyo-ku Matsugasaki, 606-8585, Kyoto, Japan.

2.6 Results and discussion

2.6.1 Macroscopic observations and pH evaluation

Glass

Figure 2.24 shows the appearance of the glass samples, both bulk and powders, before and after functionalization with polyphenols. The color of the samples changes after the treatment from colorless to brown for GA functionalization, to light yellow for GPH functionalization and to orange for TPH functionalization.

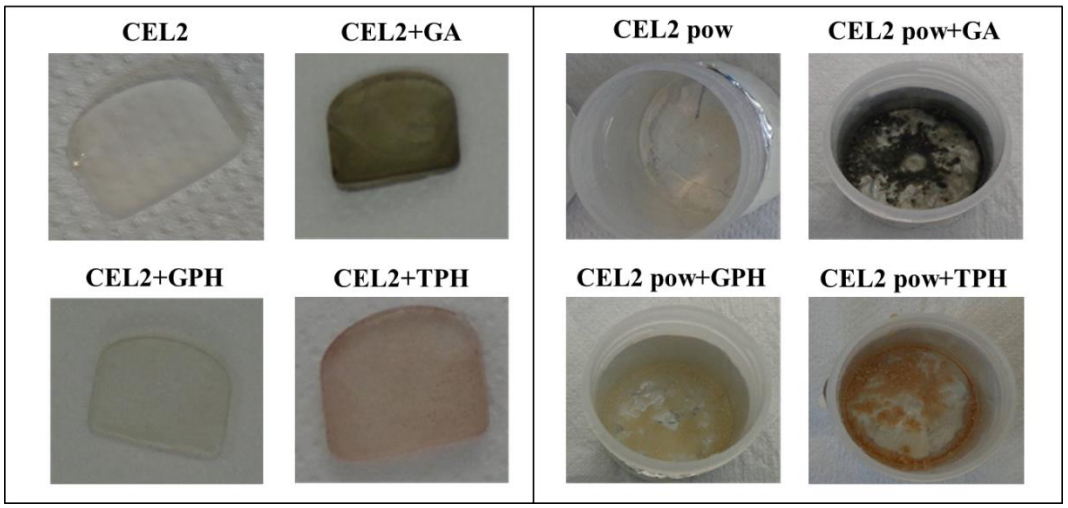

Figure 2.24: macroscopic observation of the glass samples before and after the functionalization. Bulk samples are slices of the glass and are on the left, while the powder samples (pow) are on the right.

A change in the color is also visible for the uptake solution of functionalization and it is reported in Figure 2.25 and table 2.13 with the relatives pH.

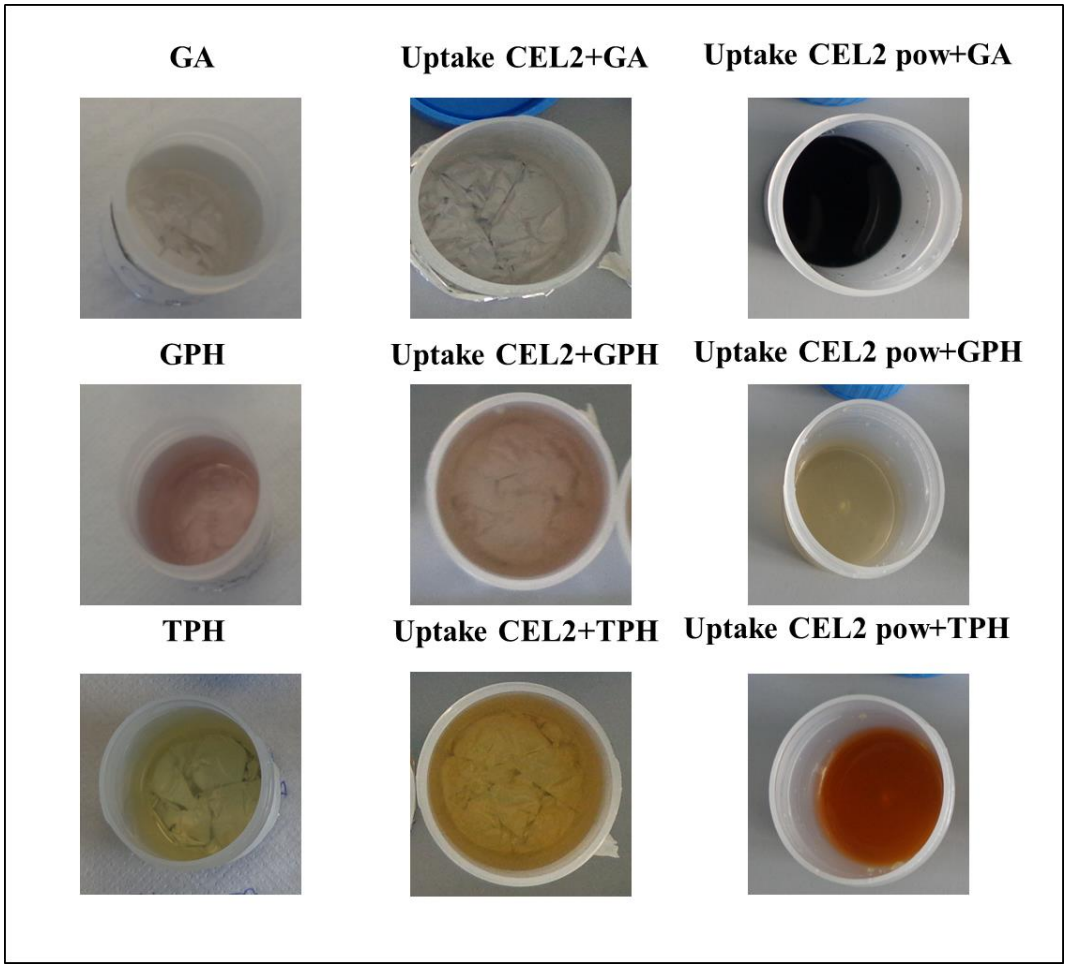

Figure 2.25: macroscopic observation of polyphenols solutions before and after functionalization. In the first column there are the pictures of the source solutions, in the second the pictures of the uptake solutions of the bulk glass samples and in the third column the pictures of the uptake solutions of the glass powder samples.

Table 2.13: pH values of the uptake and functionalization solutions and relative change in the color.

Water solution	**pH mean value**	**Standard deviation**	**Color**
GA	3.3	0.1	Colorless
Uptake CEL2+GA	4.7	0.2	Colorless
Uptake CEL2 pow+GA	8.8	0.2	Colorless
GPH	3.9	0.3	Colored
Uptake CEL2+GPH	5.6	0.5	Colored
Uptake CEL2pow+GPH	10.7	0.2	Colored
TPH	4.6	0.4	Colored
Uptake CEL2+TPH	7.7	0.2	Colored
Uptake CEL2 pow+ TPH	9.7	0.1	Colored

The source solutions of functionalization have fairly acid pH and show alkalization after the soaking of the samples. The alkalization of the solution is due to the reactivity of CEL2 glass in aqueous solutions. In literature it is widely studied that the silica amorphous network of the bioactive glass, in aqueous solution, reacts with water molecules with breakage of oxygen bridges and formation of OH• radicals. The formation of OH• radicals is also increased by the ion exchange between Na^+ ions from the glass with H_3O^+ ions from the solution [133], [134]. Furthermore the ion exchange increases in acid aqueous solutions with polyphenols[135]. The higher alkalization of the uptake solutions of the powder samples is due to the greater surface area of the samples compared with the bulk ones.

In this thesis, the time of functionalization is 3h, differently from the 24h used in previous works of the research groups[115], [116], in order to avoid molecular alteration due to strong increase in the pH. Shortening of the functionalization time reduces ions exchange from the glass and the time of permanence of the

biomolecules at basic pH reducing the risk of degradation and improving the amount of active molecules bound to the surface.
The ideal pH should remain around 7.4 that is the threshold at which the transformation of the catechol groups in quinones begin with the characteristic dark color[136], [137]. The dark color of the samples can be explained with this phenomenon. The dark color of the uptake solutions of GA for the powder samples, in spite of the not so dark color of the bulk uptake solutions, it is correlated with the high sensitivity of GA at the shift in the pH while natural extract are composed by a mix of polyphenols that are less sensible to the change of the pH [3].

Titanium alloy

The color of the Ti6Al4V samples changes from metallic to violet/green/gold (Figure 2.26) after the patented chemical treatment because of the formation of a thicker layer of titanium oxide around 100-300 nm.

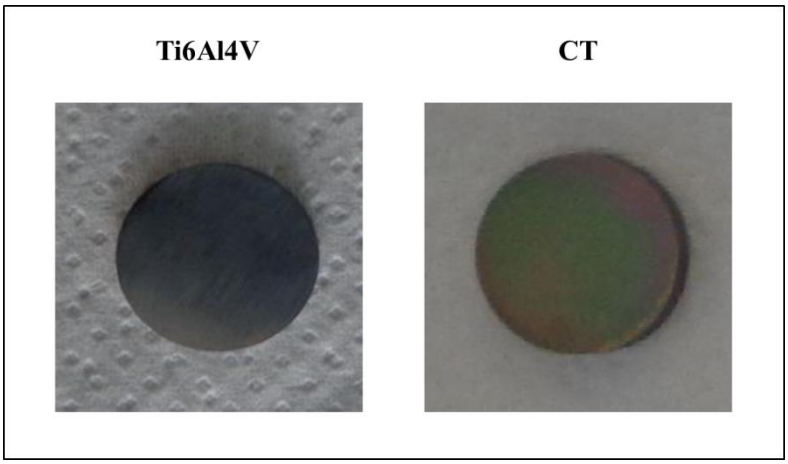

Figure 2.26: Titanium alloy samples before and after the chemical treatment.

The color of the titanium oxide changes with the change of the thickness as reported in the chart in Figure 2.27.

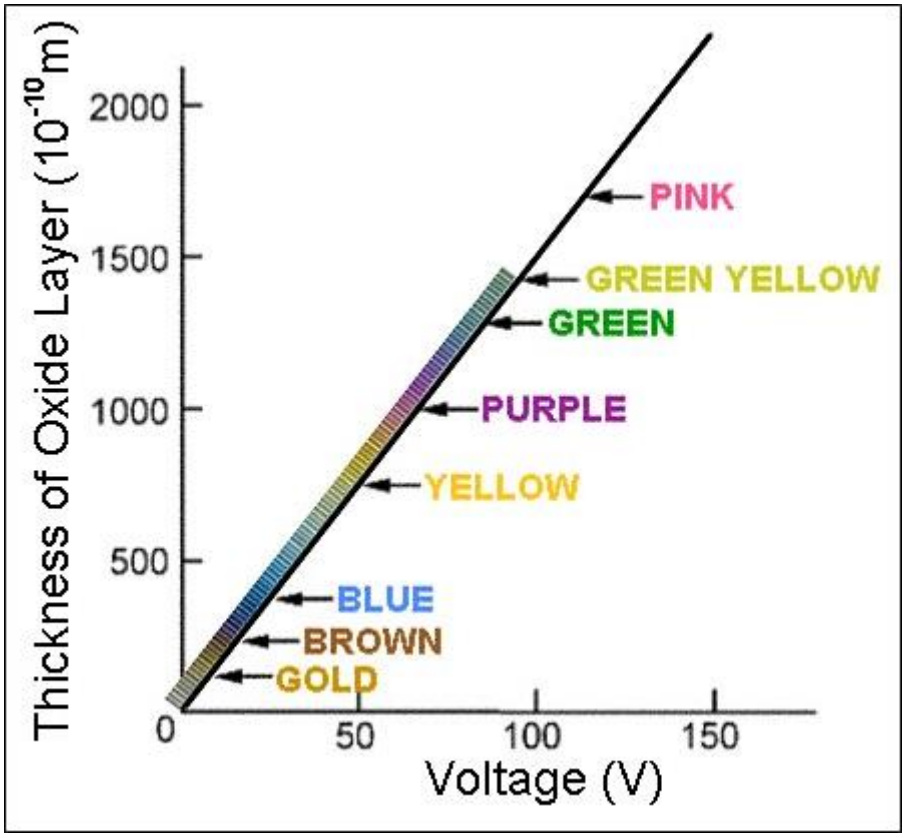

Figure 2.27: chart reporting color variation with thickness during anodization treatment [138].

The color of the samples CT after the functionalization with the polyphenols does not change.
The pH and the colors of the solution of functionalization before and after the soaking of the samples are reported in Table 2.14.

Table 2.14: pH and colors of the solutions of functionalization of chemical treated titanium alloy before and after the soaking of the samples.

Solution	**pH**	**Color of the solution**
WATER+GA_1	3.4 ± 0.1	Colorless
WATER+GA_2	3.2 ± 0.1	Colorless
SBF+GA_1	7.5 ± 0.1	Blue
SBF+GA_2	7.1 ±0.1	Blue
PBS+GA_1	6.2 ±0.1	Colorless
PBS+GA_2	4.6 ±0.1	Colorless
SBF+TPH_1	7.5± 0.1	Blue
SBF+TPH_2	7.5± 0.1	Blue
SBF+PPH_1	7.5± 0.1	Blue
SBF+PPH_2	7.4± 0.1	Blue
Uptake WATER+GA_1	3.4 ± 0.1	Colorless
Uptake WATER+GA_2	3.2 ± 0.1	Light yellow
Uptake SBF+GA_1	7.2 ± 0.1	Blue
Uptake SBF+GA_2	6.7 ± 0.1	Blue
Uptake PBS+GA_1	6.1 ± 0.1	Yellow
Uptake PBS+GA_2	4.5 ± 0.04	Colorless
Uptake SBF+TPH_1	7.48± 0.02	Blue
Uptake SBF+TPH_2	7.43± 0.01	Blue
Uptake SBF+PPH_1	7.43± 0.05	Blue
Uptake SBF+PPH_2	7.43± 0.02	Blue

The protocols of functionalization used in this thesis were developed from previous work of the research groups[115], [116] and from the literature[108].
The water solutions of the gallic acid are slightly acidic and there are not significant changes after 8h of functionalization in the color of the uptake solutions. In this range of pH, gallic acid is not deprotonated. The uptake water solution of the gallic acid 2 mg/ml has a change in the color from colorless to light yellow that can be attributed to a partial degradation of the molecules over time.
PBS and SBF have been chosen as alternative media because around the pH of this solutions, 7.4, starts the deprotonation of gallic acid that enhance the affinity to the surfaces[139], [140].
The source solutions of polyphenols 1 mg/ml in SBF maintain a pH around 7.4 that is the pH of SBF, while the solutions 2 mg/ml show a little reduction of the pH because of the high presence of polyphenols which have acidifying power.

All the solutions in SBF, both sources and uptakes, are blue because of deprotonation of the carboxylic acid of polyphenols and the formations of quinones.
The SBF and PBS uptake solutions show a decrease of the pH that is due to the tendency of the phenols to dissociate over time producing H^+ ions.
In case of PBS it is possible to observe a different behavior between the two concentrations, 1 mg/ml and 2 mg/ml.
The pH value of the source solution 1 mg/mg is 6.2 and the pH of the solution 2 mg/ml is 4.6 and they remain quite stable for the uptake solutions.
The color for the solution 2 mg/ml is colorless even after functionalization, while turns from colorless to light yellow for the solution 1 mg/ml that could mean a partial degradation of the molecules.
The time of incubation is 8h for the first attempt of functionalization and decreases at 3 h after noticing that this time is enough to reach the maximum of molecules that can be bound to the surfaces.
The scope is to maximize the amount of molecules grafted to the surfaces with a reasonable time of process and avoiding degradation of the surfaces and of the biomolecules.
In two cases, WATER + GA_2 and PBS+GA_1, the solutions used did not allow to reach the necessary conditions because degradation is highlighted by the change in the colors solutions in spite of the low pH.

2.6.2 Biomolecules detection

Glass

Figure 2.28 shows the GA equivalent concentration (mg/ml) of the polyphenols in the source solutions and in the uptake solutions after the procedure of functionalization.

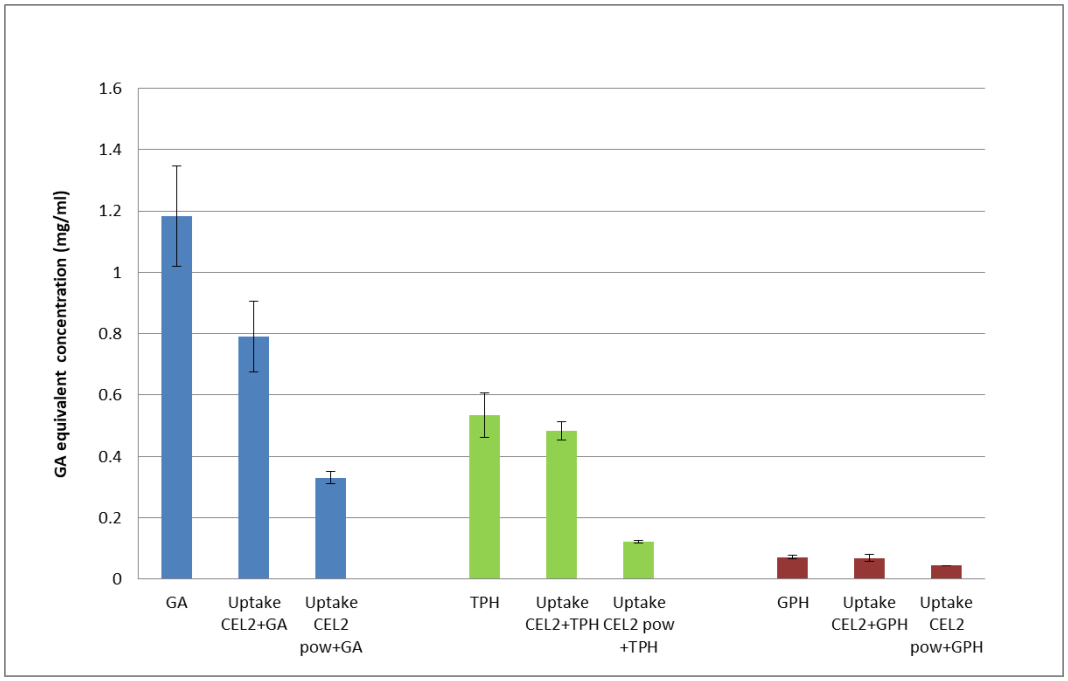

Figure 2.28: amount of the polyphenols in source solutions and uptake solutions of glass samples expresses in gallic acid equivalents (mg/ml).

The concentration of the polyphenols on the source solution of gallic acid is close to the nominal concentration because it is the solution of a pure molecule.
For the TPH source solution, the concentration is about half of the nominal ones because this is a natural extract rich in polyphenols, but containing other types of molecules extractable in hydroalcoholic solution.
GPH source solution shows a small amount of polyphenols because this natural extract contains a high amount of sugars.
The concentration of the polyphenols on the uptake solutions is significantly lower than the one of the corresponding source solutions and the decrease is more evident for the uptake solution of the powders. The decrease of the amount of polyphenols is due to the grafting of part of the biomolecules to the surface of the

samples after the procedure of functionalization like observed in previous works[115], [116].
The greatest decrease in the concentration of the uptake solutions for the powder samples with respect to the bulk samples is due to the larger surface areas of these samples that allow to bind a greater amount of molecules.
It must be also remembered that a part of this decrease is attributable to the higher increase of pH in the powder uptake solutions previously discussed and the consequent polyphenols partial degradation.
For understanding which is the amount of the molecules bound to the surface and understanding if the phenomenon of molecules degradation is considerable, it is important to perform spectrophotometric measurements with the Folin&Ciocalteu methods directly on the functionalized samples.
In Figure 2.29 it is reported the amount of the polyphenols on the surface samples after functionalization.

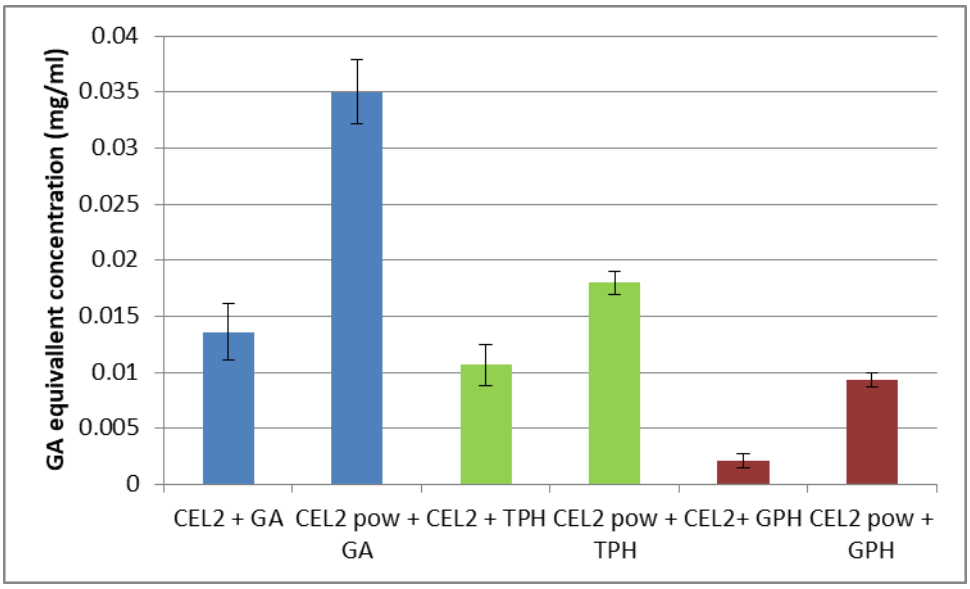

Figure 2.29: amount of the polyphenols on the glass samples surface expresses in gallic acid equivalents (mg/ml).

The results shows ability of the polyphenols, both of the pure molecule gallic acid and the natural extracts TPH and GPH, to binding the surfaces of the bioactive glass maintaining their activity , in spite of the possible degradation due to pH increase. The concentration for all the three functionalizations in greater for the powder samples than for the bulk ones because of their larger surface area.
The samples functionalized with GPH show a lower amount of biomolecules due to the lower amount of polyphenols in the source solution.

The samples are able to graft the following percentages of polyphenols present in the source functionalization solutions (the percentages were calculated considering as 100% the amount of polyphenols in the source solutions):

- CEL2+ GA : 1.18%
- CEL2 pow+ GA: 3.00%
- CEL2+ TPH : 2.00%
- CEL2 pow+ TPH: 3.40%
- CEL2+ GPH : 2.80%
- CEL2 pow+ GPH: 12.00%

These results highlight a greater ability of the natural mixture of polyphenols to graft the surface compared with the single molecule gallic acid. In particular the polyphenols from red grape skins show a great ability to bind glass surface.

In order to better investigate the bond of biomolecules to the surface their characteristic chemical functionalities has been analysed. XPS analysis was performed on the surface of glass bulk samples before and after the functionalization.

In Table 2.15 the atomic percentage of the elements detected on the surface of the bare and functionalized CEL2 samples is reported.

Table 2.15: Atomic percentage of elements on the surfaces of the glass samples detected by XPS analysis. (Uncertainty of measurements 0.3-0.1% at).

	Samples			
Elements [%at]	CEL2 washed	CEL2+GA	CEL2+TPH	CEL2+GPH
O	50.9	58.2	28	40.7
C	30.3	26.1	67.6	49
Si	6.6	11.4	-	2.5
Ca	5.4	-	1.7	3.7
Na	4.6	1.1	1.6	2.1
P	1.4	3.3	0.9	2.0
K	0.8	-	-	-
Mg	<0.1	<0.1	<0.1	0.2

The percentage of the glass constituents (Ca, Na, K) decreases after the procedure of functionalization and this result confirm the ionic exchange between the glass and the acid solution described in paragraph 2.6.1.

The percentage of Si increased after the functionalization with GA because the permanence in an aqueous solution increase the formation of silica gel on the surface, the same process is not visible for the natural molecules GPH and TPH because the bigger dimensions of this biomolecules cover the surface in a more uniform way. The variation of the amount of Na and Ca after the procedure of functionalization can be also correlated to the ability of polyphenols to bind metal ions [141], [142].

A relevant increase in the carbon content can be observed after the functionalization with GPH and TPH but not with GA.

This can be explained considering the substitution of glass carbonate after the functionalization and the bigger dimension of the GPH and TPH polyphenols compared with the small dimension of the gallic acid molecules with a consequent high amount of carbon. A variation of oxygen can also be noted, it increases for

the functionalization with gallic acid because of the –OH groups exposed by this molecules, while decrease with the natural polyphenols that are bigger molecules with a high number of carbon atoms.
The variation in the percentage of the elements on the surfaces is not enough to determine the presence of the biomolecules, so in order to understand the chemical groups on the surfaces, the high resolution spectra of carbon and oxygen were analysed.
The high resolution spectra of the carbon region for bare and functionalized samples are reported in Figure 2.30.

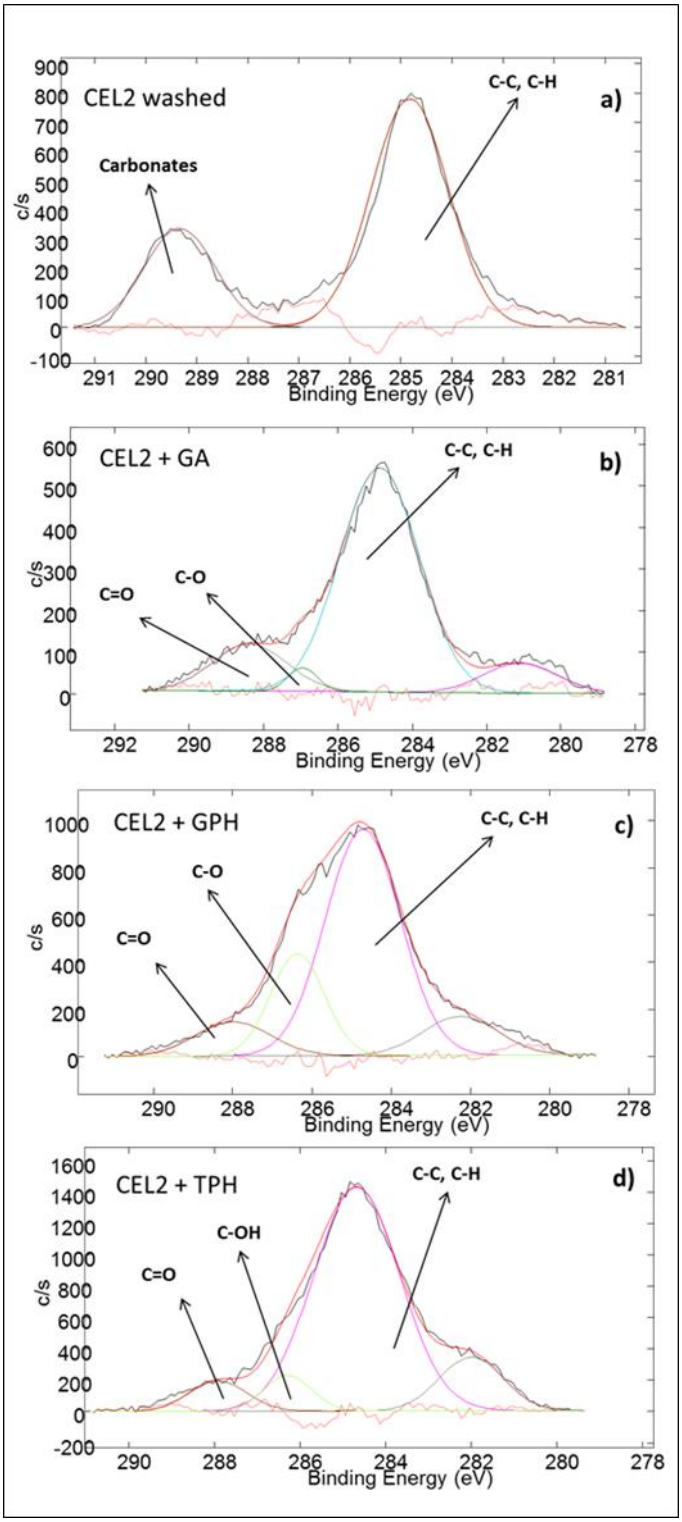

Figure 2.30: XPS high resolution spectra of the carbon region of glass samples.

The high resolution spectrum of the carbon region of CEL2 bare sample (Figure 2.30a) shows two peaks at 284.79 eV e 289.25 eV. The first signal is correlated with hydrocarbon contaminations unavoidable at the reactive surfaces [143] and previously observed for CEL2 glass[115], [116].The second peak is due to carbonates present on the surface of the class as contaminant[144].This signal disappears after functionalization (Figure 2.30 b, c and d) as previously observed for this kind of functionalization[115], [116].

The signal around 284 is still present on all the samples after functionalization regardless of the grafted molecules. That signals is due to the C-C and C-H bonds that can be correlated to both surface contaminants and polyphenols which are molecules rich of these bonds. In the spectrum of the samples functionalized, two characteristic peaks appear, one around 286 eV and the other around 288 eV. These signals are correlated to C-O and C=O bonds respectively[110] and they are observed also in previous work on glass functionalization [115], [116]. These two bonds are well present in polyphenols and can indicate the presence of these molecules on the surfaces. However the C=O group can also be correlated with the tendency of the polyphenols to oxidize into quinone.

The high resolution spectra of the oxygen region are reported in Figure 2.31 for CEL2 samples bare and functionalized.

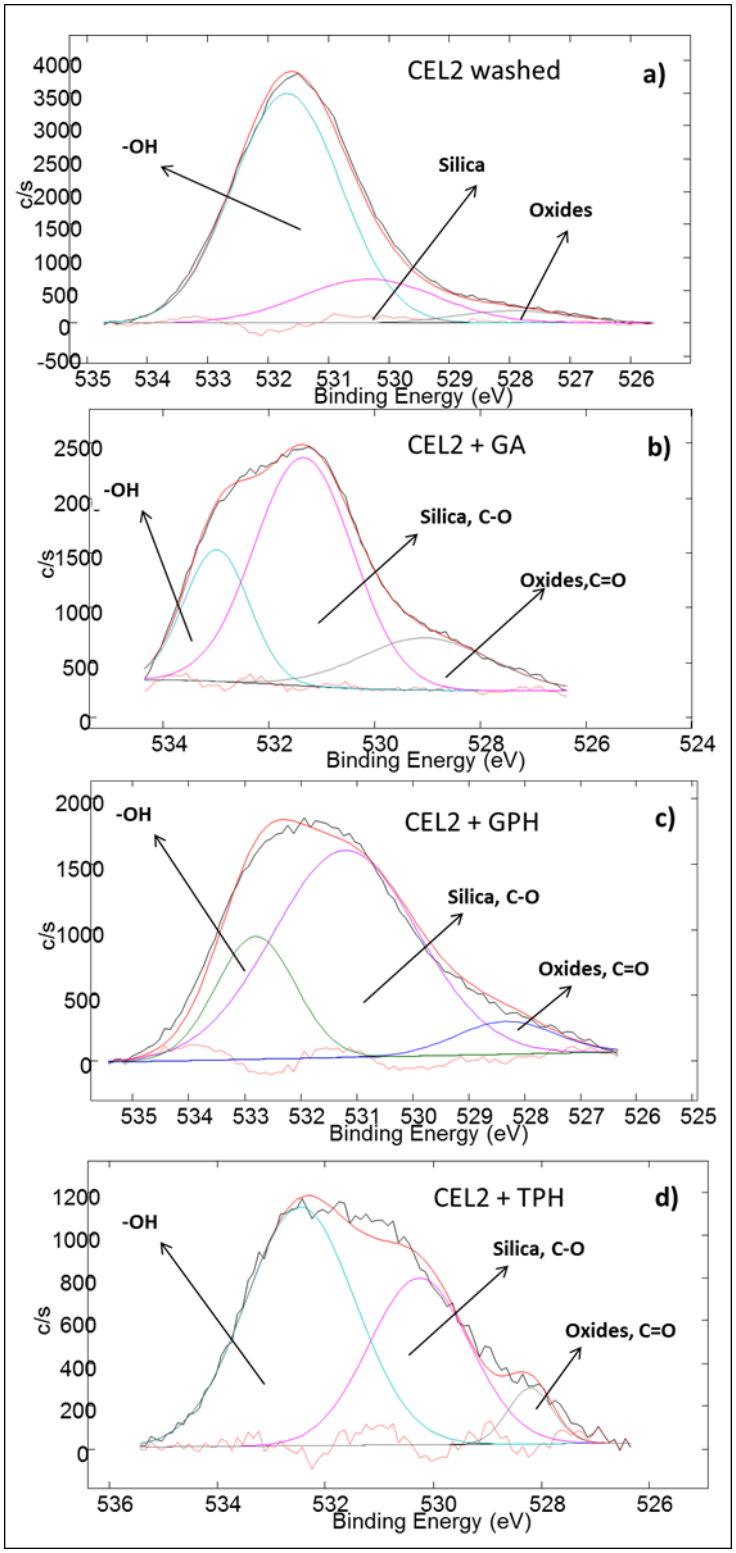

Figure 2.31: XPS high resolution spectra of the oxygen region of the glass samples.

The spectrum of the bare samples (Figure 2.31a) shows three main peaks, one at 527.93 eV, one at 530.34 eV and one at 531.69 eV. They can be respectively correlated with the oxides of the glass, silica and –OH groups[145].
The samples functionalized (Figure 2.31 b, c, d) present again three peaks with a shift to higher energies of the –OH peaks that is attributable to – OH in the phenolic group of the polyphenols[146]. With the presence of polyphenols the peak at 529 eV can be correlated both to oxides and C=O bonds and the peak at 531 eV both to silica and C-O bonds[115], [116].
A further evidence of the presence of the polyphenols on the surfaces after the functionalization is supported by the fluorescence images of the samples before and after functionalization (Figure 2.32):

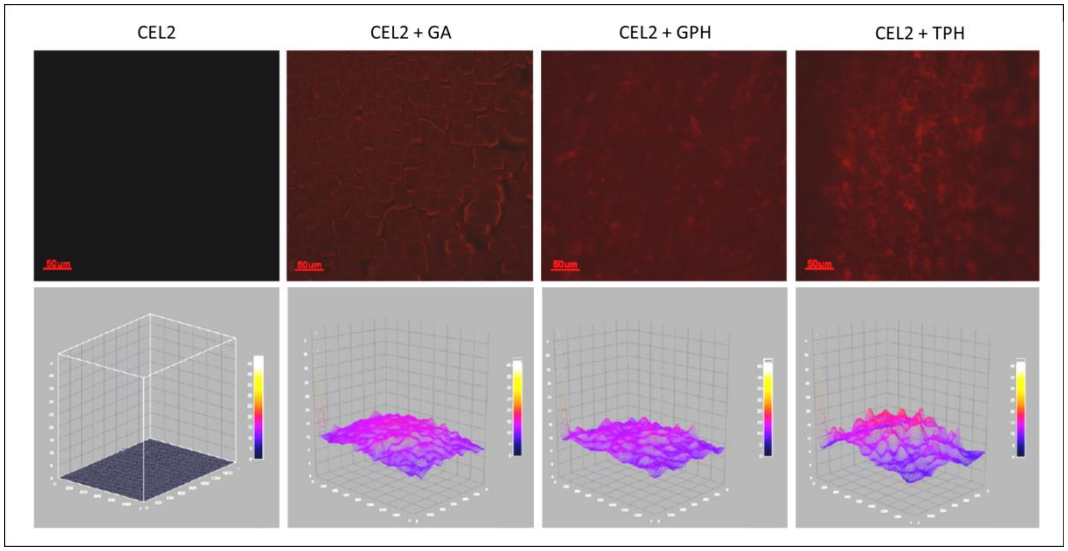

Figure 2.32: fluorescence images of the samples CEL2, CEL2+GA, CEL2+GPH and CEL2+TPH. Barscale 50 µm, magnification 20X.

The fluorescence images are present in the upper panel in which it is possible to see that the bare glass does not present any signals while the samples functionalized with polyphenols are fluorescent. In the low panel, the images were analysed with a 3D revealing software showing a homogeneous and continuous layer of biomolecules on the surfaces.
Spectrophotometric analysis with the Folin&Ciocalteu method, XPS measurements and fluorescence images proves together the successful functionalization of the bioactive glass CEL2 with polyphenols.

Titanium alloy

The first attempt of titanium alloy functionalization was performed using three different media for the functionalization of gallic acid that is the model molecules like previously described in 2.5.5. The time of functionalization was 8h as suggested from the literature [108].
The photometric measurements were performed for the source and uptake solutions and in Figure 2.33 are reported the results founded for the source solutions.

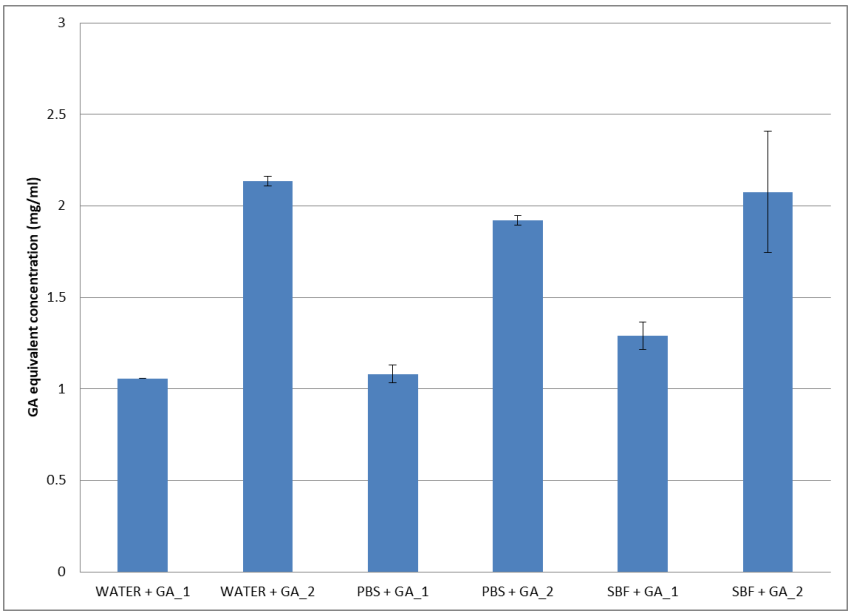

Figure 2.33: amount of gallic acid in source solutions of functionalization expressed in gallic acid equivalents (mg/ml).

The GA equivalent concentrations, in all the three media, are comparable with the nominal concentrations highlighting the stability of the chosen solvents at least for the time necessary for the functionalization.
Only the solution PBS+GA_2 shows a lower amount than the nominal one that could indicate an initial degradation of the molecules not evidenced by change in the color analysed in the previous paragraph.
The analysis on the uptake solutions, not reported in the graph, does not show significant reduction in the concentration probably because the amount of the molecules bound to the surface is too low to be significantly detected on the analysis of the solutions.

The spectrophotometric results with the Folin&Ciocalteu method are reported in figure 2.34 on the surface of the samples.

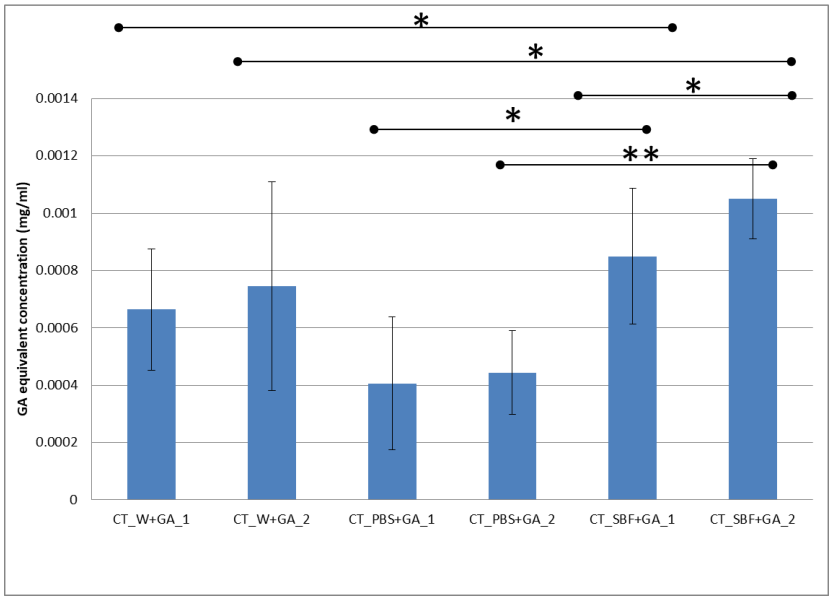

Figure 2.34: amount of the gallic acid on the titanium alloy samples surface expresses in gallic acid equivalents (mg/ml). (*p<0.05, **p<0.5).

The measurements highlight the presence of gallic acid on all the samples confirming the ability of gallic acid in aqueous solutions to bind titanium oxide surfaces[108].
The amount of gallic acid on the samples functionalized using SBF as medium is statistically higher than the one on the samples functionalized with water ($p<0.5$) or PBS ($p<0.05$) as medium.
Considering the standard deviation, there are no significant differences between the two different concentrations in the same medium (no statistical difference between groups with $p<0.05$).
This could indicate that even at the low GA concentration (1mg/ml) the surface ability of bind gallic acid is saturated and higher concentration cannot improve the amount of the molecules that can bind the surface. This result is in accordance with the negligible decrease of the amount of the molecule in the uptake solutions discussed above.
The samples are able to graft around the 0.1% of the gallic acid presents on the 1 mg/ml solution showing as expected a lower reactivity compared with the glass samples.

In order to better investigate the bond of gallic acid with the surface, their characteristic chemical functionalities are observed. XPS analysis was performed on the surface CT samples bare or functionalized in the different media and at the different concentration.
The atomic percentage of the elements detected on the surface of the bare and functionalized CT samples are reported in Table 2.16.

Table 2.16: Atomic percentages of elements on the surface of the CT samples detected with XPS analysis. (Uncertainty of measurements 0.3-0.1% at).

	Samples						
Elements [%at]	CT	CT_W+GA_1	CT_W+GA_2	CT_PBS+GA_1	CT_PBS+GA_2	CT_SBF+GA_1	CT_SBF+GA_2
O	57.0	52.6	49.6	59.0	55.5	44.7	47.8
C	19.0	29.9	31.8	19.1	20.2	45.2	39.1
Ti	18.2	15.9	14.9	15.6	15.6	6.6	8.7
Ca	-	-	-	0.8	-	3.5	3.2
Others	5.8	1.6	3,8	5,4	8,7	3.5	1.3

A certain amount of carbon is present on the surface of the CT samples because of the unavoidable hydrocarbon contamination of reactive materials [147], [148].
An increase of the amount of carbon can be observed for the samples functionalized in water and in SBF. For the samples functionalized with PBS as solvent, the increase of carbon is negligible. The increase of carbon can be correlated with the presence of gallic acid and this result is in agreement with the Folin&Ciocalteu test.
A not negligible amount of Ca is present on the surface of the samples functionalized with SBF and these data could be correlated with the tendency of gallic acid to form complexes with the calcium that is presents in the medium.
The low amount of calcium on the surface of CT_PBS+GA_1 can be considered as contaminant.
Gallic acid has the ability to bind calcium [141] through complexation reactions [149], [150]. Polyphenols are able to give complexation in solutions with metal ions and the structure of the coordination compounds can be different according to different pH. At a pH around 6-7 it is possible to hypothesize the formation of a heterogeneous ternary complex with metal ion in central position.
The complex could involve both the carboxylate ion by gallate and $Ti\text{-}O^{-}$ groups as donor.

The formation of this compound influences reactivity of polyphenols and in our case it is shown that it improves their ability to bind surfaces.
The possible mechanism of complexation and binding to the surface of the titanium alloy samples is reported in Figure 2.35.

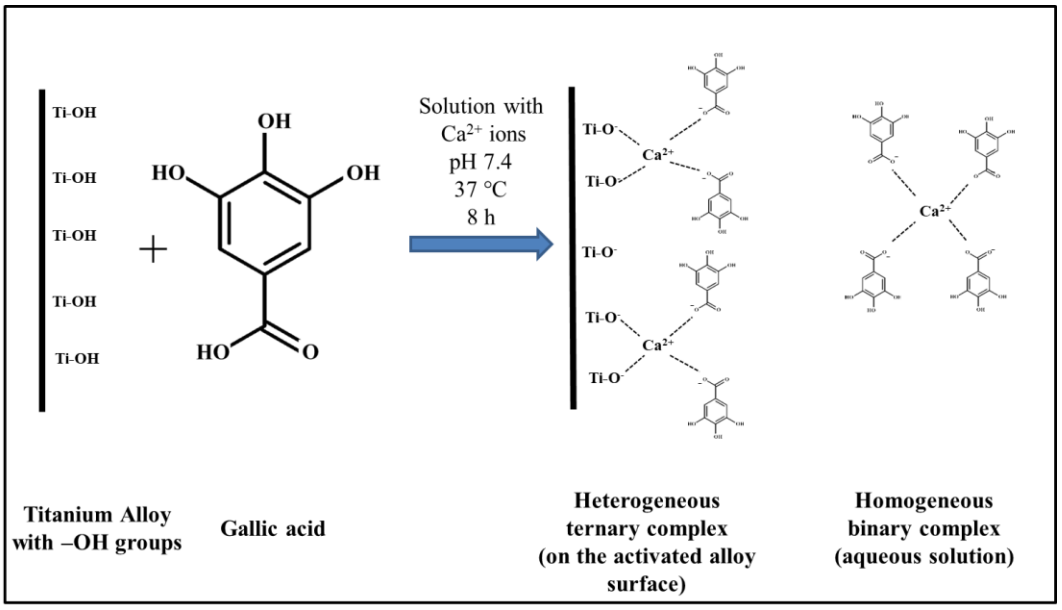

Figure 2.35: Scheme of the possible reaction of GA with the titanium alloy surface and Ca^{2+}. Planar coordination is reported, eventual equatorial coordination are omitted.

At the pH of SBF (7.4) the gallic acid in the chemical form of gallate with deprotonated carboxylic group bound to the titanium alloy surface that exposes $Ti\text{-}O^-$ groups with Ca^{2+} ions as intermediate species. A heterogeneous ternary complex is probably presents allowing the grafting of the deprotonate gallic acid to the surface alloy. In the uptake solution the free Ca^{2+} ions and the remaining gallic acid could form heterogeneous complexes with different coordination numbers.
Calcium is not present in the PBS solution this can explain the low amount of gallic acid grafted on the surfaces.
The presence of metal ions seems to be a crucial point for binding of the polyphenols to the titanium alloy surfaces.
In order to better understand the specifically functional groups exposed by the surfaces, before and after the functionalization, high resolution spectra of the carbon and oxygen region were performed.

The high resolution spectra of the carbon region of the CT samples bare and functionalized are reported in Figure 2.36.

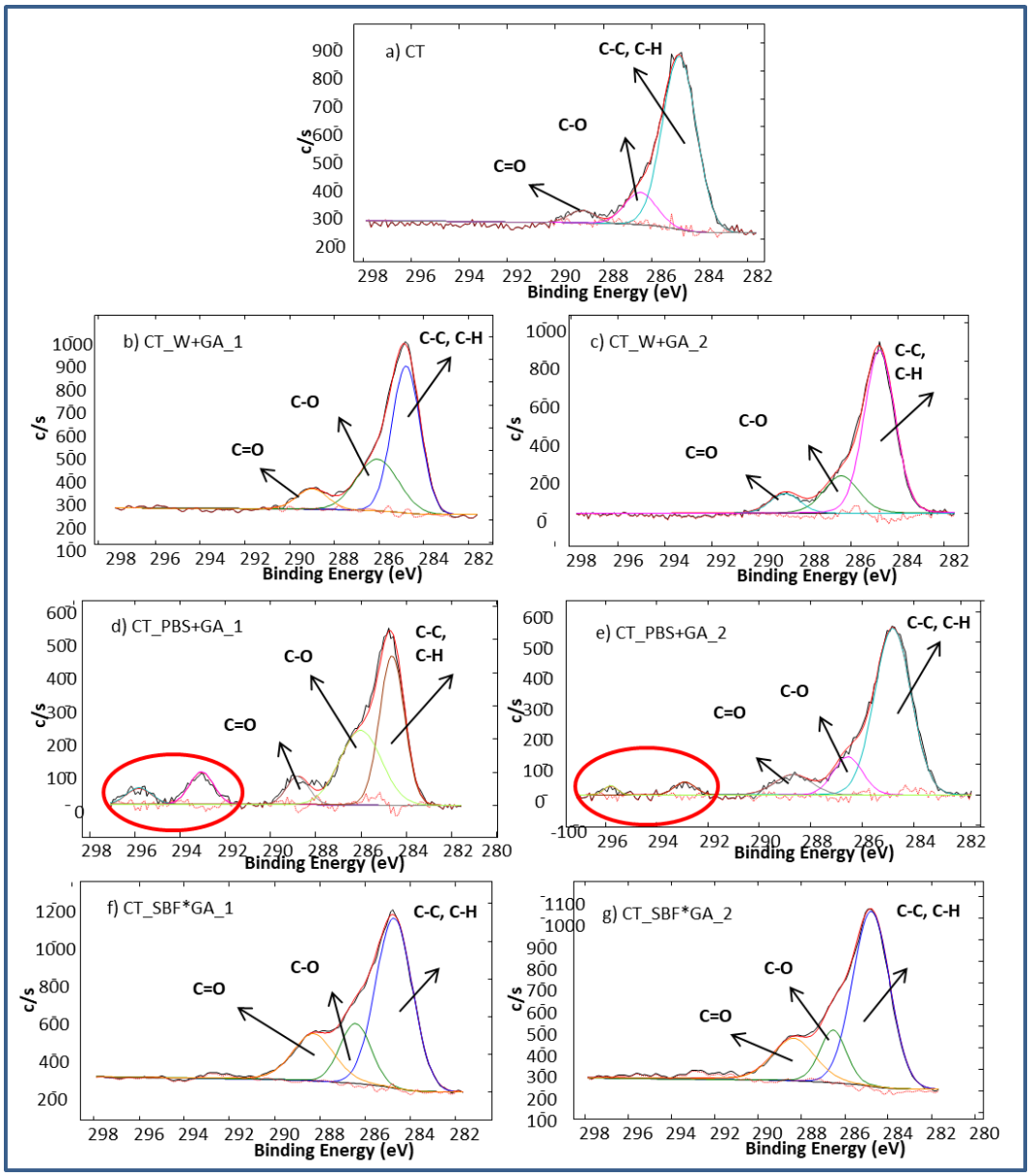

Figure 2.36: high resolution spectra of the carbon region of CT samples.

The high resolution spectrum of the carbon region of sample CT (Figure 2.36a) presents three peaks. The peak at 284.81 is correlated with C-C and C-H bonds due to hydrocarbon contaminations previously discussed [147], [148].

The others two peaks are around 286 eV and 289 eV correlated with C-O and C=O bonds[151] and because of their low intensity on this samples are due to surface contaminations.
The signal around 284 eV is still present in the spectra of the functionalized samples (Figure 2.36 b-g), but a significant increase is visible for the peaks at 286 eV and 289 eV after functionalization and in more evident manner for the samples functionalized with SBF as solvent. Regarding the peak at 284 eV, it could be correlated with hydrocarbon contaminations, but also with the C-C and C-H bonds of gallic acid. The presence of C-O and C=O groups are again correlated with gallic acids and its tendency to oxidize into quinone as such observed before in[115], [116].
A further couple of signal at 293 and 295.8 eV are present in the spectra of CT_PBS+GA_1 and CT_PBS+GA_2 samples. These two peaks are correlated with shake up satellite peaks due to aromatic rings[152] and this could indicate a different disposition of gallic acid on the surfaces with PBS as functionalization medium. The different orientation of GA can be explained by the different pH value of the source solutions if compared with the ones in SBF and water and can be related with the lower redox results obtained with the Folin&Ciocalteu test on the surfaces functionalized with PBS as medium.
The oxygen high resolution spectra of samples CT bare and functionalized are reported in Figure 2.37.

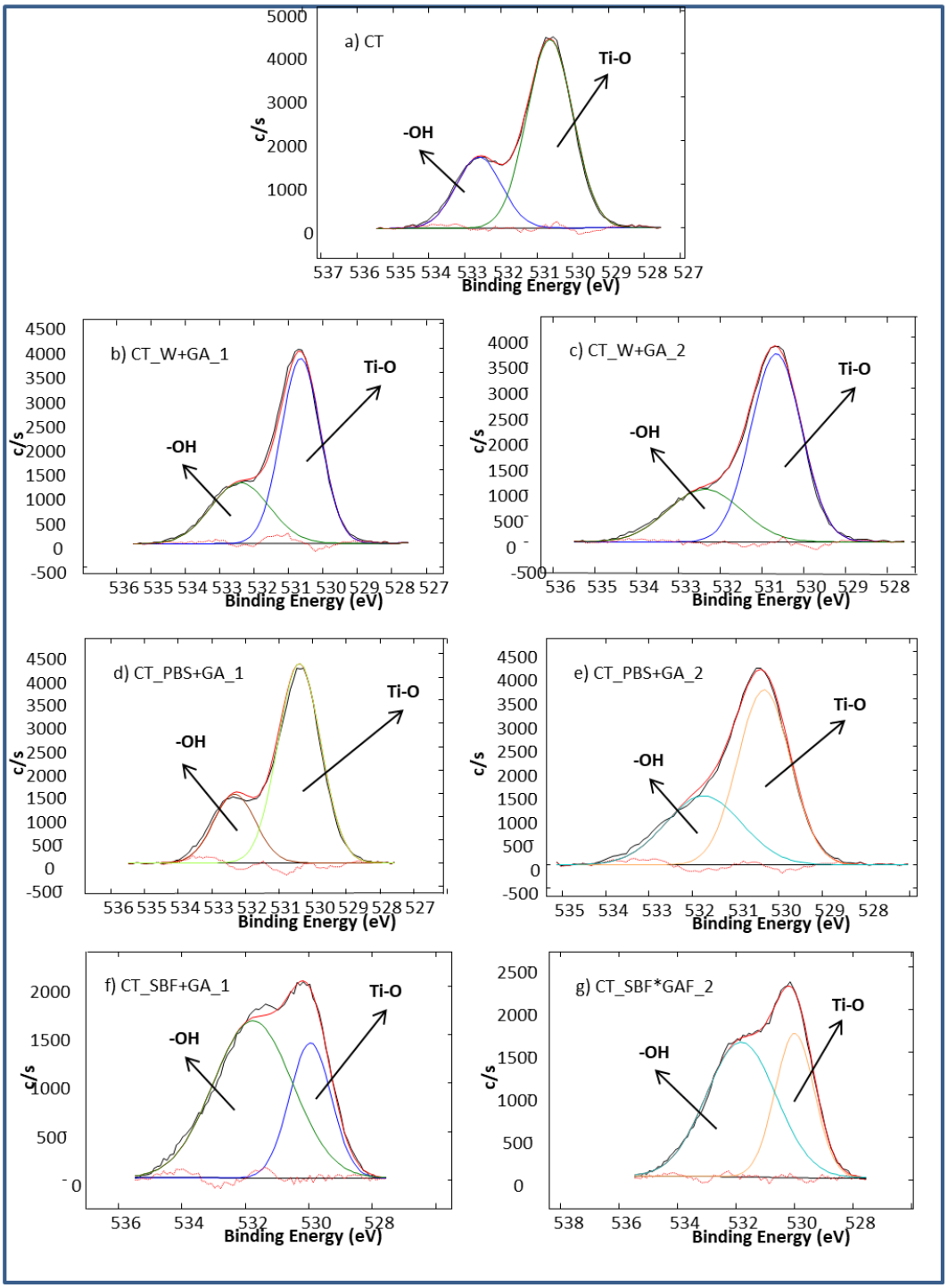

Figure 2.37: high resolution spectra of the oxygen region of CT samples.

On the spectra of all the samples, two peaks around 530 and 532 eV are present.

The first one is due to the presence of the Ti-O bonds of the titanium oxide layer and the second to the –OH groups[123], [147].
The –OH groups are abundant on the surface of the CT samples because of the chemical treatment [123], [153]. A notable increase in the –OH peaks can be observed after the grafting of gallic acid in particular manner on the samples functionalized using SBF as solvent. It can be explained considering that gallic acid exposes hydroxyl groups.
However, with PBS or water as solvents, the increase of the peak due to the presence of -OH groups is not consistent and can be correlated with a minor amount of the grafted gallic acid and with a different orientation of this biomolecule on the surface.
Since SBF as medium gave the best results in term of activity and amount of the biomolecules grafted on the surface of the titanium alloy, it was used as solvent for the investigation of shorter time of functionalization with the lower concentration (1mg/ml), in order to improve the protocol of functionalization.
Starting from the literature [108] 8 h was chosen as time for the first attempt of functionalization, then shorter time were performed.
Spectroscopic analysis with the Folin&Ciocalteu method were performed on CT samples functionalized in SBF with GA 1mg/ml for 30 minutes, 1 h, 3h and 8h and the results are reported in Figure 2.38.

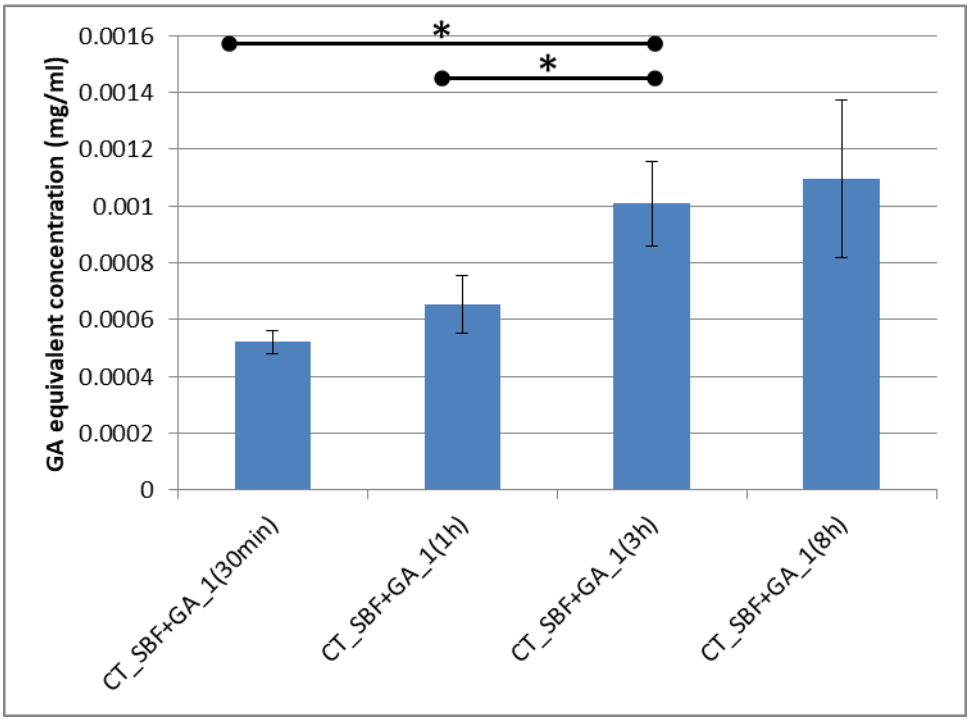

Figure 3.38: amount of the gallic acid on the titanium alloy samples surface after different time of functionalization expresses in gallic acid equivalents (mg/ml). (*p<0.05).

Active molecules of gallic acid are present on the surface of all the samples with increasing in the amount with longer time of functionalization.
Statistical significant difference ($p<0.05$) is present between the functionalization at 3h with the ones at 30 minutes and 1 h, but there are no significant difference considering media and standard deviation with t-student test between 3h and 8h of functionalization.
In the light of these results, after 3 h of functionalization, the maximum amount of molecules that can be graft to the surfaces are reached in the case of CT samples surface, and further functionalization with natural polyphenols were performed with this protocol: 3h of functionalization with SBF as solvent.
Further functionalizations with this defined protocol for CT surfaces were also performed with natural polyphenols of green tea (TPH) and natural polyphenols from red grape pomace (PPH).
The spectroscopic measurements of the source solution of PPH and TPH 1mg/ml and 2 mg/ml in SBF are reported in Figure 2.39.

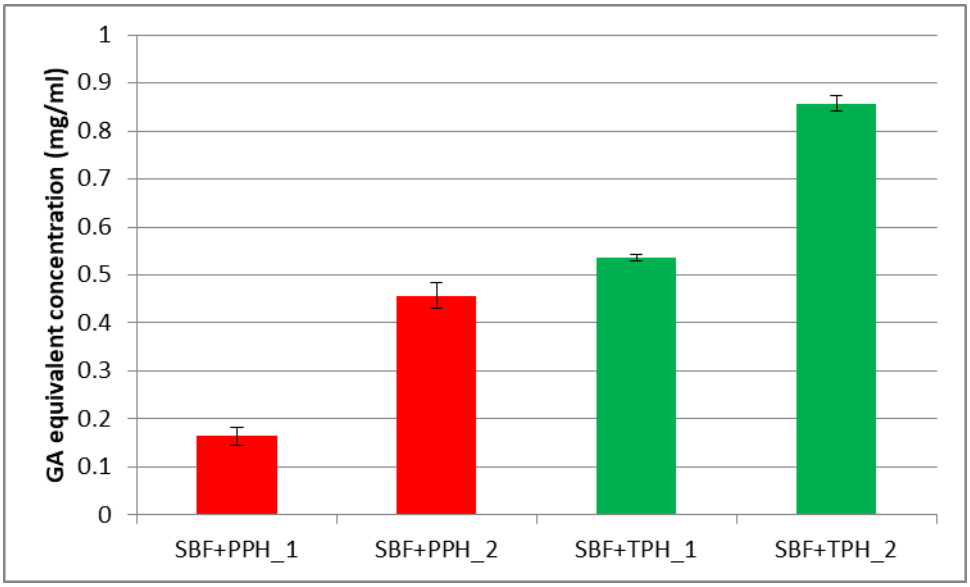

Figure 2.39: amount of the polyphenols on the SBF source solutions expresses in gallic acid equivalents (mg/ml).

For the solution with TPH 1 mg/ ml in SBF, the amount of polyphenols found is close to the one observed for the solution of TPH at the same concentration in water used for the glass functionalization and the solution SBF_TPH_2 shows a double concentration as expected.
The amount of polyphenols in the solution with grape pomace PPH in SBF, is higher than the one observed for the solution of GPH in water used for the functionalization of the glass, because the grape pomace are richer in polyphenols and has less sugar than the extract of grape skins. The concentration 2 mg/ ml is more than the double of the 1 mg/ml concentration probably because of the difficulty in weighing small amount of PPH that is a sticky substance.
A relevant amount of polyphenols is present in all the solutions tested and the uptake solutions of functionalization are not reported, as the previous case of the functionalization with gallic acid, because of the negligible reduction founded in the amount of polyphenols.
The Folin&Ciocalteu results of the samples are reported in Figure 2.40.

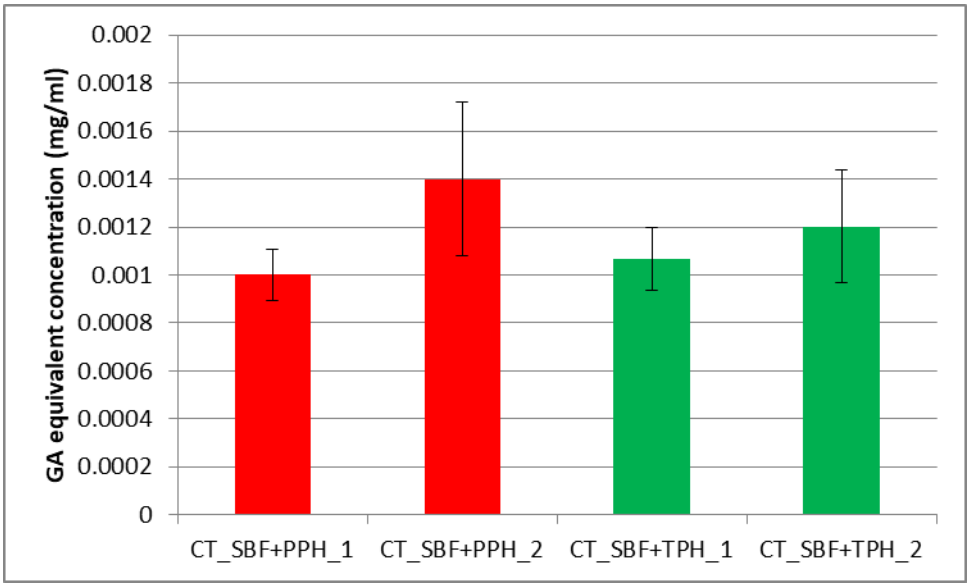

Figure 2.40: amount of the polyphenols on CT samples surfaces expresses in gallic acid equivalents (mg/ml).

The amount of polyphenols, considering media and standard deviation is the same for both the types of natural extracts and is the same for the samples functionalized with GA in SBF for 3 h and 8 h. This fact indicates that probably a low amount of polyphenols allows to saturate the possible binding sites exposed by the surfaces. The concentration 1 mg/ml was chosen for further functionalization because lower concentration can create fewer problems with weighting of polyphenols.

In order to better investigate the bond of natural polyphenols with the surface, their characteristic chemical functionalities are observed. XPS analysis was performed on the surface samples CT, CT_SBF+TPH_1 and CT_SBF+PPH_1.

The atomic percentage of the elements detected on the surface of the bare and functionalized CT samples are reported in Table 2.17.

Table 2.17: Atomic percentages of elements on the surface of the CT samples bare and functionalized detected with XPS analysis. (Uncertainty of measurements 0.3-0.1% at).

	Samples		
Elements [%at]	CT	CT_SBF+TPH_1	CT_SBF+PPH_1
O	57.0	28.5	24.1
C	19.0	68.5	74.1
Ti	18.2	1.1	0.7
Ca	-	0.8	0.5
Others	5.8	1.0	-

A remarkable increase of the amount of carbon can be observed for the samples functionalized with the natural polyphenols and this increase is correlated with the presence of the biomolecules on the substrates. A not negligible amount of Ca is present on the surface of the samples functionalized in SBF and these data could be correlated with the tendency of polyphenols to form complexes with the calcium that is presents in the medium, as discussed before. The reduction of the oxygen percentage is due to the presence of the polyphenols that covered the surfaces of the titanium oxide, data also confirmed by the reduction of the percentage of titanium relieved, forming a semi-uniform coating of molecules with a high number of carbon atoms.

In order to better understand the functional groups specifically exposed at the surfaces after the functionalization with the natural polyphenols, high resolution spectra of the carbon and oxygen region were performed.

The high resolution spectra of the carbon region of the CT samples bare and functionalized with TPH and PPH are reported in Figure 2.41.

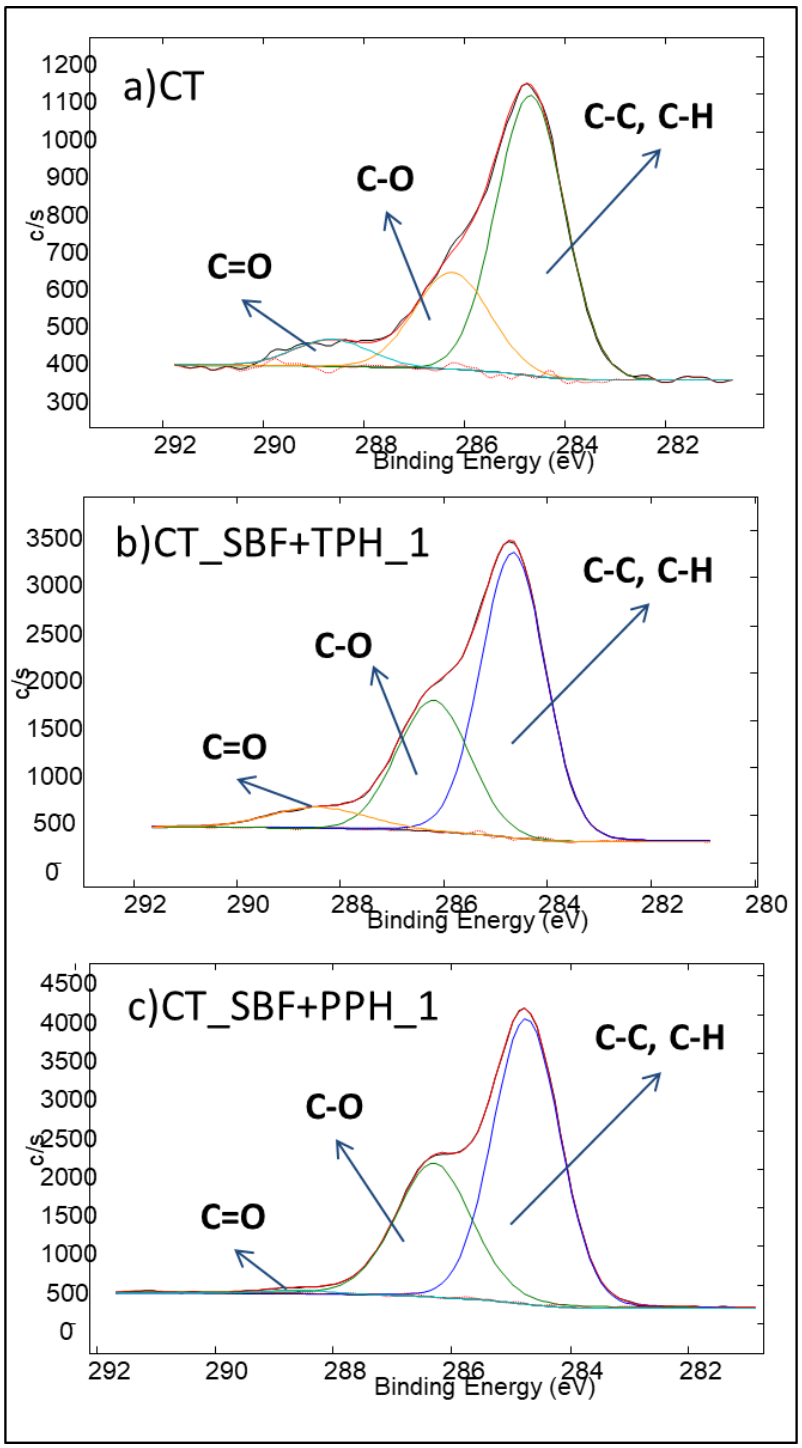

Figure 2.41: high resolution spectra of the carbon region of CT samples bare and functionalized with natural polyphenols.

The high resolution spectrum of the carbon region of sample CT (Figure 2.41a) presents three peaks. The peak at 284 eV is correlated with C-C and C-H bonds due to hydrocarbon [147], [148], while the others two peaks are around 286eV and 289 eV correlated with C-O and C=O bonds[151]. As discussed before, these peaks are due to surface contaminations.
These three peaks are observable also on the samples functionalized, but in this case they have higher intensity, for this reason, they can be attributed not only to surface contaminants, but also to C-H, C-C, C-O and C=O groups of polyphenols. For the samples CT_SBF+PPH_1, a decrease in the C=O groups contribution is also noticeable, probably because of the lower amount of polyphenols with this groups in PPH extracts. The chemical groups found in the high resolution spectra of the carbon region are amenable both to polyphenols and contaminants, for this reason the high resolution spectra of oxygen region is reported in figure 3.42 and analyzed.

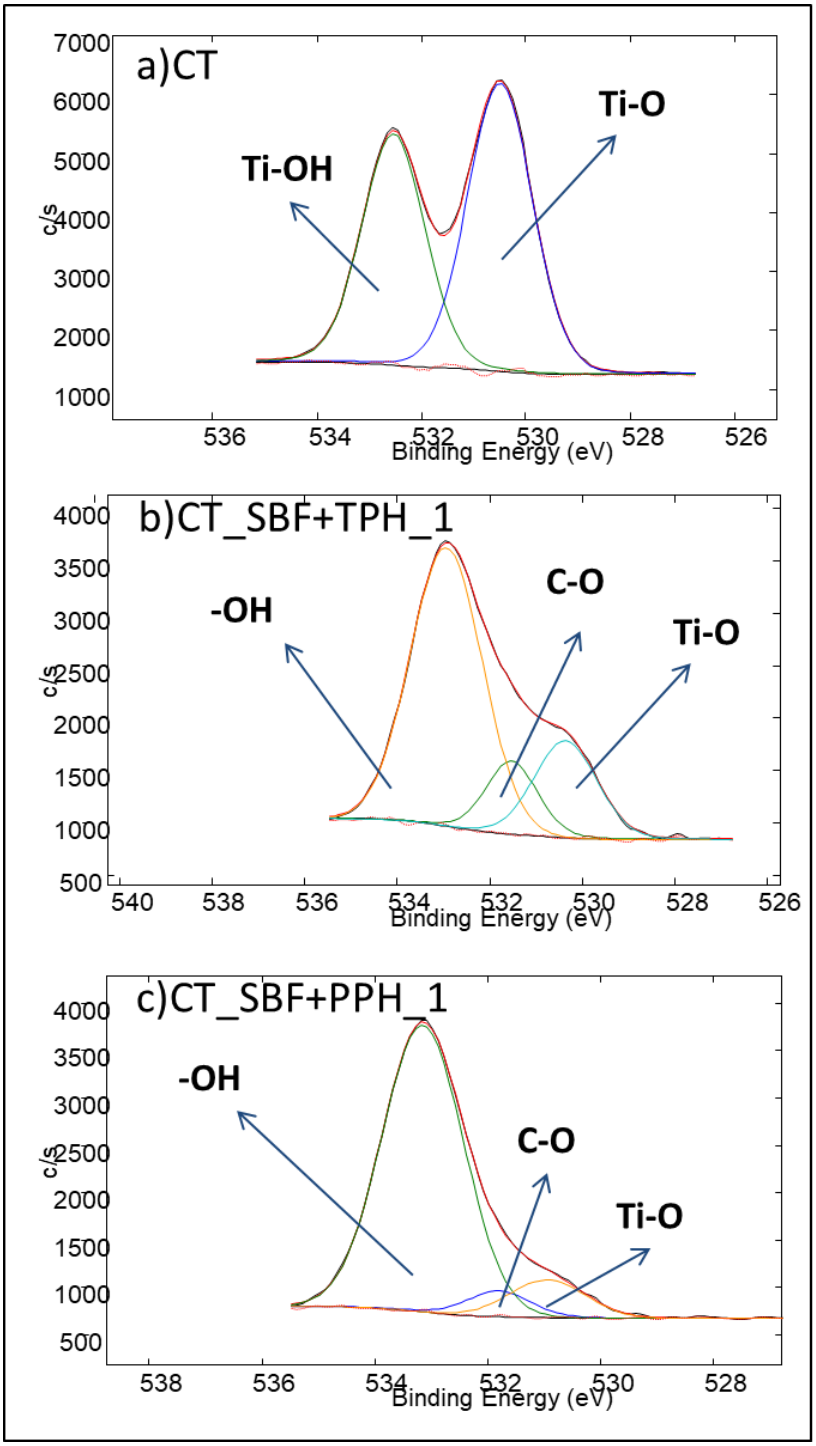

Figure 4.42: high resolution spectra of the oxygen region of CT samples bare and functionalized with natural polyphenols.

On the spectra of the samples CT, two peaks around 530 and 532 eV are observable.
The first one is due to the presence of the Ti-O bond of the titanium oxide layer and the second to the –OH groups[123], [147], as discussed before.
The spectra of the samples functionalized show a similar trend though different from the one of the bare CT samples. It is possible to see the reduction of the peak at 530 eV of the Ti-O bond of the titanium oxide because of the presence of the biomolecules on the substrates. A new peak at 531.5 eV appears correlated with C-O groups of polyphenols[154] and the peak of –OH groups considerably increases and has a small shift from 532 eV to 533 eV which could indicate the presence of aromatic –OH groups. The clear changes on the spectra of the CT samples after the functionalization with the natural extracts confirm again the success of the procedure of functionalization highlighting the presence of a thicker and more uniform layer of biomolecules if compared with the samples functionalized with gallic acid (Figure 2.37).
As observed for glass samples, the presence of the polyphenols on CT surface were also checked by means of fluorescence microscope investigation and the results are reported in figure 2.43.

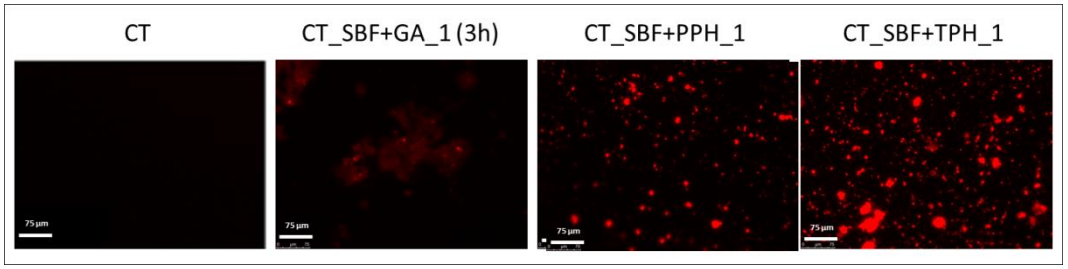

Figure 2.43: fluorescence images of the samples CT, CT_SBF+GA_1(3h), CT_SBF+PPH_1 and CT_SBF+TPH_1. Barscale 75 µm, magnification 20X.

Polyphenols are present on all the samples functionalized, the functionalization is not uniform, but the biomolecules form aggregates on the surface. The sample with GA shows a minor fluorescence if compared with the other functionalized samples. This results is in accordance with the minor amount of carbon find with XPS on the samples with GA compared to the samples with PPH and TPH and it could be correlated with an higher amount of natural polyphenols on the surface, but which are not detected by Folin&Ciocalteu method probably because of their polymerization, or with the presence of other natural molecules present in the TPH and PPH extracts.

2.6.3 Contact angle measurements

Glass

The wettability of glass surfaces before and after functionalization was tested with double distilled water and the results are reported in Figure 2.44.

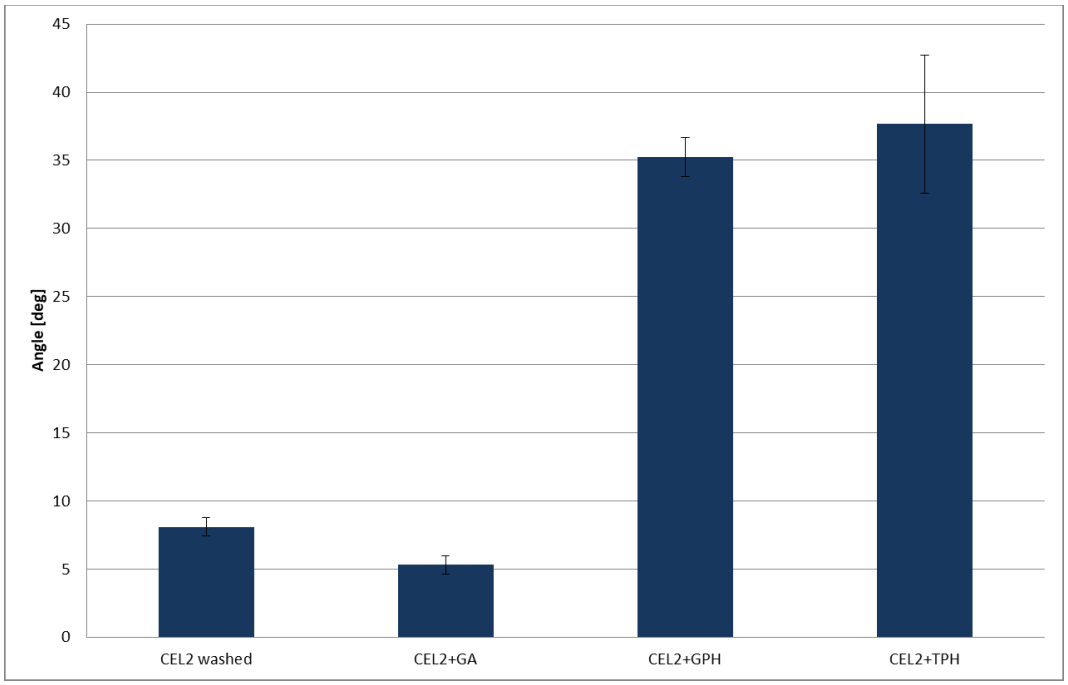

Figure 2.44: contact angles of CEL2 bulk samples, washed and functionalized.

The contact angle of the CEL2 washed is around 8° that means a high wettability of the surface due to the –OH groups exposed at the surface of the glass.
The samples functionalized with gallic acid shows a decrease of the contact angles around 5° due probably to the higher amount of –OH groups exposed by the biomolecules grafted to the surface.
The measurements on the samples CEL2+TPH and CEL2+ GPH functionalized with the natural extracts show an increase of the contact angles, 37°±5° for the CEL2+TPH samples and 35° for the sample CEL2+ GPH.
This phenomenon can be explained with the greater complexity of the natural polyphenols with longer alkyl chains and with $–CH_3$ groups that can reduce the surface wettability.

Titanium alloy

Wettability of Ti6Al4V polished up to 4000 grit, CT and CT functionalized with polyphenols was tested with double distilled water and the results are reported in Figure 2.45.

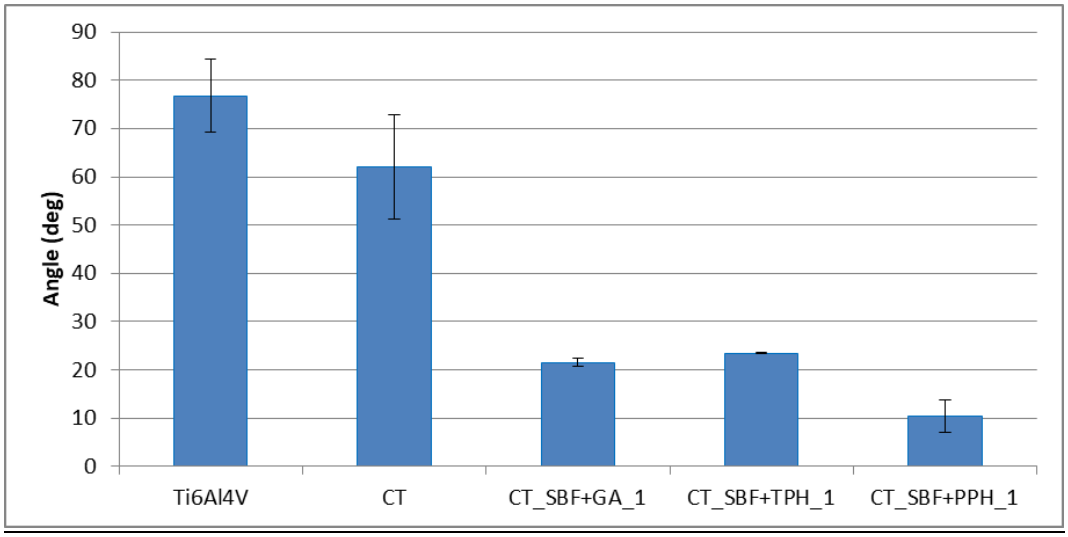

Figure 2.45: contact angles of Ti6Al4V polished up to 4000 grit, CT and CT functionalized with polyphenols.

Comparing the contact angle measurements of the bare polished titanium alloy and the chemically treated samples it is possible to observe an increase of the wettability due to the presence of the –OH groups like observed with XPS analysis. The samples functionalized with gallic acid, as observed for the bioactive glass samples leads to a reduction of the contact angles because of the –OH groups exposed by the polyphenols themselves. It can also be noted that the contact angles of the samples functionalized with GA, is 5°±0.7° for the glass samples and 22°±0.9 for the CT samples. This molecule does not uniformly cover the surfaces and the difference in the contact angles between CEL2 and CT functionalized samples are correlated with the different wettability of the substrates themselves. Regarding functionalization with the natural polyphenols, on the contrary with respect to the bioactive glass, wettability increases suggesting the ability of the CT surface to graft a different kind of molecules from the natural extracts mixtures or a different organization of the same molecules onto the surfaces. However, it can be noted that for the samples with TPH the contact angle is around 25 ° for CT samples and around 37 ° for CEL2 samples. These

two data are close considering a measurement error around 10 ° and it could be supposed that this is the contact angle of the tea polyphenols.

2.6.4 Zeta potential electrokinetic measurements

Glass

Zeta potential measurements in function of pH are reported in Figure 2.46.

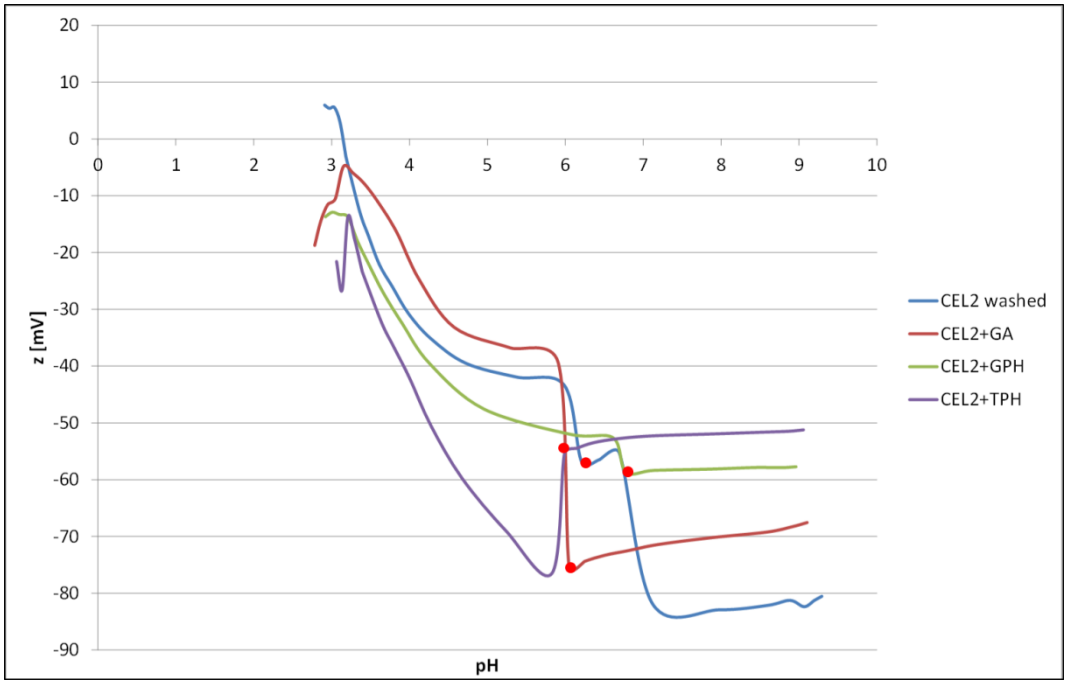

Figure 2.46: Zeta potential vs pH graph of CEL2 washed and functionalized. The red dots indicate the change of the electrolyte solution between the scanning of the acidic and basic rage.

The isoelectric point of all the samples is in the acid range and they are negatively charged at physiological pH. A defined value for IEP is detected only for the bare CEL2 glass at pH 3.14. In the case of the functionalized samples, a strong reactivity made reaching the IEP impossible without artifacts, but it is evident that the IEP can be extrapolated close to pH 3.
The titration curves of zeta potential with respect to pH are performed by making two different scanning on the same samples: a first one in the acidic range and then in the basic range: the red dots indicate the change of the electrolyte solution

between the two scanning. It can be observed that both the curves of the bare glass and those of the functionalized ones show an abrupt step in the range of pH between pH 5.8 and 6.8 that is due to the modification of the surface occurring in the acidic pH (so that when the titration in the basic range starts, the surface is changed with respect to the initial one) and/or to the surface modification around pH 6 of the glass and the polyphenols.

All the samples have negative zeta potential at the physiological pH with an evident plateau in the basic range: it is correlated with the presence of acidic hydroxyl groups on the surfaces[128]. The plateau starts off at pH around 4.5 for the curves of the bare glass and of the sample functionalized with GA: it is mainly related to the complete deprotonation of the OH groups of the glass surface (strong acid groups). The starting point of the plateau is shifted towards much more basic values (less strong acidic groups) in the case of the sample functionalized with GPH and in the case of the sample functionalized with TPH it is so shifted that it is not well detected: in these cases the glass surface appears to be much more shielded from the solution by the presence of the grafted molecules and its surface reactivity is changed.

The plateau of the functionalized samples is at a less negative potential when compared with the one of the bare CEL2. A reduction of the negative surface charge can affect the surface interaction both with proteins and cells or bacteria. For instance, it can allows higher absorption of cell adhesion proteins such as fibronectin which are negatively charged[155].

These results confirm the presence of the grafted molecules on the functionalized samples and show the different surface reactivity after functionalization.

The measurements of the z potential of the glass samples performed in SBF were reported in Figure 2.47.

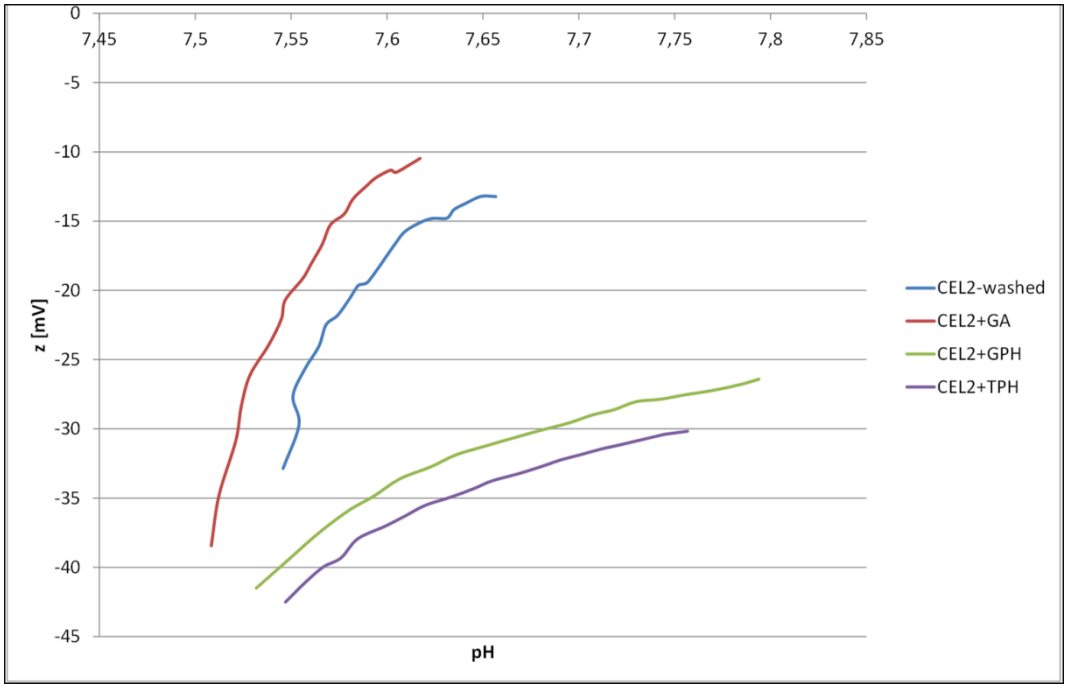

Figure 2.47: Zeta potential vs pH over time in SBF of CEL2 washed and functionalized. The measurements were repeated for 20 cycles (70 minutes).

The z potential at pH 7.4 is negative as observed previously in the KCl electrolyte solution and a moderate increase of the pH is noticeable after 20 cycles of measurements because of the ion exchange of the glass in aqueous solutions.
After the 20 cycles of measurements the z potential of all the samples became less negative and this variation is more evident for CEL2 washed and CEL2+GA. This variation can be attributed to the deposition of Ca^{2+} ions in the first stage of the cascade of bioactive reactions, as observed in literature for the bioactivity mechanism of bioactive glasses [156].
According to a shielding effect of the surface with respect to its surface chemical interaction with the fluid in the case of the samples functionalized with GPH and TPH, in these cases changing of surface charge during time is much less evident.

Titanium alloy

Zeta potential measurements in function of pH are reported in Figure 2.48.

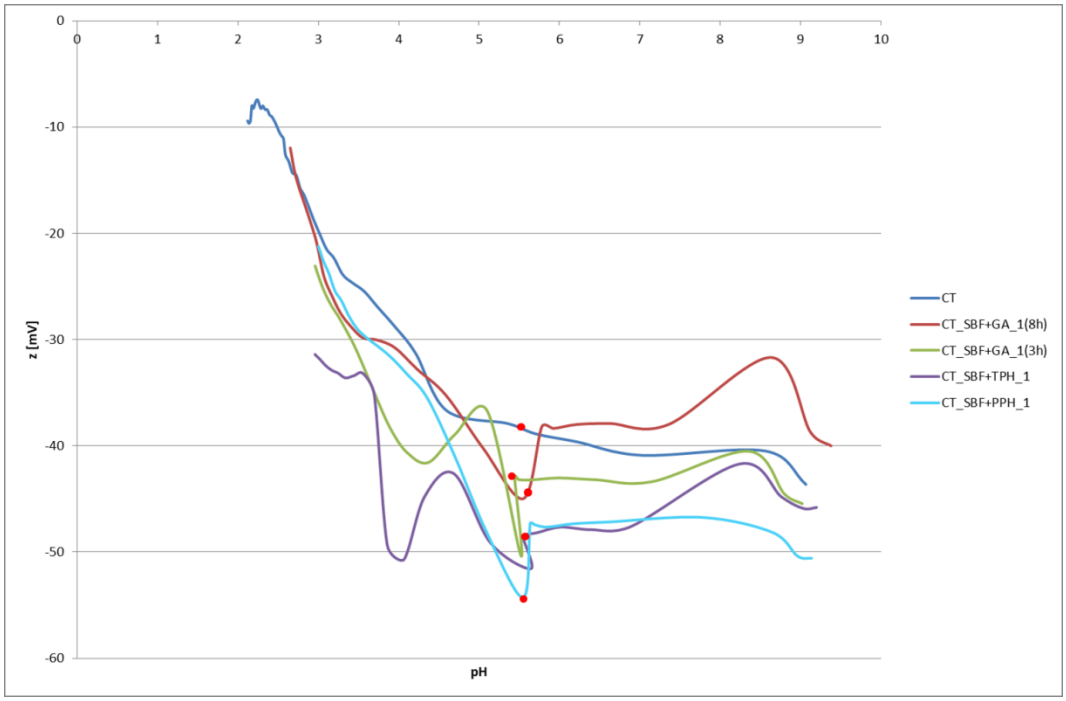

Figure 2.48: Zeta potential vs pH graph of CT bare and functionalized. The red dots indicate the change of the electrolyte solution between the scanning of the acidic and basic rage.

Because of the reactivity of the treated metal surface and of the grafted molecules, the IEP value is not detected, but it is possible to extrapolate it around pH2 for all the analyzed samples and it is also possible to observe that all the samples are negatively charged ad physiological pH.
On the curve of the CT sample, in the acid range, two changes of the slope can be observed at pH 3 and at pH 4.5-5, there is a plateau in the basic range and a trend towards negative charge at pH 8.5. The plateau in the basic range is correlated with the presence chemical groups of one single type, in this case of –OH groups, exposed by the chemical treatment[123], [128]. The change in the slope at pH 3, 4.5-5 and 8.5 at the moment cannot be correlated with specific features, but the presence of –OH groups with different pKa can be supposed[155].
For all the functionalized samples, a discontinuity can be observed between pH 5.5 and 6 and this is in part due to an artefact related to the substitution of the electrolyte solution in the interval between the scan of acid and basic ranges (a

discontinuity of 10 mV can be considered due only to this artefact), but it can be also correlated with surfaces reactions that occur during the measurement in the acid range, so that the surface at the beginning of the basic scan is changed with respect to the same surface before the test. Between the curves of samples CT_SBF+GA_1(3h) and CT_SBF+GA_1(8h) there are some differences. In the acid range, both the samples have changes in the slope between pH 5 and 3, for the samples functionalized for 8h four small changes of slope are present, while the curve of the samples functionalized for 3 h has two evident changes of slope. These changes of slope could be due to the protonation of different –OH groups[157], [158] of the GA molecules which has different acidic strength and reactivity. In the basic range, the samples have the same trend with a plateau between 6 and 7.5 due to the presence of –OH groups exposed by the substrates with the addition of the contribute of OH groups belonging to GA molecules. The changes of slope around pH 8.5 are due to the molecules degradation[3].

The samples CT_SBF+TPH_1 and CT_SBF+PPH_1 functionalized with the natural extracts showed differed behavior. In the acidic ranges, samples CT_SBF+TPH_1 have a trend similar to the one of CT_SBF+GA_1(3h), while the samples CT_SBF+PPH_1 have a trend similar to the one of CT_SBF+GA_1(8h), this behavior, as said for the gallic acid functionalization ,can be due to different arrangement of the molecules on the surfaces and, in this case, can also be due to the presence of different polyphenols with several types of –OH groups which could have different pKa [157], [158]. In the basic range, it is again present a plateau due to the exposition of deprotonated –OH groups, but for the samples with TPH there is a clear peak correlated with polyphenols degradation in the basic range, while for the samples with PPH it is not visible. This result is explainable with the higher sensitivity to pH changes of catechins, majoritarian compounds in TPH extracts if compared with the anthocyanins present in PPH extract[3]. The curves reported and analyzed suggest the success of the process of functionalization compatible with the formation of a not uniform layer of molecules considering that the surface behavior typical of the substrate is still observable.

In Figure 2.49, the measurement on samples CT_SBF+GA_1(8h) soaked for 28 days in SBF (FESEM observation are reported in the following paragraph) is reported with the curves of samples CT and CT_SBF+GA_1(8h) for comparison.

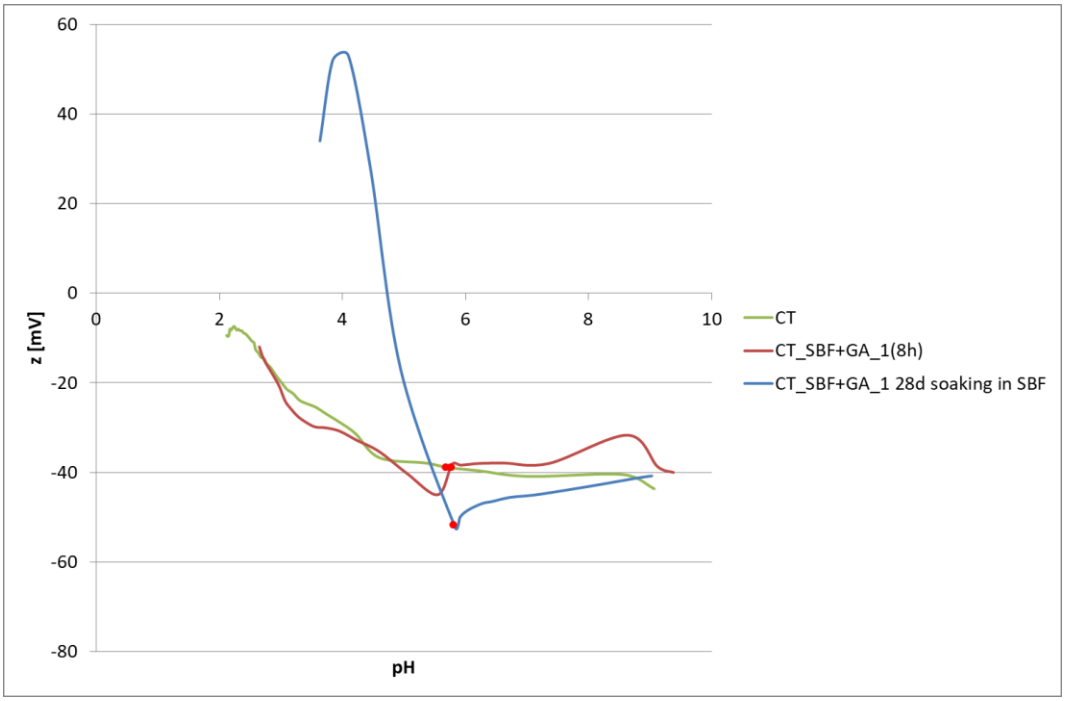

Figure 2.49: Zeta potential vs pH graph of samples CT, CT_SBF+GA(8h) and CT_SBF+GA 28 days soaking in SBF. The red dots indicate the change of the electrolyte solution between the scanning of the acidic and basic rage.

These samples are almost completely covered by hydroxyapatite. The isoelectric point of hydroxyapatite are reported in literature around pH 5[159] and the phosphate groups preferentially exposed on the surface of Hap have a z potential of – 50 mV at pH 7.4. The data obtained for the samples with GA soaked 28 days in SBF are in agreement with these values: the IEP is at pH 4.8 and the potential at physiological pH is – 45 mV. The strong decrease of the curve at pH around 4.5 is due to the decomposition of hydroxyapatite[160]. This result confirms the formation of an almost uniform layer of Hap and the great bioactivity of these samples.

2.6.5 In vitro apatite forming ability tests

Glass

Glass samples, both bulk and powder were soaked in SBF up to 14 days in order to evaluate the *in vitro* bioactivity. The samples after soaking were analyzed by means of Field Emission Scanning Electron Microscopy equipped with Energy Dispersive Spectroscopy and Fourier Transformed Infrared Spectroscopy in order to investigate the deposition of hydroxyapatite.
The pH of SBF after soaking of the samples is 7.6 for the uptake solutions of the bulk samples and 7.9 for the uptake solution of the powder samples and both these values are in the physiological range.
The powder samples were analyzed at 3, 7 and 14 days with FTIR (in pellets of KBr) and at 7 and 14 days by means of Field Emission Scanning Electron Microscopy.
The FTIR spectra of the CEL2 powder samples both bare and functionalized after 0, 3, 7, and 14 days of soaking in SBF are reported in Figure 2.50.

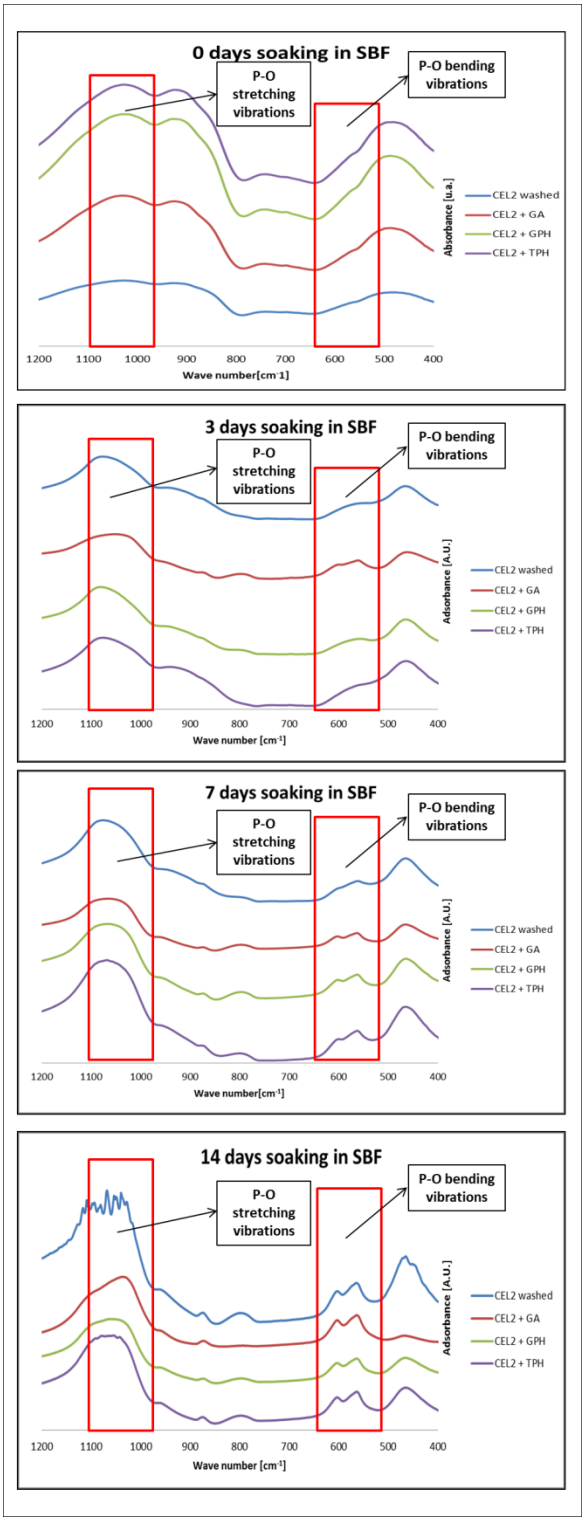

Figure 2.50: IR spectra of CEL2 powder bare and functionalized after different times of soaking in SBF. Analysis performed in transmission on pellets of the samples with KBr.

The presence of the double peak at 600 cm^{-1} and 560 cm^{-1} ant the intensification of the peak at 1025 cm^{-1} are the principal signals of the presence of hydroxyapatite on the samples and are correlated respectively with bending of the P-O bonds and with stretching vibration of phosphate in the apatite structure [156], [161]–[163].

After 3 days of soaking, these signals are well present on the samples with gallic acid and after 7 days are present on all the functionalized samples while are lower present in the spectrum of the bare one. After 14 days of soaking, the hydroxyapatite is well present on all the samples.

The FESEM micrographs of the powders samples after 7 and 14 days of soaking in SBF are reported in Figure 2.51.

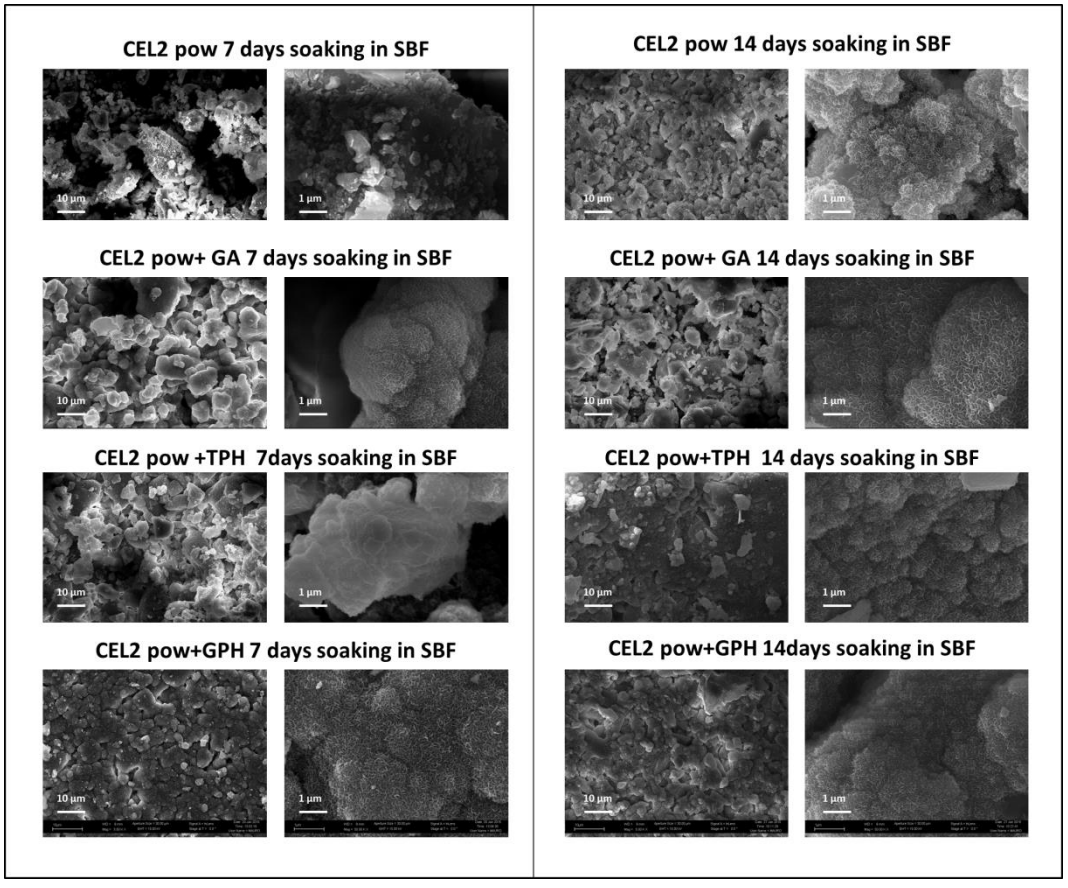

Figure 2.51: FESEM micrographs of powder glass samples after 7 and 14 days of soaking. 5.00 kX magnification and 50.00 kX magnification.

The presence of hydroxyapatite is visible for all the samples. At greater magnification the structure of the hydroxyapatite is visible. This analysis was performed also on the bulk samples, because powder samples after the drying and manipulation needed for the FESEM analysis may face the detachment of the hydroxyapatite.
These results are reported in Figure 2.52.

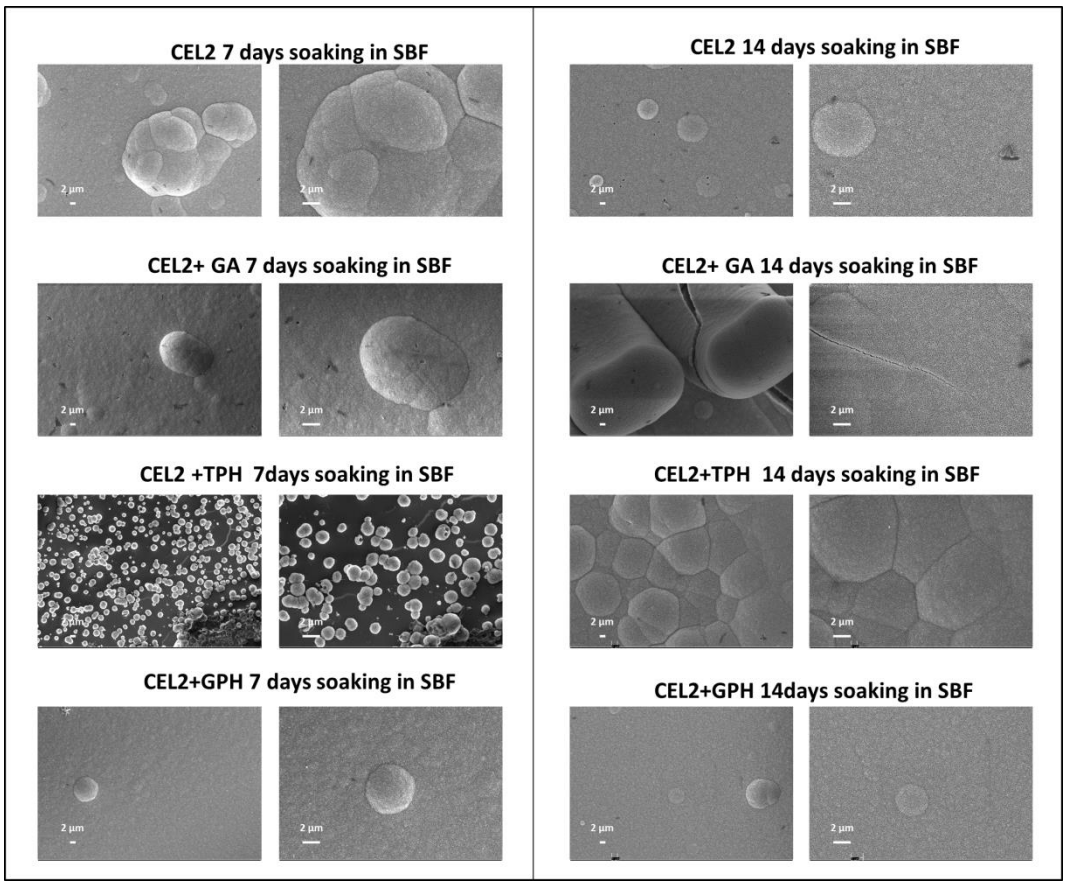

Figure 2.52: FESEM micrographs of bulk glass samples after 7 and 14 days of soaking. 5.00 kX magnification and 10.00 kX magnification.

After 7 days of soaking a lot of precipitates are present on the surface of all the samples and the EDS analysis reported in Table 2.18 confirms the presence of Ca and P with a ratio comparable with the stoichiometric one (1.67) of Hap[164].

Table 2.18: (a) EDS results of the bulk glass samples after 7 and 14 days of soaking in SBF. (b) Ca/P ratio.

(a)	Samples							
	CEL2 washed		**CEL2 + GA**		**CEL2 + GPH**		**CEL2 + TPH**	
Elements (weight %)	*7 days soaking*	*14 days soaking*	*7 days soaking*	*14 days soaking*	*7 days soaking*	*14 days soaking*	*7 days soaking*	*14 days soaking*
C	7.26	5.76	5.11	4.79	5.42	7.97	9.37	5.14
O	64.24	54.42	54.62	52.55	58.09	56.05	50.62	55.86
Na		0.64	-	-	-	-	-	-
Mg	0.93	0.64	0.67	0.8	0.74	0.77	1.94	1.15
Si	-	-	-	-	-	-	4.98	-
P	9.52	12.08	11.37	12.12	11.09	11.37	10.54	12.72
Ca	13.03	21.64	21.76	23.44	18.83	18.54	17.85	21.14
Cr	5.02	4.81	6.33	6.3	5.82	5.31	4.7	4.92

(b)	Samples							
	CEL2 washed		**CEL2 + GA**		**CEL2 + GPH**		**CEL2 + TPH**	
	7 days soaking	*14 days soaking*	*7 days soaking*	*14 days soaking*	*7 days soaking*	*14 days soaking*	*7 days soaking*	*14 days soaking*
CA/P ratio	1.37	1.79	1.91	1.93	1.69	1.63	1.69	1.66

After 7 days of soaking, the surfaces of the samples are already covered by hydroxyapatite, data confirmed by the absence of silicon in EDS analysis, the samples functionalized with the polyphenols of tea is an exception because the substrate is still visible and several spot of Hap are present.

At 14 days a uniform layer rich of Ca and P is present on the surface of all the samples.

The "cauliflower-like" structure, characteristic of HAp is present on the bare CEL2 sample, while different morphology can be observed for the functionalized ones.

The samples functionalized with tea polyphenols show a globular structure at 7 days and a carpet like structure after 14 days, due to the growth of the HAp globe that become attached one to each other.

From 7 days, the samples functionalized with the polyphenols of red grape skins show a carpet like structure that become thicker during time.
The samples functionalized with gallic acid show at 14 days a "column-like" structure of the Hap.
Polyphenols are able to regulate the precipitation and the nucleation of HAp and this can be attributable to the interaction between phenolic hydroxyl groups and Ca^{2+} ions [141], [165].

Titanium alloy

The bioactivity of the CT surfaces bare and functionalized with GA was tested by means of soaking in SBF for 28 days.
The pH was monitored during the tests and a small decrease from 7.4 to 7.2 ±0.1 for CT samples and 7.3 ±0.1 for CT_SBF+GA_1 samples was noted after the first 3 days of soaking. This decrease could be related to a partial release of the molecules from the surface of the functionalized samples, but also to the tendency of the –OH groups on the CT surface to dissociate H+ ions.
During the following refresh there were no changes in the pH.
The FESEM analyses on the samples after 28 days of soaking are reported in Figure 2.53.

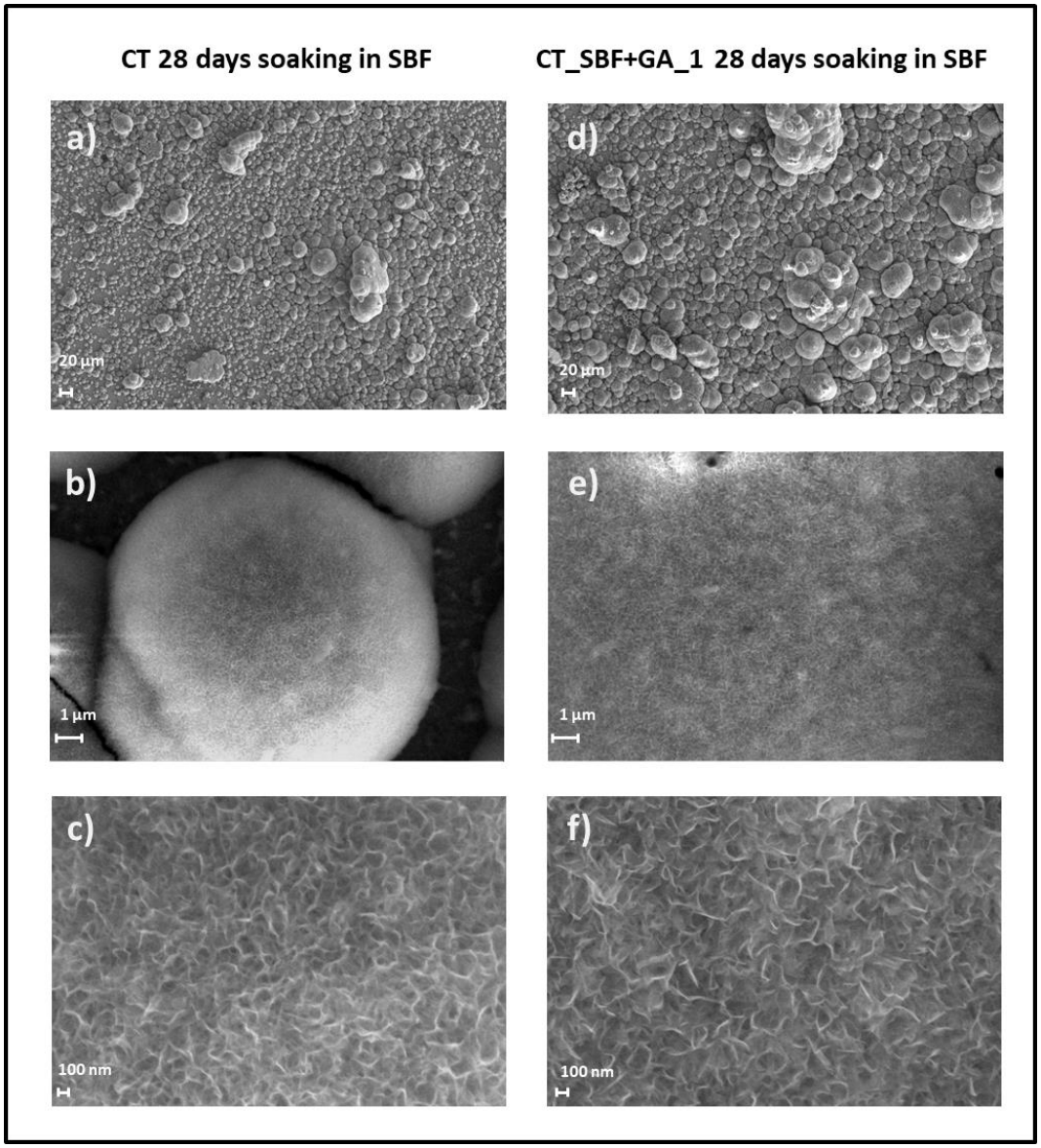

Figure 2.53: FESEM images of CT samples bare and functionalized with gallic acid after 28 days SBF soaking. a, d,) 500x magnification; b,e,) 20000x magnification; c, f,) 100000x magnification.

The micrographs reported in Figure 2.52 show that the bare CT samples after 28 days of soaking is covered by a carpet of "cauliflower-like" HAp and the same result is observable for the samples CT_SBF+GA_1.
The samples CT, like observed in previous work[123] has a great bioactive behavior and no significant change seems to be induced by the amount of gallic acid on the functionalized samples. The column-like structure of HAp observed on the samples of CEL2 glass functionalized with the gallic acid in this case is not

visible probably because the low amount of gallic acid or to a different configuration of the grafting with the surface of the titanium alloy.
EDS analyses were performed on different areas (106400 μm^2) of the samples (Figure 2.54) and the results are reported in Table 2.19.

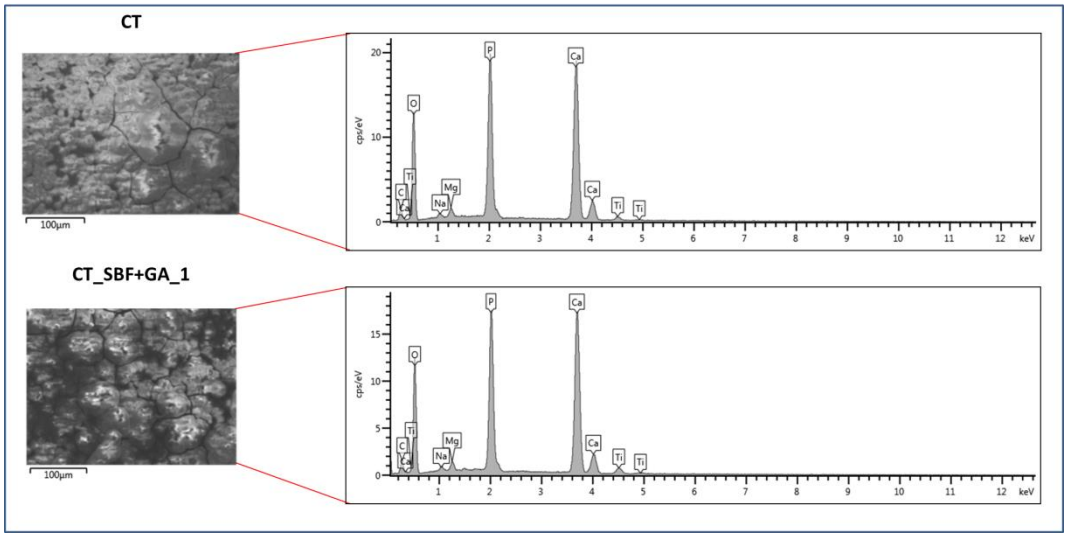

Figure 2.54: samples areas analyzed with EDS.

Table 2.19: Atomic percentages of the elements detected on the CT samples after 28 days of soaking in SBF by EDS survey.

Elements [%at]	**Samples**	
	CT	CT_SBF+GA_1
C	7.54±3,06	7.59±2.96
O	55.10±10,85	55.09±10.86
Na	0.48±0,03	0.45±0.03
Mg	0.73±0,07	0.75±0.07
P	13.32±3,54	12.71±3.37
Ca	22.18±9,68	22.18±9.67
Ti	0.78±0,42	1.25±0.67
Ca/P ratio	1.63±0.3	1.7±0.3

Both the samples present Calcium and Phosphorous on the surfaces with the radio (Ca/P) 1.63 ±0.3 for the CT samples and 1.70±0.3 for the CT_SBF+GA_1

samples. The ratios of the two samples are comparable with the stoichiometric one of hydroxyapatite (1.67) [164].

2.6.6 Evaluation of the free radical scavenging activity by means of Electron Paramagnetic Resonance

The antioxidant properties of CEL2 glass before and after the functionalization were investigated by suspension of the powder samples in a buffer solution with H_2O_2 and DMPO with the procedure described in paragraph 2.5.11.
The suspensions were analyzed by means of Electron Paramagnetic Resonance (EPR) and the intensity of the signals obtained with a double integration of the spectra are proportional to the OH• concentration.
The signal intensities after 5, 10 and 30 minutes of UV irradiation are reported in Figure 2.55.

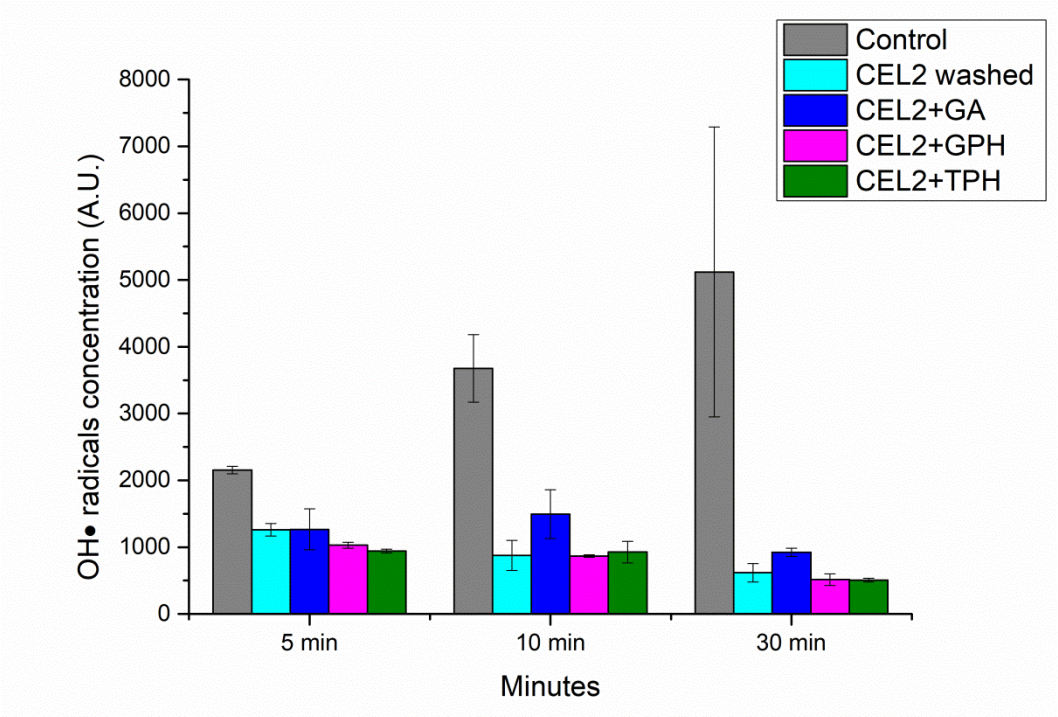

Figure 2.55: 8. Scavenging activity of HO• generated by photolysis of H_2O_2 of buffered suspensions of CEL2 powder bare and functionalized. The same experiment in the absence of the glass powder was carried out as control.

The intensities recorded for each type of sample is significantly ($p<0.05$) than the positive control and all the tested samples have scavenging activity of OH• radicals obtained by photolysis of H_2O_2.

The bare CEL2 shows scavenging activity even without the presence of polyphenols and the chemical reaction needs to be further investigated, however in literature are reported evidences of the antioxidant ability of silica hydride that is well present on the surface of the bioactive glass [166], [167].

After 5 minutes of irradiation, the scavenging activity of CEL2+TPH is higher ($p<0.05$) then the one of bare CEL2, but no significant difference were detected between the CEL2 sample and CEL2+GA and CEL2+GPH.

After 10 and 30 minutes no significant differences between the samples are notable.

The little increment in the scavenging activities showed by the samples with tea polyphenol can be correlated with the antioxidant properties of polyphenols[1], [2], [5], [11], [13], [20], [24].

The lack of scavenging activity showed by GA and GPH at each time tested and by TPH at longer times of irradiation may be due to their consumption following reaction with HO• or to UV degradation.

2.5.12 Cellular tests

Cells (U2Os and hFOB)

- Direct cytotoxicity

The results of the U2OS and hFOB cells culture on the surface of the glass samples for 1, 3 and 7 days investigated by means of their toxicity by the metabolic MTT assay are reported in Figure 2.56.

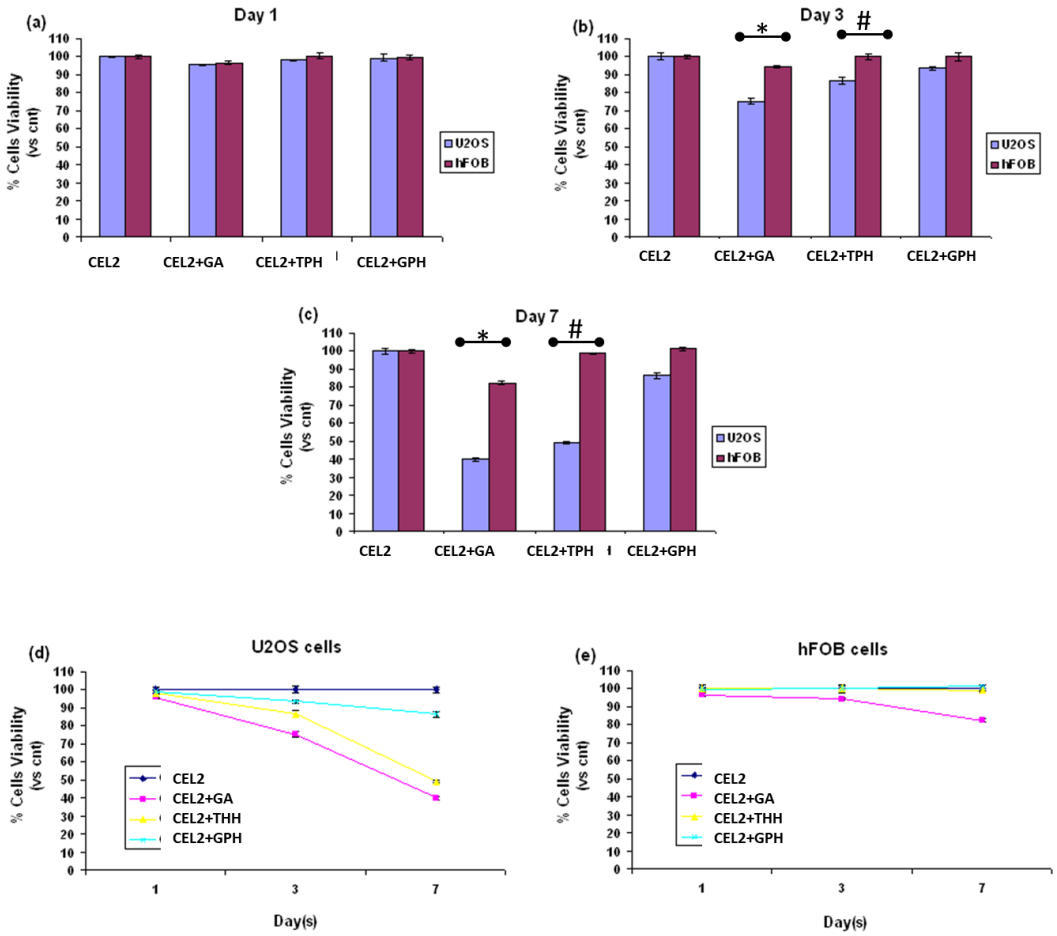

Figure 2.56: Direct cytotoxicity evaluation of cells U2OS and hFOB on CEL2 glass samples. * and # mean $p<0.05$ with t-student test.

After the first day of culture (Figure 2.56a) there is no significant difference between the viability of the different cells on the different samples.

After 3 days of culture (Figure 2.56b) a first selection in terms of viability starts to appear between healthy and tumoral cells for samples CEL2+GA and CEL2+TPH. The viability of U2OS cells decreases to 75% for the samples with GA and to 82% for the samples with TPH, while is around 94-99% for the hFOB cells. For the control samples CEL2 and the samples CEL2+GPH, no significant differences are visible between the two cells line.
After 7 days (Figure 2.56c), the selective activity of CEL2+GA and CEL2+TPH samples against tumoral cells reduces the viability of these cells x about 60% and 51% respectively, while the viability of healthy cells remain around 82-98%.
In Figure 2.56 d and e cell viability in function of times on the different samples are reported.
The tumoral cells U2OS have a significant decrease in viability after 7 days on CEL2+GA and CEL2+TPH while the hFOB viability is still >80% with no significant difference with the untreated control samples.
From this study, it results that CEL2 is in vitro cytocompatible like founded in previous work [146] and was used as control sample for the functionalized samples.
After functionalization, a different trend between the cell viability of U2OS and hFOB is reported, in particular with GA and TPH with a clear reduction of the count of tumoral cells. The growing trend GPH<TPH<GA is particularly evident after 7 days of culture. The ability of the functionalized surface of having selective effects against tumoral cells is in accordance with the results present in literature about the selective cytotoxicity of polyphenols against cancer cells[53], [55], [132], [168], [169].
In order to better understand polyphenol action mechanism of RONS and DNA damage evaluation were performed.

- RONS evaluation

The production of reactive species of oxygen and nitrogen in response to the contact with bare and functionalized CEL2 glass were studied and compared during 3 days in function of time and the results are reported in Figure 2.57. Tea polyphenols were preselected for functionalization with natural molecules on the bases of the direct test.

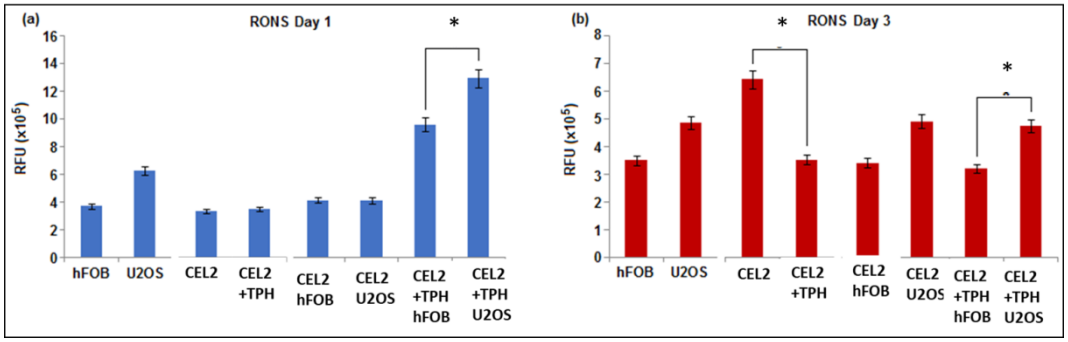

Figure 2.57: evaluation of RONS produced by cells, samples and samples with cells after a) 24h and b) 72h. $p<0.05$ indicated by *.

After the first 24 h of incubation, there are no significant differences between the RONS produced by the cells, the glass bare and functionalized without cells culture and the bare CEL2 samples with cells culture. However a significant difference appears for the samples CEL2+TPH between the two types of cells, hFOB and U2OS.

After 72h (Figure 2.57b), more differences are present between the samples tested and the functionalization with polyphenols decreases the RONS amount compared with the bare glass. When cell are present on the surface of the glass, the RONS amount is higher for the U2OS cells as previously seen at 24h.

The test reveals a certain amount of RONS in presence of cells without material due to their metabolic activity [170]. Also the presence of the bioactive glass bare or functionalize induce production of reactive species that can be correlated with the reactivity of the surfaces and is similar to the one of the cells alone, without differences between the functionalized and the bare samples at 24h.

However after 3 days a significant difference is present between CEL2 and CEL2+TPH samples because of the ability of tea polyphenols to reduce the RONS production. When both samples and cells are present, an increase of the RONS production for cancerous cells U2OS is recorded on CEL2+TPH samples, while an antioxidant and anti-inflammatory activity appears for the healthy cells on the same samples.

These results highlighted a selectivity action of the polyphenols just seen in the direct cell test. Tumoral cells showed higher level of inflammation that can be related to the minor viability seen in the MTT assay and this is correlated with the high sensitivity of cancer cells towards RONS that are largely discussed in literature[53], [55], [171], [172]. Is also reported in literature that gallic acid, catechins (abundant in tea extracts) and trans resveratrol (well present between

grape polyphenols), can modify the pathway involved in cancer generation and cause selective apoptosis of cancer cells[12], [20], [27], [43]–[45], [55], [173].

- DNA damage evaluation

In order to evaluate the DNA damage induced by polyphenols U2OS were cultivated for 3 days onto the surfaces of CEL2 and CEL2+TPH samples. After the culture the localization of 53BP1 was investigated using a fluorescence microscope and the results are reported in Figure 5.58a.
With the nuclear DAPI staining (blue dye), it is possible to note that U2OS are able to form tumor aggregates on bare CEL2, while single cells are dispersed at the surface of CEL2+TPH samples.
53BP1 signals (green dye) are most present inside the nuclei (highlighted by green arrows) confirming that a DNA damage occurred.
In the end, in order to understand if the tumoral cells are able to restore their DNA, Cyclin B1 staining was applied and the results are reported in Figure 5.58b. Also Cyclin B1 is mostly present inside the nuclei demonstrating that the tumoral cells cultured on CEL2+TPH are not able to restore their DNA

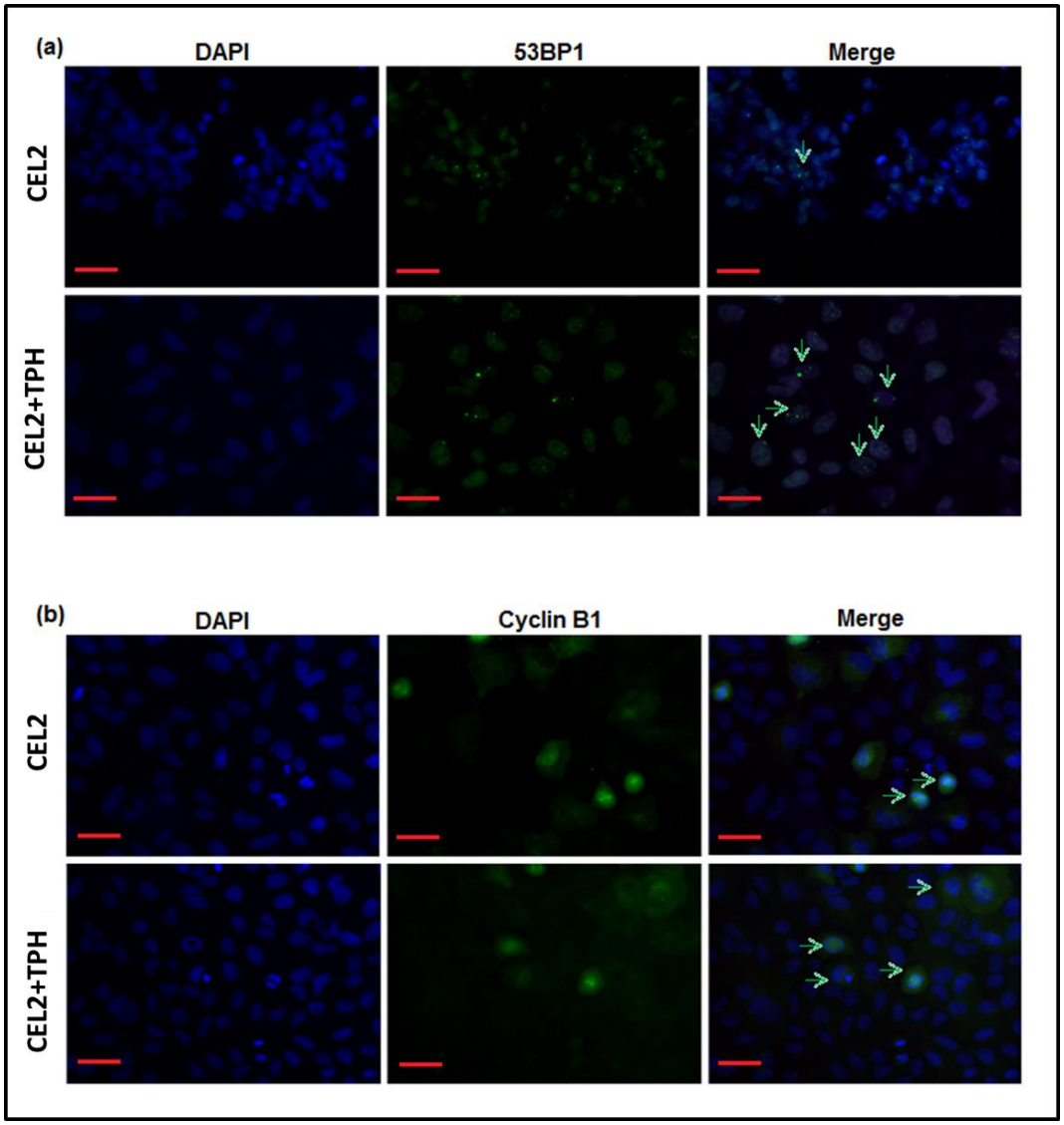

Figure 2.58: DNA damage evaluation. (a) DAPI staining (blue day), 53BP1 staining (green dye), (b) DAPI staining (blue day), cyclin B1 staining (green dye).

These results confirm the ability of polyphenols to have a selective effect against bone tumor cells. This effect can be correlated with the production of RONS in the tumoral cells with a consequent selective and irreversible DNA damage.
At the same time an anti-inflammatory action is evidenced on the healthy osteoblasts.

- Indirect cytotoxicity tests

The viability of cells cultured on 1,2,3,5 and 7 days samples' surnatans is reported on Figure 2.59.

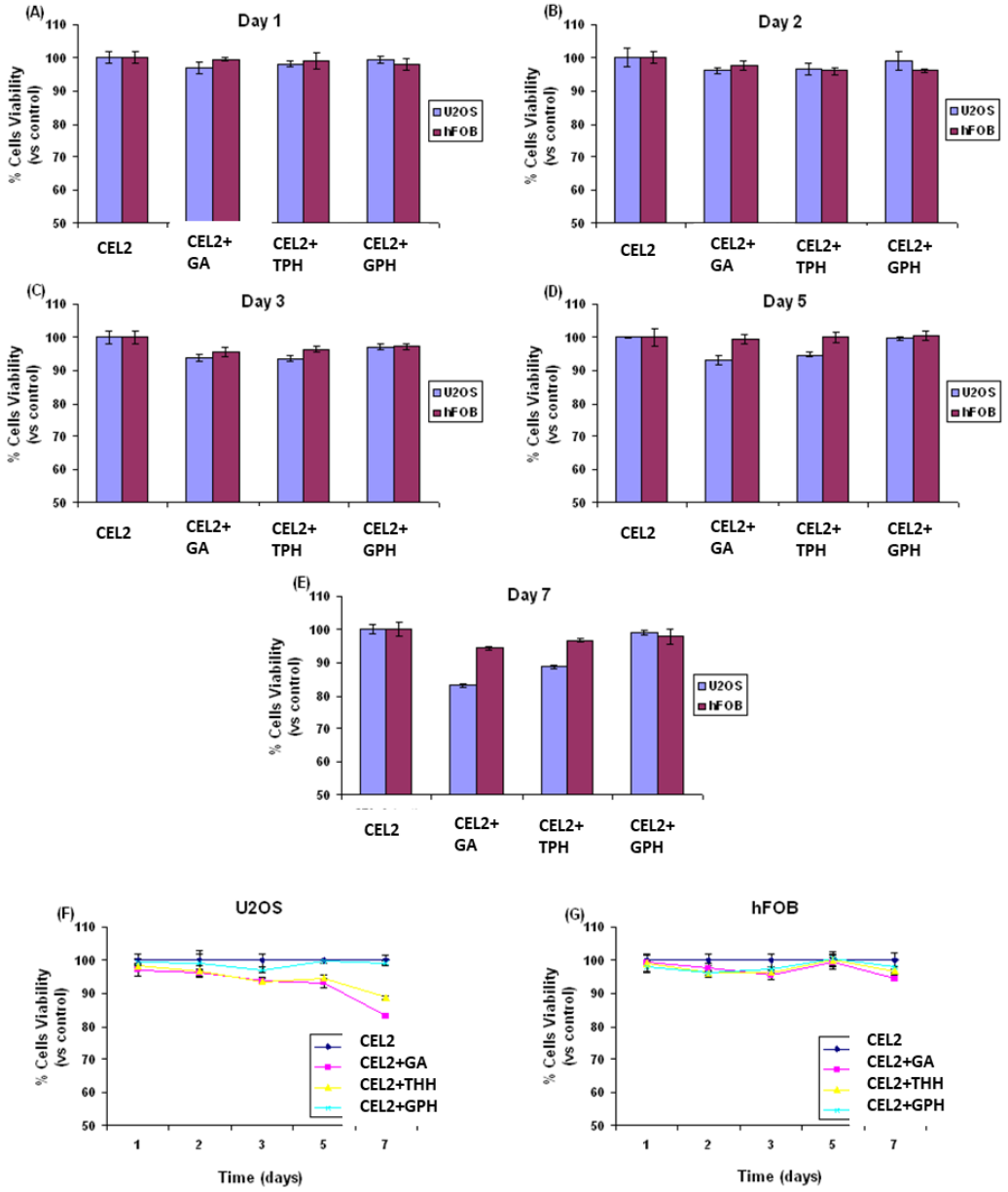

Figure 2.59: indirect evaluation cell test. Cells cultured on 1(a), 2(b), 3(c), 5(d) and 7(e) days samples' supernatants.

No differences can be evidenced between the samples in the first three days (Figure 2.59 a, b, c). For the 5 and 7 days culture a reduction in term of viability around 15-20% is notable for U2OS cell cultivated with CEL2+GA and CEL2+TPH surnatans. Between hFOB and U2OS viability, a significant difference can be observed for CEL2 and CEL2+TPH, while there are no

differences for CEL2+GPH. A reduction of cell viability is observable for U2OS on the surnatans of samples with GA and TPH in comparison with the bare glass control and no differences are being found for the healthy cells hFOB.
The viability reduction of the cancer cells is minor for the indirect tests compared with the direct ones and this result can be explained with the release tests performed on glass samples during the master thesis [121]. With spectroscopic analysis with the Folin&Ciocalteu methods it was founded that after 7 days of immersion in water, a great amount of the biomolecules were still grafted to the surface of the samples while only a small part was released. This result explains the reason because of the polyphenols are effective when the cells are directly seeded onto the surface while are less effective when cells are seeded with the surnatans of the samples.
The lower effects of the samples functionalized with GPH in both direct and indirect tests can be explained with the Folin&Ciocalteu tests performed on the functionalized samples that highlight a smaller amount of polyphenols compared with the samples functionalized with GA or TPH.

Cells (KUSA A1)

Titanium alloy

After the Kusa A1 cell culture on the samples CT and CT_SBF+TPH_1 with normal medium (NORM) or medium with osteoinductive factors (OF), FTIR spectra were acquired between 400cm^{-1} and 400 cm^{-1} and the results are reposted in Figure 2.60.

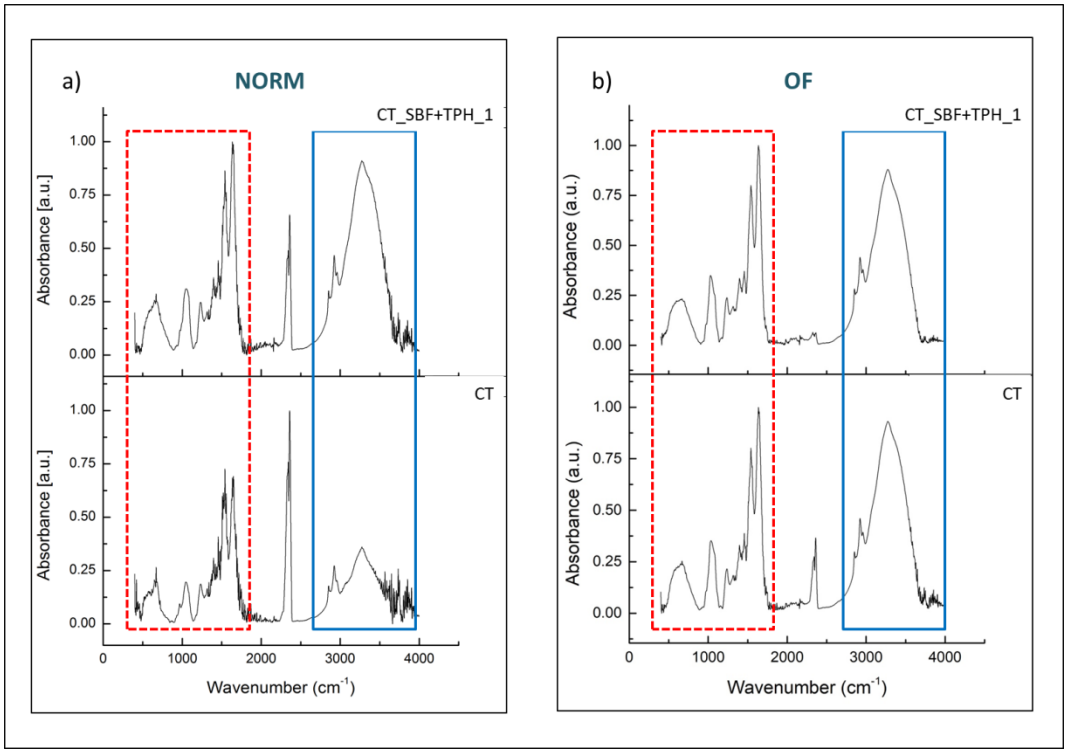

Figure 2.60: FITR spectra of samples CT and CT_SBF+TPH_1 cultured with a) normal medium (NORM), b) medium with the osteoinductive factors (OF).

The main differences between the spectra of the samples CT and CT_SBF+TPH_1 with the two different media are indicated by the red rectangle between 400 cm^{-1} and 1700 cm^{-1} and the blue rectangle between 2700 cm^{-1} and 3600 cm^{-1} .

For sample in the normal medium (Figure 2.60a), in the region in red, signals from protein vibrations and PO_4 vibration of hydroxyapatite between 400 and 600 cm^{-1} are present. The signals between 960 and 1100 cm^{-1} are due to the presence of HAp and they are higher for the spectra on the CT_SBF+TPH_1 samples.

At 1540 cm^{-1} and 1645 cm^{-1}, the bands of amide I and II, have different behavior for CT and CT_SBF+TPH_1 samples and this is clearly noticeable in the case of samples immersed in media without osteoinductive factors (Figure 2.60a).

The samples with tea polyphenols show more intense bands highlighting an increase of protein compounds, mainly collagen type I, and that suggests the ability of polyphenols to improve the formation of collagen matrix.

The signals in the red rectangle are due to the C-H stretching of proteins, vibration modes of CH_2 of lipids and to the collagen formation (2800-300 cm^{-1}). The large band between 3000-3600 cm^{-1} is correlated with the O-H stretching of water and organic compounds.

For the samples cultured in the normal medium these bands are more intense for the CT_SBF+TPH_1 samples.
Observing the two highlighted parts of the spectra it is possible to suppose that the mesenchymal stem cells Kusa A1 were differentiated into osteoblasts with deposition of hydroxyapatite and collagen because the bioactive properties of the substrate. This bioactive behavior was improved by the presence of polyphenols with an increase in the deposition of mineralized and non-mineralized extracellular matrix[162], [174]–[176].
In Figure 2.60b, for the samples cultured with osteoinductive factors, the signals of interest are present, but there are no significant differences between bare and functionalized CT samples probably because the effects of the osteoinductive factors overcome the ones of polyphenols.
The deposition of the hydroxyapatite on the surface of the samples was also investigated with RAMAN spectroscopy and the results are reported in Figure 2.61.

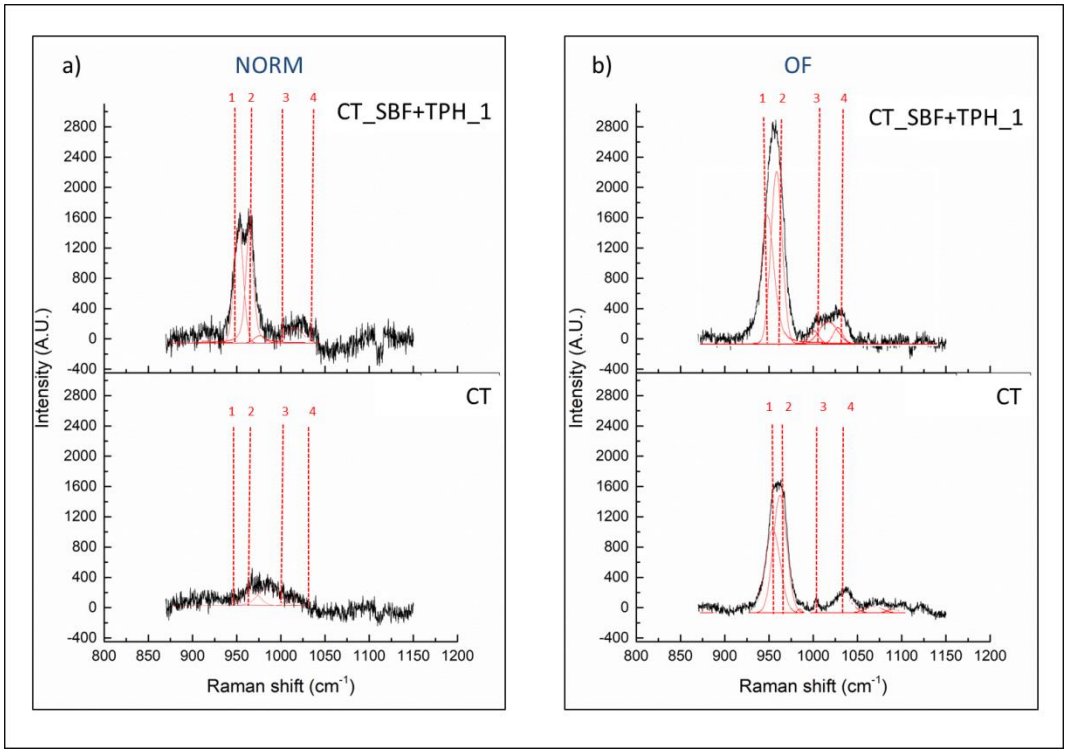

Figure 2.61: RAMAN spectra of Samples CT and CT_SBF+TPH_1 cultured with a) normal medium (NORN), b) medium with the osteoinductive factors (OF).

The main bands of interest are between 900 and 1050 cm^{-1}.
The samples cultured in the normal medium (Figure 2.61a) show peaks barely visible for the CT samples, while they are clearly present for the CT_SBF+TPH_1 samples.
This result is in agreement with the one obtained with FTIR measurements and suggests a higher deposition of HAp on the samples with polyphenols.
Deconvolution of this band into two peaks numbered with 1 and 2 at 940 cm^{-1} and 960 cm^{-1} it is possible to observe the components due to vibration of amorphous HAp (peak number 1) and crystalline Hap (peak number 2) [177], [178].
For the samples CT_SBF+TPH_1 the two peaks have the same intensity suggesting a similar amount of amorphous and crystalline Hap.
For the samples cultured with the osteoinductive factors (Figure 2.61b) , the band of HAp is well visible both for CT and CT_SBF+TPH_1 samples with the same intensity ratio 1.5 between crystalline/amorphous HAp, but for the samples with the polyphenols the observed intensity is higher. This result could be correlated with osteoinductive effects of the polyphenols synergistically with the osteoinductive factors not revealed by FTIR measurements.
At 1004 cm^{-1} with number 3 is signaled the presence/absence of the phenylalanine bands. This peak is clearly visible for the samples cultured with the osteoinductive factors while for the samples cultured with the normal medium is absent or barely visible. This band is used as a cellular viability indicator and is a little bit higher for the samples functionalized with polyphenols confirming the effect of polyphenols on cells increasing matrix deposition.
With number 4 is indicated another feature of the spectra at 1035 cm^{-1} due to the vibrational mode collagen compounds. This band is clearly present for the samples with osteoinductive factors and in particular for the samples functionalized with polyphenols suggesting one more time a stimulating effect of polyphenols on cells.
In Figure 2.62 are reported the volumes of extracellular matrix of the samples cultured with normal or enriched medium, analyzed with laser microscope.
The presence of the osteoinductive factors enhance the amount of the deposited extracellular matrix for both CT and CT_SBF+TPH_1 samples, but with both the type of cultures the presence of polyphenols allows cells to deposit an higher amount of extracellular matrix showing the stimulating effects of polyphenols on Kusa A1 cells.

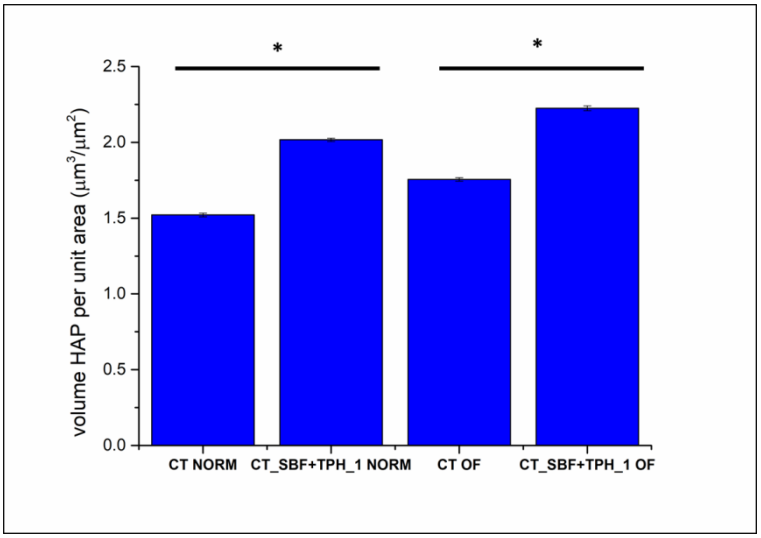

Figure 2.62: extracellular matrix quantification on the surface of the samples CT and CT_SBF+TPH_1 after the cell culture with the normal medium (NORM) and with the osteoinductive factors (OF). (*$p<0.01$).

The results of the fluorescence microscope images on samples CT and CT_SBF+TPH_1 with Kusa A1 culture are reported in Figure 2.63. The probe used was blue for nuclei (DAPI), red for dead cells (PI) and green for osteocalcin (Hoechst33342).

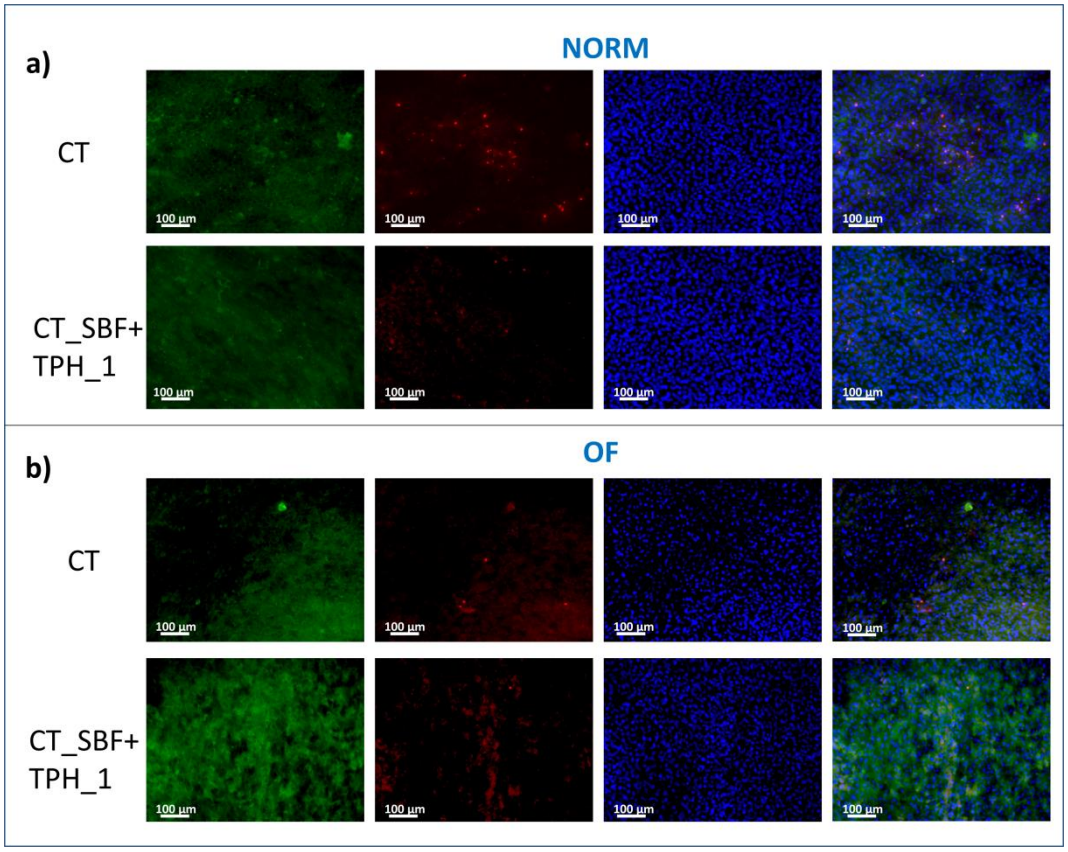

Figure 2.63: Fluorescence images obtained using blue probe for cell nucleus (DAPI), Red probe for dead cells (PI) and green probe for osteocalcin (Hoechst33342). The images were performed at 20x magnification and in Figure 5a are reported the results of the samples cultured with the normal medium (NORM) and in Figure 5b the results of the medium cultured with the osteoinductive factors (OF).

The blue probe highlights a high number of cells on all the samples.
The green probe shows the presence of osteocalcin, signal of the differentiation the mesenchymal stem cells Kusa A1 into osteoblasts with deposition of hydroxyapatite.
In Figure 2.63a osteocalcin is well visible on the surface of sample CT around cells, while for the sample CT_SBF+TPH_1 the amount of osteocalcin is higher and overlaying the cells.
For the culture performed with osteoinductive factors (Figure 2.63b), the amount of osteocalcin is high ant this protein is accumulated in one point for the sample CT and well dispersed for the sample with the polyphenols.

The red probe marks the nuclei of dead cells and a reduction of the apoptosis is visible for the functionalized samples both with and without osteoinductive factors.
The effect of the tea polyphenols on the up regulation of osteocalcin is already reported in literature[179] and is only one of the effects attributable to the polyphenols.
Tea polyphenols can promote osteoblasts differentiations trough RunX2 transcription activity[180] and by mean of the upregulation of other related genes. Osteoblasts in contact with polyphenols showed higher expression of bone morphogenic proteins and alkaline phosphatase with a greater degree of mineralization [181].An increased collagen deposition, as observed in FTIR was already reported in [182].

2.7 Conclusions

The work exposed in this chapter deals with surface functionalization of silica based bioactive glass CEL2 and titanium alloy Ti6Al4V with polyphenols. The protocol of functionalization of the glass developed during the Master thesis work was optimized in order to maximize the grafting of the polyphenols to the surface and to minimize the molecules degradation due to pH increase and alkalinizing power of the glass itself.

The presence and the activity of polyphenols were characterized by means of spectroscopic measurements with the Folin&Ciocalteu method. The presence of the polyphenols on the surfaces of the glass samples was also checked with XPS analysis, contact angles evaluation and fluorescence microscope observation.

These analyses showed the presence of all the kinds of polyphenols tested (GA, TPH and GPH) on the surface of the glass samples confirming the success of this functionalization protocol. The antioxidant activity of the polyphenols bonded to the glass surface was tested with EPR analysis and the glass itself showed scavenging activity against ROS: this activity was a little bit improved by tea and red grape skins polyphenols. Bioactivity of the samples was tested by soaking in Simulated body fluid SBF until 14 days before and after functionalization. The samples after the soaking were characterized with FESEM and FTIR analysis that highlighted the ability of the biomolecules of accelerating the kinetics of deposition of hydroxyapatite and to influence also the structure of the hydroxyapatite itself.

Concerning the use of glass as bone filler after tumor resections, the selective activity of the polyphenols against bone cells was tested highlighting a reduction of the viability of tumoral cells on the surface of the samples functionalized with TPH and GA, while the viability of healthy cells remained almost comparable with the one of the control bar CEL2 samples. The mechanism of actions of the polyphenols against tumoral cells was more in depth investigated with evaluation of RONS and DNA damage. The detection of RONS on surnatans of tumoral cells cultured on the surface of the samples functionalized with tea polyphenols was higher than the one detected for the healthy cells suggesting a role of the polyphenols on the regulation of reactive species production that could damage tumoral cells. DNA damage was detected and cells could not repair it. Furthermore cancer cells seemed to not form typical tumoral aggregate on the surface of the functionalized samples, while it is possible to see them on the surface of the bare CEL2 samples. This anti-aggregative property is another possible way of actions of polyphenols against tumoral cells, but this result needs

further investigations. Starting from the experience with glass and from literature, a protocol for the functionalization of the chemically-treated Titanium alloy Ti6Al4V. Different media, concentrations and times of functionalization were tested for gallic acid, green tea polyphenols and red grape pomace polyphenols. The Simulated body fluid SBF allowed to obtain the better results because its pH allows the deprotonation of the polyphenols, in the case of the glass this role was performed by the alkalinizing power of the glass itself, and because of the presence of calcium, present also in the composition of the bioactive glass, which seemed to be able to guide the deposition of the biomolecules onto the surface, acting as a bridging ion.

Presence and activity of polyphenols were characterized by means of spectroscopic measurements with the Folin&Ciocalteu method, contact angles measurements and XPS measurements as performed for glass samples.

The amount of polyphenols grafted to the surface of the chemically-treated titanium alloy is lower than the one found on the surface of the bioactive glass and this fact is due to the lower reactivity of the CT surface compared with the CEL2 one. Contact angle measurement, contrary to what observed for the glass, showed that functionalization with natural polyphenols did not decrease the wettability of the surfaces and that could suggest the ability of these two surface of grafting different molecules from the natural extract mixtures. However, being the contact angles detected on the two surfaces functionalized with TPH similar, it could also mean that this is the contact angle of the tea polyphenols.

The main purpose of the chemically-treated titanium alloy surface is osteointegration and bioactivity tests were performed in order to evaluate this aspect. For the investigation of osteointegrative ability of the titanium alloy before and after functionalization, in vitro bioactivity tests were performed by soaking in SBF and mineralization ability was evaluated by with cell cultures.The samples soaked in SBF for 14 and 28 days were investigated by means of FESEM observation and the presence of gallic acid, contrary to what observed for glass, did not enhance the kinetic of deposition because of the lower presence of the polyphenols. Different results were obtained with the analysis performed with mesenchymal stem cells culture onto the surfaces of CT and CT_SBF+TPH_1.

The samples after the culture were investigated with laser microscope, Raman, FTIR and with fluorescence microscope observations. The chemically treated titanium alloy surface itself was able to induce osteoblasts differentiations, but the presence of the polyphenols showed the ability to enhance the deposition of mineralized and non-mineralized extracellular matrix highlighting the osteoinductive effect of polyphenols.

These results suggest that the biomaterial surface functionalization is a promising field for the combination of polyphenols properties with those of biomaterials. It is possible to confer to biomaterial surfaces new properties using natural molecules with high value, but low price, available from the wine and food industries waste.

References:

[1] H. El Gharras, "Polyphenols: Food sources, properties and applications - A review," *Int. J. Food Sci. Technol.*, vol. 44, no. 12, pp. 2512–2518, 2009.

[2] K. B. Pandey and S. I. Rizvi, "Plant polyphenols as dietary antioxidants in human health and disease.," *Oxid. Med. Cell. Longev.*, vol. 2, no. 5, pp. 270–8, 2009.

[3] H. s. Friedman, M.; Jurgens, "Effect of pH on stability of plant phenoliccompounds," *J. Agric. Food Chem.*, vol. 48, pp. 2101–2110, 2000.

[4] F. Saura-Calixto, J. Serrano, and I. Goñi, "Intake and bioaccessibility of total polyphenols in a whole diet," *Food Chem.*, vol. 101, no. 2, pp. 492–501, 2007.

[5] L. Bravo, D. Sources, and N. Significance, "Polyphenols: chemistry, dietary sources, metabolism, and nutritional significance.," *Nutr. Rev.*, vol. 56, no. 11, pp. 317–333, 1998.

[6] R. Kushwaha and S. Karanjekar, "A critical review of methods for characterisation of polyphenolic compounds in fruits and vegetables," *Int. J. ChemTech Res.*, vol. 3, no. 3, pp. 1033–1036, 2011.

[7] F. Shahidi and M. Naczk, *Phenolics in food and nutraceuticals*. 2006.

[8] J. P. E. Spencer, M. M. Abd El Mohsen, A.-M. Minihane, and J. C. Mathers, "Biomarkers of the intake of dietary polyphenols: strengths, limitations and application in nutrition research.," *Br. J. Nutr.*, vol. 99, pp. 12–22, 2008.

[9] W. Vermerris and R. Nicholson, "Families of phenolic compounds and means of classification," in *Phenolic Compound Biochemistry*, 2006, pp. 1–34.

[10] et al. Manach C, Scalbert A, Morand C, "Polyphenols: Food sources and bioavailability," *Am. J. Clin. Nutr.*, vol. 79, pp. 727–747, 2004.

[11] R. Tsao, "Chemistry and biochemistry of dietary polyphenols," *Nutrients*, vol. 2, no. 12, pp. 1231–1246, 2010.

[12] S. Verma, A. Singh, and A. Mishra, "Gallic acid: Molecular rival of cancer," *Environ. Toxicol. Pharmacol.*, vol. 35, no. 3, pp. 473–485, 2013.

[13] N. Balasundram, K. Sundram, and S. Samman, "Phenolic compounds in plants and agri-industrial by-products: Antioxidant activity, occurrence, and potential uses," *Food Chem.*, vol. 99, no. 1, pp. 191–203, 2006.

[14] R. J. Block and E. Al., "Tannins and polyphenols.," in *Manual of paper chromatography and paper electrophoresis.*, 1958, pp. 373–379.

[15] N. C. Cook and S. Samman, "Flavonoids-Chemistry, metabolism, cardioprotective effects, and dietary sources," *J. Nutr. Biochem.*, vol. 2863, no. Ldl, pp. 66–76, 2006.

[16] I. M. Toaldo *et al.*, "Effect of grape seeds on the polyphenol bioactive content and elemental composition by ICP-MS of grape juices from Vitis labrusca L.," *LWT - Food Sci. Technol.*, vol. 53, no. 1, pp. 1–8, 2013.

[17] J. Yu and M. Ahmedna, “Functional components of grape pomace: Their composition, biological properties and potential applications,” *Int. J. Food Sci. Technol.*, vol. 48, no. 2, pp. 221–237, 2013.
[18] C. C. Ratnasooriya and H. P. V. Rupasinghe, “Extraction of phenolic compounds from grapes and their pomace using Beta-cyclodextrin,” *Food Chem.*, vol. 134, no. 2, pp. 625–631, 2012.
[19] V. Amico, R. Chillemi, S. Mangiafico, C. Spatafora, and C. Tringali, “Polyphenol-enriched fractions from Sicilian grape pomace: HPLC-DAD analysis and antioxidant activity,” *Bioresour. Technol.*, vol. 99, no. 13, pp. 5960–5966, 2008.
[20] A. Van de Wiel, P. H. M. Van Golde, and H. C. Hart, “Blessings of the grape,” *Eur. J. Intern. Med.*, vol. 12, no. 6, pp. 484–489, 2001.
[21] E. Xia, X. He, H. Li, S. Wu, S. Li, and G. Deng, “Biological Activities of Polyphenols from Grapes,” *Polyphenols Hum. Heal. Dis.*, vol. 1, pp. 47–58, 2013.
[22] Q. Deng, M. H. Penner, and Y. Zhao, “Chemical composition of dietary fiber and polyphenols of five different varieties of wine grape pomace skins,” *Food Res. Int.*, vol. 44, no. 9, pp. 2712–2720, 2011.
[23] L. Rustioni, S. Fiori, and O. Failla, “Evaluation of tannins interactions in grape (Vitis vinifera L.) skins,” *Food Chem.*, vol. 159, pp. 323–327, 2014.
[24] J. Garrido and F. Borges, “Wine and grape polyphenols - A chemical perspective,” *Food Res. Int.*, vol. 54, no. 2, pp. 1844–1858, 2013.
[25] B. Dawn, “Resveratrol: Ready for prime time?,” *J. Mol. Cell. Cardiol.*, vol. 42, no. 3, pp. 484–486, 2007.
[26] J. A. Baur and D. A. Sinclair, “Therapeutic potential of resveratrol: the in vivo evidence,” *Nat. Rev. Drug Discov.*, vol. 5, no. 6, pp. 493–506, 2006.
[27] Y. Li, C. M. Bäckesjö, L. A. Haldosén, and U. Lindgren, “Resveratrol inhibits proliferation and promotes apoptosis of osteosarcoma cells,” *Eur. J. Pharmacol.*, vol. 609, no. 1–3, pp. 13–18, 2009.
[28] “http://supplementscience.org/resveratrol.html (18 August 2017, 4:21 pm).”
[29] D. Chen and Q. P. Dou, “Tea polyphenols and their roles in cancer prevention and chemotherapy,” *Int. J. Mol. Sci.*, vol. 9, no. 7, pp. 1196–1206, 2008.
[30] G. Rusak, D. Komes, S. Likić, D. Horžić, and M. Kovač, “Phenolic content and antioxidative capacity of green and white tea extracts depending on extraction conditions and the solvent used,” *Food Chem.*, vol. 110, no. 4, pp. 852–858, 2008.
[31] M. G. Ferruzzi, “The influence of beverage composition on delivery of phenolic compounds from coffee and tea,” *Physiol. Behav.*, vol. 100, no. 1, pp. 33–41, 2010.
[32] M. G. Sajilata, P. R. Bajaj, and R. S. Singhal, “Tea polyphenols as nutraceuticals,” *Compr. Rev. Food Sci. Food Saf.*, vol. 7, pp. 229–254, 2008.

[33] C. J. Dufresne and E. R. Farnworth, “A review of latest research findings on the health promotion properties of tea,” *J. Nutr. Biochem.*, vol. 12, no. 7, pp. 404–421, 2001.
[34] A. Gramza, S. Khokhar, S. Yoko, A. Gliszczynska-Swiglo, M. Hes, and J. Korczak, “Antioxidant activity of tea extracts in lipids and correlation with polyphenol content,” *Eur. J. Lipid Sci. Technol.*, vol. 108, no. 4, pp. 351–362, 2006.
[35] Y.-D. Z. Dale G. Naglea, Daneel Ferreiraa, “Epigallocatechin-3-gallate (EGCG): Chemical and biomedical perspectives,” *Phytochemistry*, vol. 67, no. 4, pp. 661–671, 2006.
[36] G. J. Du *et al.*, “Epigallocatechin gallate (EGCG) is the most effective cancer chemopreventive polyphenol in green tea,” *Nutrients*, vol. 4, no. 11, pp. 1679–1691, 2012.
[37] S. Wolfram, “Effects of green tea and EGCG on cardiovascular and metabolic health.,” *J. Am. Coll. Nutr.*, vol. 26, no. 4, p. 373S–388S, 2007.
[38] J. B. Harborne, *Methods in Plant Biochemistry: 1. Plant Phenolics*, vol. 20, no. 3. 2014.
[39] J. B. Harborne and C. A. Williams, “Advances in flavonoid research since 1992,” *Phytochemistry*, vol. 55, no. 6, pp. 481–504, 2000.
[40] S. Quideau, D. Deffieux, C. Douat-Casassus, and L. Pouységu, “Plant polyphenols: Chemical properties, biological activities, and synthesis,” *Angew. Chemie - Int. Ed.*, vol. 50, no. 3, pp. 586–621, 2011.
[41] S. Ramos, “Cancer chemoprevention and chemotherapy: Dietary polyphenols and signalling pathways,” *Mol. Nutr. Food Res.*, vol. 52, no. 5, pp. 507–526, 2008.
[42] P. S. Makena and K. T. Chung, “Effects of various plant polyphenols on bladder carcinogen benzidine-induced mutagenicity,” *Food Chem. Toxicol.*, vol. 45, no. 10, pp. 1899–1909, 2007.
[43] S. Kuntz, U. Wenzel, and H. Daniel, “Comparative analysis of the effects of flavonoids on proliferation, cytotoxicity, and apoptosis in human colon cancer cell lines,” *Eur J Nutr*, vol. 38, no. 3, pp. 133–142, 1999.
[44] J. R. Araújo, P. Gonçalves, and F. Martel, “Chemopreventive effect of dietary polyphenols in colorectal cancer cell lines,” *Nutr. Res.*, vol. 31, no. 2, pp. 77–87, 2011.
[45] C. J. Weng and G. C. Yen, “Chemopreventive effects of dietary phytochemicals against cancer invasion and metastasis: Phenolic acids, monophenol, polyphenol, and their derivatives,” *Cancer Treat. Rev.*, vol. 38, no. 1, pp. 76–87, 2012.
[46] L. S. Wang and G. D. Stoner, “Anthocyanins and their role in cancer prevention,” *Cancer Lett.*, vol. 269, no. 2, pp. 281–290, 2008.
[47] K. Raina, S. Rajamanickam, G. Deep, M. Singh, R. Agarwal, and C. Agarwal, “Chemopreventive effects of oral gallic acid feeding on tumor growth and progression in TRAMP mice.,” *Mol. Cancer Ther.*, vol. 7, no. 5, pp. 1258–67, 2008.

[48] L. Camont *et al.*, “Radical-induced oxidation of trans-resveratrol,” *Biochimie*, vol. 94, no. 3, pp. 741–747, 2012.
[49] S. K. Goswami and D. K. Das, “Resveratrol and chemoprevention,” *Cancer Lett.*, vol. 284, no. 1, pp. 1–6, 2009.
[50] M. Athar, J. H. Back, L. Kopelovich, D. R. Bickers, and A. L. Kim, “Multiple molecular targets of resveratrol: Anti-carcinogenic mechanisms,” *Arch. Biochem. Biophys.*, vol. 486, no. 2, pp. 95–102, 2009.
[51] J. K. Kundu and Y. J. Surh, “Cancer chemopreventive and therapeutic potential of resveratrol: Mechanistic perspectives,” *Cancer Lett.*, vol. 269, no. 2, pp. 243–261, 2008.
[52] E. Xia, X. He, H. Li, S. Wu, S. Li, and G. Deng, “Biological Activities of Polyphenols from Grapes,” *Polyphenols Hum. Heal. Dis.*, vol. 1, pp. 47–58, 2013.
[53] N. Ullah *et al.*, “Green tea phytocompounds as anticancer: A review,” *Asian Pacific J. Trop. Dis.*, vol. 6, no. 4, pp. 330–336, 2016.
[54] B. Bin Hafeez, S. Ahmed, N. Wang, S. Gupta, A. Zhang, and T. M. Haqqi, “Green tea polyphenols-induced apoptosis in human osteosarcoma SAOS-2 cells involves a caspase-dependent mechanism with downregulation of nuclear factor-??B,” *Toxicol. Appl. Pharmacol.*, vol. 216, no. 1, pp. 11–19, 2006.
[55] N. Khan and H. Mukhtar, “Multitargeted therapy of cancer by green tea polyphenols,” *Cancer Lett.*, vol. 269, no. 2, pp. 269–280, 2008.
[56] K. Zhu and W. Wang, “Green tea polyphenol EGCG suppresses osteosarcoma cell growth through upregulating miR-1,” *Tumor Biol.*, vol. 37, no. 4, pp. 4373–4382, 2016.
[57] B. Halliwell, “Free radicals and antioxidants - Quo vadis?,” *Trends Pharmacol. Sci.*, vol. 32, no. 3, pp. 125–130, 2011.
[58] J. M. C. Gutteridge and B. Halliwell, “Antioxidants: Molecules, medicines, and myths,” *Biochem. Biophys. Res. Commun.*, vol. 393, no. 4, pp. 561–564, 2010.
[59] A. Scalbert, I. T. Johnson, and M. Saltmarsh, “Polyphenols: antioxidants and beyond.,” *Am. J. Clin. Nutr.*, vol. 81, no. 1, p. 215S–217S, 2005.
[60] M. Leopoldini, N. Russo, and M. Toscano, “The molecular basis of working mechanism of natural polyphenolic antioxidants,” *Food Chem.*, vol. 125, no. 2, pp. 288–306, 2011.
[61] D. Procházková, I. Boušová, and N. Wilhelmová, “Antioxidant and prooxidant properties of flavonoids,” *Fitoterapia*, vol. 82, no. 4, pp. 513–523, 2011.
[62] Z. Lu, G. Nie, P. S. Belton, H. Tang, and B. Zhao, “Structure-activity relationship analysis of antioxidant ability and neuroprotective effect of gallic acid derivatives,” *Neurochem. Int.*, vol. 48, no. 4, pp. 263–274, 2006.
[63] M. C. MJ Hynes, “The kinetics and mechanisms of the reactions of aluminium(III) with gallic acid, gallic acid methyl ester and adrenaline,” *J. Inorg. Biochem.*, vol. 84, pp. 1–12, 2001.

[64] L.-L. Lu, Y. Li, and X. Lu, “Kinetic study of the complexation of gallic acid with Fe(II),” *Spectrochim. Acta Part A Mol. Biomol. Spectrosc.*, vol. 74, no. 3, pp. 829–34, 2009.
[65] I. Gülçin, “Antioxidant properties of resveratrol: A structure-activity insight,” *Innov. Food Sci. Emerg. Technol.*, vol. 11, no. 1, pp. 210–218, 2010.
[66] P. Ryan and M. J. Hynes, “The kinetics and mechanisms of the complex formation and antioxidant behaviour of the polyphenols EGCg and ECG with iron(III),” *J. Inorg. Biochem.*, vol. 101, no. 4, pp. 585–593, 2007.
[67] S. D. Lin, E. H. Liu, and J. L. Mau, “Effect of different brewing methods on antioxidant properties of steaming green tea,” *LWT - Food Sci. Technol.*, vol. 41, no. 9, pp. 1616–1623, 2008.
[68] S. Shao, T. Zhou, and R. Tsao, *Antimicrobials from Plants - Food Preservation and Shelf-Life Extension*, Second Edi., vol. 4. Elsevier B.V., 2011.
[69] M. Bancirova, “Comparison of the antioxidant capacity and the antimicrobial activity of black and green tea,” *Food Res. Int.*, vol. 43, no. 5, pp. 1379–1382, 2010.
[70] W. Si, J. Gong, R. Tsao, M. Kalab, R. Yang, and Y. Yin, “Bioassay-guided purification and identification of antimicrobial components in Chinese green tea extract,” *J. Chromatogr. A*, vol. 1125, no. 2, pp. 204–210, 2006.
[71] S. Petti and C. Scully, “Polyphenols, oral health and disease: A review,” *J. Dent.*, vol. 37, no. 6, pp. 413–423, 2009.
[72] A. Furiga, A. Lonvaud-Funel, and C. Badet, “In vitro study of antioxidant capacity and antibacterial activity on oral anaerobes of a grape seed extract,” *Food Chem.*, vol. 113, no. 4, pp. 1037–1040, 2009.
[73] V. Sendamangalam, O. Kyun-Choi, Y. Seo, and D.-S. Kim, “Antimicrobial and Antioxidant Activities of Polyphenols against Streptococcus mutans,” *Free Radicals Antioxidants*, vol. 1, no. 3, pp. 48–55, 2011.
[74] R. Díaz-Gómez, R. López-Solís, E. Obreque-Slier, and H. Toledo-Araya, “Comparative antibacterial effect of gallic acid and catechin against Helicobacter pylori,” *LWT - Food Sci. Technol.*, vol. 54, no. 2, pp. 331–335, 2013.
[75] M. Daglia, “Polyphenols as antimicrobial agents,” *Curr. Opin. Biotechnol.*, vol. 23, no. 2, pp. 174–181, 2012.
[76] T. P. T. Cushnie and A. J. Lamb, “Recent advances in understanding the antibacterial properties of flavonoids,” *Int. J. Antimicrob. Agents*, vol. 38, no. 2, pp. 99–107, 2011.
[77] C. L. Shen, J. K. Yeh, J. J. Cao, and J. S. Wang, “Green tea and bone metabolism,” *Nutr. Res.*, vol. 29, no. 7, pp. 437–456, 2009.
[78] Y.-J. Mah *et al.*, “The effect of epigallocatechin-3-gallate (EGCG) on human alveolar bone cells both in vitro and in vivo,” *Arch. Oral Biol.*, vol. 59, no. 5, pp. 539–549, 2014.
[79] C.-L. Shen, J. K. Yeh, J. J. Cao, M.-C. Chyu, and J.-S. Wang, “Green tea

and bone health: Evidence from laboratory studies.," *Pharmacol. Res.*, vol. 64, no. 2, pp. 155–61, 2011.
[80] R. C. Casarin *et al.*, "Resveratrol improves bone repair by modulation of bone morphogenetic proteins and osteopontin gene expression in rats," *Int. J. Oral Maxillofac. Surg.*, vol. 43, no. 7, pp. 900–906, 2014.
[81] X. He, G. Andersson, U. Lindgren, and Y. Li, "Resveratrol prevents RANKL-induced osteoclast differentiation of murine osteoclast progenitor RAW 264.7 cells through inhibition of ROS production," *Biochem. Biophys. Res. Commun.*, vol. 401, no. 3, pp. 356–362, 2010.
[82] L. Forte *et al.*, "Antioxidant and bone repair properties of quercetin-functionalized hydroxyapatite: An in vitro osteoblast-osteoclast-endothelial cell co-culture study," *Acta Biomater.*, vol. 32, pp. 298–308, 2016.
[83] K. Sòllyom, R. Solà, M. J. Cocero, and R. B. Mato, "Thermal degradation of grape marc polyphenols," *Food Chem.*, vol. 159, pp. 361–366, 2014.
[84] D. T. Sponza and R. Oztekin, "Photodegradation of polyphenols and aromatic amines in olive mill effluents with Ni doped C/TiO2," *J. Chem.*, 2015.
[85] I. Volf, I. Ignat, M. Neamtu, and V. Popa, "Thermal stability, antioxidant activity, and photo-oxidation of natural polyphenols," *Chem. Pap.*, vol. 68, no. 1, 2014.
[86] J. Correa-Betanzo, E. Allen-Vercoe, J. McDonald, K. Schroeter, M. Corredig, and G. Paliyath, "Stability and biological activity of wild blueberry (Vaccinium angustifolium) polyphenols during simulated in vitro gastrointestinal digestion," *Food Chem.*, vol. 165, pp. 522–531, 2014.
[87] C. A. R.-E. Andreas R. Rechner, Gunter Kuhnle, Paul Bremner, Gary P. Hubbard, Kevin P. Moore, "THE METABOLIC FATE OF DIETARY POLYPHENOLS IN HUMANS," *Free Radic. Biol. Med.*, vol. 33, no. 2, pp. 220–235, 2002.
[88] F. Sousa, G. M. Guebitz, and V. Kokol, "Antimicrobial and antioxidant properties of chitosan enzymatically functionalized with flavonoids," *Process Biochem.*, vol. 44, no. 7, pp. 749–756, 2009.
[89] M. Božič, S. Gorgieva, and V. Kokol, "Homogeneous and heterogeneous methods for laccase-mediated functionalization of chitosan by tannic acid and quercetin," *Carbohydr. Polym.*, vol. 89, no. 3, pp. 854–864, 2012.
[90] M. Bozic, S. Gorgieva, and V. Kokol, "Laccase-mediated functionalization of chitosan by caffeic and gallic acids for modulating antioxidant and antimicrobial properties," *Carbohydr. Polym.*, vol. 87, no. 4, pp. 2388–2398, 2012.
[91] M. Moradi *et al.*, "Characterization of antioxidant chitosan film incorporated with Zataria multiflora Boiss essential oil and grape seed extract," *LWT - Food Sci. Technol.*, vol. 46, no. 2, pp. 477–484, 2012.
[92] C. Nunes, É. Maricato, Â. Cunha, A. Nunes, J. A. L. Da Silva, and M. A. Coimbra, "Chitosan-caffeic acid-genipin films presenting enhanced antioxidant activity and stability in acidic media," *Carbohydr. Polym.*, vol.

91, no. 1, pp. 236–243, 2013.
[93] K. T. Trifković *et al.*, “Chitosan microbeads for encapsulation of thyme (Thymus serpyllum L.) polyphenols,” *Carbohydr. Polym.*, vol. 111, pp. 901–907, 2014.
[94] A. Belščak-Cvitanović *et al.*, “Encapsulation of polyphenolic antioxidants from medicinal plant extracts in alginate-chitosan system enhanced with ascorbic acid by electrostatic extrusion,” *Food Res. Int.*, vol. 44, no. 4, pp. 1094–1101, 2011.
[95] M. Ramírez-Ambrosi, F. Caldera, F. Trotta, L. Berrueta, and B. Gallo, “Encapsulation of apple polyphenols in β-CD nanosponges,” *J. Incl. Phenom. Macrocycl. Chem.*, vol. 80, no. 1–2, pp. 85–92, 2014.
[96] J. P. Saikia, R. Konwarh, B. K. Konwar, and N. Karak, “Isolation and immobilization of Aroid polyphenol on magnetic nanoparticles: Enhancement of potency on surface immobilization,” *Colloids Surfaces B Biointerfaces*, vol. 102, pp. 450–456, 2013.
[97] E. B. Gloria Berliera, Lucia Gastaldib, Simona Sapinob, Ivana Milettoa and E. U. Daniela Chiriob, “MCM-41 as a useful vector for rutin topical formulations: Synthesis, characterization and testing,” *Int. J. Pharm.*, vol. 457, no. 1, pp. 177–186, 2013.
[98] Y. Chen, Y. D. Lee, H. Vedala, B. L. Allen, and A. Star, “Exploring the chemical sensitivity of a carbon nanotube/green tea composite,” *ACS Nano*, vol. 4, no. 11, pp. 6854–6862, 2010.
[99] K. Wang *et al.*, “Dual-functionalization based on combination of quercetin compound and rare earth nanoparticle,” *J. Rare Earths*, vol. 31, no. 7, pp. 709–714, 2013.
[100] S. Das and K. Y. Ng, “Colon-specific delivery of resveratrol: Optimization of multi-particulate calcium-pectinate carrier,” *Int. J. Pharm.*, vol. 385, no. 1–2, pp. 20–28, 2010.
[101] R. K. Mohanty, S. Thennarasu, and A. B. Mandal, “Resveratrol stabilized gold nanoparticles enable surface loading of doxorubicin and anticancer activity,” *Colloids Surfaces B Biointerfaces*, vol. 114, pp. 138–143, 2014.
[102] Y. Li *et al.*, “Resveratrol-conjugated poly - Caprolactone facilitates in vitro mineralization and in vivo bone regeneration,” *Acta Biomater.*, vol. 7, no. 2, pp. 751–758, 2011.
[103] C. R. Dosier, C. P. Erdman, J. H. Park, Z. Schwartz, B. D. Boyan, and R. E. Guldberg, “Resveratrol effect on osteogenic differentiation of rat and human adipose derived stem cells in a 3-D culture environment,” *J. Mech. Behav. Biomed. Mater.*, vol. 11, pp. 112–122, 2012.
[104] S. Nagarajan, B. S. R. Reddy, and J. Tsibouklis, “In vitro effect on cancer cells: Synthesis and preparation of polyurethane membranes for controlled delivery of curcumin,” *J. Biomed. Mater. Res. - Part A*, vol. 99 A, no. 3, pp. 410–417, 2011.
[105] E. S. Džunuzović, J. V. Džunuzović, A. D. Marinković, M. T. Marinović-Cincović, K. B. Jeremić, and J. M. Nedeljković, “Influence of surface

modified TiO 2 nanoparticles by gallates on the properties of PMMA/TiO 2 nanocomposites," *Eur. Polym. J.*, vol. 48, no. 8, pp. 1385–1393, 2012.
[106] F. H. Lin, G. C. Dong, K. S. Chen, G. J. Jiang, C. W. Huang, and J. S. Sun, "Immobilization of Chinese herbal medicine onto the surface-modified calcium hydrogenphosphate," *Biomaterials*, vol. 24, no. 13, pp. 2413–2422, 2003.
[107] M. Moritz and M. Geszke-Moritz, "The newest achievements in synthesis, immobilization and practical applications of antibacterial nanoparticles," *Chem. Eng. J.*, vol. 228, pp. 596–613, 2013.
[108] T. S. Sileika, D. G. Barrett, R. Zhang, K. H. A. Lau, and P. B. Messersmith, "Colorless multifunctional coatings inspired by polyphenols found in tea, chocolate, and wine," *Angew. Chemie - Int. Ed.*, vol. 52, no. 41, pp. 10766–10770, 2013.
[109] S. Erakovic, A. Jankovic, G. C. P. Tsui, C. Y. Tang, V. Miskovic-Stankovic, and T. Stevanovic, "Novel Bioactive Antimicrobial Lignin Containing Coatings on Titanium Obtained by Electrophoretic Deposition," *Int. J. Mol. Sci.*, vol. 15, no. 7, pp. 12294–12322, 2014.
[110] Y. P. Neo, S. Swift, S. Ray, M. Gizdavic-Nikolaidis, J. Jin, and C. O. Perera, "Evaluation of gallic acid loaded zein sub-micron electrospun fibre mats as novel active packaging materials," *Food Chem.*, vol. 141, no. 3, pp. 3192–3200, 2013.
[111] L. Mohan, C. Anandan, and N. Rajendran, "Drug release characteristics of quercetin-loaded TiO nanotubes coated with chitosan.," *Int. J. Biol. Macromol.*, vol. 93, pp. 1633–1638, 2016.
[112] K. Gurzawska *et al.*, "Osteoblastic response to pectin nanocoating on titanium surfaces," *Mater. Sci. Eng. C*, vol. 43, pp. 117–125, 2014.
[113] S. Seshadri, S. Thotapalli, and B. Santhosh Kumar, "Synthesis and characterization of a novel bone graft material using biphasic calcium phosphate casein chitosan with the extracts of coriandrum sativum," *Int. J. Pharm. Pharm. Sci.*, vol. 6, no. 5, pp. 358–361, 2014.
[114] S. Ferraris *et al.*, "Gallic acid grafting to a ferrimagnetic bioactive glass-ceramic," *J. Non. Cryst. Solids*, vol. 432, pp. 167–175, 2016.
[115] X. Zhang, S. Ferraris, E. Prenesti, and E. Verné, "Surface functionalization of bioactive glasses with natural molecules of biological significance , part II : Grafting of polyphenols extracted from grape skin," *Appl. Surf. Sci.*, vol. 287, pp. 341–348, 2013.
[116] X. Zhang, S. Ferraris, E. Prenesti, and E. Verné, "Surface functionalization of bioactive glasses with natural molecules of biological significance, part I: Gallic acid as model molecule," *Appl. Surf. Sci.*, vol. 287, pp. 329–340, 2013.
[117] Q. V. Vuong, J. B. Golding, C. E. Stathopoulos, M. H. Nguyen, and P. D. Roach, "Optimizing conditions for the extraction of catechins from green tea using hot water," *J. Sep. Sci.*, vol. 34, no. 21, pp. 3099–3106, 2011.
[118] C. Vitale-Brovarone, E. Verné, L. Robiglio, G. Martinasso, R. A. Canuto,

and G. Muzio, “Biocompatible glass-ceramic materials for bone substitution,” *J. Mater. Sci. Mater. Med.*, vol. 19, no. 1, pp. 471–478, 2008.
[119] E. Verné *et al.*, “Alkaline phosphatase grafting on bioactive glasses and glass ceramics,” *Acta Biomater.*, vol. 6, no. 1, pp. 229–240, 2010.
[120] E. Verné *et al.*, “Early stage reactivity and in vitro behavior of silica-based bioactive glasses and glass-ceramics,” *J. Mater. Sci. Mater. Med.*, vol. 20, no. 1, pp. 75–87, 2009.
[121] M.Cazzola, “Funzionalizzazione superficiale di materiali bioattivi con polifenoli,” 2014.
[122] “S.Spriano et al., European Patent 2214732.”
[123] S. Ferraris *et al.*, “Surface modification of Ti-6Al-4V alloy for biomineralization and specific biological response: Part I, inorganic modification,” *J. Mater. Sci. Mater. Med.*, vol. 22, no. 3, pp. 533–545, 2011.
[124] T. Kokubo, “Bioactive glass ceramics : properties and applications,” *Biomaterials*, vol. 12, pp. 155–163, 1991.
[125] M. Cazzola, I. Corazzari, E. Prenesti, E. Bertone, E. Vernè, and S. Ferraris, “Bioactive glass coupling with natural polyphenols : Surface modification , bioactivity and anti-oxidant ability,” *Appl. Surf. Sci.*, vol. 367, pp. 237–248, 2016.
[126] R. M. L.-Ravent. VERNON L. SINGLETON, RUDOLF ORTHOFER, “Analysis of Total Phenols and Other Oxidation Substrates and Antioxidants by Means of Folin-Ciocalteu Reagent,” *METHODS Enzymol.*, vol. 299, no. 1974, pp. 152–178, 1999.
[127] N. Lavid, A. Schwartz, O. Yarden, and E. Tel-Or, “The involvement of polyphenols and peroxidase activities in heavy-metal accumulation by epidermal glands of the waterlily (Nymphaeaceae),” *Planta*, vol. 212, no. 3, pp. 323–331, 2001.
[128] T. Luxbacher, *The zeta potential for solid surface analysis*. 2014.
[129] T. Kokubo and H. Takadama, “How useful is SBF in predicting in vivo bone bioactivity?,” *Biomaterials*, vol. 27, no. 15, pp. 2907–2915, 2006.
[130] M. Y. Ghotbi and M. Z. Bin Hussein, “Controlled release study of an anti-carcinogenic agent, gallate from the surface of magnetite nanoparticles,” *J. Phys. Chem. Solids*, vol. 73, no. 7, pp. 936–942, 2012.
[131] X. Kong, L. Jin, M. Wei, and X. Duan, “Antioxidant drugs intercalated into layered double hydroxide: Structure and in vitro release,” *Appl. Clay Sci.*, vol. 49, no. 3, pp. 324–329, 2010.
[132] A. Sharma, S. P. Gautam, and A. K. Gupta, “Surface modified dendrimers: Synthesis and characterization for cancer targeted drug delivery,” *Bioorganic Med. Chem.*, vol. 19, no. 11, pp. 3341–3346, 2011.
[133] L. L. Hench, N. Roki, and M. B. Fenn, “Bioactive glasses: Importance of structure and properties in bone regeneration,” *J. Mol. Struct.*, vol. 1073, no. C, pp. 24–30, 2014.
[134] L. L. H. Wanpeng Cao, “Bioactive materials,” *Ceram. Int.*, vol. 22, no. 6,

pp. 493–507, 1996.
[135] E. Vern??, C. Vitale-Brovarone, E. Bui, C. L. Bianchi, and A. R. Boccaccini, “Surface functionalization of bioactive glasses,” *J. Biomed. Mater. Res. - Part A*, vol. 90, no. 4, pp. 981–992, 2009.
[136] Z. Yang, Y. Yang, W. Yan, Q. Tu, J. Wang, and N. Huang, “Construction of polyfunctional coatings assisted by gallic acid to facilitate Co-immobilization of diverse biomolecules,” *ACS Appl. Mater. Interfaces*, vol. 5, no. 21, pp. 10495–10501, 2013.
[137] Z. Yang, J. Wu, X. Wang, J. Wang, and N. Huang, “Inspired chemistry for a simple but highly effective immobilization of vascular endothelial growth factor on gallic acid-functionalized plasma polymerized film,” *Plasma Process. Polym.*, vol. 9, no. 7, pp. 718–725, 2012.
[138] “http://web-o-rama.net/titanium/1anodization.html (08/11/2017, 09:50 am).” .
[139] Guenin, S. O. S. Hamady, and P. Bourson, “Monitoring deprotonation of gallic acid by Raman spectroscopy,” *J. Raman Spectrosc.*, vol. 46, no. 11, pp. 1062–1066, 2015.
[140] M. A. B. Araujo, P.Z., P.J. Morando, “Interaction of catechol and gallic acid Langmuir, with titanium dioxide in aqueous suspensions. 1. Equilibrium studies,” *Langmuir*, vol. 21, pp. 3470–3474, 2005.
[141] B. Tang, H. Yuan, L. Cheng, X. Zhou, X. Huang, and J. Li, “Effects of gallic acid on the morphology and growth of hydroxyapatite crystals,” *Arch. Oral Biol.*, vol. 60, no. 1, pp. 167–173, 2014.
[142] M. S. Das, V. T. Athavale, and A. E. Estabhshment, “STUDIES OF GALLIC ACID COMPLEXES WITH METALS AND THEIR ANALYTICAL APPLICATIONS,” *Proc. Indian Acad. Sci. - Sect. A*, vol. 40, no. 6, pp. 260–269, 1954.
[143] G. Berlier *et al.*, “MCM-41 as a useful vector for rutin topical formulations: Synthesis, characterization and testing,” *Int. J. Pharm.*, vol. 457, no. 1, pp. 177–186, 2013.
[144] “http://www.xpsfitting.com/2011/03/c-1s-carbonates.html (31 August 2017, 2:46 pm).” .
[145] C. Gruian, E. Vanea, S. Simon, and V. Simon, “FTIR and XPS studies of protein adsorption onto functionalized bioactive glass,” *Biochim. Biophys. Acta - Proteins Proteomics*, vol. 1824, no. 7, pp. 873–881, 2012.
[146] E. Vernè, S. Ferraris, C. Vitale-Brovarone, A. Cochis, and L. Rimondini, “Bioactive glass functionalized with alkaline phosphatase stimulates bone extracellular matrix deposition and calcification in vitro,” *Appl. Surf. Sci.*, vol. 313, pp. 372–381, 2014.
[147] M. Textor, C. Sittig, V. Frauchiger, and S. Tosatti, *Properties and Biological Significance of Natural Oxide Films on Titanium and Its Alloys*. 2001.
[148] M. Morra *et al.*, “Surface Chemistry Effects of Topographic Modification of Titanium Dental Implant Surfaces :1. Surface Analysis,” *Int. J. Oral*

Maxillofac. Implant. 41, vol. 18, no. 1, pp. 40–45, 2003.
[149] E. Prajatelistia, S. W. Ju, N. D. Sanandiya, S. H. Jun, J. S. Ahn, and D. S. Hwang, "Tunicate-Inspired Gallic Acid/Metal Ion Complex for Instant and Efficient Treatment of Dentin Hypersensitivity," *Adv. Healthc. Mater.*, vol. 5, no. 8, pp. 919–927, 2016.
[150] H. Ejima *et al.*, "One-Step Assembly of Coordination Complexes for Versatile Film and Particle Engineering," *Sci. Reports*, vol. 341, pp. 154–157, 2013.
[151] K. D. B. J.F. Mowlder, W.F. Stickle, P.E. Sobol, *HANDBOOK OF X-RAY PHOTOELECTRON SPECTROSCOPY*. 1981.
[152] M. Ö. Öteyaka, P. Chevallier, L. Robitaille, and G. Laroche, "Effect of surface modification by ammonia plasma on vascular graft: PET film and PET scaffold," *Acta Phys. Pol. A*, vol. 121, no. 1, pp. 125–127, 2012.
[153] E. V. S. Ferraris, S. Spriano, C.L. Bianchi, C.Cassinelli, "Surface modification of Ti-6Al-4 V alloy for biomineralization and specific biological response : part II , alkaline phosphatase grafting," *J Mater Sci Mater Med*, vol. 22, pp. 1835–1842, 2011.
[154] "http://xpssimplified.com/elements/oxygen.php (07/12/ 2017, 10:25 am)."
[155] A. Romdhane, M. Aurousseau, A. Guillet, and E. Mauret, "Effect of pH and ionic strength on the electrical charge and particle size distribution of starch nanocrystal suspensions," *Starch/Staerke*, vol. 67, no. 3–4, pp. 319–327, 2015.
[156] D. C. Clupper, J. E. Gough, P. M. Embanga, I. Notingher, L. L. Hench, and M. M. Hall, "Bioactive evaluation of 45S5 bioactive glass ® bres and preliminary study of human osteoblast attachment," *J. Mater. Sci. Mater. Med.*, vol. 15, pp. 803–808, 2004.
[157] T. Borkowski, H. Szymusiak, A. Gliszczyńska-Świgło, I. M. C. M. Rietjens, and B. Tyrakowska, "Radical scavenging capacity of wine anthocyanins is strongly pH-dependent," *J. Agric. Food Chem.*, vol. 53, no. 14, pp. 5526–5534, 2005.
[158] M. Of, A. Action, and O. F. Hydroxyflavones, "THE INFLUENCE OF pH ON ANTIOXIDANT PROPERTIES AND THE MECHANISM OF ANTIOXIDANT ACTION OF HYDROXYFLAVONES," *Free Radic. Biol. Med.*, vol. 31, no. 7, pp. 869–881, 2001.
[159] C. M. Botelho, M. A. Lopes, I. R. Gibson, S. M. Best, and J. D. Santos, "Structural analysis of Si-substituted hydroxyapatite: zeta potential and X-ray photoelectron spectroscopy RID B-1753-2010," *J. Mater. Sci. Med.*, vol. 13, no. 12, pp. 1123–1127, 2002.
[160] S. V Dorozhkin, "Dissolution mechanism of calcium apatites in acids: A review of literature," *World J. Methodol.*, vol. 2, no. 1, p. 1, 2012.
[161] A. El-Ghannam, P. Ducheyne, and I. M. Shapiro, "Formation of surface reaction products on bioactive glass and their effects on the expression of the osteoblastic phenotype and the deposition of mineralized extracellular matrix," *Biomaterials*, vol. 18, no. 4, pp. 295–303, 1997.

[162] K. Ishii, A. Kimura, T. Kushibiki, and K. Awazu, “Analysis of tissue specific progenitor cell differentiation using FT-IR,” *Biomed. IV*, vol. 6628, no. 1, pp. 1–8, 2007.
[163] A. Balamurugan *et al.*, “Synthesis and characterisation of sol gel derived bioactive glass for biomedical applications,” *Mater. Lett.*, vol. 60, no. 29–30, pp. 3752–3757, 2006.
[164] H. Wang, J.-K. Lee, A. Moursi, and J. J. Lannutti, “Ca/P ratio effects on the degradation of hydroxyapatite in vitro.,” *J. Biomed. Mater. Res. A*, vol. 67, no. 2, pp. 599–608, 2003.
[165] R. Zhou, S. Si, and Q. Zhang, “Water-dispersible hydroxyapatite nanoparticles synthesized in aqueous solution containing grape seed extract,” *Appl. Surf. Sci.*, vol. 258, no. 8, pp. 3578–3583, 2012.
[166] Y. W. Hsu, C. F. Tsai, W. C. Chuang, W. K. Chen, Y. C. Ho, and F. J. Lu, “Protective effects of silica hydride against carbon tetrachloride-induced hepatotoxicity in mice,” *Food Chem. Toxicol.*, vol. 48, no. 6, pp. 1644–1653, 2010.
[167] C. J. Stephanson and G. P. Flanagan, “Antioxidant capacity of silica hydride: A combinational photosensitization and fluorescence detection assay,” *Free Radic. Biol. Med.*, vol. 35, no. 9, pp. 1129–1137, 2003.
[168] A. Schuck *et al.*, “Cytotoxic and proapoptotic activities of gallic acid to human oral cancer HSC-2 cells,” *Oxid. Antioxid. Med. Sci.*, vol. 2, no. 4, p. 265, 2013.
[169] H. Lewandowska, M. Kalinowska, W. Lewandowski, T. M. Stepkowski, and K. Brzóska, “The role of natural polyphenols in cell signaling and cytoprotection against cancer development,” *J. Nutr. Biochem.*, vol. 32, pp. 1–19, 2016.
[170] S. Jebahi *et al.*, “Antioxidative/oxidative effects of strontium-doped bioactive glass as bone graft. In vivo assays in ovariectomised rats,” *J. Appl. Biomed.*, vol. 10, no. 4, pp. 195–209, 2012.
[171] X. Cheng, J. Sherman, W. Murphy, E. Ratovitski, J. Canady, and M. Keidar, “The effect of tuning cold plasma composition on glioblastoma cell viability,” *PLoS One*, vol. 9, no. 5, pp. 1–9, 2014.
[172] J. Köritzer *et al.*, “Restoration of Sensitivity in Chemo - Resistant Glioma Cells by Cold Atmospheric Plasma,” *PLoS One*, vol. 8, no. 5, 2013.
[173] M. G. Sajilata, P. R. Bajaj, and R. S. Singhal, “Tea Polyphenols as Nutraceuticals,” *Compr. Rev. FOOD Sci. FOOD Saf.*, vol. 7, pp. 229–254, 2008.
[174] S. R. R.Shazza, Z. Movasaghi, *Vibrational spectroscopy for tissue analysis*. 2013.
[175] C. Woess *et al.*, “Assessing various Infrared (IR) microscopic imaging techniques for post-mortem interval evaluation of human skeletal remains,” *PLoS One*, pp. 1–16, 2017.
[176] A. Boskey and N. P. Camacho, “FT-IR Imaging of Native and Tissue-Engineered Bone and Cartilage,” *Biomaterials*, vol. 28, no. 15, pp. 2465–

2478, 2008.
[177] G. Pezzotti *et al.*, “Vibrational algorithms for quantitative crystallographic analyses of hydroxyapatite-based biomaterials: I, theoretical foundations,” *Anal. Bioanal. Chem.*, vol. 407, no. 12, pp. 3325–3342, 2015.
[178] Z. Movasaghi, S. Rehman, and I. R. The, “Raman Spectroscopy of Biological Tissues,” *Appl. Spectrosc. Rev.*, vol. 42, no. 5, pp. 493–541, 2007.
[179] M. A. Al Mamun, M. J. Hosen, K. Islam, A. Khatun, M. M. Alam, and M. A. A. Al-Bari, “Tridax procumbens flavonoids promote osteoblast differentiation and bone formation,” *Biol. Res.*, vol. 48, pp. 1–8, 2015.
[180] L. Léotoing, M. J. Davicco, P. Lebecque, Y. Wittrant, and V. Coxam, “The flavonoid fisetin promotes osteoblasts differentiation through Runx2 transcriptional activity,” *Mol. Nutr. Food Res.*, vol. 58, no. 6, pp. 1239–1248, 2014.
[181] S. Srivastava, R. Bankar, and P. Roy, “Assessment of the role of flavonoids for inducing osteoblast differentiation in isolated mouse bone marrow derived mesenchymal stem cells,” *Phytomedicine*, vol. 20, no. 8–9, pp. 683–690, 2013.
[182] A. V. S. Perumalla and N. S. Hettiarachchy, “Green tea and grape seed extracts - Potential applications in food safety and quality,” *Food Res. Int.*, vol. 44, no. 4, pp. 827–839, 2011.

Chapter 3

Essential oils

3.1 Introduction

As mentioned in chapter 2, natural molecules have attracted more and more interest during the last years. Essential oils have been used in the folk medicine since ancient time, but it is also possible to use them in the production of food packaging and medical devices. Essential oils have well known antibacterial activity interesting for multi-purpose use because they could allow to avoid the side effects of antibiotics. In addition to antibacterial property, they have also a wide variety of effects on human health such as cardiovascular protective effects, antitumoral effects, anti-inflammatory effects, and many other for positive effects in the diseases that involves free radical proliferations because of their antioxidant property[1].
The antibacterial and the antiseptics properties are the most studied and the aim of this chapter is coupling molecules from essential oils to the surface of a chemically-treated titanium alloy suitable for bone contact applications in order to reduce bacterial contamination ant the spreading of infections after implants.
The first attempt of functionalization with essential oil in this thesis were performed with Thyme and Mentha Piperita essential oils extracted from laboratories of the Università degli studi di Torino. For the subsequent functionalizations and coatings, where a higher amount of essential oils are requested, a commercial Mentha Piperita essential oil of Pancalieri, Piedmont, Italy, was used in order to valorize the area and exploit the great antibacterial

activity of this kind of essential oil. The aim of this work is to develop a protocol for the functionalization of the titanium surface with *Mentha Piperita* oil molecules in order to confer antibacterial properties. In literature there are no standard methods for characterization of surfaces with this kind of functionalization, several analysis methods were used in order to find the most suitable protocol for the grafting of essential oils. This chapter includes bibliographic data about chemical composition and the main characteristics of essential oils and in particular of Mentha Piperita essential oil, the exposure and discussion of the methods employed and of the results obtained.

3.2 Definition and chemical composition of essential oils

The definition of essential oils given by European Pharmacopoeia 7th edition is: "Odorant product, generally of a complex composition, obtained from a botanically defined plant raw material, either by driving by steam of water, either by dry distillation or by a suitable mechanical method without heating. An essential oil is usually separated from the aqueous phase by a physical method that does not lead to significant change in its chemical composition"[2].
They are mixtures of lipophilic compounds contained in families of plants like *Rutaceae. Asteraceae, Lamiaceae, Cupressaceae, Pinaceae, Poaceae, Myrtaceae,* and *Apiaceae*. Most of essential oils in plants are mainly located in special oil cells, but they are also present in oil intercellular compartments divided into schizogenic and lysigenic. Essential oils can also be founded in plant-surface glad and milk tube. The compounds present in essential oils have a central role for the plants atmosphere control because of their fast reaction with reactive oxygen species (ROS) and –OH radicals[1].
The composition of essential oils is complex and it is includes a lot of different substances often chemically related. Many compounds are derived from hydrocarbon isoprene (Figure 3.1)

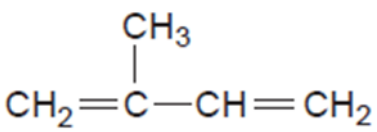

Figure 3.1: isoprene structure [3].

The component of the essential oils can be classified in [3]:

- Terpenes (hydrocarbons and alcohols)
- Oxygenated compounds
- Alcohols
- Phenols
- Aldehydes
- Ketones
- Ethers
- Esters
- Lactones,
- Coumarins
- Oxides

- **Terpene Hydrocarbons**

  -Monoterpenes: are terpenes molecules derived from isoprene units with 10 carbon atoms and with one or more double bonds. They could be linear or cyclic. Terpene hydrocarbons react quickly if exposed to oxygen or high temperature. They have anti-inflammatory, antiseptic, antiviral and antibacterial properties.

  -Sesquiterpenes: are formed by 15 carbon atoms and they have therapeutic properties. One of the most knows sesquiterpene is farnesene (Figure 3.2) that was used in the past with the same purpose of ibuprofen or aspirin.

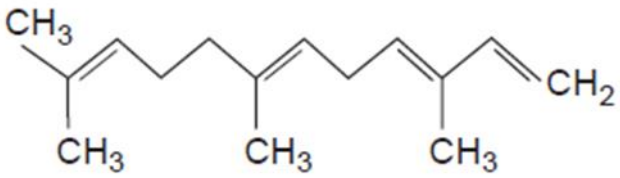

Figure 3.2: farnesene structure[3].

- **Terpene Alcohols:**

  -Monoterpene alcohols: the most abundant are linalool, terpinol, and citronellol, geraniol. They have antibacterial, anti-fungal and antiviral effect with few side effects.

  -Sesquiterpene alcohols: are not common in essential oils, but can be found in german chamomile, sandwood, ginger, patchouli, carrot seed and vetiver. They are oxidative derivatives of sesquiterpenes and they are glandular and liver stimulant, anti-allergen and anti-inflammatory.
- **Aldehydes:** are present in melissa, lemon grass and citronella giving their characteristic lemon-like fragrance. They also have anti-inflammatory, anti-fungal

and sedative effects. A high presence of these compounds in the oil could however cause sensitivity and skin irritation.

- **Ketones:** usually they can be toxic, but at appropriate concentration can also be used for medical purpose.
- **Esters:** they are formed starting prom acids and alcohols and they confer to the essential oils their fruity character. These compounds are antispasmodic and sedative. One of the most known is linalyl acetate (Figure 3.3) that is present in clary sage and lavender.

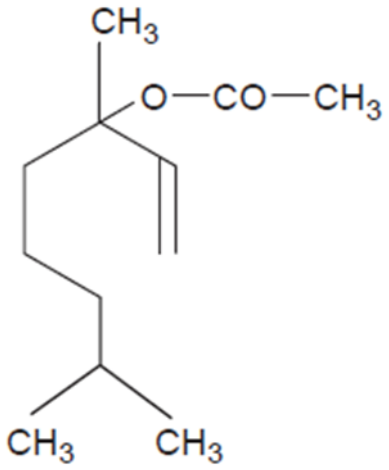

Figure 3.3: linalyl acetate structure [3].

- **Ethers:** they are presents in a very low amount in essential oils under phenolic form and the most representative are anethol from aniseed oil and methyl chavicol from basil and terragon oils.
- **Oxides:** oxides as such 1, 8-cyneol (eucalyptol) present in eucalypt essential oil are responsive of the decongestant property of this oil.
- **Lactones and coumarins:** lactones are the results of an intramolecular reaction involving an ester with the elimination of water. Coumarins are types of lactones with an aromatic ring. They contain oxacycloalcan with a C=O group. The amount of lactones and coumarins is very small, but they can act as sedatives and antispasmodics. In high amount they can cause neurotoxic effects, irritation and sanitizing of skin.
- **Phenols:** the phenols present in the essential oils usually have an aliphatic chain and they have antiseptic properties[1], [3], [4].

3.2.1 Chemical composition of Mentha Piperita essential oils

Mentha Piperita essential oil is obtained from the leaves of *Mentha Piperita Linnaeus* developed with the crossbreeding of *Mentha Acquatica* and *Mentha Spicata Linnaus*. This plant is native from Europe but has spread to the world.
The essential oil is colorless with the characteristic odor and taste. Mentha Piperita oil is widely used and it is composed by up to 50 % menthol, 10 to 30 % menthone, 1 to 5 % limonene, up to 10% methyl esters and other monoterpene derivatives like piperitone, pulegone and menthofurane[5]–[8].
Menthol ($C_{10}H_{20}O$) is a cyclic terpene alcohol present in high percentage (around 50%) in Mentha Piperita oil. The cyclohexaring of menthol has three asymmetric carbon atoms and allows menthol to have four opticaliomers: (-)- and (+)-menthol, (-)- and (+)-neomenthol, (-)- and (+)-isomentho1 and (-)- and (+)-neoisomenthol (Figure 3.4)[9].

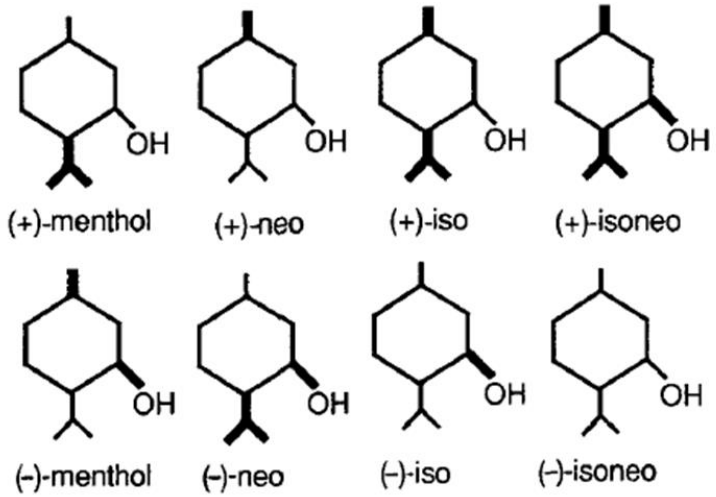

Figure 3.4: structure of the four pair of menthol opticalisomers [9].

This molecule confers to the Mentha oil its characteristic flavor and is employed in several fields as such cosmetics, pharmaceutical, pesticides and as flavoring agent. For medical purpose it has beneficial effects on common cold, musculoskeletal pain, gastrointestinal disorders and it also has antiseptic and analgesic effects [10].
Menthone ($C_{10}H_{18}O$) is a terpene belonging to the class of menthane monoterpenoids (Figure 3.5). Like menthol it is abundant in mint oils (around 10 to 30 %) and It is used in flavor compounds, cosmetics and perfumery [11].

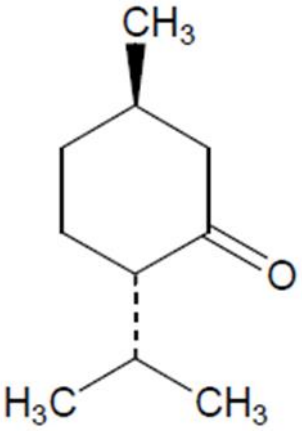

Figure 3.5: l-menthone structure [8].

Pulegone ($C_{10}H_{16}O$) (Figure 3.6) is a monoterpene ketone. It is a minor compound in several Mentha species essential oils and its percentage is between 0.5% and 4.6% in Mentha Piperita essential oil.

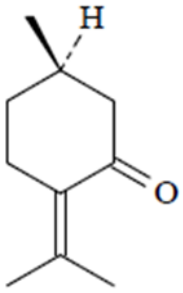

Figure 3.6: pulegone structure [12].

In nature it occurs with two enantiomeric forms. A high intake of this molecule could be hepatotoxic. The control of the amount of this molecules in the composition of the oils is important for their quality and beneficial effects on human health [12], [13]. It is also the precursor of menthofurane formation[14].
Menthofurane (C10H14O) (Figure 3.7) is a terpenic oxide minor constituent of Mentha Piperita oil. Despite of its low amount, it is fundamental for the organoleptic properties of this oil[15].

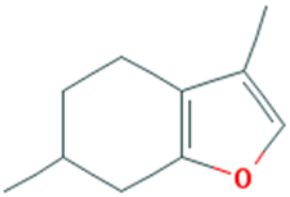

Figure 3.7: menthofuran structure [15].

Limonene ($C_{10}H_{16}$) (Figure 3.8) is a cyclic monoterpene, precursor of carvone, abundant in orange oil and present in small amount in Mentha Piperita oil (around 1 to 5%)[16].
The pure molecule is used as solvent for industrial painting and cleaner in the electronic industries. It is also used as fragrance additives in cleaning products, perfumes and food[16].

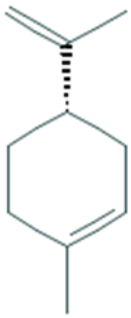

Figure 3.8: limonene structure[16].

Carvone ($C_{10}H_{14}O$) (Figure 3.9) is a volatile terpenoids present in percentage under 1% in Mentha Piperita oil. This molecule is sometimes present in human biologic fluids of normal individuals and was used for medical purpose by the ancient Romans[17].

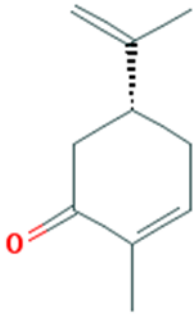

Figure 3.9: carvone structure [17].

Piperitone ($C_{10}H_{16}O$) (Figure 3.10) is a cyclic monoterpene ketone present in some essential oils with two stereoisomers, D-form and L-form. The D-form has a Mentha Piperita like aroma [18].

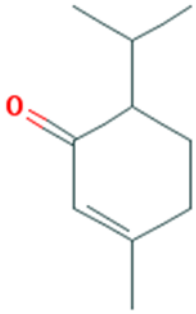

Figure 3.10: piperitone structure [18].

The composition of Mentha Piperita essential oil is influenced by several factors like: age of the plant at the time of harvesting, period of the harvesting, fertilization of soil, sun irradiation, soil moisture, place of cultivation and method of extraction[19], [20].

Mentha Piperita of Pancalieri

"Mentha Piperita of Pancalieri" or "Mentha Piperita Pancalieri Piedmont" is a plant species with the scientific name "*Mentha piperita Luds, kind Officinalis Sole, form Rubescens Camus*". It is also known as "Mentha of Mitcham" from the name of the English place where the first cultivation started.
The essential oil is obtained by steam distillation from the whole plant not ground [21]. The Mentha Piperita of Pancalieri essential oil is a P.D.O. (Protected Designation of Origin) product famous for its flavor and taste [21]. This oil is

used in food, liquor and pharmaceutical industries after a procedure of "rectification" in order to correct the amount of some component such as terpenes that could be toxic for human health [22].

3.3 Properties of essential oils

More than 300 types of essential oils are commercialized and they have different medical and biological properties based on their composition. Essential oils have several applications in food industries, agriculture, cosmetics and health applications. The use of essential oils in medicine has been started in ancient time of the human history. The biological properties of essential oils are many and various and they include antibacterial, antimutagenic, antioxidant, antiviral, immunomodulatory, anticancer and anti-inflammatory activity.

The increase of antibiotic resistance of bacteria has induced the scientific community to research alternative antibacterial agents such as essential oils.

Essential oils extracted from plant families such as *Poaceae, Apiaceae, Alliaceae, Asteraceae, Myrtaceae, Lamiaceae* and *Rutaceae* have been studied for their medical properties reported in Table 3.1[23].

Table 3.1: medical properties of essential oil from selected plant families [23].

Sr. no.	Plant family	Essential oil	Medicinal properties
1	Apiaceae (Umbelliferae)	*Carum nigrum* (Black caraway); *Anethum graveolens* (Dill); *Apium graveolens* (Celery); *Foeniculum vulgare* (Fennel); *Pimpinella anisum* (Anise); *Cuminum cyminum* (Cumin); *Corriandrum sativum* (Coriander)	Antibacterial; Antifungal; Anticancer; Antiviral; Anti-diabetic
2	Asteraceae (Compositae)	*Artemisia judaica*; *A.* annua; *A. absinthium* (Wormwood); *A. dracunculus* (Tarragon)	Antifungal; Anticancer; Antiviral
3	Geraniaceae	*Pelargonium graveolens* (Rose Geranium);	Antibacterial
4	Lamiaceae/Labiateae	*Origanum vulgare* (Origano); *Melissa officinalis* (Lemon balm); *Salvia officinalis* (Sage); *Mentha* sp.; *Mentha longifolia* (Wild Mint); *M. piperita* (Peppermint); *M. spicata* (Spearmint); *Ocimum basilicum* (Sweet Basil); *O. sanctum*; *Rosmarinus officinalis* (Rosemary); *Lavandula officinalis* (Lavender); *Lavandula* sp.; *Salvia sclarea* (Sage Clary)	Antibacterial; Antifungal; Anticancer; Antiviral; Antidiabetic; Antimutagenic, Antiprotozoal; Anti-inflammatory; Antioxidant
5	Lauraceae	*Cinnamomum* sp. (Cinnamon)	Antimicrobial; Anti-inflammatory; Antimutagenic
6	Liliaceae	*Allium sativum* (Garlic); *Allium cepa* (onion)	Antifungal; Antiviral; Antiprotozoal
7	Myrtaceae	*Syzigium aromaticum* (Clove); *Thymus vulgaris* (Thyme); *Thymus* sp.; *Melaleuca alternifolia* (Tea tree); *Eucalyptus globulus* (Blue gum); *Myristica fragrans* (Nutmeg)	Antibacterial; Antifungal; Anticancer; Antiviral; Antimutagenic Anti-inflammatory Antiprotozoal
8	Oleaceae	*Jasminum* sp.; *Olea europaea* (Olive)	Antibacterial, Anticancer
9	Piperaceae	*Piper nigrum* (Black pepper)	Antibacterial; Antifungal; Anticancer; Antiprotozoal
10	Pinaceae	*Cedrus libani* (Cedar wood oil)	Antifungal
11	Poaceae	*Cymbopogon martini* (Palmarosa); *Cymbopogon citrates* (Lemon grass); *Cymbopogon nardus* (Citronella grass);	Antifungal; Anticancer
12	Rutaceae	*Citrus* sp. (Lemon); *C. paradisi* (Grape fruit)	Antibacterial; Antifungal; Anticancer
13	Rosaceae	*Rosa* sp.;	Antifungal
14	Santalaceae	*Santalum* sp.; *Santalum album* (Sandalwood)	Antiviral
15	Zingiberaceae	*Zingiber officinale* (Ginger); *Zingiber montanum; Curcuma longa* (Turmeric); *Elettaria cardamomum* (Cardamom)	Antifungal; Anticancer; Antioxidant; Antimutagenic

Essential oils from plants of the *Apiceae* family, such as *Pimpinella* anisum and *Coriandrum sativum* are known for their antiviral, antimicrobial, antioxidant and

anti-inflammatory properties. These properties belong also to the oils extracted from plants of *Lamisceae* family, such as *Mentha Piperita* and *Rosmarinus officinalis*. Plants of this family are also used against bronchitis and gastrointestinal disorder and have antitumoral activity [8]. Plants from *Myrtaceae*, such as *Eucalyptus globus* and *Myrtus communis*, have antiviral, antibacterial, antitumor and antifungal properties. Essential oils from the *Pomaceae* family extracted for example from Lemmon grass (*Cymbopogon citratus*) and Citronell (*Cymbopogon nardus*), containing limonene, show antibacterial and antitumoral actions. Geranium and sandalwood oils, extracted from plants of the *Geraniaceae* and *Santalaceae* families, have antibacterial action. Other families plants as like *Hypericaceae , Liliaceae, Cupressaceae, Fabaceae, Zygophyl- laceae* and *Pinaceae* have also antibacterial properties [23].

3.3.1 Antibacterial properties of essential oils

The incidence of bacteria drug resistance is increasing and the side effects and toxicity limits the long term use of antibiotics. Essential oils have been shown to have antibacterial effects against Gram-positive and Gram-negative bacteria and they may respond to the need of novel alternative biocides molecules [23].
The majority of essential oils is more effective against Gram-positive bacteria than against Gram-negative ones [23].
Gram-positive bacteria and Gram-negative bacteria stand out for the composition of their cellular wall (Figure 3.11).

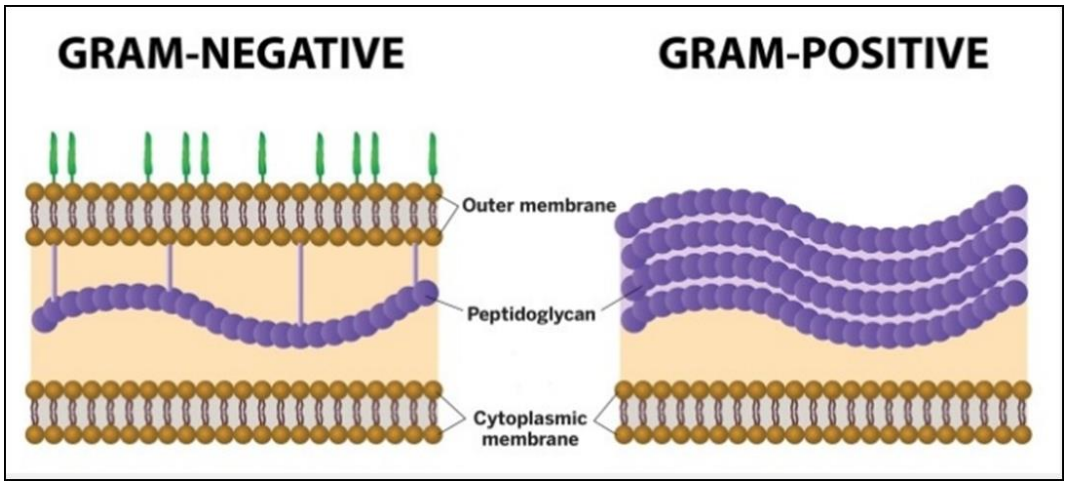

Figure 3.11: schematic representation of the composition of the cellular wall of Gram-negative and Gram-positive bacteria [24].

Gram-positive bacteria have a membrane composed by a thick wall of peptidoglycans with teichoic acid and some other proteins linked. Gram-negative bacteria are more complex with a single layer of peptidoglycans and the presence of outer membrane and periplasmatic space. Gram-positive bacteria have a structure that easily allows the hydrophobic molecules to penetrate the cells and that could explain the stronger effects on this kind of bacteria of essential oils which are rich in hydrophobic molecules [25]. The effects are dose dependent and can interfere with enzymatic process at low concentration and denature proteins at higher concentration. Gram-negative bacteria are almost impermeable at the passage of hydrophobic compounds but a small part can still enter through porins. The mechanism of actions of essential oils against bacteria depends on their composition. Terpenes do not show high antibacterial activity, while terpenoids that are terpenes with added oxygen molecules or that have methyl groups moved or removed show antibacterial activity related to their functional group. The presence of phenolic groups and of delocalized electrons is an important aspect for the antibacterial action of these molecules.

Phenylpropenes are present in a small number of essential oils and their antibacterial ability is conferred by the eventual presence of free hydroxyl groups. The antibacterial property of essential oils is not only do to a single mechanism but to a sequence of reaction acting on the whole bacterium (Figure 3.12).

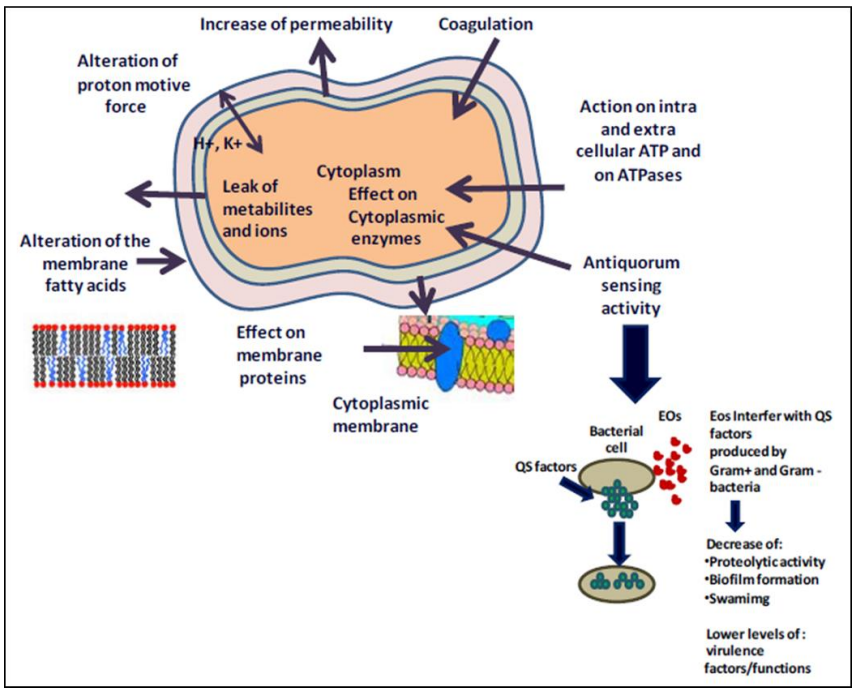

Figure 3.12: scheme of the site of actions of the essential oils on bacterial cell[26].

The hydrophobicity of essential oils disrupts the bacteria wall [27]and increases its permeability interfering with cellular process like energy balance, solute transport and regulation of metabolism. After degradation of cell wall, essential oils are able to damage the cytoplasmic membrane, coagulate the cytoplasm, denature proteins, reduce the ATP synthesis, reduce proton motive force and reduce the membrane potential [26]. Interacting with membrane, essential oils can also reduce the production of toxins by bacteria disrupting the phospholipid bilayer limiting the transmembrane transport and reducing the release of toxins.
The production of ATP in bacteria occurs both in cytosol and in cell wall by glycolysis and essential oils can alliterate the energetic balance reducing the intracellular ATP. Also the bacteria protein synthesis is modified by the essential oils and for examples p-cymene and carvacrol, two essential oil components, can induce the synthesis of heat shock proteins in bacteria. Essential oils modify the internal pH of bacterial cells interfering in cell homeostasis and influencing the capacity of block protons. The internal pH change interferes also with DNA transcription. Quorum sensing is a mechanism that bacterial cells use to communicate one with each other's producing molecules named autoinducers. Gram-negative bacteria produce acyl homoserine lactones and Gram-positive bacteria produce oligopeptides. Quorum sensing is involved in virulence, stress resistance, biofilm production, swarming and mobility and by controlling this way of communication is impossible to control infections and to decrease bacterial resistance. The way of action of essential oils on quorum sensing are still under investigation[28], [29]. The tested effects of several essential oils on different bacteria are resumed in Table 3.2.

Table 3.2: resume of the antibacterial effects of several tested essential oil.

Essential oils	**Bacteria**	**Effects**	**References**
Thymus vulgaris, Origanum vulgare, Cinnamomum zeylanicum, Rosmarinus officinalis and *Salvia officinalis* essential oils	Food pathogens (*Staphylococcus aureus, Listeria monocytogenes, Salmonella enteritidis, Campylobacter jejuni*) and five enterotoxin produced by S.*aureus* and *L.monocytogenes*	Antibacterial and antitoxic effects suitable for food industries	[30], [31]
Thyme, Laurel, Orange, Myrtle ad	*Escherichia coli, Listeria*	Antibacterial and bacteriostatic	[32]

Sage essential oils	*monocytogenes*, *Staphylococcus aureus* and *Candica Albicans*	activity. *L. monocytogenees* resulted to be less sensitive to essential oils action	
Fennel seeds (Principal compounds trans-anethole and estragole) essential oil	*Staphylococcus albus, Bacillus subtilis, Salmonella typhimurium, Shigella dysenteriae* and *Escherichia coli*	Antibacterial effect. The greatest effect was showed against *Shigella dysenteriae*	[33]
Anise, bay leaves, cinnamon bark, clove, fennel, hop, Istanbul oregano, Izmir oregano, mint, myrtus, orange peel, sage, thyme, and Turkish oregano essential oils	Four Gram-positive bacteria (*Listeria innocua, coagulase-negative staphylococci, Staphylococcus aureus, and Bacillus subtilis*) and six Gram-negative bacteria (*Yersinia enterocolitica, Salmonella Enteritidis, Salmonella Typhimurium, Proteus mirabilis, Escherichia coli* O157:H7 and *Klebsiella oxytoca*)	Essential oils of oreganos, cinnamon, and thyme had the highest inhibitory effects, while orange peel essential oil had the lowest inhibitory effect	[34]
Clove, laurel, cinnamon ceylan, pimento and winter savory essential oils	Three Gram positive bacteria (*S. aureus, L. monocytogenes* and *B. cereus*) and three Gram negative bacteria (*E. coli, S. Typhimurium, and P. aeruginosa*)	Antibacterial activity against both Gram-positive and Gram-negative bacteria, but were ineffective against *P. aeruginosa*	[35]
Thyme essential oil	Several bacteria present on human skin	Reducing bacterial contamination of cotton fibers	[36]
Lippia multiflora, Eugenia	Five oral-dental bacterial strain:	MIC obtained for these oils ranged	[37]

caryophyllata, *Mentha piperita* and *Zingiber officinale* essential oils	*Micrococcus luteus*, *Staphylococcus aureus* ATCC 29213, *Proteus mirabilis* ATCC 24974, *Pseudomonas aeruginosa* ATCC 27853 and *Candida albicans* IP 4872	from 0.078 to 5 mg/ml and the MBC ranged from 0.078 to 10 mg/ml. Highest MIC and MBC were observed for *Pseudominas aeruginosa* and lowest for *Micrococcus luteus*	
Mentha piperita essential oil	*Staphylococcus Epidermis* and *Escherichia coli*	Plasmidic elimination	[8]
essential oil and methanol extract of *Mentha longifoglia ssp. longifoglia*	Bacteria strain reported in Table 3.3	Essential oils showed strong antimicrobial activity, while the methanol extract was almost inactive	[38]
Peppermint and Chocolate mint essential oils	*P. aeruginona*, *Escherichia coli*, *S. aureus*	The obtained MIC for peppermint oil was 0.15 % v/v for *E. coli*, 0.08 %v/v for *S. aureus* and 0.92% v/v for *P. aeruginona*, while for the Chocolate mint the MIC founded are higher, 0.23, 0.09 and 1.22 % v/v respectively for *E.coli*, *S. aureus* and *P. aeuriginosa*	[5]

Table 3.3 Effects of *Mentha longifoglia ssp. longifoglia* against several tested bacteria[38].

Test microorganisms	Plant extract (MeOH)		Essential oil		Antibiotics	
	DD[b]	MIC[d]	DD[c] (mm)	MIC[d]	DD[a] (mm)	MIC[e] (max)
Acinetobacter baumanii-A8	–	–	14	31.25	18 (OFX)	31.25
Bacillus macerans-M58	–	–	22	15.62	19 (OFX)	15.62
Bacillus megaterium-M3	–	–	9	–	9 (SCF)	15.62
Bacillus subtilis-ATCC-6633	–	–	8	62.50	28 (OFX)	62.50
Bacillus subtilis-A57	–	–	–		28 (OFX)	125
Brucella abortus-A77	–	–	–	–	12 (SCF)	62.50
Burkholdria cepacia-A225	–	–	8	62.50	22 (SCF)	125
Clavibacter michiganense-A227	–	–	–	–	25 (SCF)	16.62
Enterobacter cloacae-A135	–	–	11	62.50	20 (NET)	31.25
Enterococcus faecalis-ATCC-29122	–	–	12	62.50	18 (SCF)	31.25
Escherichia coli-A1	–	–	18	31.25	20 (OFX)	62.50
Klebsiella pneumoniae-A137	–	–	14	31.25	12 (OFX)	125
Proteus vulgaris-A161	–	–	9	125	12 (OFX)	125
Proteus vulgaris-KUKEM1329	–	–	12	62.50	13 (OFX)	125
Pseudomonas aeruginosa-ATCC9027	–	–	–	–	22 (NET)	31.25
Pseudomonas aeruginosa-ATCC27859	–	–	–	–	22 (NET)	15.62
Pseudomonas syringae pv.*tomato* A35	–	–	–	–	24 (OFX)	125
Salmonella enteritidis-IK27	–	–	8	62.50	27 (SCF)	62.50
Staphylococcus aureus-A215	–	–	21	15.62	22 (SCF)	31.25
Staphylococcus aureus-ATCC-29213	–	–	14	31.25	22 (SCF)	62.50
Staphylococcus epidermis-A233	–	–	13	62.50	12 (SCF)	15.62
Streptococcus pyogenes-ATCC-176	–	–	–	–	10 (OFX)	62.50
Streptococcus pyogenes-KUKEM-676	–	–	–	–	13 (OFX)	31.25
Xanthomonas campestris-A235	–	–	–	–	20 (SCF)	31.25

The antibacterial activity of Mentha species in particular, is mainly attributable to the presences of phenols and alkanoids [39]. Menthol and menthone, compounds contained in high percentage in Mentha Piperita oils, showed as well as other monoterpenes great antibacterial activity and moreover, combining menthol with antibiotics such as oxacillin a synergistic antibacterial effects was obtained because of the increase of membrane permeability due to menthol action [40].

3.3.2 Antioxidant properties of essential oils

The inflammatory process is correlated with the production of ROS as described in chapter 2 paragraph 2.3.2 which are related with several diseases due to cell damage. Essential oils have shown antioxidant properties in several biochemical model simulating pathway or reactions in biological pathogenesis. They have antioxidant effects on lipid peroxidation that can cause cell death and by means of this capacity they can show protective effects on cell and reduce the inflammatory process[1]. Antioxidant properties of essential oils can be related by the ability of their compounds to stop the organic matter oxidation. Phenols, as reported in the previous chapter and some terpenoids are the main actors of the essential oils antioxidant properties. The organic matter oxidation mainly regards lipids, carbohydrates and proteins and occurs with a peroxyl radicals (ROO•) radical

chain mediated reaction in parallel with hydrocarbons autoxidation. This oxidative process is reported in figure 3.13.

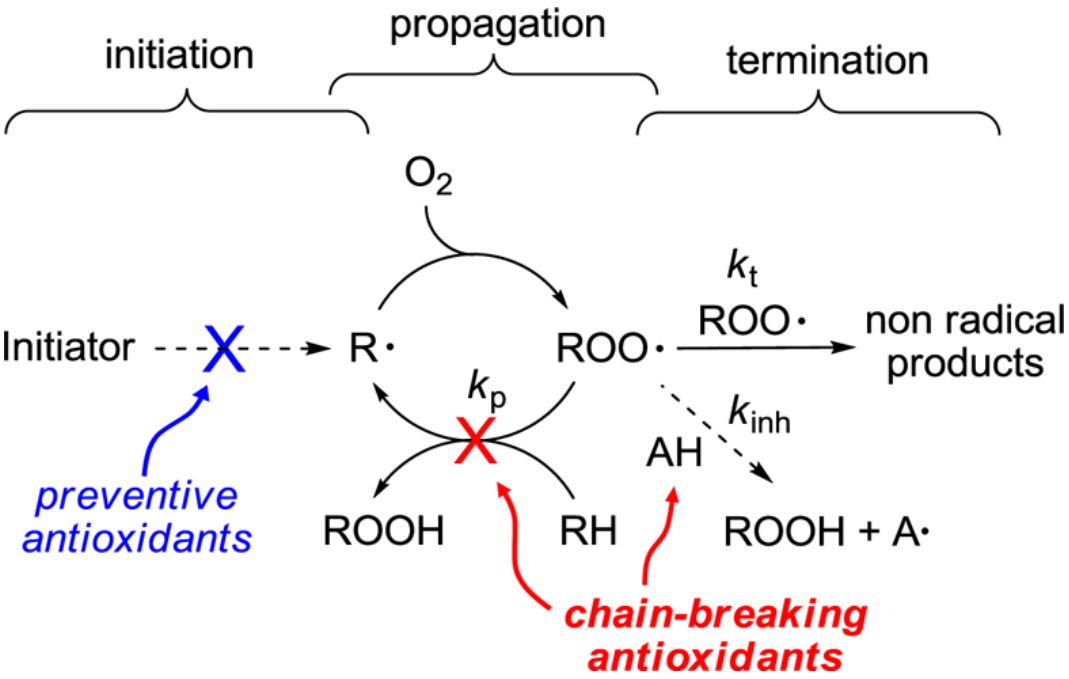

Figure 3.13: scheme of reactions of hydrocarbon autoxidation and antioxidant properties [41].

The reaction is started by a radical species reacting with RH (lipid) producing a R• radical which reacts with oxygen forming a peroxyl radical ROO•.
ROO• attacks cyclically a new organic molecule forming a hydroperoxide ROOH and another radical. This process continues until two radical species meet each other's in the termination steps. Substances with preventive antioxidant capacity can act directly in the initiation process, while chainbraking antioxidants reduce or block autoxidation interfering with the propagation of the reactions.
Phenolic compounds quench peroxyl radicals stopping the reaction with fast radical-radical reactions. Terpenoids can react with peroxyl radicals leading to reactive alkyl radicals, but there are several exceptions like terpenoids with cyclohexadiene structure that can conduce to chain termination. Cycloexadiene-terpenes are termination-enhancing antioxidants and they oxidize with a very fast termination process reducing the rate of oxidation. The complex nature itself of essential oils, with several antioxidants and oxidizable components required a study of essential oils composition in order to investigate the one with the best antioxidant ability and a synergic effects of their compounds [41], [42],[43].

In Table 3.4 are reported the antioxidant effects of different essential oils and their main compounds.

Table 3.4: antioxidant effects of several essential oils.

Essential oil	**Main antioxidant compounds**	**Antioxidant effects**	**References**
Piper nigrum L. essential oil obtained by hydrodistillation or by supercritical carbon dioxide distillation	β-caryophyllene, limonene	DPPH assay showed an higher scavenging activities for the hydrodistilled essential oil which contains a greater amount of β-caryophyllene	[44]
Oregano essential oil	Phenols: carvacrol ant thymol	Used since ancient time to avoid oxidative degradation of lard in food production	[42]
Salvia sharifii essential oil	Linalool	Moderate antioxidant activities (IC_{50} = 16.8 μg/mL)	[45]
Peppermint oil	Terpinene, rosmarinic acid, caffeic acid, eriocitrin, and luteolin (Figure 3.14)	Reduces polysaccharide-induced inflammation and prevents lipoperoxidation	[43]
Peppermint and chocolate mint essential oils	Alcohol (43.47-50.10%), terpene (18.55-21.07%) and (28.19-30.35%).	DPPH assay and β-carotene-linoleic assay showed a greater antioxidant activity of peppermint essential oils compared with chocolate mint essential oil, respectively the IC_{50} (inhibitory concentration needed to quench to 50% of the radicals present in	[5]

		the solution was 4.45 µl/mL and 19.86 µl/mL)	
Mentha longifolia essential oil	Limonene, isomenthone, menthol and linalool	The oil showed great antioxidant activity by means of DPPH assay with IC_{50} 0.86±0.01 mg/ml	[6]

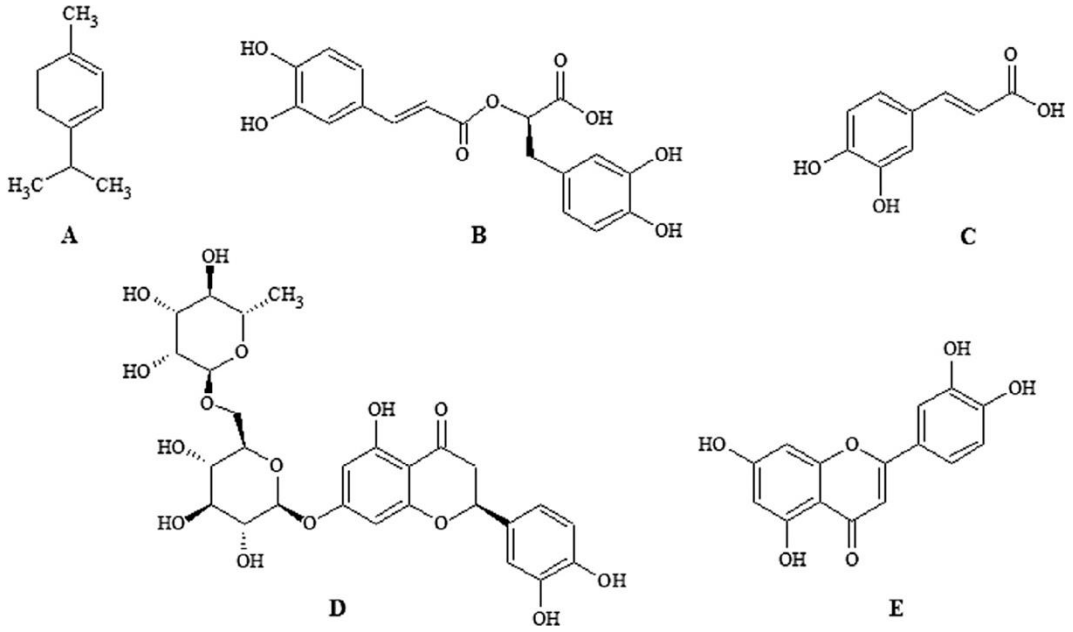

Figure 3.14: most recurrent antioxidant compounds in mint essential oil : A terpinene, B rosmarinic acid, C caffeic acid, D eriocitrin, E luteolin[43].

Carotenoids, retinoids, tocopherols, ascorbic acid, phenolic acids, flavonoids, terpenoids and polyphenols are all antioxidant molecules which could be contained in essential oils, but a good guideline for the choose of an essential oil with high antioxidant properties is a large content of phenolic compounds and a low contend of unsaturated terpenes with the exception of cyclohexadiene-like components[41], [42],[43],[45].

3.3.3 Anticancer activities of essential oils

It is reported in literature that essential oils have therapeutics effects on several cancer cells such as breast cancer, glioma, human liver tumor, colon cancer and pulmonary tumor. They can also be applied in prevention strategies. Polyphenols and some terpenoids content in essential oils can prevent tumor proliferation inducing apoptosis and necrosis of tumoral cells. The effects against tumor cells of several essential oils are reported in Table 3.5[23].

Table 3.5: antitumoral activities of some essential oils and their compounds.

Essential oil	Main compounds	antitumoral effects	References
Cymbopogon martini essential oil	Geraniol	Interferences with membrane functions and cell signaling of cancer cell lines	[23]
Atractylodes lancea oil	β-eudesmol	Help in prevent malignant tumors	[23]
Many essential oils	Terpenoids and polyphenol	Prevention of tumor cell proliferation through necrosis or induction of apoptosis	[23]
Myristica fragrans essential oil	Myristicin	Induction of apoptosis as displayed in neuroblastoma cells	[23]
Lemongrass essential oil	Citral	Active in vitro against early phase of rat hepatocarcinogenesis	[23]
M. alternifolia essential oil	Terpinen-4-ol	Reduced incidence of human melanoma	[23]
Chamomile essential oil	α-bisabolol	Induced apoptosi in glioma cells	[46]
Many essential oils	Geraniol	Reduced expression of thymidylate synthase and thymidine kinase decreasing the resistance at 5-	

		Fluorouracil (chemotherapeutic agent) of colon cancer cells	
Many essential oils	Limonene	Proapoptotic and antiangiogenic effects against human gastric cancer in dose and time dependent manner and enhance the effects of 5-Fluorouracil. Diallyl trisulfide, compound presents in garlic essential oil, arrests the division of human liver tumor cells probably acting on the regulation of cyclin B1 and Cdk7 expression	[46]
Eucalyptus essential oil	1,8-cineol	Induced morphological changes on human leukemia HL-60 cell	[46]
Lemon balm essential oil		Activity against A549, MCF-7, Caco-2, HL-60, K562 human cancer cell line	[46]
Artemisia annua L. essential oils		Apoptosis in SMMC-7721 hepatocarcinoma cells	[46]
Hydrodistilled frankincense and myrrh essential oils		MCF-7 and HS-1 cells showed sensitivity	[47]
Essential oils of *Tagetes erecta L.*, *Tetradenia riparia*, *Bidens sulphurea*		Effects against several tumoral lines: murine melanoma (B16F10),	[48]

and *Foeniculum vulgare*		human colon carcinoma (HT29), human breast adenocarcinoma (MCF-7), human cervical adenocarcinoma (HeLa), human hepatocellular liver carcinoma(HepG2), and human glioblastoma (MO59J, U343, and U251)	

Essential oils result effective against several tumoral lines because of their antioxidant effects and their ability to interfere with mitochondrial function of mammalian cells. They are able to reduce metabolic events such as increased cellular metabolism and mitochondrial overproduction characteristic of cancer development [23].

3.3.4 Toxicity of essential oils

US Food and Drug Administration (FDA) define 160 essential oils as "generally recognized as safe". In food industry sage, thyme, citrus, clove, coriander, rosemary and oregano essential oils are mainly used. International organisms like FDA and Council of Europe (CoE) established toxicological and chemical analysis protocols for essential oils with guidelines defining the maximal and minimal amount of volatile components that essential oils can contain.

Food Chemical Codex (FCC) classifies the constituents of essential oils commercialized as food flavors in three classes. The first class includes low toxic compounds with "fifth percentile no-observed-effect-level" (NOEL) of 3.0 mg/kg/d, the second class includes less safe compounds than the first class with NOEL of 0.91 mg/Kg/d and the third class contains compounds with relevant high toxicity with NOEL of 0.15 mg/kg/d[49], [50].

The first target of essential oils is the cytoplasmic membrane with its disruption and permeabilization. This ability confers to the essential oils their antibacterial activity, but it can also cause side effects such as cell necrosis or apoptosis. Aldehydes and phenolic compounds are the main actors of the cytotoxicity of essential oils against

bacteria, but they are also involved in negative effects towards hosts. They can cause corrosiveness, sensitization, irritation, phototoxicity, acute toxicity and carcinogenesis. The possible side effects of the essential oils depend on their composition and the toxic effects of singles compound were studied [23].
Essential oils are safe al low concentration and fortunately the acute toxicity due to oral intake is low with LD_{50} (Lethal dose 50) of 2-5 g/Kg, however some components such as pulegone, contained in Mentha Species, has a LD_{50} around 0.47 g/kg and it is important to control the amount of this compounds in Mentha essential oils for human use [1]. Regarding Mentha Piperita, rich of menthol, some side effects were observed in a woman that smoked a high number of menthol cigarettes every days becoming irritable and developing gastrointestinal disease probably caused by the major cell permeability induced by menthol, however after 17 days without menthol cigarettes the woman completely recovered. Another case of toxicity was reported for an old woman after 18 years of peppermint oil injections that developed severe pulmonary edema, again probably due to the increase of the pulmonary permeability[8].

3.3.5 Stability of essential oils

As illustrated in the previous paragraphs, essential oils are complex mixtures, with a composition depending on several factors. For this reason it is impossible to define general guidelines for the stability of all the essential oils, however some factors which are usually involved in the degradation of organic molecules can be considered (Figure 3.15).

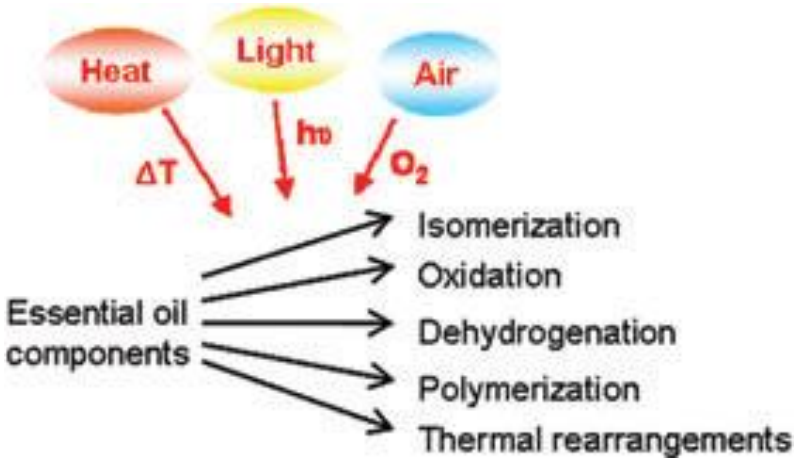

Figure 3.15: possible factors thatinfluence the stability of essential oils[51].

Visible and ultraviolet light accelerate autoxidation of essential oils enhancing the formation of alkyl radicals. Monoterpenes are the compounds most sensible to light irradiation. Essential oils undergo to degradation in different manner and this degradation is speed up by light in different way for each oils.
Temperature is an important factor influencing chemical reactions which are accelerated by heat. The oxidative process that leads to degradation of the essential oils is speed up by increasing temperature, but at the same time lower temperature enhances the oxygen solubility that can reduce the stability of oils. This aspect was not extensively studied, but some investigations on single essential oils were performed. After 3 months of storage in the fridge, for the essential oil of rosemary, the oxidation can be prevented demonstrating a good stability of this oil. Pine essential oil, instead, forms peroxides even at 5°C. At high temperature, terpenoids, which are thermolabile, can face rearrangement process. Obviously the presence of oxygen plays a decisive role in oxidation of essential oils. The consumption of oxygen by monoterpenes was recorded to influence the physiochemical properties of the oils and this phenomenon is more pronounced in containers not completely full of oil. The spoilage of the oils accelerates with the increase of dissolved oxygen and is a function of temperature and pressure. Another aspect that could influence stability of essential oils is the presence of metal ions such as ferrous ions and copper ions, present as contaminants, that can promote autoxidation[51]. Essential oils spoilage can be noted with change in the color and viscosity and the alteration of the properties, for examples generation of peroxides in tea tree oil, can lead to irritating activities. As general recommendation it is suggested to store essential oils in the dark, away from heat sources and in full sealed containers or in nitrogen atmosphere[1].

3.4 Functionalization with essential oils

As mentioned for the polyphenols in chapter 2 paragraph 2.4, natural molecules are attracting more and more interest in the scientific community, but a massive study was started only in the last few years. Performing a search in PubMed with keyword “essential oil” in title and abstracts of articles between 01/01/1970 and31/12/2016, 7420 articles were found. The number of articles has been growing in exponential manner with a maximum in 2016 as reported in Figure 3.16.

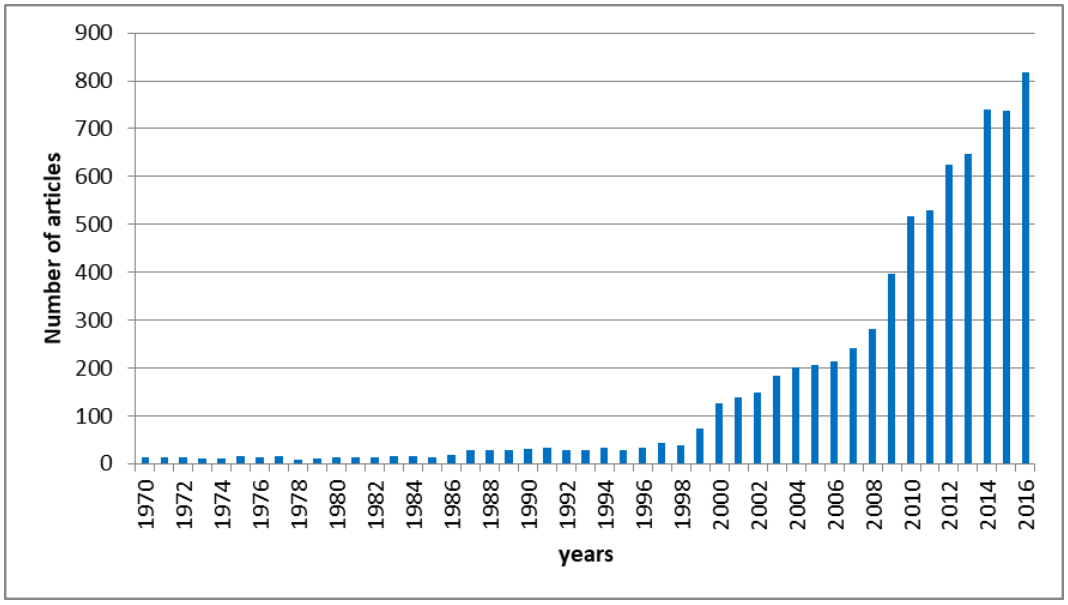

Figure 3.16: number of articles for years from 01/01/1970 to 31/12/2016 found on PubMed with the keyword "essential oil".

Despite the increasing interest in essential oil properties, as previously reported for polyphenols, a low number of attempts of coupling essential oils with material are presented in literature. Performing search in PubMed with keywords "essential oil and titanium" in title and abstracts of articles between 01/01/1970 and 31/12/2016 only 4 articles were found and none focused on functionalization. Performing search in PubMed with keywords "essential oil and glass" in title and abstracts of articles between 01/01/1970 and the 31/12/2016 only 35 articles were founded and again none focused on the functionalization procedures.
Some attempts of use of essential oils in combination with other materials or for their treatment are reported below in Table 3.6.

Table 3.6: resume of the attempts of the combined use of essential oils and materials.

Essential oil/ compound	**Use**	**Results**	**References**
Salvia officinalis essential oil	Magnetic nanofluid used for coupling the oil as nanoparticles on the surfaces of the prosthetic implant Provox	Avoid biofilm formation	[52]
Cinnamon essential oil	Coating of stainless steel orthopedic prosthesis	avoid biofilm formation by *Staphylococcus Epidermis*	[53]
Artemisia Mesatlantica essential oil	Adsorption on carbon steel	Corrosion inhibitor	[54]
Mentha Spicata Essential Oil	Adsorption on steel	Avoid corrosion	[55]
Eugenol	Presence of the compounds in oral environment with titanium implant	Reduced corrosion	[56]
Oregano essential oils	Functionalization of alginate film	Increased elongation at break and thickness of the film itself and conferring it antibacterial properties	[57]
Carvacrol and thymol isolated from the essential oil of *Origanum dictamnus* and *Artemisia arborescens L.*	liposomal embedded	Preserved antiviral and antimicrobial activities	[58], [59]
Cinnamon essential oil	Encapsulation in a sol-gel produces hybrid silica matrix	Antibacterial effect	[60]
Menthol	Menthol-PCl micro and nanoparticles for the	Avoid bacterial and mycotic	[61]

	functionalization of cotton tissue	contamination	
Eugenia carryophyllata essential oil	Core/ shell Fe_3O_4/oleic acid nanoparticles with a coating of adsorbed essential oil	Improved resistance to mycotic colonization of catheter surface pellicles	[62]
Anethum graveolens and *Salvia officinalis* essential oils	Coating by adsorption of magnetic nanoparticles	Production of a wound dressing surface resistant to *Candida Albicans* adhesion	[63]
Mentha Piperita essential oil	Coating of magnetic nanoparticles	Reduced bacterial contamination of prosthetic devices	[64]
Peppermint essential	Production of nanoparticles	Antibacterial effect	[65]
Thymol	Encapsulation in ethylcellulose/ methylcellulose submicronspheres	Antibacterial effect	[66]
Thyme oil	Encapsulation in chitosan and benzoic acid-based nanogel	Preserved half-live and antifungal activity	[67]
Essential oils of Cassia, Oregano and Red Thyme	Encapsulation in zein nanospheres by means of phase separation	Antibacterial effect	[68]
Peppermint essential oil	Encapsulation by means of coacervation method into gelatin/gum Arabic microcapsule	Protects it to degradation in the gastric transition	[69]
Metha Spicata L. essential oil	Encapsulation in chitosan matrix	Relieving skin irritation	[70]

3.5 Materials and methods

3.5.1 Characterization of the essential oils

Three different essential oils were considered for the surface functionalization of titanium alloy:

- Thyme essential oil
- Mentha Piperita essential oil
- Mentha Piperita of Pancalieri essential oil

Thyme oil and Mentha Piperita essential oil were extracted by means of steam distillation at the Plant Physiology Unit, Department of Life Sciences and Systems Biology, University of Turin, Via Quarello 15/A, 10135 Turin, Italy. Mentha Piperita of Pancalieri oil is instead a commercial not deterpenated essential oil produced by the Azienda Agricola EssenzialMente Pancalieri.
The essential oils of Thyme and Mentha were available only in a low amount, so the larger functionalization campaign was performed with the Mentha Piperita essential oil of Pancalieri which is available in greater amount and has good antibacterial activity[20]. The essential oils were characterized by means of gas chromatography analysis in order to understand their composition with the sequent protocol. Following the addition of 3 mL of MilliQ water and 1 mL of n-hexane at the essential oil, the sonicated samples were mixed vigorously by vortex for 20 sec and then centrifuged at 1000 RPM for 5 min using a table top centrifuge. The organic upper phase was then dehydrated in a glass column packed with anhydrous magnesium sulphate (Fluka, USA) and concentrated by a constant flow of nitrogen (N_2) to 100 µl before GC-MS analysis.
Qualitative and quantitative analyses of the different compounds were performed by GC-MS on an Agilent 6890N gas chromatograph coupled to Agilent 5973A mass spectrometer. The GC was equipped with a HP5-MS column (30 m length, 250 µm diameter, 0.25 µm thickness). Helium was used as carrier gas at constant flow of 1 mL min-1. The following temperature program was used: 60°C as initial temperature, thermal gradient of 3°C min-1 up to 250°C. Post time lasted 2 minutes at 250 °C. Injector port was set at 250°C in splitless mode. Transfer line temperature to MSD was 280 °C and ionization energy (EI) was 70 eV. Mass spectra were acquired in full scan mode with 50 – 350 m/z range.

In total 3 µl of each sample were injected in the GC-MS and the identification of compounds was based on the comparison of their mass spectra with NIST 98 by the NIST v2.0 research software.
The Mentha Piperita essential oil of Pancalieri was also characterized by means of FTIR (FTIR, Alpha, Bruker Optics, Ettlingen, Germany) in ATR mode in order to understand the chemical groups present in the essential oils which will later be researched on the surface of the functionalized samples.

3.5.2 Antibacterial characterization of essential oils

Essential oils of Thyme and Mentha Piperita distilled at the Plant Physiology Unit, Department Life Sciences and Systems Biology, University of Turin, were tested against several bacteria acquired from the American Type Culture Collection (ATCC) or isolated from patients. These analyses were performed at the Department of Public Health and Pediatrics of the University of Torino. The strain acquired from ATCC were three Gram-positive bacteria *Staphylococcus aureus* (ATCC 29213), *Staphylococcus epidermidis* (ATCC 35984), *Enterococcus faecalis* (ATCC 29212), while the strain isolated from patients were Gram-positive bacteria *Staphylococcus aureus*, *Staphylococcus epidermidis* and *Enterococcus faecalis* and Gram-negative bacteria *Escherichia Coli* and *Klebsiella pneumoniae*. In order to evaluate the antibacterial activity of each oil, the samples were tested two times in serial dilution with factor 2 in order to found the minimum inhibitory concentration (MIC) and minimum bactericidal concentration (MBC). This analysis was performed in order to select suitable essential oils for titanium alloy samples functionalization.

3.5.3 Preparation of Ti6Al4V samples

Ti6Al4V samples were prepared as reported in chapter 2 paragraphs 2.5.4 and 2.5.5 and the procedure is repeated below. The material used was Ti6Al4V (ASTM B348, Gr5, TitaniumConsulting and Trading). The samples were cut into slices with thickness of 2 mm from cylindrical bars (10 mm diameter) with an automatic cutter (Struers Accutom 5). After the cutting the samples were signed with a letter on one side and polished on the opposite one with abrasive SiC papers (up to 4000). The samples for the functionalization with 2% essential oils were cut in half before the washing steps. The polished samples were washed in

acetone for 5 minutes in an ultrasonic bath and then ultrasonically washed twice for 10 minutes in ultrapure water. After washing the samples were dried at room temperature under laminar flow. In order to make the titanium alloy samples bioactive and functionalizable, they were treated with a patented chemical treatment developed by the research group[71], [72]. This treatment consists in an acid etching with diluted hydrofluoric acid and a reoxydation in hydrogen peroxide. The surface obtained has a specific pattern at the nanometric and micrometric scale inducing a good response of osteoblasts and rich of hydroxyl groups which allow the functionalization with biomolecules In order to improve the reactivity of the –OH groups the samples were exposed for 1h to UV irradiation. The samples treated with the chemical treatment and irradiated with UV are named CT (chemical treated).

3.5.4 Surface functionalization of the samples with 2% essential oils

The first attempts of functionalization were performed by soaking for 24 h the samples in a 2% solution of essential oil in ethanol. This percentage was chosen on the basis of the one usually used for antibacterial tests with essential oils. The oils used for this functionalization were Thyme oil and Mentha Piperita oil chosen on the basis of the antibacterial test on the bare oils [73], [74]. One sample was functionalized with Thyme essential oil, one sample with Mentha Piperita oil (both samples are disks of titanium alloy cut in half because the low quantity of oil available) and another sample (an entire disk), was not functionalized, but only soaked in ethanol as reference. An amount of 50 µl of Thyme essential oils was diluted in a holder containing 2450 µl of ethanol, and the same dilution (2% of oil) were used in a different holder for the Mentha Piperita essential oil. By contrast, 5 ml of ethanol was put in the holder for the sample which was not divided in half. All the holders were covered by thin aluminum foil. The holders were placed in incubator at 37 °C for 24 h. After the incubation, the samples functionalized with the two types of essential oils were washed in ethanol and then in ultrapure water, whereas the specimen CT_ ethanol_water washed was washed only in ultrapure water and dried at room temperature. The samples were dried at room temperature under laminar flow and stored in the dark.
The samples were indicated respectively as:
- CT 2% Thyme oil_ethanol washed_water washed
- CT 2% Mentha Piperita oil_ethanol washed_water washed

- CT_ ethanol_water washed (control sample)

3.5.5 Surface functionalization of the samples with Mentha Piperita essential oil of Pancalieri

Several attempts were performed in order to define the best protocol of functionalization of bioactive chemically-treated titanium alloy CT with Mentha essential oils. No references were found in literature about this kind of functionalization and several protocols of functionalization or coating were developed and investigated in order to understand the reactivity of the essential oils and the affinity of its biomolecules with the surface. The main scope of this work is to develop an appropriate protocol of functionalization which allows to bind the chemical molecules of essential oils to the materials' surface conferring the main properties of the essential oil while avoiding cytotoxic effects. In a first attempt the CT samples were placed on a holder covered with aluminum foil in order to avoid UV degradation and a drop (5 μl) of Mentha Piperita of Pancalieri essential oil was placed on each sample using a micropipette. Finally, the samples were placed in incubator at 37°C for 48 hours until the formation of a layer of polymerized essential oil. After polymerization the samples were washed twice in ultrapure water and dried under laminar flow and stored in the dark. These samples were named from now on CT_Metha oil_water washed. Some samples were not washed after coating and were named CT_Mentha oil.

In a second attempt samples with different protocols of coating were performed and listed below:

- CT_Metha oil_ethanol washed: After the treatment described for the CT_Mentha oil protocol the samples were not washed in ultrapure water but only one time in ethanol.
- CT_Metha oil_ethanol washed_water washed: After the treatment described for the CT_Mentha oil protocol the samples were washed one time in ethanol and one time in ultrapure water.
- CT_50% Mentha oil _wash ethanol _wash water: after the treatment described for the CT_Mentha oil samples the samples were washed one time in ethanol and one time in ultrapure water.

For the functionalization with the essential oil, several protocols were investigated and are reported below:

- CT_20% Mentha oil (soaking)_ethanol washed_water washed: the CT samples were placed in a holder covered with a tin aluminum foil and covered with 2.5 ml

of a solution of functionalization of 20% Mentha oil in ethanol. The samples were placed at 37°C for 48h and then washed one time in ethanol and one time in ultrapure water.

- CT_20% Mentha oil(soaking)_ethanol washed: the CT samples were placed in a holder covered with a tin aluminum foil and covered with 2.5 ml of a solution of functionalization of 20% Mentha oil in ethanol. The samples were placed at 37°C for 48h and then washed one time in ethanol.
- CT_20% Mentha oil(soaking): the CT samples were placed in a holder covered with a tin aluminum foil and covered with 2.5 ml of a solution of functionalization of 20% Mentha oil in ethanol. The samples were placed at 37°C for 48h and then dried at room temperature without washing steps.
- CT_30% Mentha oil(soaking)_ethanol washed_water washed: the CT samples were placed in a holder covered with a tin aluminum foil and covered with 2.5 ml of a solution of functionalization of 30% Mentha oil in ethanol. The samples were placed at 37°C for 48h and then washed one time in ethanol and one time in ultrapure water.
- CT_40% Mentha oil(soaking)_ethanol washed_water washed: the CT samples were placed in a holder covered with a tin aluminum foil and covered with 2.5 ml of a solution of functionalization of 40% Mentha oil in ethanol. The samples were placed at 37°C for 48h and then washed one time in ethanol and one time in ultrapure water.
- CT_50% Mentha oil(soaking)_ethanol washed_water washed: the CT samples were placed in a holder covered with a tin aluminum foil and covered with 2.5 ml of a solution of functionalization of 50% Mentha oil in ethanol. The samples were placed at 37°C for 48h and then washed one tine in ethanol and one time in ultrapure water.
- CT_50% Mentha oil(soaking)_water washed: the CT samples were placed in a holder covered with a tin aluminum foil and covered with 2.5 ml of a solution of functionalization of 50% Mentha oil in ethanol. The samples were placed at 37°C for 48h and then washed one time in water.
- CT_50% Mentha oil(soaking): the CT samples were placed in a holder covered with a thin aluminum foil and covered with 2.5 ml of a solution of functionalization of 50% Mentha oil in ethanol. The samples were placed at 37°C for 48h and then dried at room temperature without washing steps.

Two more kinds of samples were prepared in order to investigate the effects of the ultrapure water and ethanol washing on the surface of CT samples.

- CT_48h ethanol(soaking): the CT samples were soaked for 48h at 37°C in ethanol and then dried under chemical hood at room temperature.

- CT_48h ethanol(soaking)_ water washed: the CT samples were soaked for 48h at 37°C in ethanol and then washed in ultrapure water and dried under chemical hood at room temperature.
  The protocols of functionalization and coating are schematically represented in Figure 3.17.

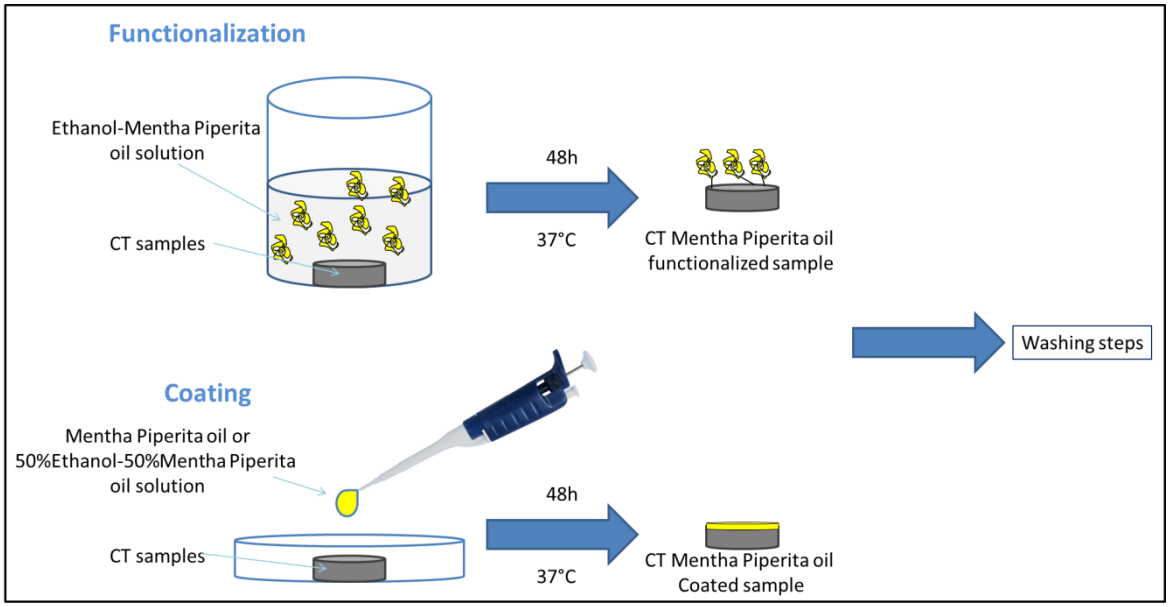

Figure 3.17: scheme of the CT surface functionalization/coating with Mentha Piperita of Pancalieri essential oil.

3.5.6 Fluorescence microscope observation

Presence and distribution of the essential oil in the surface of the CT samples were investigated by fluorescence microscope (Leica DM5500 BLeica Microsystems, IL, USA) exploiting the autofluorescence of essential oil [8].

3.5.7 Gas chromatography analysis

Gaschromatographic analysis were performed on the samples coated/functionalized in order to understand which molecules of the essential oils are able to bind the surface of the CT sample. The analysis was performed on solutions obtained from the samples reported below:

- CT as control sample
- CT_Mentha oil(soaking)
- CT_Mentha oil(soaking)_water washed
- CT_20%Mentha oil (soaking)_ethanol washed_water washed
- CT_50% Mentha oil (soaking)_ethanol washed_water washed

After coating/functionalization, the compounds of the oil grafted to the surfaces of the samples were detached sonicating each sample in 3 ml of ethanol for 10 minutes in a plastic holder covered with aluminum in order to avoid UV degradation of the biomolecules. With a first analysis, no peaks were revealed, so the solutions were concentrated with the use of hexane. The ethanol in which were sonicated the samples were placed in glass tube and 3 ml of ultrapure water and 1 ml of Hexane was added. The solutions were maintained under stirring for 20 seconds and then centrifuged for 5 minutes at 1000 rpm. The Hexane upper phase were transferred in another holder and concentered at 100 µl. 3 µl of the concentrated solution were injected in the gaschromatograph and the analysis were performed with the program reported in paragraph 3.5.1

3.5.8 Contact angles measurements

Wettability tests were performed on the samples as reported in chapter 2 paragraph 2.5.8 and reported below. The surface wettability was evaluated by means of measurements of the contact angle with sessile drop method before and after the functionalization on bulk samples. Each sample was placed on the support of the machine (Kruss DSA 100) in front of the camera with the treated side upward and a drop of 5 µl of ultrapure water was deposited with a micropipette on the surface. The images were acquired with the camera and elaborated by the software obtaining the value of the contact angle. The measures were performed in triplicate on each kind of samples produced.

3.5.9 Fast Fourier transform infrared spectroscopy

Fast Fourier transform infrared spectroscopy (FTIR, Hyperion 3000) analysis in transmittance mode were performed in order to highlight the chemical groups present on the surface of the samples after the functionalization and revealed the presence of essential oil. Spectra were acquired between 400 and 4000 cm^{-1}. Each

sample was positioned on the focal plan by means of the optic microscope of the instrument and irradiated with IR, two random points for each samples were acquired and the two spectra were collected with the software SCOPUS and mediated.

3.5.10 X-ray photoelectron spectroscopy

X-ray photoelectron spectroscopic analysis (XPS, PHI 5000 VERSAPROBE, PHYSICAL ELECTRONICS) were performed in order to determine the chemical composition of the samples surface before and after the functionalization. High resolution spectra of carbon and oxygen regions were acquired in order to identity the chemical groups characteristic of essential oils. This analysis was performed on samples:

- CT
- CT_Mentha oil
- CT_Mentha oil_water washed
- CT_Mentha oil_ethanol washed_water washed
- CT_20%Mentha oil(soaking)_ethanol washed_water washed
- CT_50%Mentha oil(soaking)_ethanol washed_water washed

3.5.11 Zeta potential electrokinetic measurements

Electrokinetic measurements were performed as reported on chapter 2 paragraph 2.5.9 and the procedure is briefly summarized below. Measurements of the z potential were performed on the samples before and after functionalization by means of the streaming potential technique using an electrokinetic analyzer (SurPASS, Anton Paar). For each measurement, a couple of samples is needed and the zeta potential of the surface was analyzed in function of pH in a 0.001M KCl electrolyte solution varying the pH with the addition of 0.05 M HCl or 0.05 M NaOH trough the automatic titration unit of the instrument according with the standard procedure[75] .

Z potential measurements were performed for samples:

- CT
- CT_ethanol(soaking)_water washed
- CT_20% Mentha oil(soaking)_ethanol washed_water washed

- CT_50%Mentha oil(soaking) _ethanol washed_water washed
- CT_Mentha oil_water washed
- CT_Mentha oil_ethanol washed_water washed

3.5.12 Tape test

Tape test was performed on sample CT_Mentha oil_water washed in order to evaluate the adhesion of the essential oil coating to the CT surface. This test, performed in accordance with the standard ASTM D 3359[76] evaluates the adhesion of coating films to substrates by applying and removing a strip of pressure sensitive tape over cuts made in the film with a sharp razor blade.
Cuts were made on the polymerized film with a razor along a grid and any detached chippings were removed with a brush. A rubber based adhesive tape was applied on the selected area over the grid and then removed with a rapid pull. Then the grid area were observed with an optical microscope and the adhesion was classified in accordance to standard ASTM D 3359 (Figure3.18).

CLASSIFICATION OF ADHESION TEST RESULTS		
CLASSIFICATION	PERCENT AREA REMOVED	SURFACE OF CROSS-CUT AREA FROM WHICH FLAKING HAS OCCURRED FOR SIX PARALLEL CUTS AND ADHESION RANGE BY PERCENT
5B	0% None	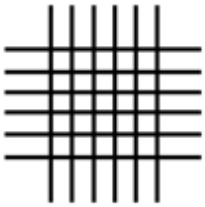
4B	Less than 5%	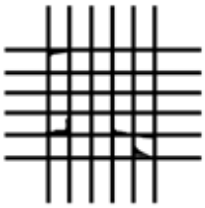
3B	5 – 15%	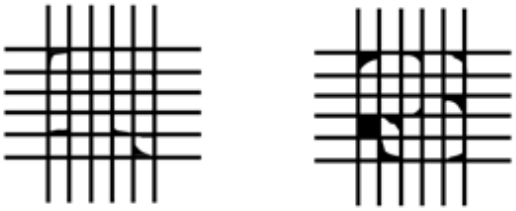
2B	15 – 35%	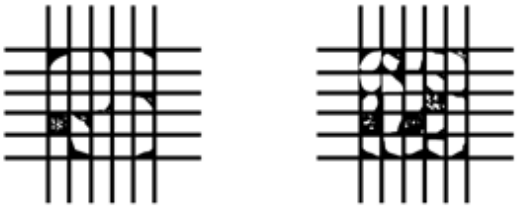
1B	35 – 65%	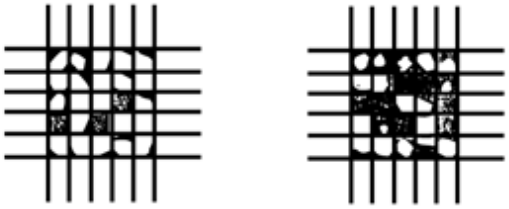
0B	Greater than 65%	

Figure 3.18: classification of adhesion test in accordance with ASTM D3359[76].

3.5.13 Biological tests

Antibacterial tests

In order to understand the antibacterial properties of the coated/functionalized CT samples, different antibacterial tests were performed.

Kirby Bauer test:

The antibacterial effects of the CT_Mentha oil_water washed samples was evaluated by means of Kirby Bauer test. The bacterium employed was *Staphylococcus aureus* ATCC 29213 acquired from the American
Type Culture Collection (ATCC). *Staphylococcus aureus* is a common Gram-positive bacterium in periprosthetic infections. The bacterial broth was prepared from lyophilized pellet of bacteria introducing them in the highly nutritive growth medium Brian Heart Broth and incubating it for 24 h at 35°C. After 24 h the brothel with the bacteria were shaded on a blood agar plate (Figure 3.19) and incubated again for 24h at 35°C.

Figure 3.19: Blood agar plate with *Staphylococcus aureus* ATCC 29213 culture.

Then a 0.5 Mc Farland solution of the bacteria was prepares and passed with a swab on a Muller Hilton plate in order to cover the entire surface. The samples were placed on then Muller Hilton plate whit the bacteria with the antibacterial surface in contact with the plate and incubated for 24 h at 35°C.
The last step was the analysis of the shadow produced by the samples on the plate in case of release of antibacterial molecules and the presence of the bacteria on the surface of the sample itself in order to investigate bacteriostatic properties. After these observations the samples were detached from the plate, eventually bacteria present on the surface were fixed with heath and metallized with chromium for a subsequent FESEM observation.

Broth dilution method:

Bacteria adhesion tests were performed in order to quantify the amount of bacteria adherent on the sample surface of the samples after culture in the bacterial broth. The tested bacteria is the same of the Kirby Bauer test *Staphylococcus aureus* ATCC 29213. In the adhesion tests, the samples were incubated in bacterial broths with inoculum of 10^4 CFU/ml for 24 h and then the evaluation of the adherent and non-adherent bacteria were performed. The tests consist in several steps explained below:

- The broth culture (mycorrhiza helper bacteria MHB) was prepared overnight at 37°C starting from pellet of microbank stored bacteria.
- N. 5 tubes were prepared. 5 ml of the broth were placed in the first test tube and dilution of 100 µl to 100µl was repeated until tube 5.
- Test tube n.5 was centrifuged at 4000 rpm for 10 minutes.
- The pellet was resuspended in 100µl of MHB.
- 5 ml of physiological solution 0.9% 0.5 Mc Farland were prepared (10^8 CFU/ml).
- The bacteria inoculum were prepared
  - 0.1ml of the 0.5 Mc Farland (10^8)+9.9 MHB→10^6
  - Final inoculum: 0.2ml of the 10^6 inoculum+19.8 MHB→10^4
- The samples were placed in a multiwell plate and covered with 5 ml of the final inoculum (10^4 CFU/ml), a CFU plate counting was also prepared with the final inoculum in order to control the concentration.
- The samples and the control were incubated at 37°C for 24h.
- For the counting of non-adherent bacteria 0.5 ml of the broth culture of each sample were progressive diluted in sterile water and the relative CFU plating count on nutrient agar was performed.

- For the counting of adherent bacteria, the bacteria were removed from the surface of the samples. The samples were transferred into sterile bags with 1.5 ml of physiological solution 0.9% and sonicated at 43 Hz for 7 minutes in order to detach the bacteria from the surface.
- The samples were removed from the bags and the bags were placed in a vortex mixer.
- 0.5 ml of the physiological solution were taken from each bags progressive diluted with sterile water.
- For each samples were performed CFU plate counting obtaining the amount of the adherent bacteria.

This test was performed on the samples listed below:

- Ti6Al4V mirror polished
- CT
- CT_Mentha oil_water washed
- CT_Mentha oil_ethanol washed_water washed
- CT_20%Mentha oil(soaking) ethanol washed_water washed
- CT_50%Mentha oil(soaking) ethanol washed_water washed

These analyses were performed at the Department of Public Health and Pediatrics of the University of Torino.

Antibacterial Properties Evaluation:

Bacteria strain and growth conditions

A single colony of a multi-drug resistant (MDR) *Staphylococcus aureus* (reference strain ATCC 25923, purchased from the American Type Culture Collection, Manassas, USA) from an overnight culture onto selective Mannitol Salt Agar plate (Sigma-Aldrich) was resuspended in 9 mL of Luria Bertani broth (LB, Sigma-Aldrich) and incubated at 37°C for 18 h. After incubation, a new fresh LB tube diluted 1:10 was prepared. The new tube was incubated at 37°C for 3 hours in order to achieve the logarithmic growth phase. Finally, a fresh broth-culture was prepared prior each experiment by diluting bacteria in LB broth until optical density (o.d.) resulted as 0.005 at 600 nm, thus corresponding to a final concentration of 1x105 cells /ml.

Biofilm formation

Sterile specimens were placed in a 24 multiwell plate (Nunclon Delta Surface, Thermo Scientific) and submerged in 1 ml of LB medium containing $1*10^5$ cells /

ml prepared as previously described. The plate was incubated for 90 minutes at 37°C under agitation at 120 rpm (adhesion phase). Supernatants were then extracted to remove floating planktonic cells (separation phase) and specimens gently washed 3 times with PBS to remove non-adherent cells. Then, each specimen was rinsed with 1 ml of fresh LB medium and plate incubated for 24, 48 and 72 h at 37°C for biofilm culture.

Bacterial Cell Viability

To assess the growth capacity of the bacterial strains after 24, 48 and 72 h of direct contact compared to that of untreated controls, bacterial viability was evaluated by the validated quantitative colorimetric metabolic 2,3-bis (2-methoxy-4-nitro-5-sulphophenyl)-5-[(phenyl amino) carbonyl]-2H-tetrazolium hydroxide assay (XTT, Sigma-Aldrich). Briefly, 20 µL of XTT solution (3 mg mL−1 in acetone containing 0.1M menadione) were added to each well and plates were incubated at 37°C for 5 h in the dark. Then, 50 µL were collected from each well and centrifuged for 2 min at 480 g to remove any debris, and the optical density was evaluated using a spectrophotometer (SpectraCount, IBM) at 490 nm. Mirror-polished specimens were considered as control.

Live/Dead Assay

To determine the viability of bacteria a Live/Dead BacLight bacterial viability kit (Molecular Probes, Life Technologies Italia, Monza, Italy) was used. The kit includes two fluorescent nucleic acid stains: SYTO9 and propidium iodide. SYTO9 penetrates and stains both viable and nonviable bacteria, while propidium iodide enters only damaged/dead cells and quenches SYTO9 fluorescence.

For assessing viability, 1 mL of stock solution of each stain was added to 3 mL of PBS and, after mixing, the solution was distributed into the plates containing the materials specimens and incubated at RT for 15 min in the dark. Stained biofilms were examined by fluorescent microscope (Leica 6500, Leica Microsystems, Basel, Switzerland). Finally, the number of dead bacteria was calculated and expressed as % of total bacteria number by ImageJ (NIH, Bethesda, USA) software.

These analyses were performed at the Department of Health Sciences, Università del Piemonte Orientale UPO, Via Solaroli 17, 28100 Novara, Italy on the samples:

- Ti6Al4V mirror polished
- CT
- CT_Mentha oil_water washed

- CT_50%Mentha oil_ethanol washed water washed

Cytotoxicity assay

Cell tests were performed in order to investigate the cytotoxic effects of the essential oil on the coated/functionalized samples.
Samples cytocompatibility was evaluated towards human osteoblasts progenitor cells (hFOB 1.19) that were purchased from the American Type Culture Collection (ATCC, Manassas, USA, ATCC CRL-11372). hFOB were cultured in DMEM: Ham's F12 mixture (50:50, Sigma) supplemented with 10% fetal bovine serum, 1% antibiotics and 0.3 mg/ml neomycin (G418 salt, Sigma). Cells were cultured at 34°C, 5% CO_2 until 80–90% confluence, detached with trypsin–EDTA solution (Sigma) and used for experiments.
Samples produced in clean conditions were gently collected with surgical tweezers avoiding any surface impairment and seeded onto a new 24 well plate; cells (hFOB) were seeded in a defined number ($1x10^4$ cells/specimen) directly onto specimens' surface and cultivated using 1 ml of fresh medium for 24, 48 and 72 h at 37°C, 5% CO_2. Afterwards, at each selected time-point, cells viability was evaluated by the Alamar blue colorimetric assay (alamarBlue, Thermo Fisher) following manufacturer's instruction. Briefly, 100 µl of the ready-to-use Alamar solution was added to each well containing cells-seeded specimens and the plate was incubated 4 h at 37°C in the dark. Then, 100 µl of each supernatants were collected and transferred to a new black-bottom 96 wells plate; after gently shaking the plate, fluorescence intensity was detected at 600 nm with a spectrophotometer (Victor, IBM). Mirror-polished specimens were considered as control.
These analyses were performed at the Department of Health Sciences, Università del Piemonte Orientale UPO, Via Solaroli 17, 28100 Novara, Italy on the samples:

- Ti6Al4V mirror polished
- CT
- CT_Mentha oil_water washed
- CT_20%Mentha oil_ethanol washed water washed
- CT_50%Mentha oil_ethanol washed water washed

3.6 Results and discussion

3.6.1 Characterization of the bare essential oils

In Tables 3.7, 3.8, 3.9, are reported the results of gas chromatography analysis on essential oil of Thyme, Mentha Piperita and Mentha Piperita of Pancalieri with the % area of the peaks of the different compounds. The compounds resulted of contaminations, on the basis of the experience in this analysis, were removed from the list.

Table 3.7: Gaschromatographic analysis of Thyme essential oil.

Compound	Retention time	% Area	%Area corrected removing contaminants
(-)-β-Pinene	4.14	0.01	0.02
α-Thujene	4.24	0.05	0.08
α-Pinene	4.48	1.75	2.65
Isosylvestrene	4.81	0.19	0.29
Camphene	4.87	0.48	0.73
Sabinene	5.56	2.00	3.03
β-Pinene	5.82	0.76	1.15
p-Cymene	6.92	1.65	2.50
1,8-Cineol	7.27	29.47	44.69
|trans|-Sabinene hydrate	8.40	0.63	0.96
Linalool	9.62	6.43	9.75
Camphene	9.96	0.08	0.12
|cis|-Pulegol	10.37	0.03	0.05
Isopinocarveol	10.98	0.10	0.15
Sabinene	12.21	2.02	3.06
Terpinolen	13.28	4.26	6.46
Thymol	17.58	3.53	5.35
Bicyclogermacrene	18.73	0.49	0.74
A-Cubebene	19.34	0.03	0.05
α-Copaene	20.50	0.08	0.12
β-Bourbonene	20.81	0.54	0.82

α-Gurjunene	21.75	0.17	0.26
Clovene	22.68	0.12	0.18
Isolongifolen	23.51	0.13	0.20
Valencene	23.86	0.50	0.76
γ-Cadinene	23.96	0.05	0.08
Bicyclosesquiphellandrene	24.74	0.63	0.96
β-Selinene	25.03	0.11	0.17
Bicyclogermacrene	25.33	1.02	1.55
Hinesene	25.62	0.27	0.41
β-Bisabolene	26.01	2.96	4.49
_d_-Amorphene	26.29	0.52	0.79
|cis|-Calamenene	26.39	0.11	0.17
Spathulenol	28.56	3.67	5.57
trans-Caryophyllene	29.81	0.20	0.30
4-|epi|-β-Patchoulene	30.17	0.12	0.18
Isospathulenol	30.63	0.36	0.55
α-Cadinol	31.50	0.26	0.39
(-)-AR-Curcumene	32.29	0.03	0.05
Longipinocarvone	34.08	0.13	0.20

Thyme essential oil is a complex mixture of several compounds and the most abundant (above the threshold of 5%) are 1,8-cineol (eucalyptol), terpinolen, thymol, linalool and spathulenol. In this oil there are a predominance of oxygenated compounds (66.7%) and a 33.3% of terpenes.

1,8-cineol, linalool and thymol are monoterpenoids oxide or alcohol and they have antibacterial, anti-inflammatory and antioxidant effects on human health as cited before in the bibliographic part of this chapter. Terpinolen is a terpene with antibacterial and antioxidant properties[77] and spathulenol is a terpenoid with antibacterial effects[78].

The structure of these molecules is reported in Figure 3.20.

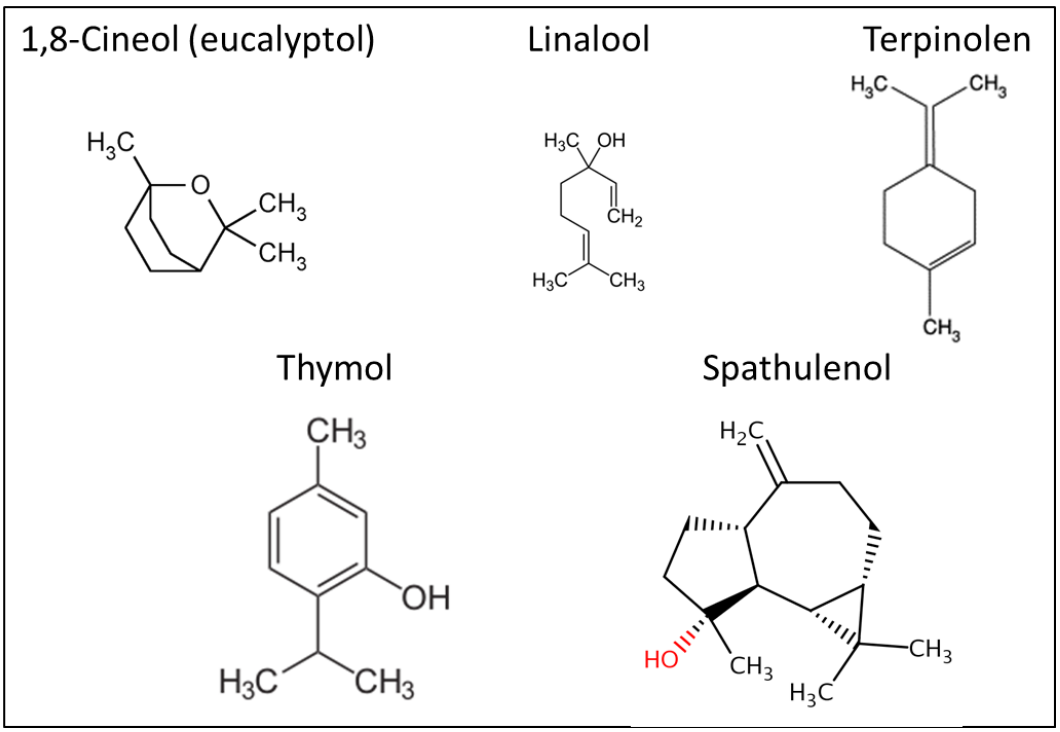

Figure 3.20: chemical structure of the main compounds of Thyme essential oil: 1,8-cineol, linalool, terpinolen, thymol and spathulenol[79]–[83].

Table 3.8: Gaschromatographic analysis of Mentha Piperita essential oil.

Compound	**Retention time**	**% Area**	**%Area corrected removing contaminants**
1,8-Cineol	7.13	0.35	0.59
γ-Terpinene	7.92	0.03	0.05
Menthone	11.90	12.84	21.60
Isomenthone	12.22	4.94	8.31
Menthyl-acetate	12.34	0.61	1.03
Menthol	13.17	19.97	33.59
Camphene	13.57	1.25	2.10
Pulegone	15.09	1.13	1.90
Carvone	15.27	0.14	0.24
Piperitone	15.78	2.05	3.45
Thymol	17.37	0.88	1.48
Teresantalol	18.38	0.01	0.02
Bicycloelemene	18.79	0.07	0.12

cis-Ocimene	19.44	0.07	0.12
Eugenol	19.65	0.12	0.20
Phenol	20.28	0.03	0.05
α-Copaene	20.55	0.11	0.19
Camphane	20.68	0.01	0.02
Sesquisabinene-A	20.75	0.03	0.05
β-Bourbonene	20.88	0.58	0.98
β-Ylangene	21.06	0.04	0.07
β-Elemene	21.16	0.28	0.47
Isolimonene	21.35	0.16	0.27
trans-Caryophyllene	21.71	0.01	0.02
Caryophyllene	22.44	4.70	7.91
β-Copaene	22.74	0.29	0.49
γ-Muurolene	23.30	0.12	0.20
β-Cubebene	23.56	0.11	0.19
α-Humulene	23.74	0.25	0.42
|trans|-β-Bergamotene	23.85	0.36	0.61
γ-Cadinene	24.84	1.94	3.26
Menthofuranone	25.43	0.21	0.35
δ-Cadinene	26.31	0.56	0.94
β-Ionone	28.12	0.08	0.13
Spathulenol	28.64	1.62	2.72
Caryophyllene oxide	28.76	1.39	2.34
β-Selinene	28.88	0.05	0.08
Viridiflorol	29.24	1.52	2.56
β-Neoclovene	29.54	0.05	0.08
α-Cadinol	31.52	0.28	0.47
Cycloisolongifol-5-ol	32.08	0.21	0.35

The main compounds found in this Mentha Piperita essential oil by means of gaschromatographic analysis are menthone, isomenthone, menthol and caryophyllene. In this oil there are a 57.7% of terpenes and a 42.3% of oxygenated compounds. The amount of pulegone that could have toxic effects on human health is low. Menthone, isomenthone and menthol have antibacterial, anti-inflammatory and decongestant properties as reported previously in the bibliographic part of this chapter. Caryophyllene is a bycyclosesquiterpene with

antibacterial, antitumoral and anti-inflammatory effects [84]. The structure of these molecules is reported in Figure 3.21.

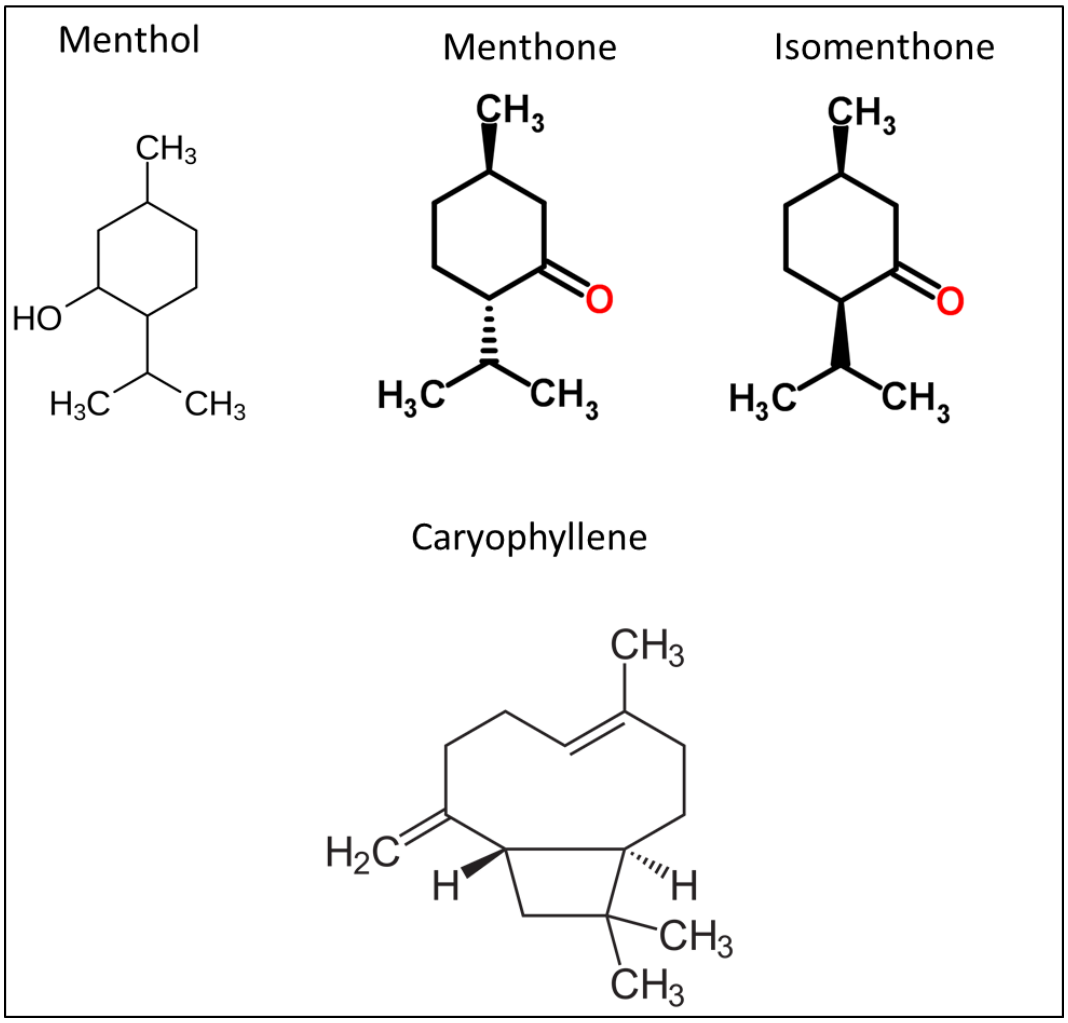

Figure 3.21: chemical structure of the main compounds of Mentha Piperita essential oil: menthol, menthone, isomenthone, and caryophyllene [85]–[87].

Table 3.9: Gaschromatographic analysis of Mentha Piperita essential oil of Pancalieri. Boiling point and vapor pressure are reported for further discussion.

Compound	**Retention time**	**% Area**	**%Area corrected removing contaminants**	**Boiling point** °C @ 760.00 mm Hg	**Vapor pressure** mm/Hg @ 25.00 °C
cis-Ocimene	4.37	0.23	0.27	169	1.971
γ-Terpinene	4.48	0.42	0.48	181	1.075
α-Pinene	5.31	0.14	0.16	155	4.750
Sabinene	5.45	0.46	0.53	163	2.630
δ-3-carene	5.54	0.59	0.68	170	3.720
dl-Limonene	6.94	0.87	1.00	178	1.550
1,8-Cineol	7.10	5.12	5.90	90	1.900
(-)-CIS-2-Carene	8.42	0.34	0.39	167	3.720
Camphene	8.46	0.43	0.50	159	3.00
Menthone	11.59	13.12	15.12	209	0.256
Menthofuran	11.88	13.24	15.26	-	0.275
ISO-Methylacetate	12.34	0.61	0.70	56	368.350
-(-)-Menthol	12.70	30.39	35.03	212	0.032
-neo-menthol	13.11	0.34	0.39	95	0.032
Pulegone	14.91	5.71	6.58	220	0.093
Camphane	17.11	5.88	6.78	160	4.931
α-Copaene	20.52	0.13	0.15	246	0.038
α-Bourbonene	20.82	0.69	0.80	254	0.026
Trans-caryophyllene	22.28	3.06	3.53	254	0.013
3,7-Guaiadiene	22.70	0.16	0.18	-	-
δ-Cadinene	23.27	0.11	0.13	280	0.007
α-Humulene	23.70	0.14	0.16	166	0.008
Bicyclo-sesqui-phellandrene	24.75	1.27	1.46	270	0.011
Butyl-methoxy-benzene	25.12	0.64	0.74	-	-

1- Menthofurarone	25.40	1.38	1.59	86*	0.275
2- Menthofurarone	26.28	0.18	0.21	86*	0.275
(-)-Mintlactone	26.57	0.23	0.27	302	0.001
(+)-Aromadendrene	29.24	0.88	1.01	260	0.023

The main compounds of the Mentha Piperita oil of Pancalieri, resulting from this analysis, are 1,8-Cineol, menthone, menthofuran, -(-)-menthol, camphane and trans-caryophyllene. The oxygenated compounds are the 41.3 % while terpenes are 58.7%. In this mint oil, the amount of pulegone is higher than in the previous tested Mentha Piperita oil, so is important control the amount of this molecule that could be grafted or remain on the surface of the samples.
The structure of these molecules is reported in Figure 3.22.

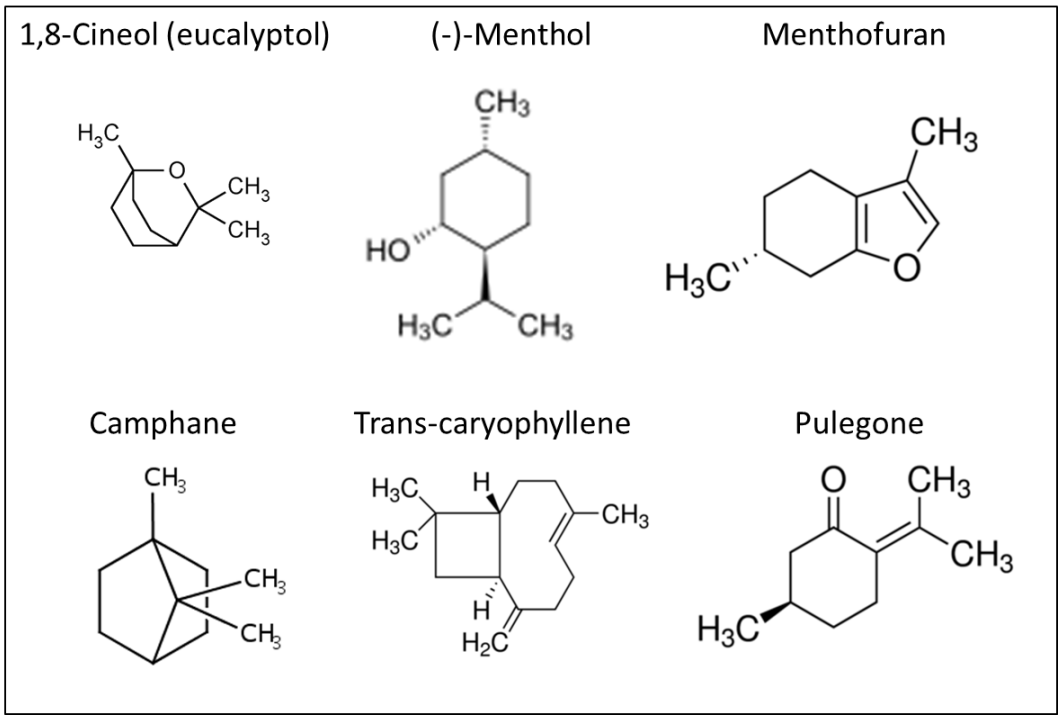

Figure 3.22: chemical structures of the main compounds of Mentha Piperita of Pancalieri essential oil: 1,8 cineol, (-)-menthol, menthofurane, camphene, trans-caryophyllene and pulegone[79], [87]–[91].

The Mentha Piperita essential oil of Pancalieri was also characterized by means of FTIR (FTIR, Alpha, Bruker Optics, Ettlingen, Germany) in ATR mode and the results are reported in the graph in Figure 3.23.

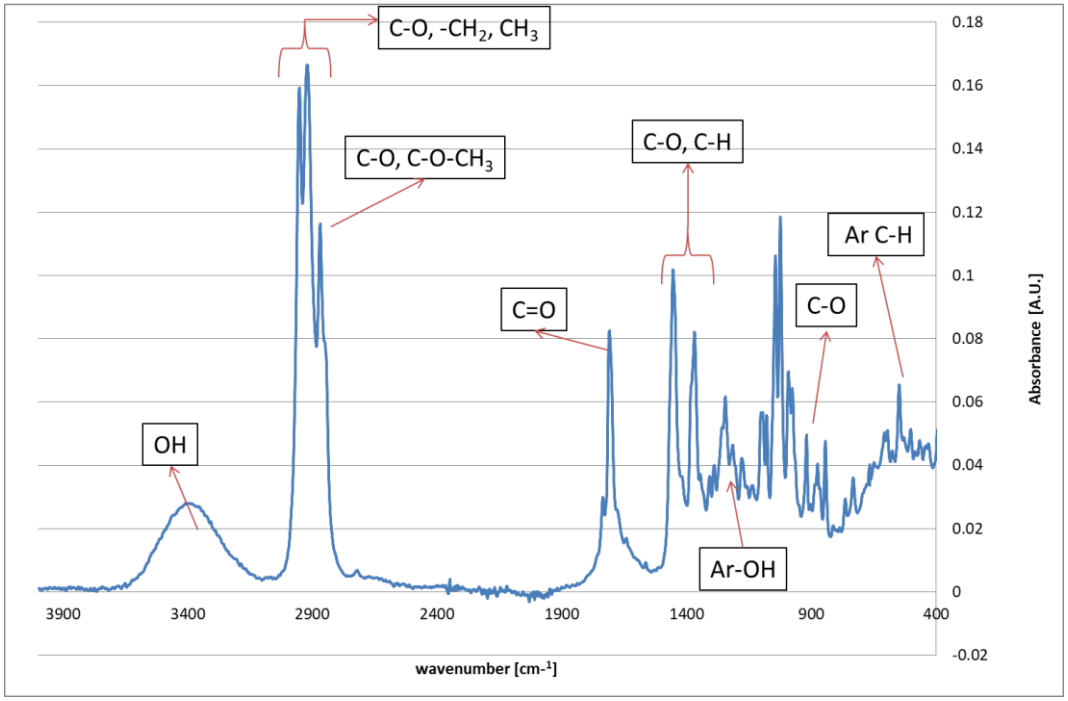

Figure 3.23: FTIR mediated spectrum of Mentha Piperita essential oil of Pancalieri.

The graph gives information about the chemical bonds and functional groups of the oil. The main peaks, with their possible assignments, are indicated in Table 3.10. Essential oils of Mentha species show an abundant presence of oxygenated monoterpenes as results from the gaschromatographic analysis and confirmed by the FTIR signals.

Table 3.10: IR peaks of Mentha of Pancalieri essential oil.

WAVENUMBER (cm^{-1})	**ABSORBANCE (A.U.)**	**ASSIGNEMENT**
3407	0.03	O-H stretch[92]
2952 2921	0.16 0.11	Chelate compounds, primary alcohols, Aliphatic- CH_3 and CH_2 stretching, O-H and C-O stretching [92]
2869	0.11	C-O-CH_3 group, C-O stretching [92]
2721	0.01	C-H stretching [92]
1710	0.08	C=O stretching vibration

		[92]
1456 1369 1307	0.09 0.08 0.05	C-H deformation of- CH_2 or CH_3 groups in aliphatic [92] Primary alcohols, C-O stretching [92]
1215 1245 1258 1289	0.04 0.04 0.05 0.06	Ester carbonyl group, phenol [92]
1025	0.12	C-O [93]
974	0.06	C-O skeletal vibration[77]
549	0.06	Aromatic C-H[93]

The peaks identified in the oil are useful in order to check the presence of some oil compounds on the surface of CT samples after coating/functionalization.

3.6.2 Antibacterial characterization of bare essential oils

The efficacy of Thyme and Mentha Piperita essential oils is tested and the minimal inhibitory concentration (MIC) and the minimal bactericide concentration (MB) concentration are found. The results on Gram-positive bacteria and Gram-negative bacteria are reported respectively in Table 3.11 and 3.12.

Table 3.11: MIC and MBC of thyme and Mentha Piperita essential oils against Gram-positive bacteria.

Bacterial strain		**Thyme** (2% v/v)		**Mentha** (2% v/v)	
	Inoculum (CFU/ml)	**MIC (% v/v)**	MBC (% v/v)	**MIC (% v/v)**	MBC (% v/v)
Staphylococcus aureus ATCC 29213	10^4	**1**	1	**1**	1
	10^6	**1**	>1	**1**	>1

Staphylococcus aureus (swab from ulcer)	10^4	**0.5-1**	0.5	**0.5**	0.5
	10^6	**1**	>1	**1**	1
Staphylococcus epidermidis ATCC 35984	10^4	**0.25**	0.5	**0.25-0.5**	0.5
	10^6	**1**	>1	**0.5**	>1
Staphylococcus epidermidis 93	10^4	**1**	>1	**0.5-1**	>1
	10^6	**1**	>1	**1**	>1
Enterococcus faecalis ATCC 29212	10^4	**1**	1->1	**1**	1->1
	10^6	**1- >1**	>1	**1**	>1

Table 3.12: MIC and MBC of thyme and Mentha Piperita essential oils against Gram-negative bacteria

Bacterial strain		**Thyme** (2% v/v)		**Mentha** (2% v/v)	
	Inoculum (CFU/ml)	**MIC (% v/v)**		Inoculum (CFU/ml)	MBC (% v/v)
Escherichia coli ATCC 25922	10^4	**0.5**	0.5	**0.25**	0.25
	10^6	**0.5**	0.5	**0.5**	0.5
Escherichia coli (pus)	10^4	**0.5-1**	0.5-1	**>1**	>1
	10^6	**1**	1	**>1**	>1
Klebsiella pneumoniae pneumoniae (from bile)	10^4	**1**	1	**1->1**	1
	10^6	**1**	1	**>1**	>1

The oils were tested against concentrations of 10^4 and 10^6 CFU/ml of several bacteria with a 2% dilution of the oils that is usually considered as safe

concentration for topical applications. As reported in Table 3.11, *Staphylococcus aureus* results less sensitive than *Staphylococcus epidermidis* to the action of these two oils. Between Gram-positive bacteria the best results was obtained with Mentha oil against *Staphylococcus epidermidis* ATCC 35984 with a MIC of 0.25 for the 10^4 concentration and 0.5 for the 10^6 concentration. Between the Gram-negative bacteria reported in Table 3.12, Mentha oil is the most effective against *Escherichia coli* with a MIC of 0.25 for the 10^4 concentration and 0.5 for the 10^6 concentration.
For these two bacteria, such as in most cases, MIC and MBC are equivalent indicating a bactericidal action of the essential oils tested. Observing the general results, Mentha oil results slightly more antibacterial than thyme oil.

3.6.3 Characterization of the samples functionalized with 2% essential oils

After the functionalization of CT samples with 2% solutions of essential oil of Thyme or Mentha Piperita no macroscopic changes are observable on the surfaces. XPS and FTIR analysis and wettability tests are below reported in order to analyze the possible presence of the biomolecules on the surface.
XPS survey spectra of samples CT, CT_ ethanol_water washed, CT_2% Thyme oil_ethanol washed_water washed and CT_2% Mentha Piperita oil_ethanol washed_water washed show the compositions of the surfaces reported in Table 3.13.

Table 3.13: Atomic percentage of the elements on the surface of the samples CT, CT_ ethanol_water washed CT_2% Thyme oil_ethanol washed_water washed and CT_2% Mentha Piperita oil_ethanol washed_water washed.

	Samples			
Elements (%at)	CT	CT_ ethanol_water washed	CT_2% Thyme oil_ethanol washed_water washed	CT_2% Mentha Piperita oil_ethanol washed_water washed
O	60.7	53.7	50.4	46.6
C	20.7	26.1	30.9	35.4
Ti	16.2	16.1	14.7	13.7
Al	-	1.7	1.9	2.1
N	2.3	2.3	2.1	2.2

Between the CT samples and the samples soaked with ethanol or ethanol with essential oil few little differences are observable in the atomic percentage of the elements reveled by XPS. The percentage of the titanium remains almost the same while the percentage of aluminum varies, however this aspect is due to the chemical treatment itself which can shows on the surface a percentage of aluminum low, but variable. The presence of nitrogen is due to surface atmospheric contamination of reactive surfaces.

It is possible to observe a reduction of the oxygen and an increase of the carbon of the samples after the soaking and these changes are almost the same of the samples soaked with bare ethanol and with ethanol+ 2% essential oil. These data are not enough to confirm or denied the presence of the biomolecules on the surface and for this reason high resolution spectra of carbon and oxygen region were performed.

High resolution spectra of the carbon region are reported in Figure 3.24.

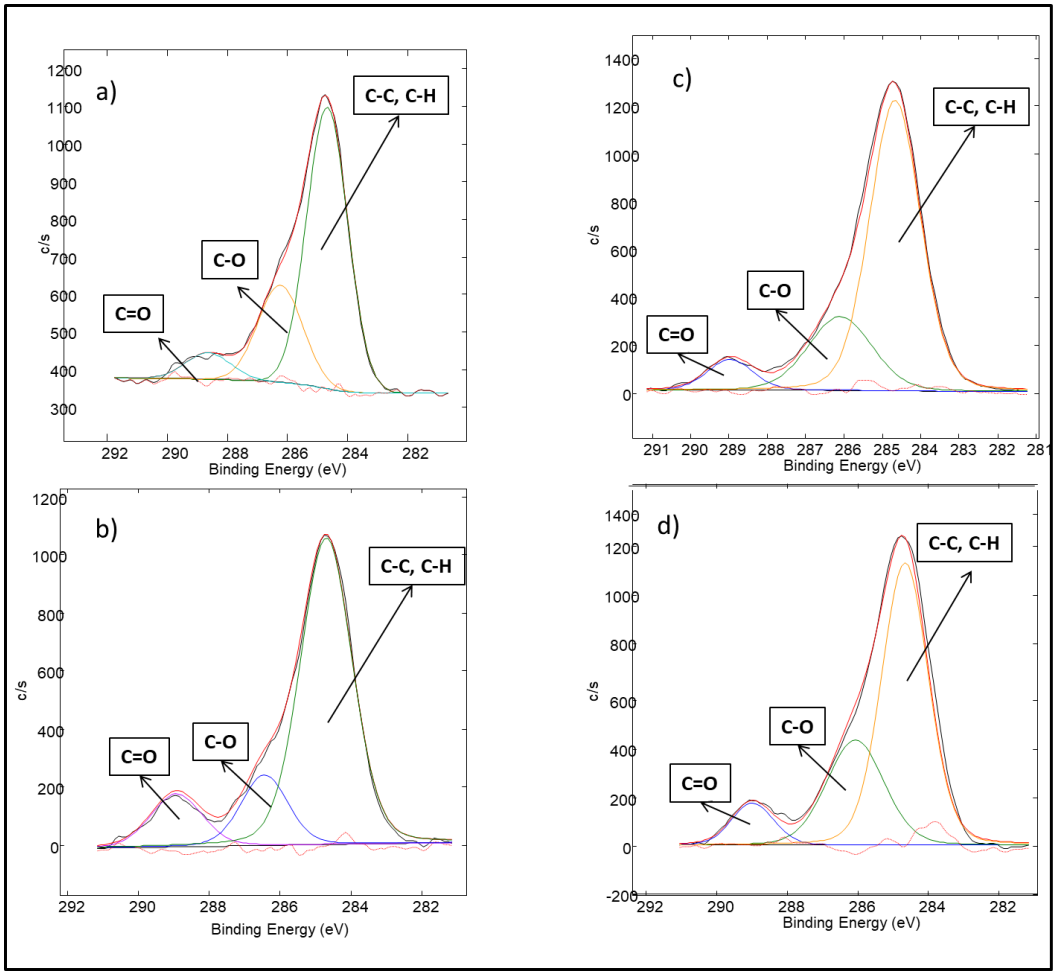

Figure 3.24: carbon XPS high resolution spectra of samples a) CT, b) CT_ ethanol_water washed, c)CT_2% Thyme oil_ethanol washed_water washed and d)CT_2% Mentha Piperita oil_ethanol_washed_water washed.

The high resolution spectra of the carbon region show that for all the samples is present a peak at a binding energy around 284 eV. The peak is attributable to the surface contaminants with carbon of the samples [94], [95]. Together with the carbon contaminants peak, other signals can be observed: one at 286 eV and the second one at 289 eV. They can be attributed to C-O and C=O bonds[96], [97]. In particular, for the C1s spectra of the samples CT_ ethanol_water washed, CT_2% Thyme oil_ethanol washed_water washed and CT_2% Mentha Piperita oil_ethanol washed_water washed, these two peaks are also associated to chemisorbed ethanol: a peak at about 284 eV assigned to the carbon atom in the methyl (H_3C-) group and a peak at about 286 eV assigned to the carbon atom in the hydroxymethyl (-CH_2OH) group) [98]. The presence of C-C bonds, associated

to the contaminants, could be partially due to the oils in the functionalized specimens, but overall, XPS analysis does not allow in this specific case to recognize the presence of the essential oils on the sample surfaces, due to the similar pattern of the spectra.

Figure 3.25 reports the XPS detailed analysis of the oxygen region of the CT, CT_ ethanol_water washed , CT_2% Thyme oil_ethanol washed_water washed and CT_2% Mentha Piperita oil_ethanol washed_water washed.

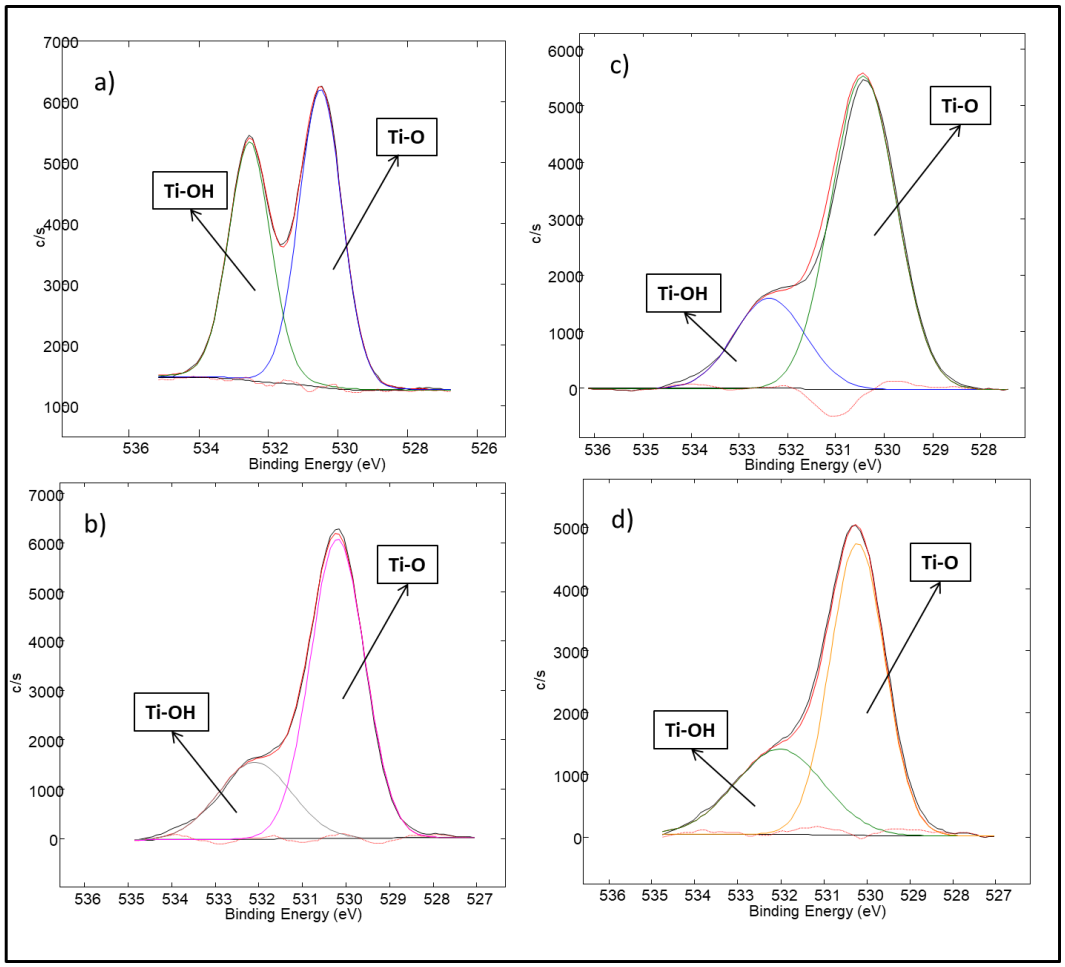

Figure 3.25: oxygen XPS high resolution spectra of samples a) CT, b) CT_ ethanol_water washed, c)CT_2% Thyme oil_ethanol washed_water washed and d)CT_2% Mentha Piperita oil_ethanol washed_water washed.

All the samples have an intense peak at a binding energy of 530 eV, attributable to bulk oxygen in titanium oxide[99], and a peak due to the Ti-OH bonds around 532 eV[95], [100], which can be attributed to -OH groups. In the O1s spectra of the samples CT_ ethanol_water washed, CT_2% Thyme oil_ethanol washed_water

washed and CT_2% Mentha Piperita oil_ethanol washed_water washed, the peak at about 532.1-532.3 eV is also correlated to chemisorbed ethanol (C_2H_5OH) (i.e. ethanol that is bonded directly to the surface atoms) [98]. The presence of the peak related to the hydroxyl groups on the CT sample confirms the success of the surface chemical treatment, which allows to obtain a high density of -OH groups on the sample surfaces[72]. By contrast, no significant differences between the samples functionalized with 2% of essential oil and the non- functionalized sample, were found, which could be due to the absence of the oils or to the absence of specific bonds with oxygen.
FTIR analyses were performed on CT and CT_2% Mentha Piperita oil_ethanol washed_water and the results are reported in Figure 3.26.

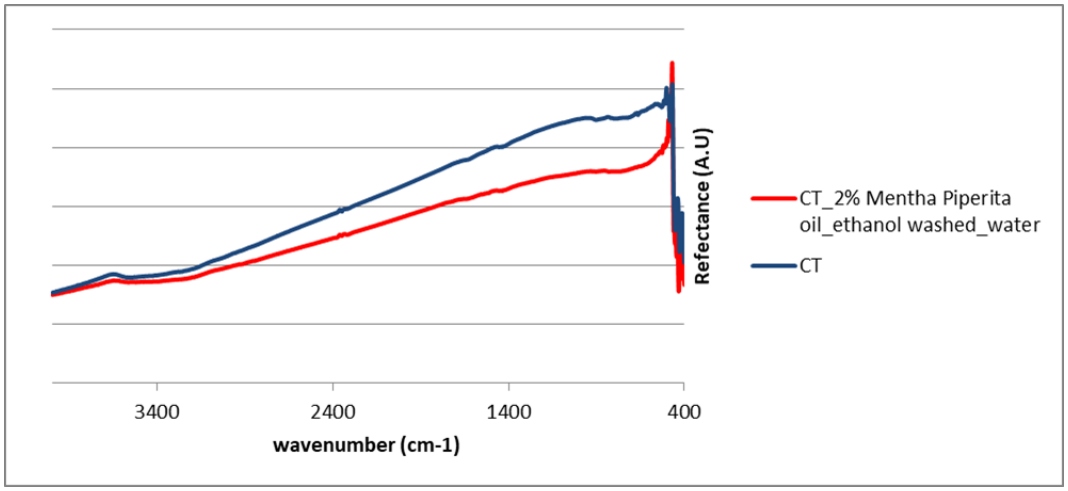

Figure 3.26: FTIR spectra of samples CT and CT_2% Mentha Piperita oil_ethanol washed_water.

Between the spectra obtained, no difference can be noted and through this analysis it is impossible to observe any molecule adsorbed onto titanium oxide surface.
The wettability test was performed in order to better understand the interactions between the modified surfaces and biological fluids and eventually to prove that the functionalization has occurred. The mean values and the corresponding standard deviations achieved from the test are shown in the bar graph in Figure 3.27.

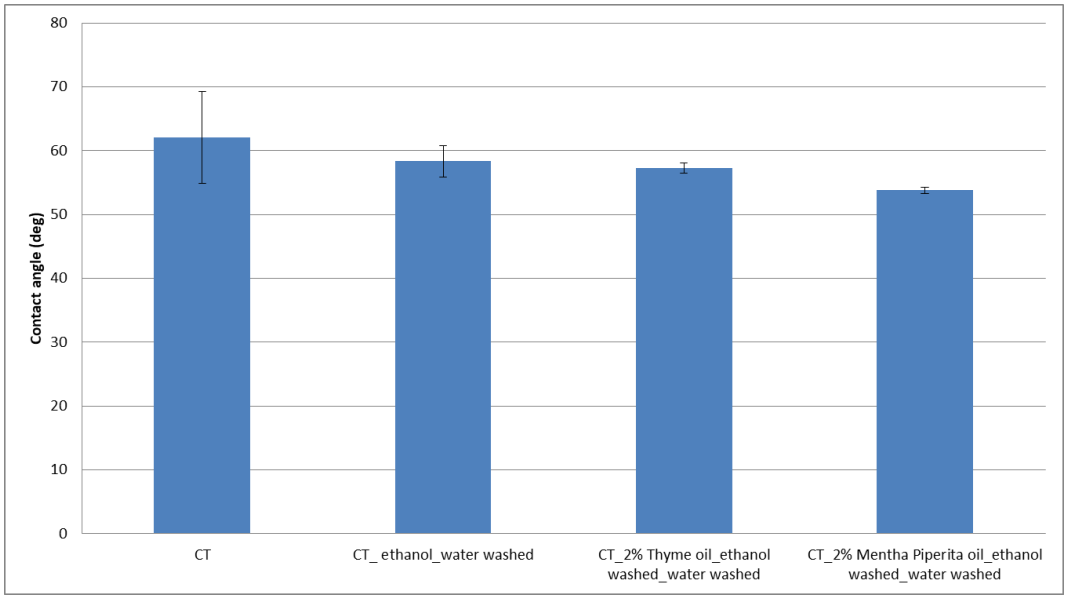

Figure 3.27: contact angle of the samples a) CT, b) CT_ ethanol_water washed, c)CT_2% Thyme oil_ethanol washed_water washed and d)CT_2% Mentha Piperita oil_ethanol washed_water washed.

According to the bar chart in Figure 3.26, the values measured on the samples are similar and no significant statistic differences are notable. The CT presents a contact angle of 62.1±7.2°, while the sample CT_ ethanol_water washed shows an angle of 58.3±2.5°. The specimens indicated as CT_2% Mentha Piperita oil_ethanol washed_water washed and CT_2% Thyme oil_ethanol washed_water washed, instead, have respectively a contact angle of 53.8±2.5° and 57.3±0.8°. Therefore, the functionalization process with essential oils does not induce a relevant modification in the surface wettability of the samples.
On the basis of XPS, FTIR and wettability results on the samples functionalized with 2% essential oils, protocols of functionalization with solution of higher concentration of Mentha Piperita of Pancalieri essential oil were developed and characterized.

3.6.4 Macroscopic observation of samples functionalized/coated with Mentha Piperita of Pancalieri essential oil

After the procedure of coating with pure or 50% diluted Mentha essential oil of Pancalieri or functionalization with 20% or 50% diluted Mentha Piperita essential oil of Pancalieri, macroscopic differences of the surface of the samples can be noted. Images of some samples as exemplification are reported in Figure 3.28.

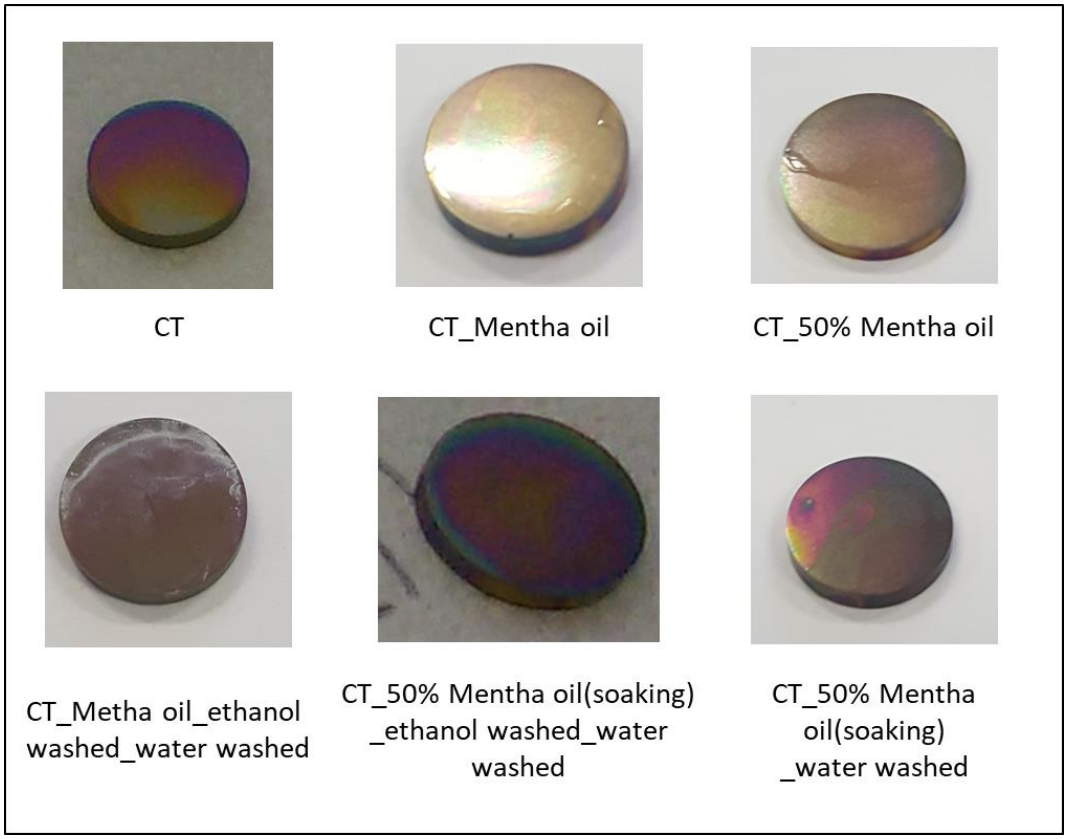

Figure 3.28: appearance of samples CT, CT_Mentha oil, CT_50% Mentha oil, CT_Mentha oil_ethanol washed_water washed, CT_50%Mentha oil(soaking)_ethanol washed_water washed, CT_50% Mentha oil(soaking)_water washed.

Sample CT has changing colors due to the surface titanium oxide layer created by means of the patented chemical treatment cited in the materials and methods section of this chapter [71], [72]. The samples with pure polymerized Mentha oil and polymerized 50% Mentha oil show a transparent coating on the surface also after washing in water. The samples coated in the same way, but washed in

ethanol or one time in ethanol and one time in water, after polymerization, show on the surface a whitish not uniform coating. The samples functionalized by means of soaking in different concentration of Mentha oil after ethanol washing or after one wash in ethanol and one in water present surfaces identical to the bare CT surface, while the samples only washed in water after soaking show once dried the presence of a not uniform coating of polymerized essential oil. This result suggest that with the purpose of obtaining a real functionalization the two washing steps in ethanol and water are needed in order to remove the exceeding oil and avoid its polymerization when exposed to air, while, on the other hand, no washing in ethanol must be performed in order to achieve a continuous coating.

3.6.5 Fluorescence microscope observation

In Figure 3.29 the fluorescence microscope images of samples coated or functionalized with Mentha oil of Pancalieri are reported.

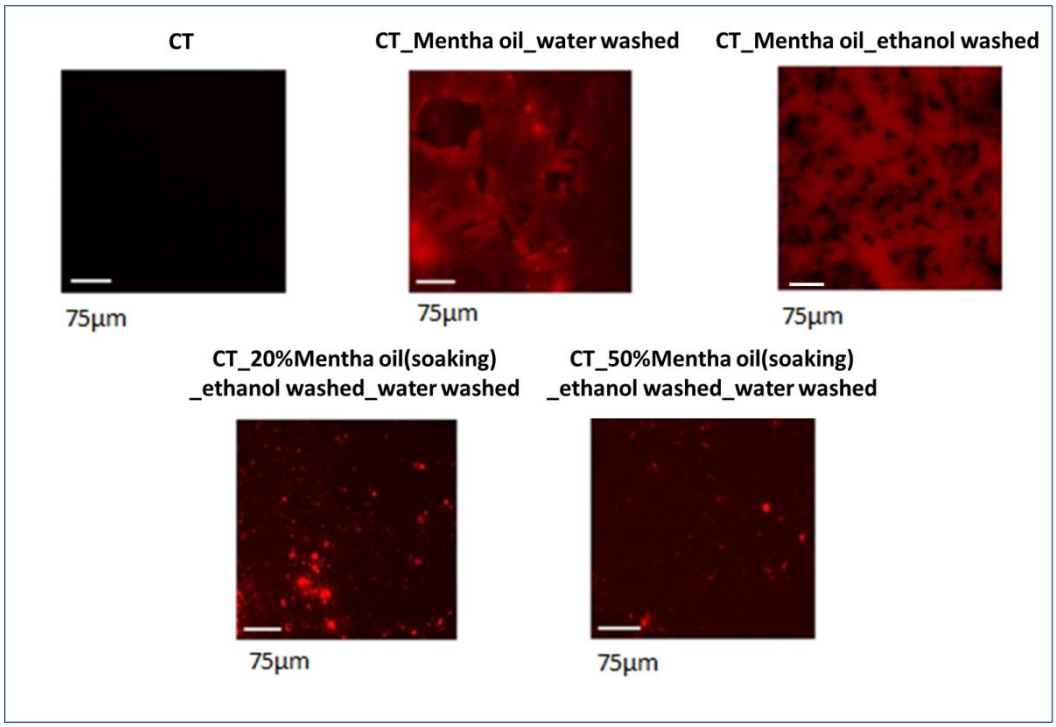

Figure 3.29: fluorescence microscope images of samples CT, CT_Mentha oil_wather washed, CT_Mentha oil_wather ethanol washed, CT_20%Mentha oil_ethanol washed_water washed, CT_50%Mentha oil_ethanol washed_water washed.

As expected the bare CT samples does not emit any fluorescent signals while the samples with the Mentha oils are fluorescent[8]. The sample CT_Mentha oil_water washed shows an homogeneous fluorescence on all the surface of the samples because of the presence of the continuous polymerized Mentha oil layer, while the ethanol washing of sample CT_Mentha oil_wather ethanol washed selectively remove compounds from the coating. Indeed, the functionalized samples CT_20%Mentha oil_ethanol washed_water washed and CT_50%Mentha oil_ethanol washed_water washed showed intense fluorescence spots highlighting the grafting of biomolecules occurred with a not uniform functionalization, but the biomolecules result grafted to the CT surface forming aggregates. The fluorescence microscope observation results a suitable technique for the control of the presence of Mentha molecules on the substrates.

3.6.6 Gas chromatography analysis

Gas chromatography analysis performed on the solutions obtained by extracting the molecules from the coating or grafted on the surfaces (as explained in paragraph 3.5.7) from the samples CT_Mentha oil_water washed, CT_50%Mentha oil _water washed, CT_20% Mentha oil(soaking)_ethanol washed water washed and CT_50% Mentha oil(soaking)_ethanol washed water washed highlight the presence of the sequent compounds on the samples: menthol, hydroxyl-menthofuran, menthyl-acetate, 1-menthofuranone, 2-menthofuranone, diethyl-methoxy-benzene, beta-cubebene and trans-caryophyllene.
The same analysis was performed as control on the solution in which was soaked a bare CT samples and no compounds correlated with the essential oils was found.
The compounds found for each samples are reported in Table 3.14.

Table 3.14: compound found on samples CT_Mentha oil_water washed, CT_50%Mentha oil _water washed, CT_20% Mentha oil(soaking)_ethanol washed water washed and CT_50% Mentha oil(soaking)_ethanol washed_water washed and relatives % areas. [87], [101]–[105].

Samples	Compound identified	RT	Area % compared to total extracted compounds	Area % excluding contaminants	Chemical structure
CT_Mentha oil_water washed	Menthol	12.17	3.34	44.13	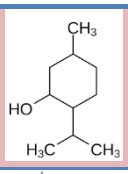
	Hydroxyl-menthofuran	13.53	2.42	32.03	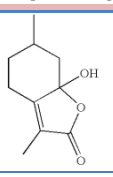
	Menthyl-acetate	14.41	0.35	4.68	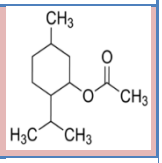
	Beta-cubebene	24.17	1.45	19.16	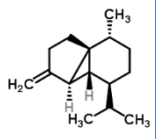
CT_50%Mentha oil_water washed	Hydroxyl-menthofuran	13.58	0.80	6.29	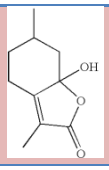
	1-menthofuranone	19.01	0.28	2.19	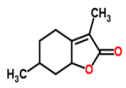
	2-menthofuranone	21.13	2.39	18.84	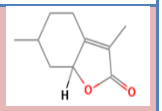

	Diethyl-methoxy-benzene	24.97	3.03	23.88	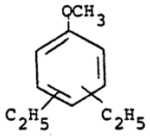
	Beta-cubebene	24.28	6.20	48.81	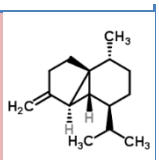
CT_20%Mentha oil(soaking)_ethanol washed_water washed	Beta-cubebene	24.22	8.47	96.52	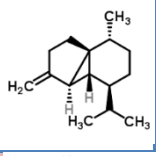
	Trans-caryophyllene	21.83	0.30	3.48	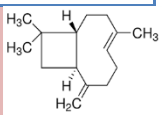
CT_50%Mentha oil(soaking)_ethanol washed_water washed	Beta-cubebene	24.26	0.33	44.86	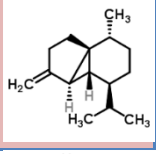
	Trans-caryophyllene	21.81	0.41	55.13	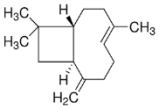

Comparing these results with the composition of the Mentha Piperita of Pancalieri essential oil, it is possible to observe that menthol, menthyl-acetate, trans-caryophyllene and 1- and 2- menthofuranone are among the components of the oil.

The hydroxyl-menthofuran is a metabolite of menthofuran which is present in the initial composition of the oil and the beta-cubebene is an isomer of α-copaene also present in the initial composition of the oil [106]. The presence of this compound could be correlated with a rotation of the molecules during the functionalization and the grafting to the surface or during the extraction from the surface. Diethyl-methoxy-benzene is a derivative compound of butyl-methoxy-benzene present in the oil composition. The cited compounds present in the composition of the oil are listed in paragraph 3.4.12 Table 3.9.

The coating on the samples CT_Mentha oil_water washed result composed by 44% of menthol, 32% Hydroxyl-menthofuran, 20% of beta-cubebene and 4% of menthyl-acetate. The menthol is the only oxygenated compounds found on the samples surfaces and it is present only on this sample probably because the

formation of the coating is able to avoid its evaporation. The samples CT_50%Mentha oil _water washed with the coating obtained with the oil diluted in ethanol is composed by 50% beta-cubebene, 24% diethyl-methoxy-benzene, 19% 1- menthofuranone, 2% 2- menthofuranone and 6% hydroxyl-menthofuran.
The menthol is no more present and the amount of not oxygenated compounds is increased. This result can be correlated with the process of depolymerization and solubilization of the polymerized coating by ethanol.
On the samples functionalized CT_20% Mentha oil(soaking)_ethanol washed water washed and CT_50% Mentha oil(soaking)_ethanol washed_water washed, only beta- cubebene and trans-caryophyllene are found and it is interesting to note that these compounds are minor fractions of the initial Mentha oil composition. These compounds have $=CH_2$ bonds and are not oxygenated and for this reason it is possible to hypothesis an affinity between the CT surface and this molecules because of the high affinity between titanium and carbon and less affinity of these biomolecules with solvents (water and ethanol). Trans-caryophyllene and α-copaene, beta-cubebene precursor, have also a low vapor pressure as reported in Table 3.9 that could be a factor involved in the selective graft of these biomolecules to CT surfaces. This hypothesis needs more investigation.

3.6.7 Contact angles measurements

Measurements of the contact angles with ultrapure water were performed on all the kinds of samples produced and the results are reported in Figure 3.30.

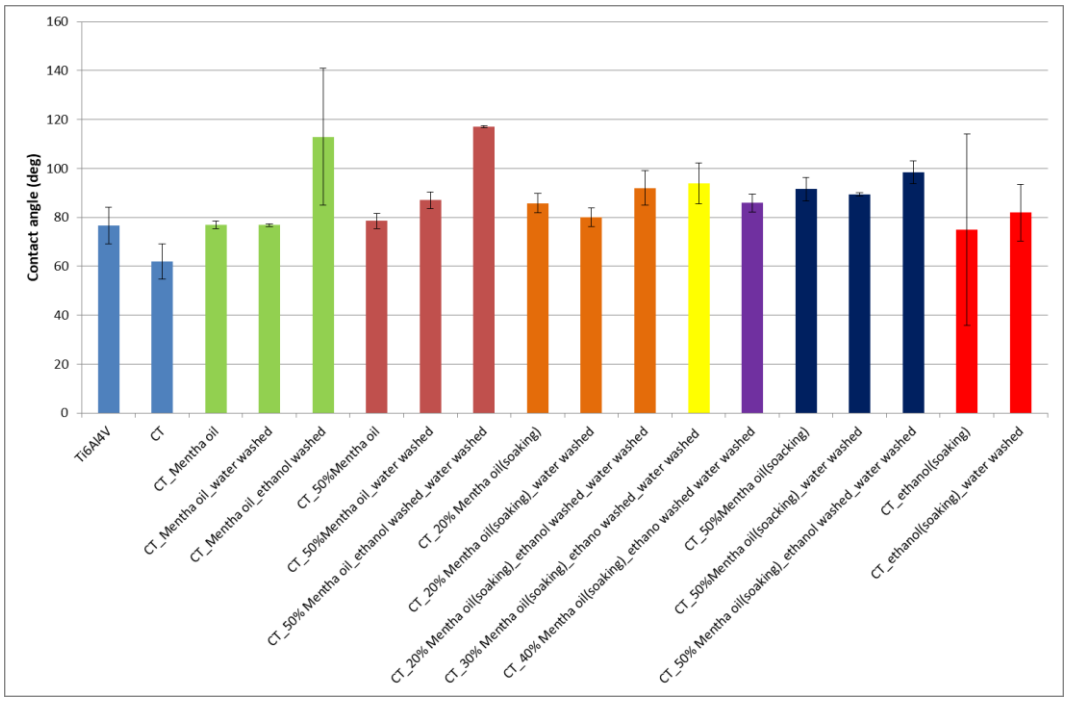

Figure 3.30: contact angles of samples of Ti6Al4V polished up to 4000, CT, and CT coated or functionalized with Mentha Piperita essential oil.

The patented chemical treatment CT induces a higher wettability (62°±7.2°) compared with the bare titanium alloy (77°±7.5°) because of the –OH groups exposed by the surface and the nanotopography. The coating or functionalization with Mentha oil reduce the wettability of the surface because of the presence of hydrophobic groups that bring the contact angle around 80-90°. The greatest increase of the contact angle is observable for samples CT_Mentha oil_ethanol washed and CT_50% Mentha oil_ethanol washed_water washed in which the washing with ethanol of the polymerized coating creates an irregular surface finishing, enhancing the roughness and increasing the contact angle. For the samples CT_ethanol(soaking) an high standard deviation is reported because the contact angles depends on the uncontrolled amount of ethanol molecules that remain on the sponge like oxide layer at the time of the measurement. On the basis of this result, all the samples treated with Mentha oil were dried under the chemical hood with laminar flow for two hours in order to avoid, as much as

possible, the effects induced by ethanol washing after the treatments. In conclusion the change of the contact angles after the functionalization or coating is present, but it is similar to the one induced only by soaking in ethanol and washing in water, for this reasons this technique of analysis is not suitable to prove with certainty the presence of the oil molecules onto the surface in the case of the functionalized samples and further analysis were performed.

3.6.8 Fast Fourier transform infrared spectroscopy

FTIR spectra of samples CT and CT_ethanol(soaking)_water washed are reported in figure 3.31 in order to investigate any eventual change induced on the surface of the CT samples by the washing steps.

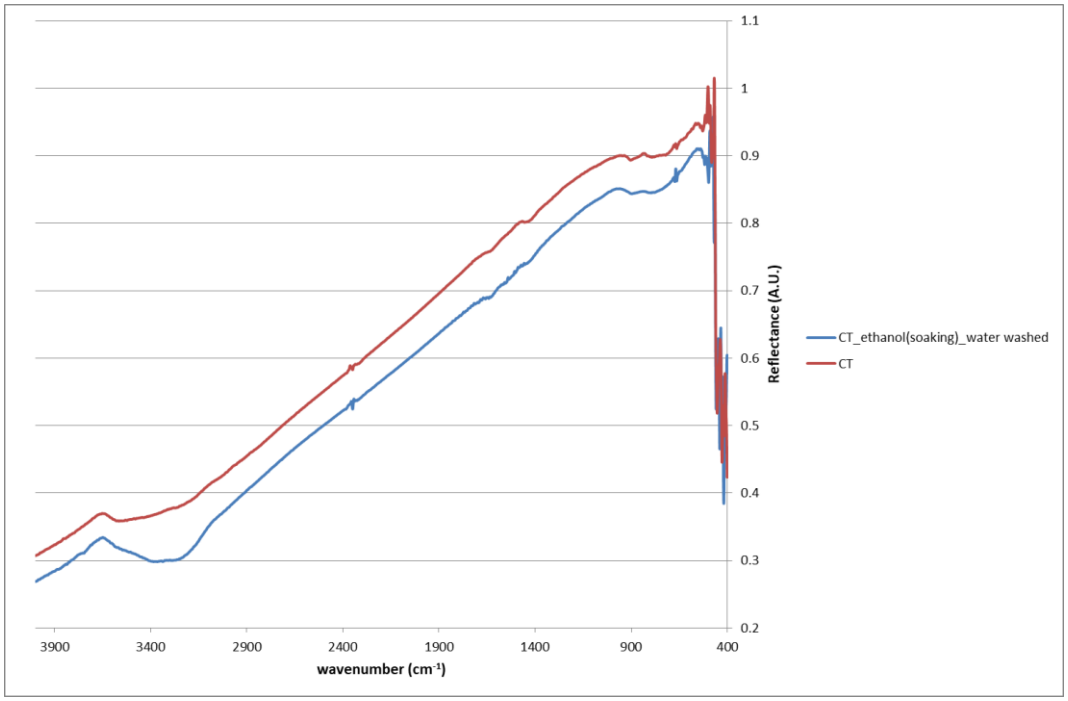

Figure 3.31: FTIR spectra of samples CT and CT_ethanol(soaking)_water washed between 400 and 4000 cm^{-1}.

The two spectra are almost the same with the exception of the band between 3450-3200 cm^{-1} due to -OH stretching vibration[107]. The presence of the –OH groups on sample CT is due to the patented chemical treatment and it was already seen in a previous work[72]. The enhancing of this band could be correlated to the presence of some remaining water or ethanol molecules in the sponge like

structure of the oxide layer of the CT samples. It highlighted that the soaking in ethanol and the water washing, as showed by contact angles measurements, can influences the surface properties. The comparative graphs of the different coating / functionalization procedures are shown below.

The spectra of the pure Mentha oil coated samples are reported in Figure 3.32 in the range between 400-4000 cm^{-1} (Fig3.32a), 2400-4000 cm^{-1}(Fig3.32b) and 2400-1000 cm^{-1}(Fig3.32c).

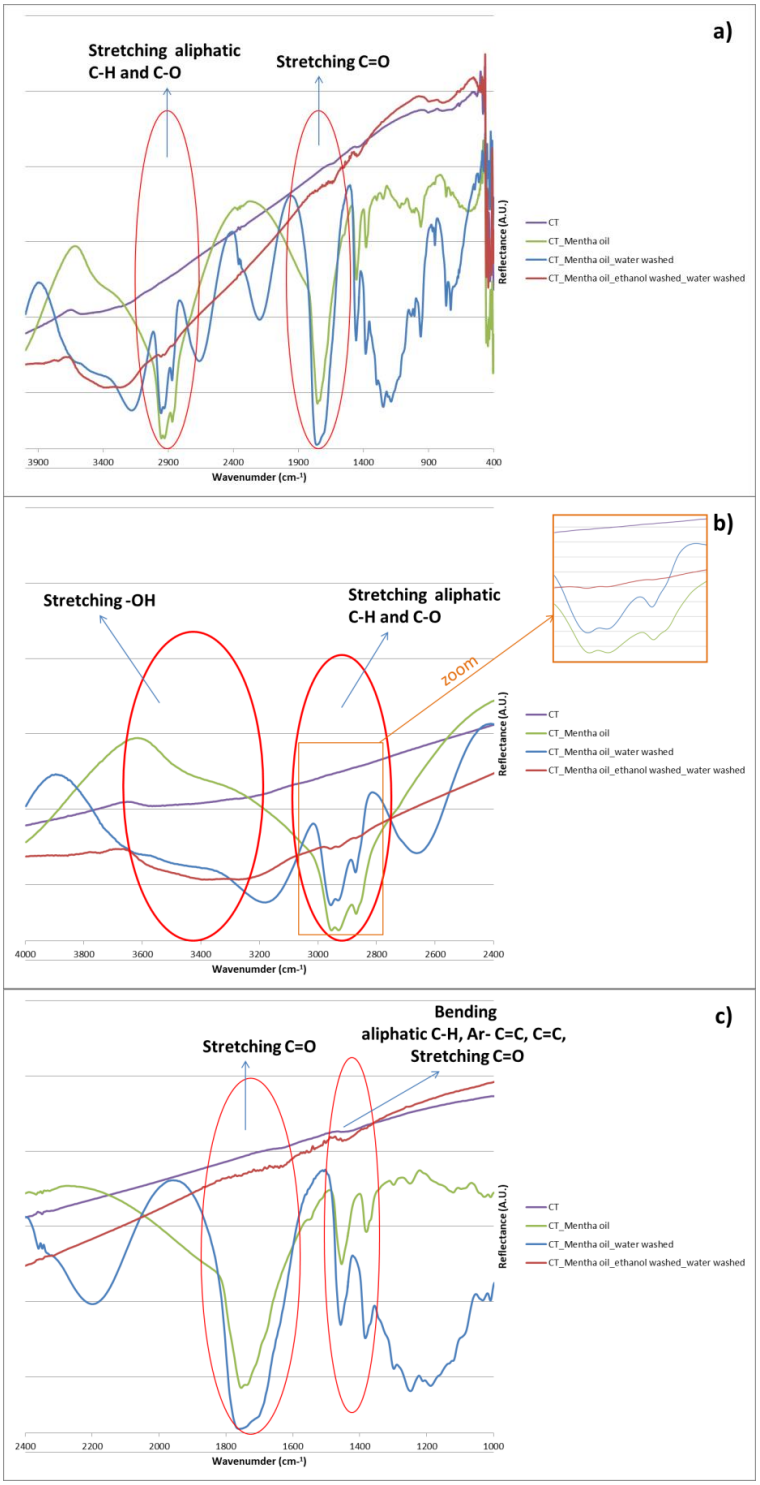

Figure 3.32: FTIR spectra of samples CT, CT_Mentha oil, CT_Mentha oil_water washed, CT_Mentha oil_ethanol washed_water washed in the range a) 400-4000 cm^{-1},b)2400-4000 cm^{-1} c) 1000-2400 cm^{-1}.

The spectra of the samples CT_Mentha oil, CT_Mentha oil_water washed are really different from the CT spectrum, but it is difficult to identify with certainty the peaks of the Mentha coating itself. This coating is thick and semitransparent creating internal reflection of the IR light disturbing the measurements. The spectrum of the sample CT_Mentha oil_ethanol washed_water washed has less pronounced signals because the ethanol washing reduces the thickness of the polymerized Mentha layer that become also opaque avoiding internal reflection. However, for all the coated samples the same peaks between 2960-2870 cm^{-1} due to stretching vibration of C-H aliphatic bonds and C-O bonds are present [92], [108] (Fig.3.32a,b) and for the coated samples not washed or water washed a peak between 1780-1700 cm^{-1} due to C=O stretching[92] (Fig. 3.32 c) is present. These peaks are not present on the spectrum of the CT sample and in the case of the sample washed in ethanol and in water the main peak is shifted towards lower energy and this could be correlated to a higher amount of C=C bonds. Between 1500 and 1440 cm^{-1} are also present three peaks, the peak at 1450 cm^{-1} could be correlated with the bending of aliphatic C-H, but also to the stretching of aromatic C=C bonds or bending of aliphatic C=C bonds[109]. The aromatic C=C bonds are present in the molecules found in Mentha coatings with GC (dietyl-menthoxy-benzene and hydroxyl-menthofuran), but this peak is also present, even if less intense, on the spectrum of the sample CT and in this case the most plausible attribution is to C-H bonds due to organic contamination.

The two peaks between 1400-1370 cm^{-1} could also have a double attribution, to the stretching of C=O bonds or to stretching of $=CH_2$ [109] bonds both present in the molecules of the oil found on the samples by GC(hydroxyl-menthofuran, menthyl-acetate and beta-cubebene).

These signals can be correlated to the presence of the molecules of Mentha oil and are present also in the spectrum of the liquid oil reported in paragraph 3.5.1 Figure 3.31.

The spectrum of the 50% Mentha oil coated samples are reported in Figure 3.33 in the range between 400-4000 cm^{-1}(Fig3.33a), 2400-4000 cm^{-1}(Fig3.33b) and 2400-1000 cm^{-1}(Fig3.33c).

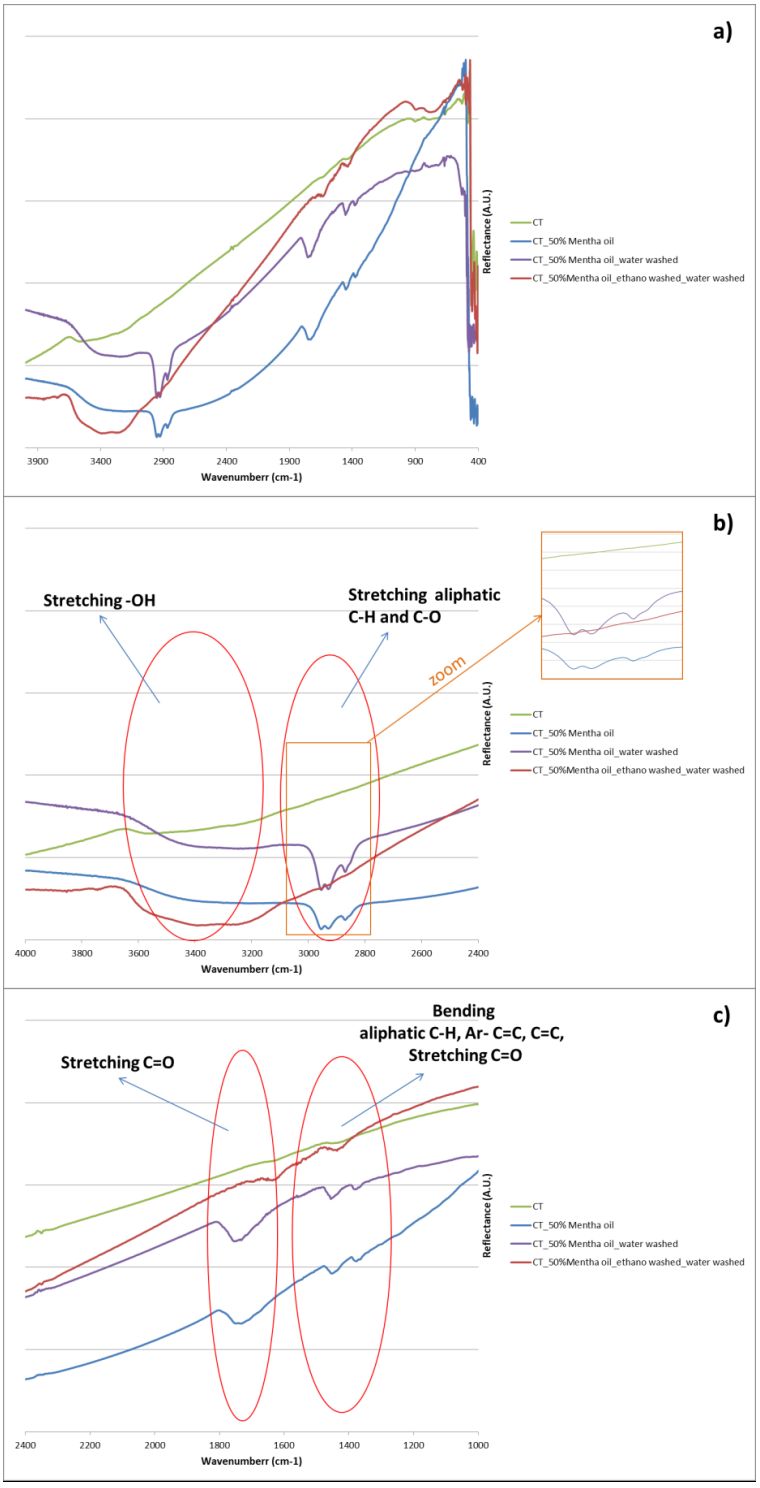

Figure 3.33: FTIR spectra of samples CT, CT_50%Mentha oil, CT_50%Mentha oil_water washed, CT_50%Mentha oil_ethanol washed_water washed between a) 400-4000 cm^{-1}, b)2400-4000 cm^{-1} and c) 1000-2400 cm^{-1}.

In Figure 3.33a some differences between the spectrum of the CT sample and the spectra of the 50% Mentha oil coated samples are visible and are reported more in details in Figure 3.31b

In Figure 3.30a are reported the spectra between 4000-400 cm^{-1} and some differences, highlighted by the red ovals, can be noted between 3450-3200 cm^{-1} and 2960-2870 cm^{-1}. Between 3450-3200 cm^{-1} the stretching band of the –OH groups [107] is present for all the samples, but with an evident change in intensity and the three peaks between 2960-2870 cm^{-1}, due to the stretching of aliphatic C-H groups and C-O [92] groups, are present on the samples with Mentha oil, but not on the bare CT samples, as mentioned before, confirming the presence of the Mentha oil molecules on the samples. These signals are high for the samples CT_50%Mentha oil, CT_50%Mentha oil_water washed, while they are very low for the samples CT_50%Mentha oil_ethanol washed_water washed for which the ethanol washing could have washed out a large amount of the coating, preferentially the molecules with C=O bonds. In Figure 3.30b are reported the spectra between 1000-2400 cm^{-1} and the region of interest are highlighted by the two red ovals.

Around 1780-1700 cm^{-1} there is the signal due to the C=O bonds[77] of Mentha oil and it is well visible for the samples CT_50%Mentha oil, CT_50%Mentha oil_water washed and really low for the samples CT_50%Mentha oil_ethanol washed_water washed for the reason mentioned before. Between 1500 and 1440 cm^{-1}, such as for the previous set of samples, three peaks are present. The peak around1450 cm^{-1} could be correlated with the bending of aliphatic C-H, but also to the stretching of aromatic C=C bonds or bending of aliphatic C=C bonds[109]. The aromatic C=C bonds are present in the molecules found in 50% Mentha coatings with GC (hydroxyl-menthofuran, menthofuranone and dietyl-menthoxy-benzene).

The two peaks between 1400-1370 cm^{-1} could also have a double attribution, to the stretching of C=O bonds or to stretching of $=CH_2$ [109] bonds both present in the molecules of the oil observed with GC (hydroxyl-menthofuran, menthyl-acetate and beta-cubebene).

These signals, due to the presence of Mentha oil molecules, are present for all the 50%Mentha oil coated samples and they are low on the sample CT_50%Mentha oil_ethanol washed_water.

The spectra of the 50% Mentha oil functionalized samples are reported in Figure 3.34 in the range between 400-4000 cm^{-1}(Fig3.34a), 2400-4000 cm^{-1}(Fig3.34b) and 2400-1000 cm^{-1}(Fig3.34c).

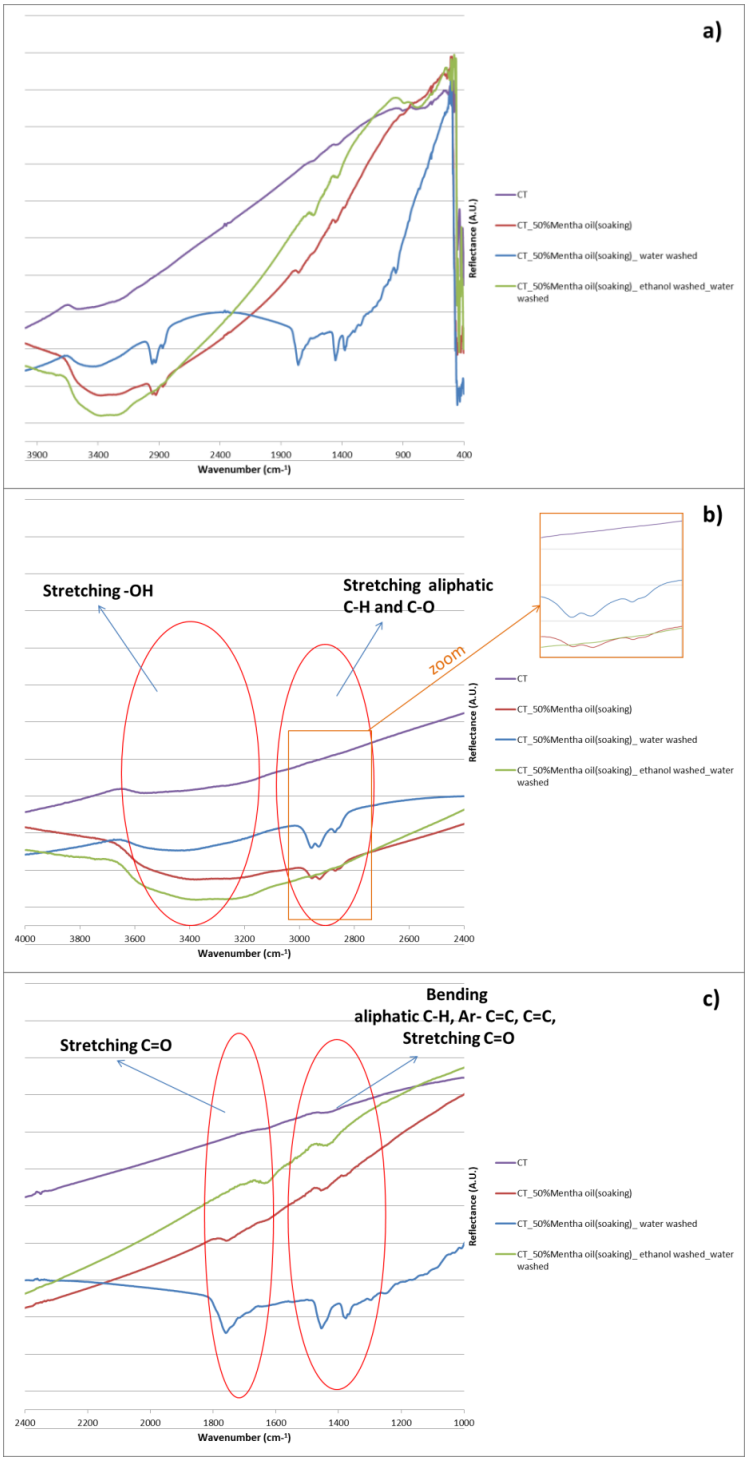

Figure 3.34: FTIR spectra of samples CT, CT_50%Mentha oil(soaking), CT_50%Mentha oil(soaking)_water washed, CT_50%Mentha

oil(soaking)_ethanol washed_water washed between a) 400-4000 cm^{-1}, b)2400-4000 cm^{-1} and c) 1000-2400 cm^{-1}.

In Figure 3.34a the differences between the CT spectrum and the spectra of the functionalized samples with 50% Mentha oil are visible and analyzed in details in Figure 3.34b and 3.34c. The principal peaks are the same analyzed for the samples coated with 50% Mentha oil. In Figure 3.34b the bands between 3450-3200 cm^{-1} of the –OH stretching [107] is present on all the samples while the peaks between 2960-2870 cm^{-1} due to the stretching of aliphatic C-H groups and C-O [92] are clearly visible for the sample CT_50%Mentha oil(soaking) and CT_50%Mentha oil(soaking)_water washed on which is present a polymerized layer on mint oil while they are lower on the sample CT_50%Mentha oil(soaking)_ethanol washed_water washed because it is not covered by a polymerized layer but has some Mentha oil molecules bonded to the surface. The peak around1450 cm^{-1} could be correlated with the bending of aliphatic C-H, but also to the stretching of aromatic C=C bonds or bending of aliphatic C=C bonds[109]. The aromatic C=C bonds are present in the molecules found in 50% Mentha soaking with GC (trans-caryophyllene).

The two peaks between 1400-1370 cm^{-1} could also have a double attribution, to the stretching of C=O bonds or to stretching of $=CH_2$ [109] bonds both present in the molecules of the oil. For the samples not washed the C=O attribution is plausible while for the samples ethanol washed water washed the signals could be correlated with $=CH_2$ bonds of beta-cubebene and trans-caryophyllene.

The spectra of the 20% Mentha oil functionalized samples are reported in Figure 3.35 in the range between 400-4000 cm^{-1} (Fig3.35a), 2400-4000 cm^{-1}(Fig3.35b) and 2400-1000 cm^{-1}(Fig3.35c).

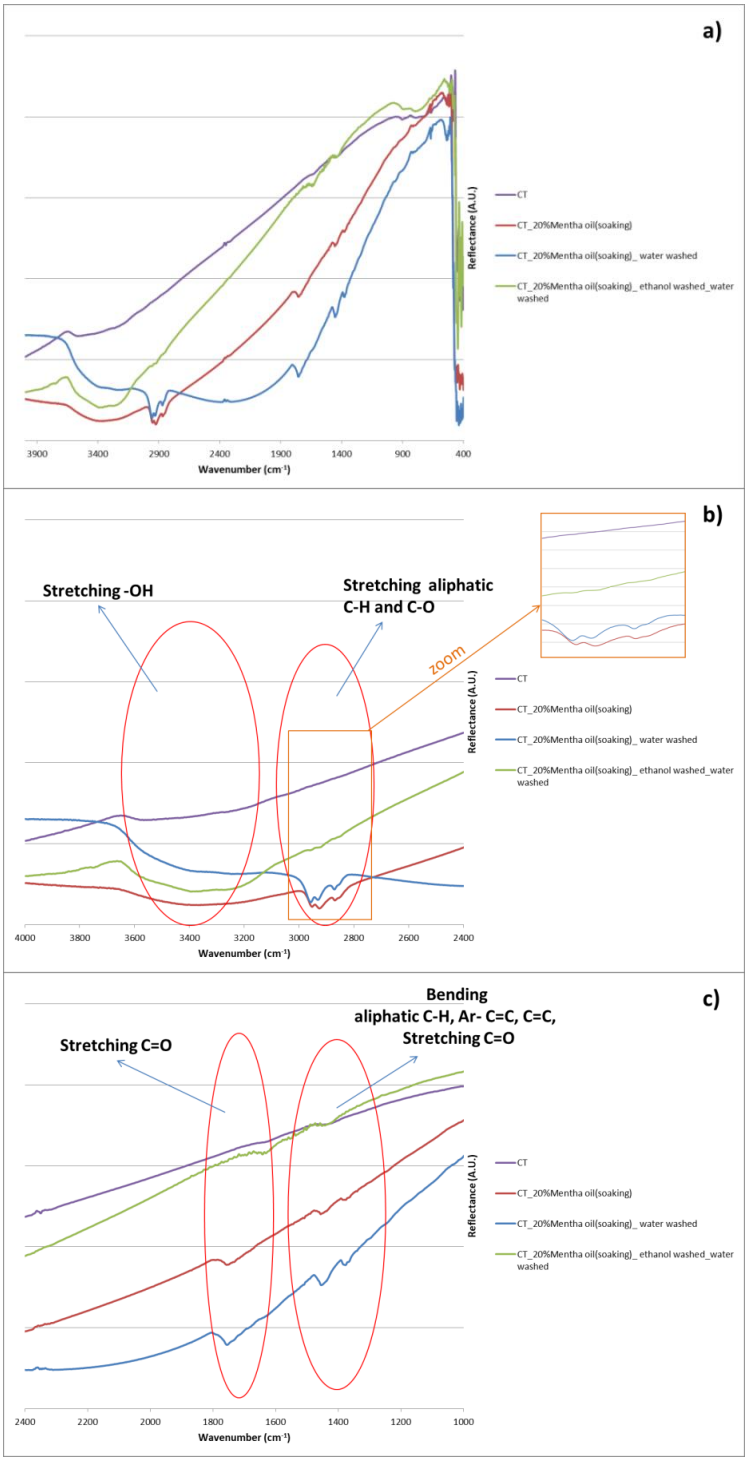

Figure 3.35: FTIR spectra of samples CT, CT_20%Mentha oil(soaking), CT_20%Mentha oil(soaking)_water washed, CT_20%Mentha oil(soaking)_ethanol washed_water washed between a) 400-4000 cm^{-1}, b)2400-4000 cm^{-1} and c) 1000-2400 cm^{-1}.

The spectra of the samples functionalized with 20% Mentha oil are similar to the ones of the samples functionalized with 50% Mentha essential oils. In Figure 3.35b the bands of the –OH stretching is present and the signals between 2960-2870 cm^{-1} due to the stretching of aliphatic C-H and C-O groups [92] are also well visible on the samples with the functionalization protocols without the wash in ethanol because of the polymerized Mentha layer that covered not uniformly the surfaces. For the samples with the ethanol and water washing, that result properly functionalized, these signals are weak, but still present indicating the presence of the Mentha oil molecules. As for the samples soaked in 50% Mentha oil the peak around1450 cm^{-1} could be correlated with the bending of aliphatic C-H, but also to the stretching of aromatic C=C bonds or bending of aliphatic C=C bonds[109]. The aromatic C=C bonds are present in the molecules found in 50% Mentha soaking with GC (trans-caryophyllene).
The two peaks between 1400-1370 cm^{-1} could also have a double attribution, to the stretching of C=O bonds or to stretching of $=CH_2$ [109] bonds both present in the molecules of the oil. For the samples not washed the C=O attribution is plausible while for the samples ethanol washed, water washed the signals could be correlated with $=CH_2$ bonds of beta-cubebene and trans-caryophyllene.
These results suggest that the water washing of the coating does not induce any change in the coating and could be useful to remove contaminant or dust from the surface of the coating, while the washing with ethanol could remove totally or partially the coating. Regarding the procedure of functionalization the two washing steps are required in order to remove the exceeding Mentha oil and avoiding the formation of a thick coating. The FTIR spectra of the samples modified with the more promising protocols are reported for comparison in Figure 3.36.

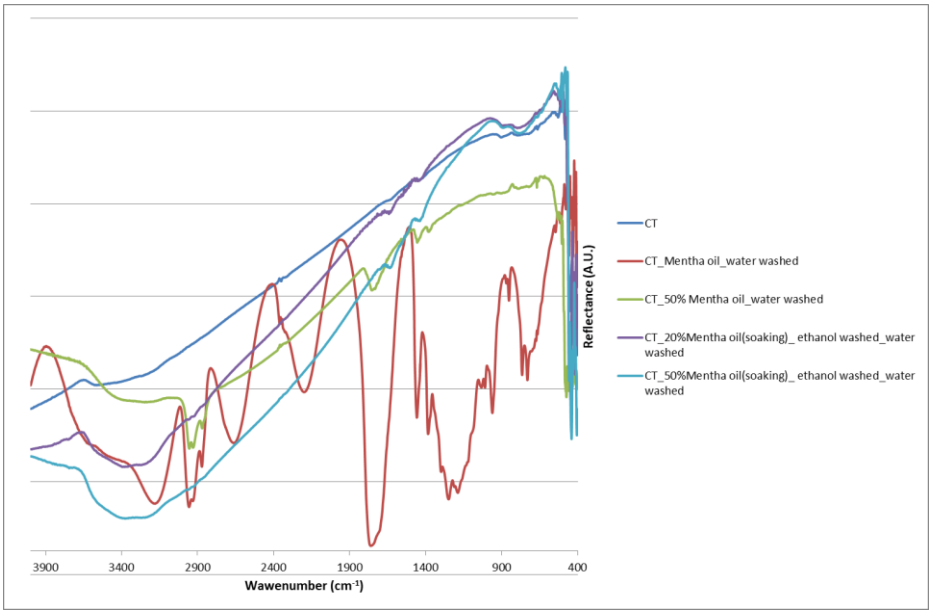

Figure 3.36: FTIR spectra between 400-4000 cm^{-1} of the samples CT, CT _Mentha oil_water washed, CT_50%Mentha oil_water washed, CT_50%Mentha oil8(soaking)_ethanol washed_water washed, CT_20%Mentha oil8(soaking)_ethanol washed_water washed.

The signals analyzed before indicated the presence of compounds of the Mentha oil on the surfaces of all these samples highlighting the successful of the coating or functionalization.
On the basis of the gas chromatography analysis, it is possible to interpret the signals found with FTIR analysis reported in paragraph 3.6.6 correlating the peaks with the chemical bonds of the compounds found on the samples and resumed in Table 3.15.

Table 3.15: correlation of FTIR results and gas chromatography results.

Wavenumber (cm^{-1})	**Assignement**	**Compound of the oil**
3450-3200 cm^{-1}[107]	***Stretching* O-H**	Menthol Hydroxy-menthofuran
2960-2870 cm^{-1}[92]	***Stretching* C-H**	Menthol Hydroxy-menthofuran Menthyl-acetate Menthofuranone diethyl-methoxy-benzene Trans-Caryophyllene Beta-cubebene
2960-2870 cm^{-1} [92]	***Stretching* C-O**	Menthol Hydroxy-menthofuran Menthyl-acetate Menthofuranone Diethyl-methoxy-benzene
1670-1820 cm^{-1} [92]	***Stretching* C=O**	Menthyl-acetate Menthofuranone
1450 cm^{-1}[109]	***Aromatic C-C***	Hydroxy-menthofuran Menthofuranone Diethyl-methoxy-benzene Trans-Caryophyllene
1450 cm^{-1} [109]	**Bending C-H,**	Menthol Hydroxy-menthofuran Menthyl-acetate Menthofuranone diethyl-methoxy-benzene Trans-Caryofphyllene Beta-cubebene
1400-1370 cm^{-1} [109]	**stretching of $=CH_2$**	Trans-Caryofphyllene Beta-cubebene
1400-1370 cm^{-1} [109]	**Stretching C=O**	Menthyl-acetate Menthofuranone

3.6.9 X-ray photoelectron spectroscopy

XPS analysis were performed on the samples CT, CT_Mentha oil, CT_Mentha oil_water washed, CT_ Mentha oil_ ethanol washed_ water washed, CT_20%Mentha oil(soaking)_ethanol washed_water washed and CT_50% Mentha oil(soaking)_ethanol washed_water washed and the atomic percentage of the elements found on the surfaces of the samples in the survey spectra are reported in Table 3.16.

Table 3.16: Atomic percentage of the elements on the surface of the samples CT, CT_Mentha oil, CT_Mentha oil_water washed, CT_ Mentha oil_ ethanol washed_ water washed, CT_20%Mentha oil(soaking)_ethanol washed_water washed and CT_50% Mentha oil(soaking)_ethanol washed_water washed.

	Samples					
Elements (at %)	**CT**	**CT_Mentha oil**	**CT_Mentha oil_water washed**	**CT_ Mentha oil _ethanol washed _water washed**	**CT_20% Mentha oil(soaking) _ethanol washed_water washed**	**CT_50% Mentha oil(soaking) _ethanol washed_water washed**
C	20.7	86.1	86	81.1	50.7	39.1
O	60.7	13.7	13.4	18.4	39.2	45
N	2.3	0.1	0.5	0.5	-	-
Ti	16.2	-	-	-	8.9	13.8
Al	-	-	-	-	-	1.7
Cl	-	-	-	-	1.2	0.4

For the coated samples CT_Mentha oil, CT_Mentha oil_water washed and CT_Mentha oil_ ethanol washed_ water washed it is evident that the titanium alloy substrate is no more detectable because of the thick coating present on the surface, The percentage of carbon grows considerably because of the presence of the organic layer and the percentage of oxygen decrease because of the titanium oxide hydroxylate layer is not detectable and the molecules of Mentha oil can expose less oxygen after polymerization. For the samples functionalized CT_20%Mentha oil(soaking)_ethanol washed_water washed and CT_50% Mentha oil(soaking)_ethanol washed_water washed the chemically treated titanium alloy substrate is still detectable. Also on these samples an increase of the carbon percentage and a decrease of the oxygen percentage are visible, in a smaller quantities if compared with the coated samples, which could be correlated

with the presence of Mentha molecules grafted to the substrate without the presence of a thick coating. For a better understanding of the chemical groups present on the surfaces of the samples, high resolution analysis of the regions of carbon and oxygen were performed and the list of the peaks found for each sample is reported on Table 3.17.

Table 3.17: Carbon and oxygen contributions and possible literature assignments.

CT					
Region C			**Region O**		
Position	**Area%**	**Assignment**	**Position**	**Area%**	**Assignment**
284.69	67.43	C-C, C-H[94]–[96]	530.50	55.64	Ti-O[99], [110]
286.25	25.43	C-O[96]	532.54	44.16	Ti-OH[72], [94], [111]
288.66	7.14	C=O[96]			
CT_ Mentha oil					
Region C			**Region O**		
Position	**Area%**	**Assignment**	**Position**	**Area%**	**Assignment**
284.74	82.34	C-C, C-H[94]–[96]	532.36	66.6	C=O[95], [99]
286.03	13.98	C-O[96]	533.4	33.4	C-O[95], [99]
288.2	3.68	C=O[96]			
CT_ Mentha oil_water washed					
Region C			**Region O**		
Position	**Area%**	**Assignment**	**Position**	**Area%**	**Assignment**
284.84	88.26	C-C, C-H[94]–[96]	532.55	78.18	C=O[95], [99]
286.41	10.71	C-O[96]	533.77	21.82	C-O[95], [99]
288.34	1.04	C=O[96]			
CT_Mentha oil_ethano washed_water washed					
Region C			**Region O**		
Position	**Area%**	**Assignment**	**Position**	**Area%**	**Assignment**

284.78	72.81	C-C, C-H[94]–[96]	532.22	11.16	C=O[95], [99]
285.12	20.24	C-O[96]	532.98	88.84	C-O[95], [99]
288.33	6.96	C=O[96]			
CT_20% Mentha oil(soaking)_ethanol washed_water washed					
Region C			**Region O**		
Position	**Area%**	**Assignment**	**Position**	**Area%**	**Assignment**
284.67	74.87	C-C, C-H[94]–[96]	530.47	68.16	Ti-O[99], [110]
285.92	22.13	C-O[96]	532.17	31.84	Ti-OH[72], [94], [111]
288.82	3	C=O[96]			
CT_50% Mentha oil(soaking)_ethanol washed_water washed					
Region C			**Region O**		
Position	**Area%**	**Assignment**	**Position**	**Area%**	**Assignment**
284.76	74.06	C-C, C-H[94]–[96]	530.54	70.43	Ti-O[99], [110]
285.94	22.83	C-O[96]	532.41	29.57	Ti-OH[72], [94], [111]
288.69	4.11	C=O[96]			

Figure 3.37 shows in the details the high resolution XPS carbon region of the examined samples.

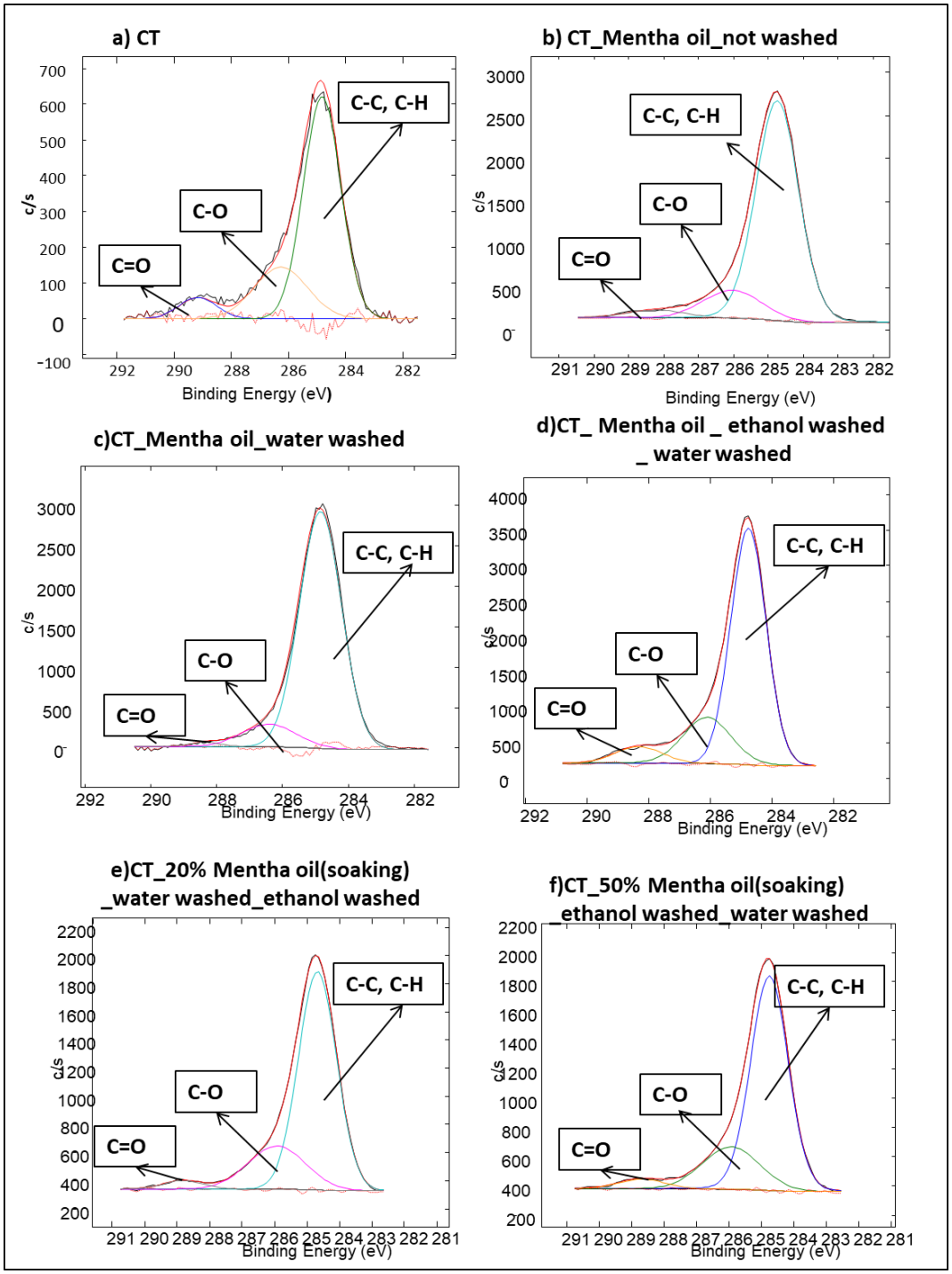

Figure 3.37: XPS detailed analysis of the carbon region of the samples a) CT, b) CT_Mentha oil, c) CT_Mentha oil_water washed, d) CT_ Mentha oil_ ethanol washed_ water washed, e) CT_20%Mentha oil(soaking)_ethanol washed_water washed and f) CT_50% Mentha oil(soaking)_ethanol washed_water washed.

For all the samples, the same three peaks are detected. The peak around 284 eV is due to C-C and C-H bonds [94]–[96] correlated to unavoidable atmospheric contamination, but also to the presence of organic molecules from the oil.
The peaks at 286 eV and 288,5 eV, instead, are related respectively to C-O and C=O bonds[96] that could be again correlated with contaminants ,but also with the molecules of the oil. These three peaks are more intense in the spectra of the samples coated/ functionalized with Mentha oil than for the bare CT spectra, but because of the presence of the same carbon bonds in the atmospheric contaminants and in the bonds of the compounds of Mentha oil, the analysis of the carbon region is not suitable to highlight significant differences between the samples.
Figure 3.38 shows in the details the high resolution XPS oxygen region of the examined samples.

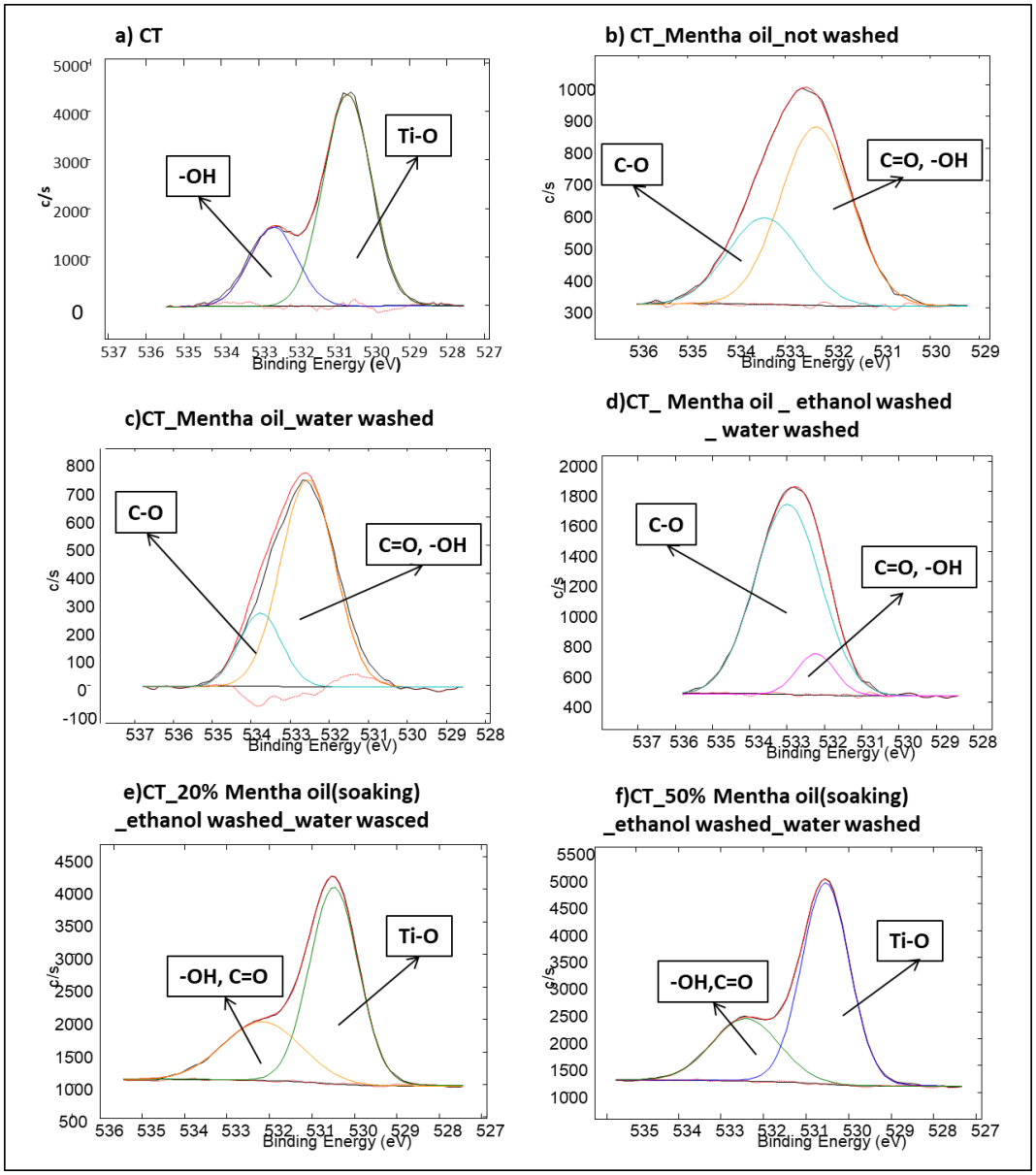

Figure 3.38: XPS detailed analysis of the oxygen region of the samples a) CT, b) CT_Mentha oil, c) CT_Mentha oil_water washed, d) CT_ Mentha oil_ ethanol washed_ water washed, e) CT_20%Mentha oil(soaking)_ethanol washed_water washed and f) CT_50% Mentha oil(soaking)_ethanol washed_water washed.

The spectrum of the CT sample displays the characteristic peak of titanium oxide at 530 eV, and the peak associated to -OH bonds of Ti-OH groups at about 532 eV[72], [111]. These peaks are shifted in the high resolution spectra of the specimens CT_Mentha oil: the first, that appears at 532 eV, can be associated to aliphatic C=O bonds (the attribution to –OH groups of the Ti substrates is not

possible because titanium is not detected in the survey spectrum), while the second at 533 eV is related to C-O bonds [95], [112] due to the presence of the polymerized essential oil. For the sample CT_Mentha oil_ ethanol washed_water washed it is possible see an inversion of the intensity of these two peaks correlated with the breaking of some double bonds and the selective washing of some molecules by means of the ethanol washing as observed before with FTIR analysis. These results highlight the presence of the compounds of Mentha oil coating on the surface of the CT samples. Regarding the functionalized samples CT_20%Mentha oil(soaking)_ethanol washed_water washed and CT_50% Mentha oil(soaking)_ethanol washed_water washed two peaks at 530 eV and 532 eV are present, the first is correlated with the Ti-O and the second with Ti-OH [97], [111] characteristic of the CT substrate. The peak at 532 eV could be also due to C=O bonds [95], [112] but in this case, on the basis of the gas chromatography analysis which did not show the presence of compounds with C=O groups, are probably correlated with surface contamination. These spectra show a probable low amount of the molecules of the oil on the substrate after the functionalization, but this technique is not suitable to detect these biomolecules grafted to the surface by means of functionalization procedure because of the nature of the surface itself which has almost the same chemical groups than the Mentha oil compounds.

3.6.10 Z potential electrokinetic measurements

In Figure 3.39 the results of the z potential vs pH measurements performed on the CT samples coated or functionalized with Mentha Piperita essential oil are reported. The samples tested are all washed in water because of the procedure of the electrokinetic measurement itself that needs washing of the samples in electrolyte during the start of the analysis in order to adjust the gap between the samples and washing in water between the basic and the acidic range of measurements.

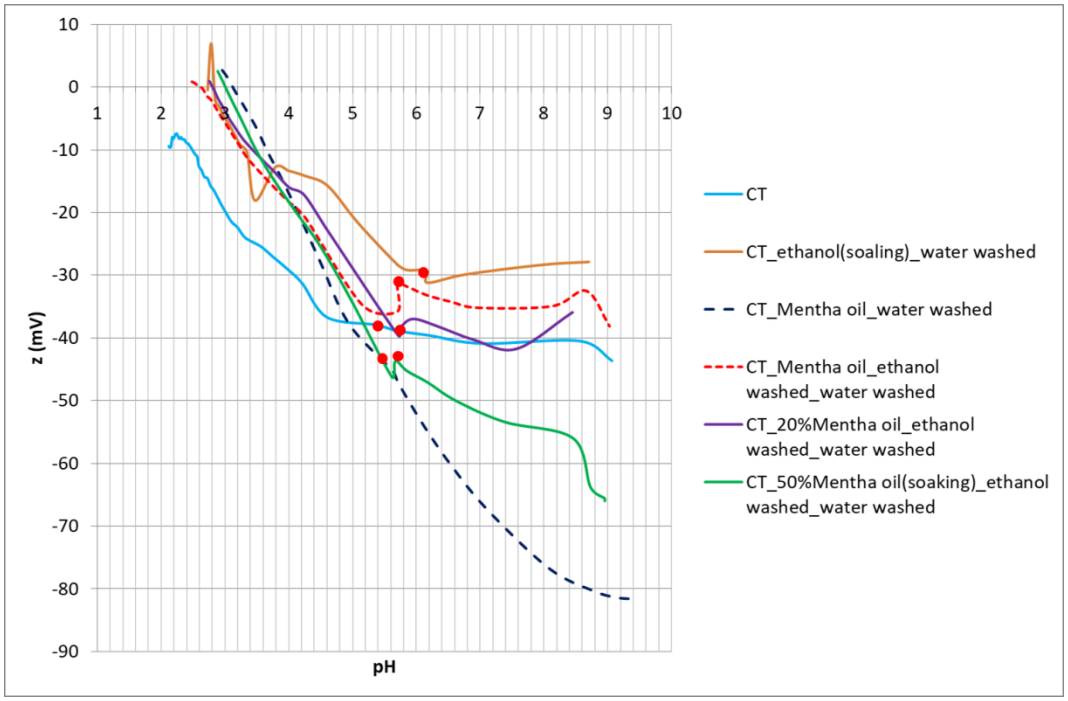

Figure 3.39: Zeta potential vs pH graph of samples CT, CT_ethanol(soaking)_water washed, CT_Mentha oil water washed, CT_Mentha oil_ethanol washed_water washed, CT_20% Mentha oil(soaking)_ethanol washed water washed and CT_50% Mentha oil(soaking)_ethanol washed water washed. The red dots indicate the change of the electrolyte solution between the scanning of the acidic and basic rage.

The principal results reported in Figure 3.39 are summarized in Table 3.18.

Table 3.18: summary of z potential results.

Samples	**IEP**	**z (pH=7.4) [mV]**	**z (pH= 6) [mV]**	**Z (pH= 8) [mV]**	**Δ Plateau [mV] z(pH=8)-z(pH=6)**
CT	<2	-40	-39	-40	-1
CT_ethanol(soaking)	2.83	-28	-28	-29	-1
CT_Mentha oil_water washed	3.12	-70	-54	-76	-22
CT_Mentha oil_ethanol washed _water washed	2.61	-35	-33	-34	-1
CT_20% Mentha oil(soaking)_ethanol washed_water washed	2.81	-40	-37	-35	2
CT_50% Mentha oil(soaking)_ethanol washed_water washed	3.01	-57	-47	-56	-9

All the samples show a shift of the isoelectric point (IEP) if compared with the IEP of the bare samples CT. The shift of the isoelectric point is observable also for the samples soaked in ethanol and washed in water without any treatment in Mentha oil combined with a shift of the starting points of the plateau in the basic range. In the case of the zeta potential titration, curves confirm that this technique is sensitive to any surface modifications and able to evidence several differences of surface chemistry. At first, it confirms that washing of CT samples with ethanol leaves a surface contaminations able to shift the IEP and the starting point of the plateau in the basic range because of the lower acidic strength of the –OH groups of ethanol exposed on the surface. This is in agreement with the contact angle measurements where a different contact angle was measured on the CT samples after washing in ethanol.

In the case of CT_Mentha oil_water washed samples show a negative charge for pH over 3, highlighting the negative potential of the samples.

The plateau present for the samples CT and CT_ethanol(soaking)-water washed, due to the presence on the surface of chemical groups of the same type (–OH groups) [113] exposed by the substrate as a consequence of the chemical treatment[71], [72], is no more visible. This result suggests that the Mentha coating is completely covering the surface, exposing several different functional groups and that the surface of the CT sample is no more exposed.

The samples, CT_Mentha oil_ethanol washed_water washed have a behavior similar to the one of the CT_Mentha oil _water washed in the acidic range, but it shows the presence of the plateau due to the exposition of probably C-O groups of

the oil compounds or –OH groups of the substrate as seen by means of XPS measurements. This plateau is at a different negative potential with respect to the sample only soaked in ethanol suggesting the presence of the Mentha coating on the samples.
The functionalized samples CT_20% Mentha oil(soaking)_ethanol washed water washed and CT_50% Mentha oil(soaking)_ethanol washed water washed have a behavior similar to the one of CT_ethanol(soaking)_water washed samples, but the plateau in the acidic range are at a more negative potential because of the presence of the Mentha oil molecules. In the basic range (pH ≈ 9) of these two samples, two deflections from the plateau that could indicate the detachment or the degradation of the grafted biomolecules on the samples are also visible.
In the end, this technique allows to confirm the presence of a polymeric film due to the Mentha oil polymerization on the samples and allows also to observe the change of the potential of the surface induced by the grafting of biomolecules of the oil and due to ethanol contamination.

3.6.11 Tape test

The sample CT_ Mentha oil_water washed was subjected to the tape test and after the test, it was observed with an optical microscope at different magnifications. The aspect of the essential oil coating is shown in Figure 3.40.

Figure 3.40: Aspect of the sample CT_Mentha oil_water washed before and after making the incisions.

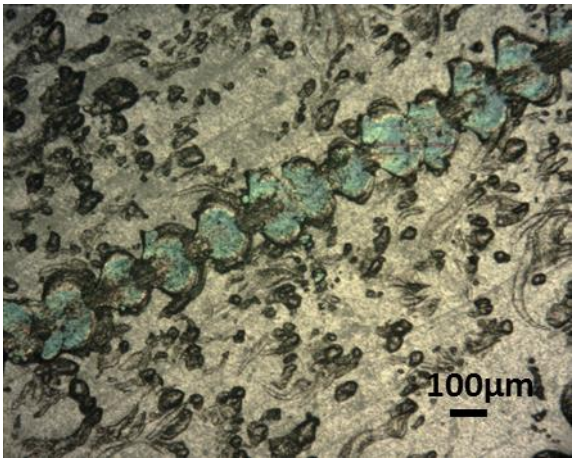

Figure 3.41: Aspect of the sample CT_Mentha oil_water washed after the tape test (magnification 5x).

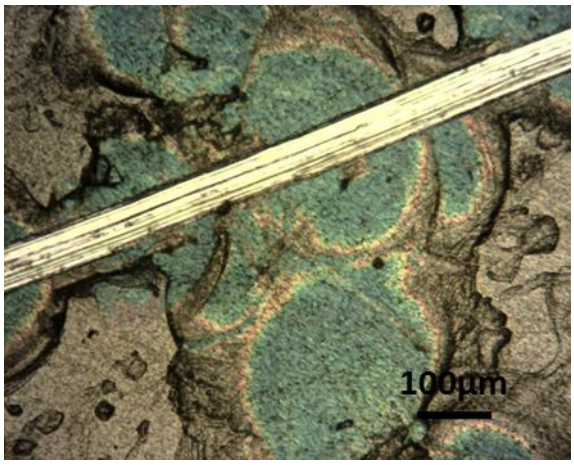

Figure 3.42: Aspect of the sample CT_Mentha oil_water washed after the tape test (magnification 10x).

Figures3.40, 3.41, 3.42 show that the coating of essential oil presents a good adhesion to the underlying material, as highlighted by the fact that, although the oil adheres clearly to the tape, it remains also attached on the sample in the test area. In addition, the detachment of the essential oil layer from the underlying material occurs in the form of bubbles. This form of separation is known as boiling. The adhesion can be classified as 3B/4B in accordance to standard ASTM D 3359: the damage indeed is limited to the incision area[76].

3.6.12 Biological tests

Antibacterial tests

Kirby Bauer test:

The sample CT_Mentha oil_water washed subjected to the Kirby-Bauer test with *Staphylococcus aureus*, does not show an inhibition zone (Fig.3.43, 3.44), related to the fact that any release of antibacterial agents occurred as expected.

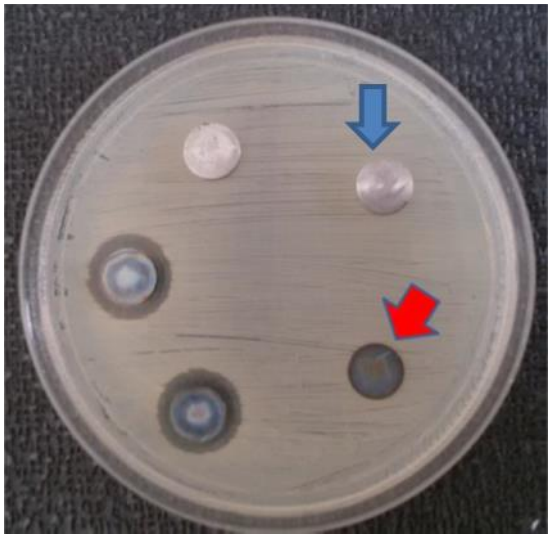

Figure 3.43: Mueller Hinton plate containing the CT_Mentha oil_water washed sample. The red arrow highlights the samples, while the blue arrow highlights the control sample (Ti6Al4V mirror polished).

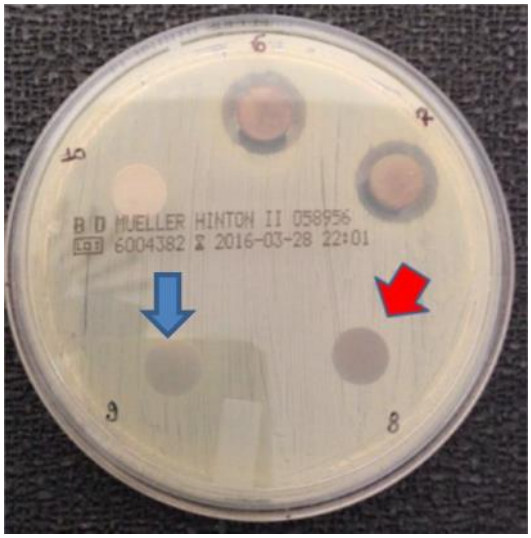

Figure 3.44: Mueller Hinton plate containing the CT_Mentha oil_water washed sample. Backside. The red arrow highlights the samples, while the blue arrow highlights the control sample (Ti6Al4V mirror polished).

The presence of bacterial proliferation on the samples was observed and subsequently confirmed by a Field Emission Scanning Electron Microscope, as shown in Figure 3.45.

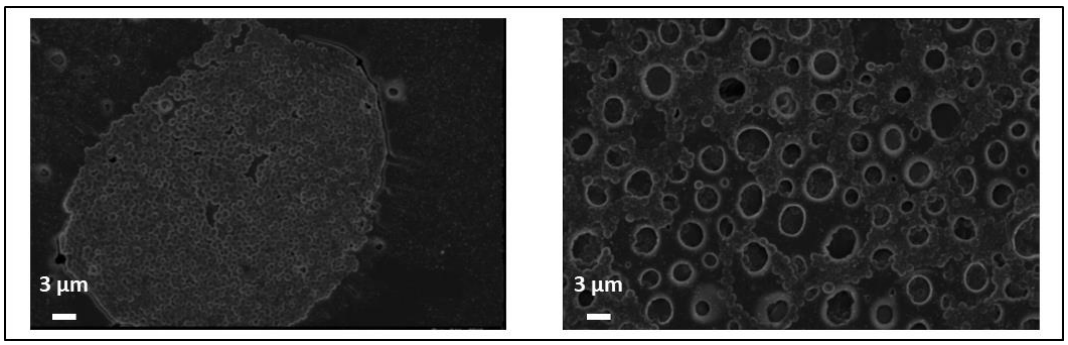

Figure 3.45: FESEM images of the bacterial proliferation on the CT_Mentha oil_water washed sample.

This result could be due to the polymerization of the essential oil on the surface of the sample, which probably reduces the antibacterial action of the chemical components of the oil. It is also possible to suppose that the presence of some discontinuities on the polymerized layer have allowed the bacteria to go under the polymerized film contaminating the substrates. This test proves that the Mentha molecules were not released from the coating, but more tests were performed in order to investigate more in depth the antibacterial behavior.

Broth dilution method:

The CFU plate counting of the bacterial (*Staphylococcus aureus*) adhesion test performed on the samples treated with Mentha oil is reported on Figure 3.46 and 3.47. CT and Ti6Al4V samples were used as control series.

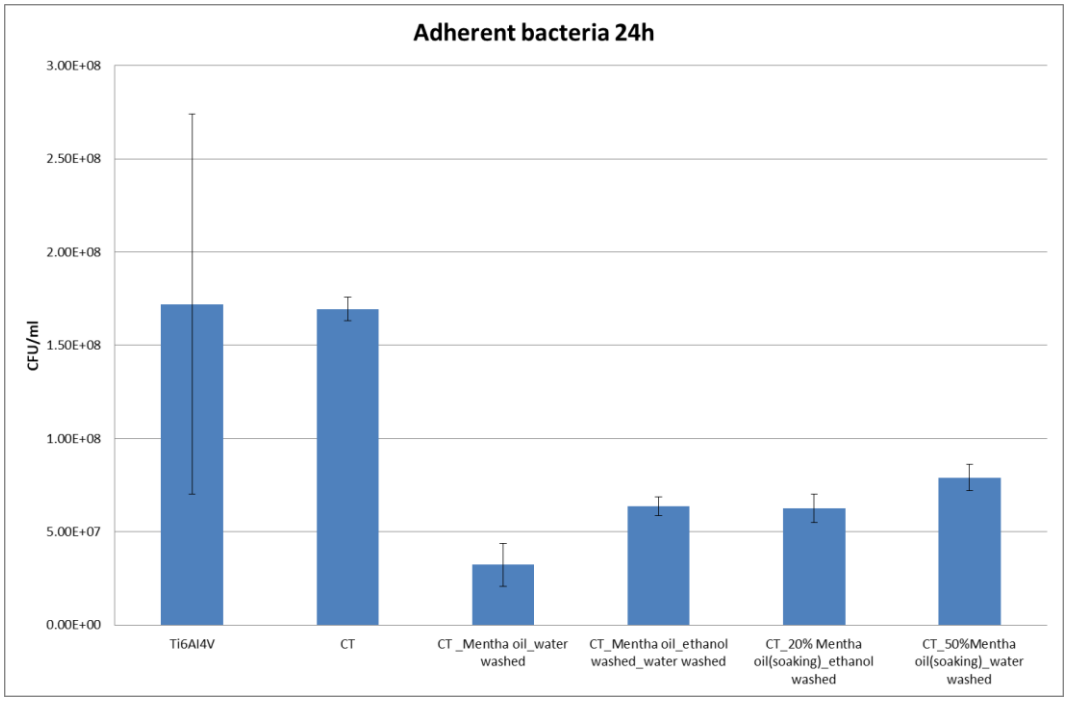

Figure 3.46 amount of adherent bacteria on examined samples.

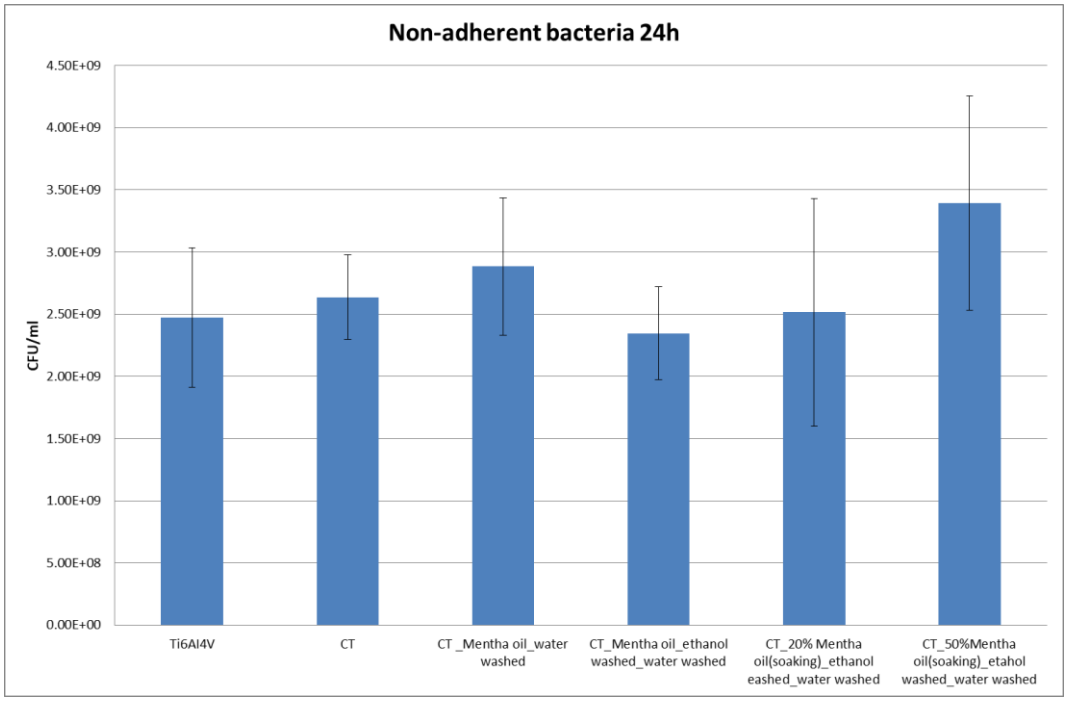

Figure 3.47: amount of non-adherent bacteria on examined samples.

The medium amount of the adherent bacteria present on the control samples after 24h of incubation is $1.72*10^8$ for the samples Ti6Al4V and $1.7*10^8$ CFU/ml for samples CT. The standard deviation for the samples Ti6Al4V is high because of some scratches or irregularity introduced on the surface of the samples during the polishing procedure or during the manipulation for the tests. For the samples treated with Mentha oil, the count results an order of magnitude minor and is respectively $3.23*10^7$ for the samples CT_Mentha oil_water washed, $6.36*10^7$ for the samples CT_Mentha oil ethanol washed_water washed, $6.\ 27*10^7$ for the samples CT_20%Mentha oil(soaking)_ethanol washed_water washed and $7.91*10^7$ for the samples CT_50%Mentha oil(soaking)_ethanol washed_water washed. The reduction of the adherent bacteria for the coated and functionalized samples is significant and it is greater for the samples CT_Mentha oil_water washed because of the higher amount of antibacterial chemical compound as highlighted by gas chromatography analysis.

Indeed, as expected and reported in Figure 3.47, the amount of the non-adherent bacteria does not change between the control samples and the functionalized or coated samples because no release, as shown in the Kirby Bauer test, was detected.

Antibacterial Properties Evaluation:

Results related to the samples' antibacterial activity are reported in Figure 3.48.
In general, treatment with Mentha oil is successfully in reducing bacteria viability only when applied as pure extract; in fact, better results were achieved after 24 hours (Fig. 3.48a) in comparison to both untreated and 50 % oil functionalized samples. The same results were obtained after 48(Fig. 3.48b) and 72(Fig.3.48 c) hours. In any case, the antibacterial activity is lower than what observed for the bare oil in the liquid form, suggesting that polymerization reduces the effectiveness of the compounds of the oil. When mint extract was used as 50 % dilution for functionalize the samples, the killing effect is noticeably reduced. It is also possible to observe a reduction of the bacterial contamination on the bare samples CT if compared with the Ti6Al4V samples because of the surface treatments that confer to the surface a nanometric roughness and the presence of negative –OH groups able to reduce bacterial contamination[109]

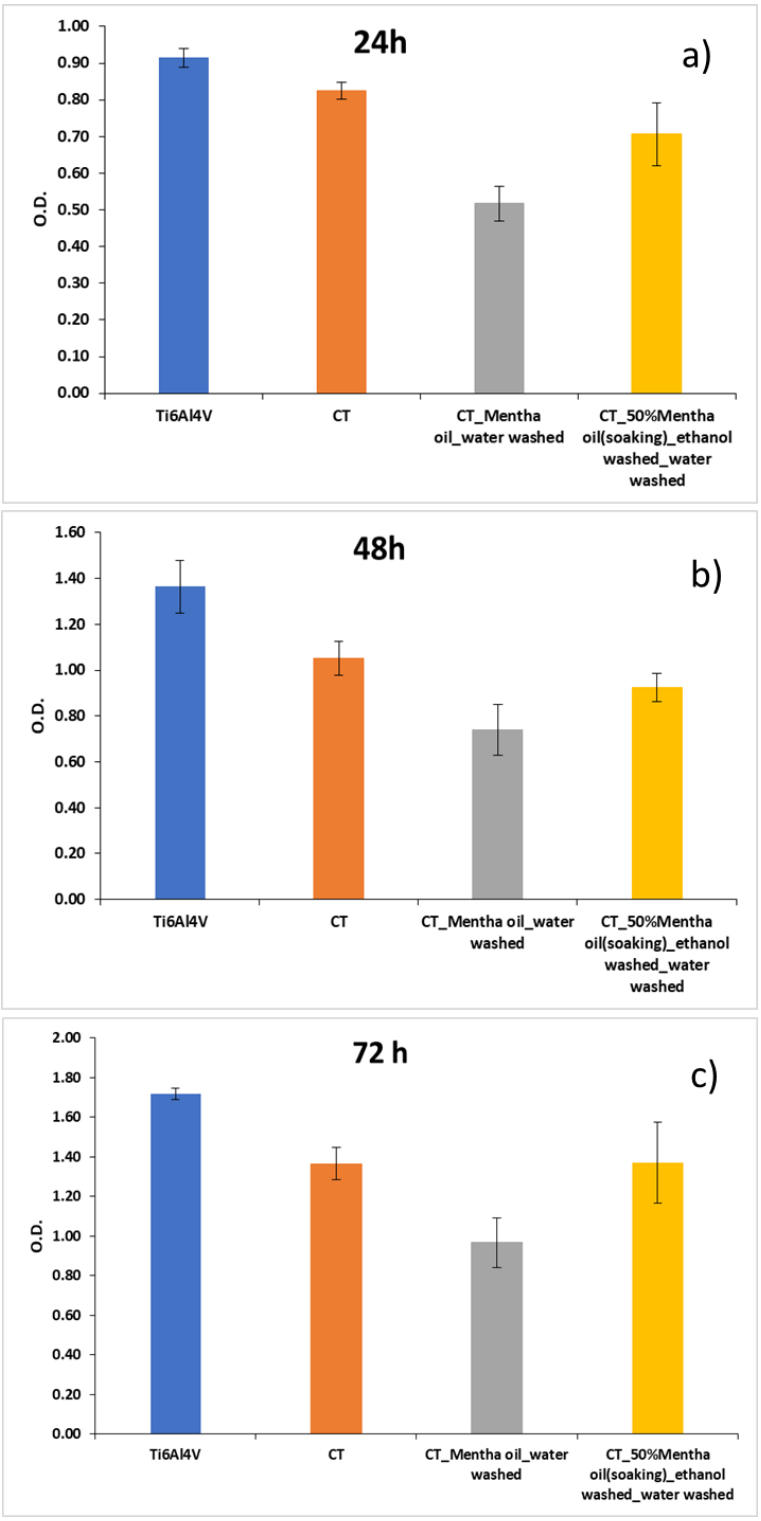

Figure 3.48: S. aureus biofilm viability after 24 a), 48 b) and 72 c) hours samples' infection. Only pure mint extract was effective in reducing bacteria viability in comparison with control groups. Results expressed in Optical density (O.D.)

Finally, results are expressed as optical density increasing in function of time in Figure 3.46 and as percentage of bacteria viability in comparison with mirror-like Ti6Al4V in Figure 3.49.

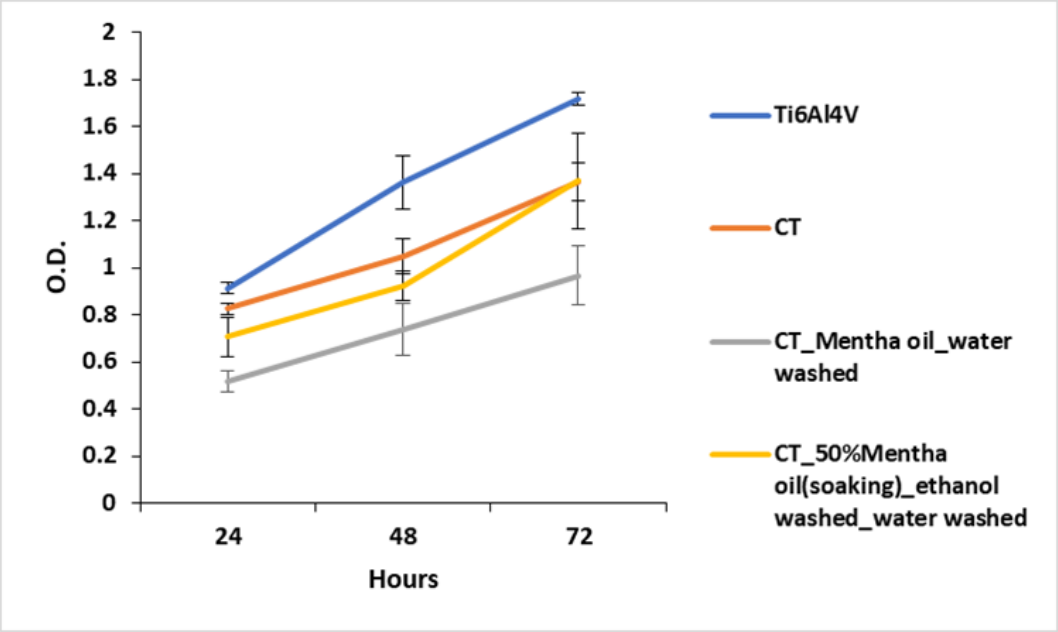

Figure 3.49: results of figure 3.48 expressed as optical density increasing in function of time.

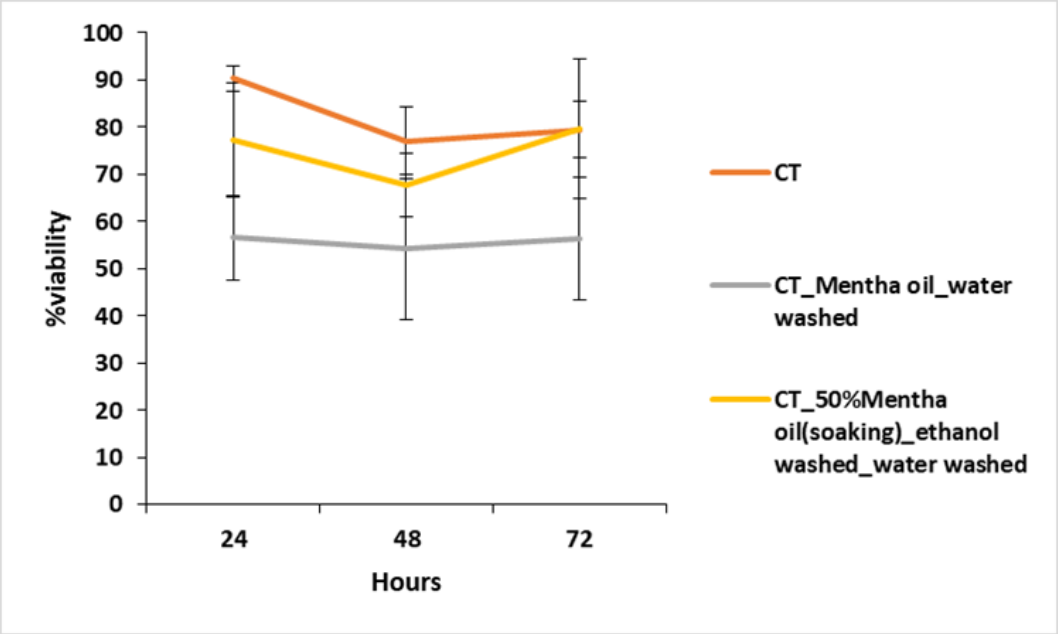

Figure 3.50: percentage of bacteria viability in comparison with mirror-like Ti6Al4V.

Accordingly, it is possible to notice that bacteria viability is increased during the 72 hours experimentation thus suggesting a bacteriostatic effect due to the mint treatment rather than a bactericide effect; moreover, biofilm cells viability was never lowered less than 50 %. Data obtained by XTT analysis were confirmed by the Live/Dead assay reported in Figure 3.51. In fact, the number of dead bacteria (stained in red) markedly increased with the introduction of pure Mentha oil coating and 50 % Mentha oil functionalization.

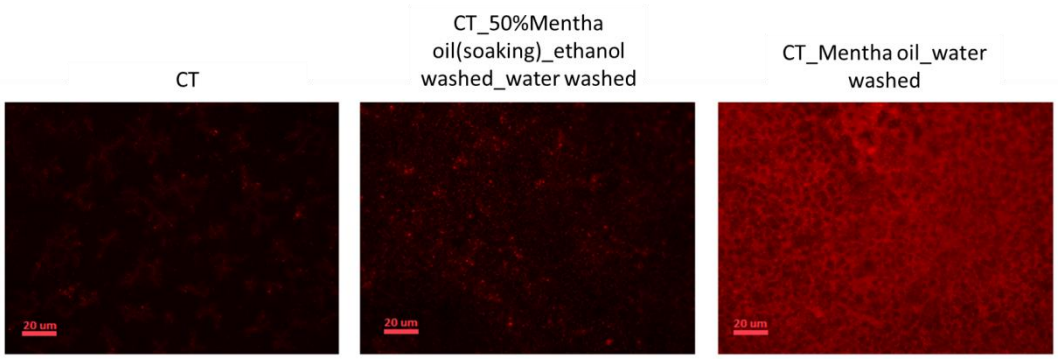

Figure 3.51: 72 hours S. aureus biofilm Live/dead assay. The number of dead bacteria (stained in red) was noticeably increased due to the introduction of Mentha (pure coating and 50 % Mentha functionalization) in comparison with bare CT surfaces. Magnification = 20x, bar scale = 20 um.

Cytotoxicity assay

Results related to samples cytocompatibility activity of hFOB cells are reported in Figure 3.52 .In general, pure Mentha oil coating results in a marked cells viability decrease that was immediately noted after 24 hours (Fig.3.52a). The toxic effect lasted for the subsequently 48 (Fig.3.52b) and 72 (Fig. 3.52c) hours.

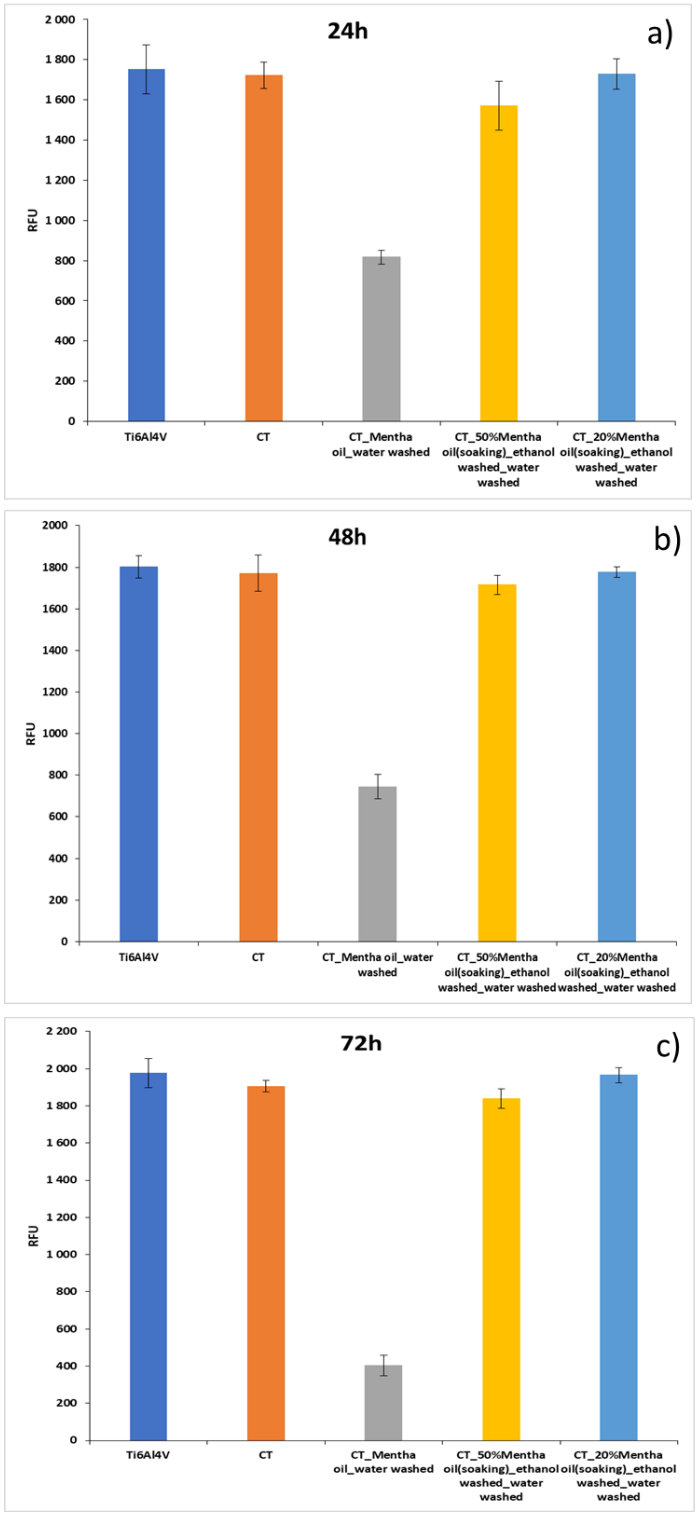

Figure 3.52: hFOB cells viability after 24 s), 48 b) and 72 d) hours direct contact onto samples surfaces. Results expressed in Relative fluorescent units (RFU).

The summarized effects of the Mentha treatments on hFOB cells viability are reported in Figure 3.53 as RFU in function of time and as percentage of cell viability in comparison with mirror-like Ti6Al4V in Figure 3.54.

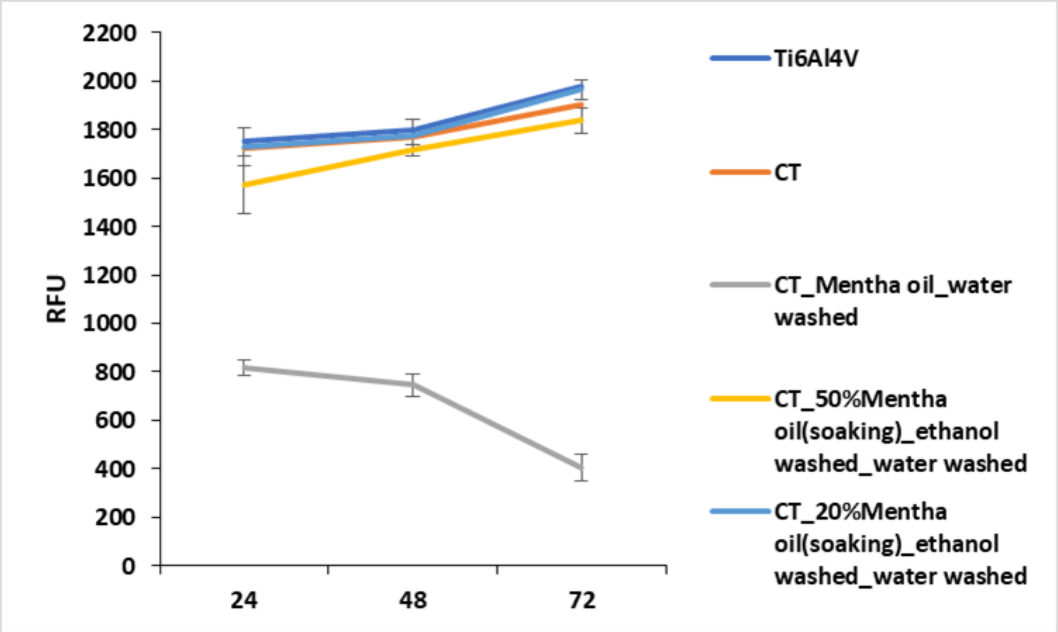

Figure 3.53: summarized results of figure 3.52 expressed as RFU in function of time.

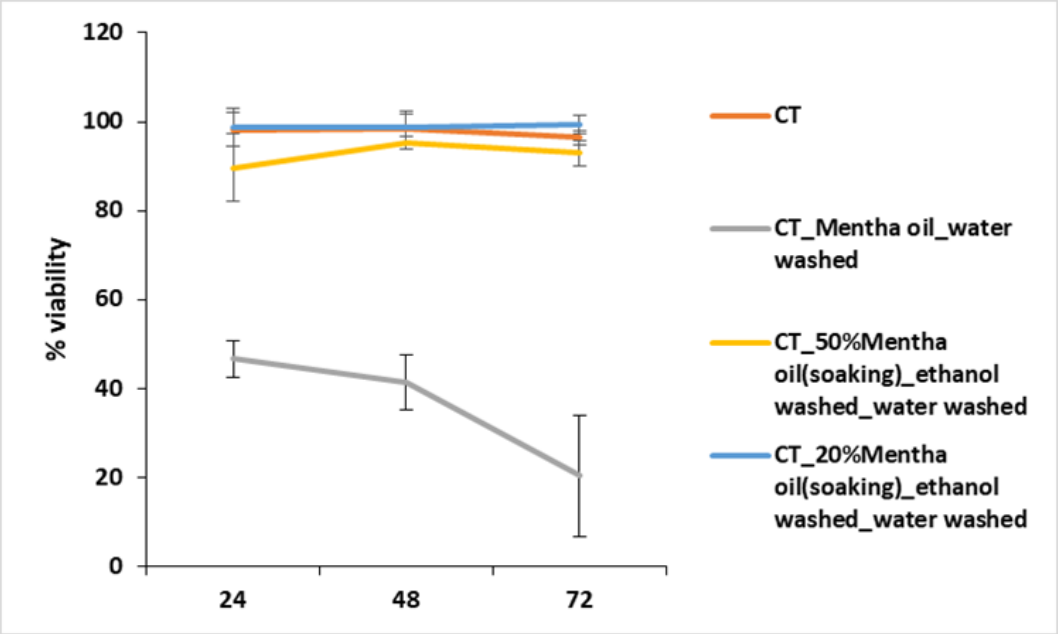

Figure 3.54: percentage of cell viability in comparison with mirror-like Ti6Al4V.

Because of the cytotoxic effects of Mentha oil, cells viability was lowered until 20 % after 72 hours (Figure 3.43). On the opposite, the 50% and 20% Mentha oil functionalization do not cause any significant toxic effect, thus allowing cells proliferation (Fig. 3.42) as viability was never < 90 % (Fig. 3.43)
These results highlighted the possible cytotoxicity of Mentha oil already known in the literature[8], [9], [50] and highlights the needs of tailoring the amount and species of Mentha oil molecules on the surface of the samples in order to enhance the antibacterial action of the Mentha compounds avoiding cytotoxic affects.

3.7 Conclusions

The work exposed in this chapter deals with the surface coating or functionalization of chemically-treated titanium alloy Ti6Al4V with essential oils and in particular with the Mentha Piperita essential oil of Pancalieri. The aim of the work is to develop protocols of coating and functionalization of this surface with essential oils and to find the appropriate methodology of characterization in order to confer to the surface antibacterial properties. The antibacterial property of essential oil is well known in literature and was tested in this chapter in order to find the MIC and MBC values of the oil that result to coincide highlighting the bactericidal effects of the essential oils.

A Mentha coating was created in loco on the surface of the samples by polymerization of the oil at 37°C and the surface functionalization were performed by means of soaking in ethanol solution with different concentration of Mentha oil.

The effects of ethanol and water washing after coating or functionalization was investigated by means of macroscopic observation, contact angle measurements, fluorescence microscopy observations, FTIR analysis, XPS analysis and gas chromatography analysis. For the coated samples, no modification was introduced by the water washing, that could however be useful in order to remove contaminants and dust that may deposit on the samples. The washing in ethanol indeed selectively removes compounds from the coating, as highlighted by fluorescence microscope images, and depolymerizes the coating removing compounds containing C=O bonds as suggested from XPS and FTIR analysis. The single wash in water seems to be the best post-treatment for the coated samples. The coating was also investigated by means of tape tests that showed a strong adhesion of the coating to the substrates.

For the soaked functionalized samples the effect of the washing seems to be determinant in order to obtain a real functionalization. The samples not washed or only washed in water after the soaking showed after drying the presence of a not uniform polymerized coating due to the high amount of Mentha oil. In order to obtain a real functionalization, a washing in ethanol suitable to remove the excess Mentha oil and a washing in water in order to remove the ethanol and eventual dust contamination are needed. The gas chromatography analysis highlighted on the surface of the functionalized samples the presence of only two compounds which are a minority fraction in the oil, trans-caryophyllene and beta-cubebene. The surface of the CT samples and/ or the functionalization/ coating procedure seems to be selective towards not oxygenated compounds probably because of the

high affinity of titanium with respect to carbon and because of the ethanol washing removes preferentially species containing C=O bonds as suggested by XPS and FTIR analysis. However, more investigations are requested in order to understand the reason that allows these two molecules to graft preferentially to the surface and how strong could be the antibacterial effects of these two compounds if grafted in a greater amount. The antibacterial tests performed highlighted that the Mentha oil molecules were not released by the coating or by the functionalized surface, but they have bacteriostatic effect on adherent bacteria. This effect is greater for the coated samples probably because of the presence of menthol that is an antibacterial compound and lower for the functionalized. The absence of terpenoids grafted on the surface of the functionalized samples can be related with the lower antibacterial effects of these surfaces, considering that aromatic oxygenated compounds are well known for their efficacy against bacteria. On the other side, caryophyllene and cubebene, are reported in literature to be effective compounds against Gram-positive bacteria and *Staphylococcus aureu*s with a dose dependent action. Their low activity on the functionalized samples could be due to the low grafted amount. The cytotoxicity on hFOB cells was tested highlighting a cytotoxic effect of the coated samples due to the high amount of Mentha molecules present and it is well known in literature that the cytotoxicity effect of the essential oil is dose dependent. For the functionalized samples the cytotoxic effects are reduced in agreement with literature, where caryophyllene is reported to have no cytotoxic effect.

At the light of these results, the use of FTIR analysis and gas chromatography measurements in combination seems to be a good way to understand which compounds are present on the surface after the coating or functionalization and fluorescent microscope observation allows to see the distribution of this biomolecules on the surfaces. It is also clear by the biological test that the amount of Mentha oil molecules on the surfaces of the samples needs to be tailored in order to improve the antibacterial effect and avoid cytotoxicity effects.

After these first attempts of combining the properties of the essential oils with those of the metallic bioactive materials, the surface functionalization seems to be a promising green way to reduce the bacterial contamination of prosthetic and in particular dental implants also thinking to the appeal that the use of essential oils could have on the market. On the basis of this research work, the use of different essential oils can be also tested in the future following specific rationale. Considering the ability of the developed method with respect to grafting caryophyllene and terpenes, oils rich in these compounds and with a proved antibacterial action (such as *Salvia Triloba*, some species of basil and cinnamon,

oregano, lavender and hops) must be considered with caution because caryophyllene is coupled with other cytotoxic compounds such as eugenol. Lavender essential oil could be of interest for its low cytotoxicity. The Mentha coating can also be investigated in future works in applications without direct contact with cells.

References:

[1] J Grassmann and E F Elstner, "Essential Oils/ Properties and Usage," in *Essential Oils*, 2003, pp. 2177–2184.

[2] A. El Asbahani *et al.*, "Essential oils: From extraction to encapsulation," *Int. J. Pharm.*, vol. 483, no. 1–2, pp. 220–243, 2015.

[3] J. Wright, "Essential oils," in *Food flavorings*, no. August, 1991, pp. 25–57.

[4] "http://essentialoils.co.za/components.htm#Monoterpene (10/10/2017, 03:57 pm)."

[5] M. L. Tsai, C. T. Wu, T. F. Lin, W. C. Lin, Y. C. Huang, and C. H. Yang, "Chemical composition and biological properties of essential oils of two mint species," *Trop. J. Pharm. Res.*, vol. 12, no. 4, pp. 577–582, 2013.

[6] A. de Sousa Barros *et al.*, "Chemical composition and functional properties of essential oils from Mentha species," *Ind. Crops Prod.*, vol. 76, pp. 557–564, 2015.

[7] S. Kizil, N. Haşimi, V. Tolan, E. Kilinç, and U. Yüksel, "Mineral content, essential oil components and biological activity of two mentha species (M. piperita L., M. spicata L.)," *Turkish J. F. Crop.*, vol. 15, no. 2, pp. 148–153, 2010.

[8] S. Alankar, "A review on peppermint oil," *Asian J. Pharm. Clin. Res.*, vol. 2, no. 2, pp. 27–33, 2009.

[9] R. ECCLES, "Menthol and Related Cooling Compounds," *J. Pharm. Pharmacol.*, vol. 46, no. 8, pp. 618–630, 1994.

[10] T. Patel, Y. Ishiuji, and G. Yosipovitch, "Menthol: A refreshing look at this ancient compound," *J. Am. Acad. Dermatol.*, vol. 57, no. 5, pp. 873–878, 2007.

[11] "http://foodb.ca/compounds/FDB013800 (12/10/2017, 10.51 am)."

[12] F. Farley, "Pulegone," in *IARC- monographs*, 2012, pp. 141–154.

[13] E. A. Petrakis, A. C. Kimbaris, C. S. Pappas, P. A. Tarantilis, and M. G. Polissiou, "Quantitative determination of pulegone in pennyroyal oil by FT-IR spectroscopy," *J. Agric. Food Chem.*, vol. 57, no. 21, pp. 10044–10048, 2009.

[14] S. S. Mahmoud and R. B. Croteau, "Menthofuran regulates essential oil

biosynthesis in peppermint by controlling a downstream monoterpene reductase," *Proc. Natl. Acad. Sci.*, vol. 100, no. 24, pp. 14481–14486, 2003.
[15] "https://pubchem.ncbi.nlm.nih.gov/compound/Menthofuran#section=Top (12/10/2017, 11:26 am)."
[16] "https://pubchem.ncbi.nlm.nih.gov/compound/_-_-Limonene#section=Top (12/10/2017, 12:14)."
[17] "https://pubchem.ncbi.nlm.nih.gov/compound/_-_-Carvone#section=Top (12/10/2017, 12:38)."
[18] "https://pubchem.ncbi.nlm.nih.gov/compound/piperitone (12/10/2017, 01:10 pm)."
[19] A. Aflatuni, "The yield and essential oil content of mint (Mentha ssp.) in Northern Ostrobothnia," 2005.
[20] M. Marotti, R. Piccaglia, E. Giovanelli, S. G. Deans, and E. Eaglesham, "Effects of planting time and mineral fertilization on peppermint (mentha x piperita l.) essential oil composition and its biological activity," *Flavour Fragr. J.*, vol. 9, no. 3, pp. 125–129, 1994.
[21] "http://www.parcopotorinese.it/dettaglio_prodotto.php?id_prodotti=1974 (12/10/2017, 5:18 pm)."
[22] "http://www.saporidelpiemonte.net/blog/prodotti-tipici-del-piemonte/olio-essenziale-di-menta-piperita-piemonte-o-pancalieri-piemonte/(12/10/2017, 08: 20 pm)."
[23] J. S. Raut and S. M. Karuppayil, "A status review on the medicinal properties of essential oils," *Ind. Crops Prod.*, vol. 62, pp. 250–264, 2014.
[24] "https://cen.acs.org/articles/93/web/2015/04/New-Spin-Old-Gram-Stain.html (23/10/2017, 04:01 pm)."
[25] J. C. Lopez-romero, H. González-ríos, A. Borges, and M. Simões, "Antibacterial Effects and Mode of Action of Selected Essential Oils Components against Escherichia coli and Staphylococcus aureus," *Evidence-Based Complement. Altern. Med.*, vol. 2015, pp. 1–9, 2015.
[26] F. Nazzaro, F. Fratianni, and L. De Martino, "Effect of Essential Oils on Pathogenic Bacteria," *Pharmaceuticals*, vol. 6, pp. 1451–1474, 2013.
[27] A. G. M. ROSANGELA DI PASQUA, GAIL BETTS, NIKKI HOSKINS, MIKE EDWARDS, DANILO ERCOLINI, "Membrane Toxicity of Antimicrobial Compounds from Essential Oils," *J. Agric. Food Chem.*, vol. 55, pp. 4863–4870, 2007.
[28] M. L. Faleiro, "The mode of antibacterial action of essential oils," in *Science against microbial pathogens: communicating current research and technological advances*, 2011, pp. 1143–1156.
[29] M. K. Swamy, M. S. Akhtar, and U. R. Sinniah, "Antimicrobial Properties of Plant Essential Oils against Human Pathogens and Their Mode of Action : An Updated Review," *Evidence-Based Complement. Altern. Med.*, vol. 2016, pp. 1–21, 2016.
[30] E. Abdollahzadeh, M. Rezaei, and H. Hosseini, "Antibacterial activity of

plant essential oils and extracts : The role of thyme essential oil , nisin , and their combination to control Listeria monocytogenes inoculated in minced fi sh meat," *Food Control*, vol. 35, pp. 177–183, 2014.
[31] G. Pesavento *et al.*, "Antibacterial activity of Oregano , Rosmarinus and Thymus essential oils against Staphylococcus aureus and Listeria monocytogenes in beef meatballs," *Food Control*, vol. 54, pp. 188–199, 2015.
[32] N. Celikel and G. Kavas, "Antimicrobial Properties of Some Essential Oils against Some Pathogenic Microorganisms," *Czech J. Food Sci.*, vol. 26, no. 3, pp. 174–181, 2007.
[33] W. Diao, Q. Hu, H. Zhang, and J. Xu, "Chemical composition , antibacterial activity and mechanism of action of essential oil from seeds of fennel (Foeniculum vulgare Mill .)," *Food Control*, vol. 35, no. 1, pp. 109–116, 2014.
[34] G. A. Evrendilek, "Empirical prediction and validation of antibacterial inhibitory effects of various plant essential oils on common pathogenic bacteria," *Int. J. Food Microbiol.*, vol. 202, pp. 35–41, 2015.
[35] D. Dussault, K. D. Vu, and M. Lacroix, "In vitro evaluation of antimicrobial activities of various commercial essential oils , oleoresin and pure compounds against food pathogens and application in ham," *Meat Sci.*, vol. 96, no. 1, pp. 514–520, 2014.
[36] J. Walentowska and J. Foksowicz-flaczyk, "Thyme essential oil for antimicrobial protection of natural textiles," *Int. Biodeterior. Biodegradation*, vol. 84, pp. 407–411, 2013.
[37] F. T. and L. B.-M. J Bonou, F Baba-Moussa, Z Adéoti, H Ahouandjinou, V Dougnon, D Dossa, JD Gbenou and Abstract, "Antimicrobial activity of essential oils of Lippia multiflora, Eugenia caryophyllata, Mentha piperita and Zingiber officinale on five oral-dental microorganisms," *J. Pharmacogn. Phytochem.*, vol. 5, no. 5, pp. 471–476, 2016.
[38] M. Gulluce, F. Sahin, M. Sokmen, H. Ozer, and D. Daferera, "Antimicrobial and antioxidant properties of the essential oils and methanol extract from Mentha longifolia L . ssp . longifolia," *Food Chem.*, vol. 103, pp. 1449–1456, 2007.
[39] G. B. Nagar and U. Pradesh, "In vitro antimicrobial activity , phytochemical analysis and total phenolic content of essential oil from Mentha spicata and Mentha piperita," *Int. Food Res. J.*, vol. 22, no. 6, pp. 2440–2445, 2015.
[40] G. P. P. Kamatou, I. Vermaak, A. M. Viljoen, and B. M. Lawrence, "Menthol : A simple monoterpene with remarkable biological properties," *Phytochemistry*, vol. 96, pp. 15–25, 2013.
[41] R. Amorati, M. C. Foti, and L. Valgimigli, "Antioxidant Activity of Essential Oils," *J. Agric. Food Chem.*, vol. 61, pp. 10835–10847, 2013.
[42] A. Brenes and E. Roura, "Essential oils in poultry nutrition : Main effects and modes of action," *Anim. Feed Sci. Technol.*, vol. 158, no. 1–2, pp. 1–

14, 2010.
[43] G. Ruberto and M. T. Baratta, “Antioxidant activity of selected essential oil components in two lipid model systems,” *Food Chem.*, vol. 69, pp. 167–174, 2000.
[44] H. Bagheri, M. Yazid, B. Abdul, and Z. Solati, “Antioxidant activity of Piper nigrum L . essential oil extracted by supercritical CO 2 extraction and hydro-distillation,” *Talanta*, vol. 121, pp. 220–228, 2014.
[45] M. I. F. Bakkali, S. Averbeck, D. Averbeck, “Biological effects of essential oils – A review,” *Food Chem. Toxicol.*, vol. 46, pp. 446–475, 2008.
[46] A. E. Edris, “Pharmaceutical and Therapeutic Potentials of Essential Oils and Their Individual Volatile Constituents: A Review,” *Phyther. Res.*, vol. 21, pp. 308–323, 2007.
[47] Y. Chen *et al.*, “Composition and potential anticancer activities of essential oils obtained from myrrh and frankincense,” *Oncol. Lett.*, vol. 6, no. 4, pp. 1140–1146, 2013.
[48] P. F. de Oliveira *et al.*, “Cytotoxicity screening of essential oils in cancer cell lines,” *Brazilian J. Pharmacogn.*, vol. 25, no. 2, pp. 183–188, 2015.
[49] M. Hyldgaard, T. Mygind, R. L. Meyer, and D. Debabov, “Essential oils in food preservation : mode of action , synergies , and interactions with food matrix components,” *Front. Microbiol.*, vol. 3, pp. 1–24, 2012.
[50] C. Dima and S. Dima, “Essential oils in foods: extraction, stabilisation and toxicity,” *Curr. Opin. Food Sci.*, vol. 5, pp. 29–35, 2015.
[51] C. Turek and F. C. Stintzing, “Stability of essential oils: A review,” *Compr. Rev. Food Sci. Food Saf.*, vol. 12, no. 1, pp. 40–53, 2013.
[52] I. Anghel *et al.*, “PROTECTIVE EFFECT OF MAGNETITE NANOPARTICLE / SALVIA OFFICINALIS ESSENTIAL OIL HYBRID NANOBIOSYSTEM AGAINST FUNGAL COLONIZATION ON THE PROVOX ® VOICE SECTION PROSTHESIS,” *Dig. J. Nanomater. Biosctructures*, vol. 7, no. 3, pp. 1205–1212, 2012.
[53] R. Magetsari, P. Dewo, B. Saputro, and Z. Lanodiyu, “Cinnamon Oil and Chitosan Coating on Orthopaedic Implant Surface for Prevention of Staphylococcus Epidermidis Biofilm Formation,” *Malaysian Orthop. J.*, vol. 8, no. 3, pp. 11–14, 2014.
[54] K. Boumhara, M. Tabyaoui, C. Jama, and F. Bentiss, “Journal of Industrial and Engineering Chemistry Artemisia Mesatlantica essential oil as green inhibitor for carbon steel corrosion in 1 M HCl solution : Electrochemical and XPS investigations,” *J. Ind. Eng. Chem.*, vol. 29, pp. 146–155, 2015.
[55] M. Znini *et al.*, “Chemical Composition and Inhibitory Effect of Mentha Spicata Essential Oil on the Corrosion of Steel in Molar Hydrochloric Acid,” *Int. J. Electrochem. Sci.*, vol. 6, pp. 691–704, 2011.
[56] L. Kinani, R. Najih, and A. Chtaini, “Corrosion Inhibition of Titanium in Artificial Saliva Containing Fluoride,” *Leonardo J. Sci.*, vol. July-Decem, no. 11, pp. 33–40, 2007.
[57] S. Benavides, R. Villalobos-Carvajal, and J. E. Reyes, “Physical,

mechanical and antibacterial properties of alginate film: Effect of the crosslinking degree and oregano essential oil concentration," *J. Food Eng.*, vol. 110, no. 2, pp. 232–239, 2012.
[58] C. C. Liolios, O. Gortzi, S. Lalas, J. Tsaknis, and I. Chinou, "Liposomal incorporation of carvacrol and thymol isolated from the essential oil of Origanum dictamnus L. and in vitro antimicrobial activity," *Food Chem.*, vol. 112, no. 1, pp. 77–83, 2009.
[59] C. Sinico *et al.*, "Liposomal incorporation of Artemisia arborescens L. essential oil and in vitro antiviral activity," *Eur. J. Pharm. Biopharm.*, vol. 59, no. 1, pp. 161–168, 2005.
[60] O. Vega, J. J. Araya, M. Chavarría, and E. Castellón, "Antibacterial biocomposite materials based on essential oils embedded in sol–gel hybrid silica matrices," *J. Sol-Gel Sci. Technol.*, vol. 79, no. 3, pp. 584–595, 2016.
[61] R. Mossotti *et al.*, "Cotton fabric functionalisation with menthol/PCL micro- and nano-capsules for comfort improvement," *J. Microencapsul.*, vol. 32, no. 7, pp. 650–660, 2015.
[62] A. M. Grumezescu *et al.*, "Hybrid Nanomaterial for Stabilizing the Antibio fi lm Activity of Eugenia carryophyllata Essential Oil," *IEEE Trans. Nanobioscience*, vol. 11, no. 4, pp. 360–365, 2012.
[63] I. Anghel, A. M. Holban, E. Andronescu, A. M. Grumezescu, and M. C. Chifiriuc, "Efficient surface functionalization of wound dressings by a phytoactive nanocoating refractory to Candida albicans biofilm development," *Biointerphases*, vol. 8, no. 12, pp. 1–8, 2013.
[64] I. Anghel and A. M. Grumezescu, "Hybrid nanostructured coating for increased resistance of prosthetic devices to staphylococcal colonization," *Nanoscale Res. Lett.*, vol. 8, no. 6, pp. 2–7, 2013.
[65] M. L. Kung *et al.*, "Bifunctional peppermint oil nanoparticles for antibacterial activity and fluorescence imaging," *ACS Sustain. Chem. Eng.*, vol. 2, no. 7, pp. 1769–1775, 2014.
[66] A. Wattanasatcha, S. Rengpipat, and S. Wanichwecharungruang, "Thymol nanospheres as an effective anti-bacterial agent," *Int. J. Pharm.*, vol. 434, no. 1–2, pp. 360–365, 2012.
[67] S. Zhaveh *et al.*, "Encapsulation of Cuminum cyminum essential oils in chitosan-caffeic acid nanogel with enhanced antimicrobial activity against Aspergillus flavus," *Ind. Crops Prod.*, vol. 69, pp. 251–256, 2015.
[68] N. Parris, P. H. Cooke, and K. B. Hicks, "Encapsulation of essential oils in zein nanosperical particles," *J. Agric. Food Chem.*, vol. 53, no. July 2005, pp. 4788–4792, 2005.
[69] H. Pakzad, I. Alemzadeh, and A. Kazemi, "Encapsulation of peppermint oil with arabic gum-gelatin by complex coacervation method," *Int. J. Eng. Trans. B Appl.*, vol. 26, no. 8, pp. 807–814, 2013.
[70] N. Mishra *et al.*, "Encapsulation of Mentha Oil in Chitosan Polymer Matrix Alleviates Skin Irritation," *AAPS PharmSciTech*, vol. 17, no. 2, pp. 482–492, 2016.

[71] "S.Spriano et al., European Patent 2214732."
[72] S. Ferraris *et al.*, "Surface modification of Ti-6Al-4V alloy for biomineralization and specific biological response: Part I, inorganic modification," *J. Mater. Sci. Mater. Med.*, vol. 22, no. 3, pp. 533–545, 2011.
[73] N. Mandras *et al.*, "Liquid and vapour-phase antifungal activities of essential oils against Candida albicans and non-albicans Candida," *BMC Complement. Altern. Med.*, vol. 16, no. 1, pp. 1–7, 2016.
[74] V. Tullio *et al.*, "Antifungal activity of essential oils against filamentous fungi determined by broth microdilution and vapour contact methods," *J. Appl. Microbiol.*, vol. 102, no. 6, pp. 1544–1550, 2007.
[75] T. Luxbacher, *The zeta potential for solid surface analysis*. 2014.
[76] "ASTM D3359-Standard Test Methods for Rating Adhesion by Tape Test," *Annu. B. ASTM Stand.*, pp. 1–7, 2009.
[77] F. A. Al-Bayati, "Isolation and identification of antimicrobial compound from Mentha longifolia L. leaves grown wild in Iraq," *Ann. Clin. Microbiol. Antimicrob.*, vol. 8, no. 1, pp. 8–20, 2009.
[78] A. Rahman *et al.*, "In vitro antibacterial properties of essential oil and organic extracts of Premna integrifolia Linn," *Arab. J. Chem.*, vol. 9, pp. S475–S479, 2016.
[79] "https://www.sciencedirect.com/science/article/pii/S008367290572015X (28/11/2017, 05:06 pm)."
[80] "http://www.pharmacopeia.cn/v29240/usp29nf24s0_m32430.html (28/11/2017, 05:09 pm)."
[81] "https://greenflowerbotanicals.com/terpene-profile-linalool/(28/11/2017, 05:02 pm)."
[82] "https://en.wikipedia.org/wiki/Thymol (28/11/2017, 05:05 pm)."
[83] "https://comptox.epa.gov/dashboard/dsstoxdb/results?search=Spathulenol%2C+%28-%29- (28/11/2017, 05:00 pm)."
[84] J. Legault and A. Pichette, "Potentiating effect of β-caryophyllene on anticancer activity of α-humulene, isocaryophyllene and paclitaxel," *J. Pharm. Pharmacol.*, vol. 59, no. 12, pp. 1643–1647, 2007.
[85] "https://en.wikipedia.org/wiki/Caryophyllene (28/11/2017, 05:15 pm)."
[86] "https://commons.wikimedia.org/wiki/File:Menthone_isomenthone_ChemSpider.png (28/11/2017, 05:11 pm)."
[87] "https://de.wikipedia.org/wiki/Menthol (19/11/2017, 02:45 pm)."
[88] "https://www.sigmaaldrich.com/catalog/product/sial/63661?lang=it&region=IT (28/11/2017, 05:22 pm)."
[89] "https://chem.nlm.nih.gov/chemidplus/rn/464-15-3 (28/22/2017, 05:20 pm)."
[90] "https://www.sigmaaldrich.com/catalog/product/sigma/c9653?lang=it&region=IT (28/11/2017, 05:18 pm)."

[91]"https://www.sigmaaldrich.com/catalog/product/aldrich/376388?lang=it&region=IT (28/11/2017, 05:17 pm)."
[92] R. Kattel, B. Devkota, and K. C. Laxman, "Fourier Transform Infrared Spectroscopy Analysis of Oil of Menthaarvensis Grown At Sites Varying With Vehicular Traffic Loads in Lucknow City, India," *Int. J. Environ.*, vol. 4, no. 3, pp. 130–139, 2015.
[93] S. K. Kasi Marimuthu, Kathiresan Sathasivam, "Phytochemical analysis and antimicrobial potential of methanolic leaf extract of peppermint (Mentha piperita: Lamiaceae)," *J. Med. Plants Res.*, vol. 6, no. 2, pp. 331–335, 2012.
[94] M. Morra *et al.*, "Surface Chemistry Effects of Topographic Modification of Titanium Dental Implant Surfaces :1. Surface Analysis," *Int. J. Oral Maxillofac. Implant. 41*, vol. 18, no. 1, pp. 40–45, 2003.
[95] M. Textor, C. Sittig, V. Frauchiger, and S. Tosatti, *Properties and Biological Significance of Natural Oxide Films on Titanium and Its Alloys*. 2001.
[96] "http://www.xpssimplified.com/elements/carbon.php (15/11/2017, 10:46 am)."
[97] X. Zhang, S. Ferraris, E. Prenesti, and E. Verné, "Surface functionalization of bioactive glasses with natural molecules of biological significance, part I: Gallic acid as model molecule," *Appl. Surf. Sci.*, vol. 287, pp. 329–340, 2013.
[98] C. J. Weststrate, W. Ludwig, J. W. Bakker, A. C. Gluhoi, and B. E. Nieuwenhuys, "Ethanol adsorption, decomposition and oxidation on Ir(111): A high resolution XPS study," *ChemPhysChem*, vol. 8, no. 6, pp. 932–937, 2007.
[99] "http://xpssimplified.com/elements/oxygen.php (07/12/ 2017, 10:25 am)."
[100] L.-T. W. Xiong Lu, Yingbo Wang, Xiudong Yang, Qiyi Zhang, Zhanfeng Zhao and Y. Leng, "Spectroscopic analysis of titanium surface functional groups under various surface modification and their behaviors in vitro and in vivo," *J. Biomed. Mater. Res. Part A*, vol. 84A, no. 2, pp. 523–534, 2008.
[101] "https://www.google.com/patents/US6720302(19/11/2017, 02:50)."
[102] "http://www.ganfyd.org/index.php?title=Menthyl_acetate (19/11/2017, 03:01 pm)."
[103] "http://www.chemspider.com/Chemical-Structure.85151.html?rid=33ea536e-855a-4387-95a3-82612b5abd1e /19/11/2017, 03:05 pm)."
[104]"https://www.sigmaaldrich.com/catalog/product/sigma/c9653?lang=it&region=IT (19/11/2017, 03:10 pm)."
[105] "http://www.chemspider.com/Chemical-Structure.84031.html (19/11/2017, 03:16 pm)."
[106] S. C. Khojasteh-bakht, W. Chen, L. L. Koenigs, R. M. Peter, and S. D. Nelson, "METABOLISM OF (R) - (⁷ⁿ) -PULEGONE AND (R) - (⁷ⁿ) -

MENTHOFURAN BY HUMAN LIVER CYTOCHROME P-450s : EVIDENCE FOR FORMATION OF A FURAN EPOXIDE ABSTRACT :," *Drug Metab. Dispos.*, vol. 27, no. 5, pp. 574–580, 1999.
[107] "http://www2.lbl.gov/mmartin/bl1.4/IRbands.html (16/11/2017, 01:12 pm)."
[108] T. A. Sandosh, M. P. J. Peter, and J. Y. Raj, "Phytochemical Analysis of Stylosanthes fruticosa using UV-VIS , FTIR and GC-MS," *Res. J. Chem. Sci.*, vol. 3, no. 11, pp. 14–23, 2013.
[109] T. R. Renato Cozzi, Pierpaolo Protti, "Bande di assorbimento ir," in *Elementi di analisi chimica strutturare*, 2000, pp. 2–35.
[110] S. Rtimi, J. Nesic, C. Pulgarin, R. Sanjines, M. Bensimon, and J. Kiwi, "Effect of surface pretreatment of TiO2 films on interfacial processes leading to bacterial inactivation in the dark and under light irradiation," *Interface Focus*, vol. 5, no. 1, pp. 20140046–20140046, 2014.
[111] H. J. Song, S. H. Park, S. H. Jeong, and Y. J. Park, "Surface characteristics and bioactivity of oxide films formed by anodic spark oxidation on titanium in different electrolytes," *J. Mater. Process. Technol.*, vol. 209, no. 2, pp. 864–870, 2009.
[112] Y. P. Neo, S. Swift, S. Ray, M. Gizdavic-Nikolaidis, J. Jin, and C. O. Perera, "Evaluation of gallic acid loaded zein sub-micron electrospun fibre mats as novel active packaging materials," *Food Chem.*, vol. 141, no. 3, pp. 3192–3200, 2013.
[113] S. Roessler, R. Zimmermann, D. Scharnweber, C. Werner, and H. Worch, "Characterization of oxide layers on Ti6Al4V and titanium by streaming potential and streaming current measurements," *Colloids Surfaces B Biointerfaces*, vol. 26, no. 4, pp. 387–395, 2002.

Chapter 4

Silver nanoparticles

4.1 Introduction

One of the biggest problems of prosthetic implants, as explained in chapter 1, is the bacterial contamination and infection. The bacteria can reach the implants during the surgery or subsequently and they cause prosthetic infections. The infections are usually treated with systemic administration of antibiotics and/or local use during the surgery, but this kind of treatment is not able to act against biofilm if it is just formed and can induce resistance of the bacterial strains[1]–[5]. The infection chronicization can lead to the removal and replacement of the prosthesis with stress and pain for the patients and increasing hospitalization time and cost.

Regarding titanium alloys implant surfaces, several attempts were performed over time in order to make the surface suitable for osteointegration, but also with antibacterial activity avoiding infection and biofilm formation[6]–[8]. The functionalization of the surface of the implants with metallic nanoparticles such as silver, copper or zinc nanoparticles have been studied and seem to be a promising way in order to reduce bacterial contamination avoiding the formation of resistant bacterial strain. Many works are reported in literature about silver nanoparticles, but several aspects like dimension, shape, surface chemistry and release from the surface are still open issues[9]–[11].

In this chapter, different protocols of in situ reduction of silver nanoparticles during the growth of the oxide layer of a chemically treated titanium alloy were

developed. In order to obtain a higher amount of nanoparticles the reducing activity of polyphenols was exploited using gallic acid as additive. Another additive, poly vinyl alcohol, was used in combination with gallic acid in order to stabilize the nanoparticles. After functionalization, the samples were characterized by means of Field Emission Scanning Electron Microscopy (FESEM) and Transmission Electron microscopy (TEM) observations investigating shape, size and distribution into the titanium oxide layer of the nanoparticles. Silver release tests were performed in order to control the amount of silver ions released over time. Bacterial and cell cultures were performed in order to check and tailor the antibacterial effects of silver nanoparticles avoiding cytotoxic effects. This chapter includes bibliographic data about the antibacterial effects of silver and the state of the art of silver nanoparticles, the explanation of the method of the in situ reduction of the nanoparticles and the discussion of the result obtained, aimed at tailoring the silver release from the surface of titanium alloy implants engineered for osteointegration.

4.2 Antibacterial activity of silver nanoparticles

Antibacterial properties of silver have already been treated in ancient texts. Already Herodotus described that the King of Persia was used to boil water for his supplies in silver flasks. Raulin in 1869 reported that Aspergillus Nigrum is not able to grow in silver jar. In 1893 the botanic von Nägeli defined silver as "oligodynamic" meaning a substance active in a very small quantity against bacteria. In 1910 Henry Crookes reported that some colloidal metals are highly germicidal and in 1919 Halfred B. Seartle wrote "The use of colloids in Health and diseases". In 1970 Doctor Robert O. Becker studied the silver effects on electrochemical body processes and he could be considered as the pioneer of the modern studies on medical application of silver[12], [13]. Today the nanotechnological use of silver is not only studied for biomedical applications, but also commonly used in products such as water filters, antibacterial sprays, detergents, cell phone cases, clothing, keyboards and many other objects of common use[11].

The antibacterial effects of silver nanoparticles were attributed by Marambio-Jones and Hoek[11] to three possible mechanisms of actions:

- Release of silver ions with actions against ATP production and DNA replication
- Generation of ROS by silver nanoparticles and silver ions

- Direct damage of bacteria membrane by silver nanoparticles attachment

The same mechanisms were sustained by Prabhu and Polouse [14] highlighting the central role of the silver ions release against bacteria.
The release of silver ions from the silver nanoparticles core Ag^0 involves the role of the nanoparticles as reservoir for the release of ions by means of oxidative dissolution. The following reaction has been proposed for the oxidative dissolution of the nanoparticles:

$$2Ag + H_2O_2 + 2H^+ \rightarrow 2\ Ag^+ + 2\ H_2O$$

This reaction can occur in mitochondria where high concentration of H^+ are present and at the membrane where there is proton motion force.
Another possible reaction that leads to the formation of silver ions starting from silver nanoparticles was proposed in presence of oxygen and is reported below:

$$4Ag + O_2 + 2H_2O \rightarrow 4Ag^+ + 4\ OH^-$$ [11]

Ag^+ is affine to many biological compounds such as amines, thiols, phosphates and selenols forming quasi-covalent bonds. It could also acts as bridging agent between thiols forming irreversible aggregates. For these reasons the silver ions are able to damage biological systems such as bacteria inactivating several moieties. The principal targets that bring bacteria to die are DNA and peptides of membrane or cytoplasm, however the silver ions are not selective and bind every molecule which they are affine to, for this reason it is difficult to identify a specific pathway for their actions. Nerveless, just this lack of selectivity could explain the broad spectrum activity of silver as well as its limited resistance development.
Another investigated way of actions is the generation of ROS[15]. Because of their affinity with thiol and selenols Ag^+ ions can interfere with the regulation system of ROS interacting with reductase enzymes or scavenging glutathione increasing their intracellular ROS concentration[16]. A schematic representation of the effects of silver and silver nanoparticles is reported in Figure 4.1.

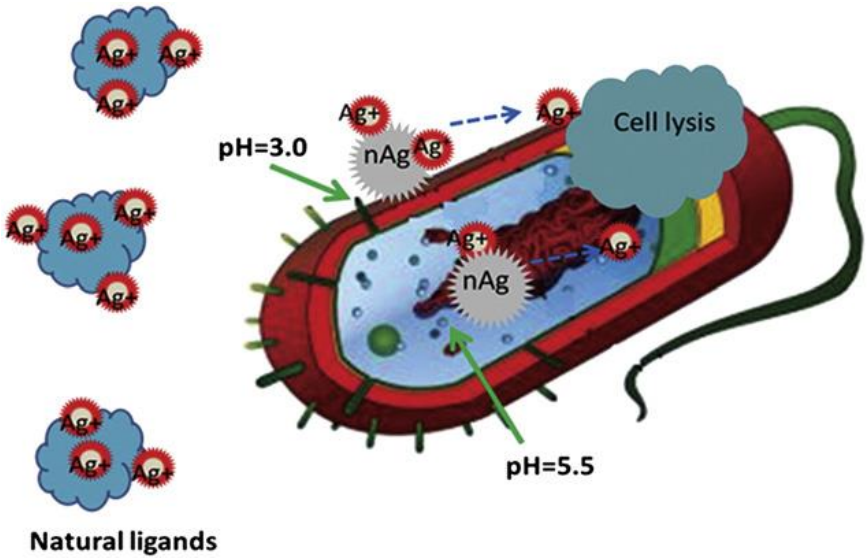

Figure 4.1: scheme of interaction between bacteria and Ag^+ and silver nanoparticles[17].

The core nanoparticles Ag^0 can face the bacteria membrane, compromising their integrity and leading to bacteria death[16].
The effect of the nanoparticles depends of their size, shape and surface chemistry and these aspects will be discussed in a further paragraph.
The antibacterial effects of silver and silver nanoparticles were proved against several Gram-positive and Gram-negative. Because of its multiple ways of actions silver is active against both these type of bacterial. In Table 4.1 are reported the mode of actions of silver nanoparticles against some Gram-positive and gram negative bacteria.

Table 4.1: mode of actions of silver nanoparticles against some Gram- positive and Gram- negative bacteria[18].

Bacterial Strain	**AgNPs size (nm)**	**Mode of action**
Gram-positive		
Bacillus subtilis	5 10	Cell membrane damage; leakage of reducing sugars Degradation of chromosomal DNA; increase in ROS levels
Clostridium diphtheria	23.42	Rupture of the cell wall; denaturation of proteins
Listeria monocytogenes	- 23 ±2	Penetration inside the bacteria DysfunctionofelectrontransportchainincreaseinROSlevelsatcellmembrane
Staphylococcus aureus	- 5 25	Adhesion to cell wall; cell membrane detachment from cell wall; DNA condensation; inhibition of replication; inactivation of proteins Cell membrane damage; leakage of reducing sugars Interaction with cell membrane; interaction with S- and P-containing compounds; inhibition of respiration
Gram-negative		
Escherichia coli	5±2 - 10 5 1-10 25 16 - 9.3	Interaction with cell membrane; interaction with S- and P-containing compounds Adhesion to cell wall; cell membrane detachment from cell wall; DNA condensation; Inhibition of replication; inactivation of proteins Interaction with S- and P-containing compounds Cell membrane damage; leakage of reducing sugars Interaction with cell membrane; increase in membrane permeability; improper transport activity; leakage of cellular components Interaction with S- and P-containing compounds Interaction with cell membrane; interaction with S- and P-containing compounds Destabilization of ribosomes; inhibition of protein synthesis; inhibition of expression of enzymes required for ATP generation Interaction with cell membrane
Klebsiella pneumonia	<50	Interaction with DNA; inhibition of cell division
Pseudomonas aeruginosa	5±2 10 28	Interaction with cell membrane; interaction with S- and P-containing compounds Penetration inside the cell Attenuation of quorum sensing
Salmonella typii	5±2 2-23	Interaction with cell membrane; interaction with S- and P-containing compounds Cell wall lysis
Vibrio cholera	5±2 90-100	Interaction with cell membrane; interaction with S- and P-containing compounds Inhibition of metabolic pathways

The Minimum Inhibitory Concentrations (MIC) of silver ions and silver nanoparticles has been studied and reported in literature.

For silver nanoparticles with diameter between 3 and 95 nm, it was reported a MIC between 3-180 μg/ml on several bacterial strains including *Escherichia coli*, *Staphylococcus aureus* and *Staphylococcus epidermis*[10], [19]–[21].

The MIC reported for silver nitrate $AgNO_3$ was between 75-300 μg/ml for Gram-positive bacteria such as *Escherichia coli*[22], *Serratia liquefaciens* and *Serratia proteamaculans*, and in the range of 150-300 μg/ml for *Pseudomonas aeuruginosa* and *Preudomonas chlororaphis* [23].
However, it must always be kept in mind that, because of the high affinity of silver ions to react with other ions or biomolecules, the effects of silver and silver ions can change with the medium in which the tests are performed.

4.3 Synthesis of silver nanoparticles

A large variety of approaches have been studied for the synthesis of silver nanoparticles. The ways of nanoparticles preparation can be classified in: physical methods, chemical methods and green approach.
The principal physical approaches are the evaporation-condensation synthesis and laser ablation. The evaporation condensation process involves the use of a tubular furnace at a temperature around 500°C and at atmospheric pressure[24]. The source material is placed at the center of the furnace and a carrier gas is vaporized. This technique allows to obtain nanoparticles of several metals, but the furnace occupies large space, requires high energy and a lot of time to achieve the needed temperature[25]. However it is also possible to synthetize silver nanoparticles through a small ceramic heater with a located heating area obtaining small nanoparticles in high concentration[26].
Silver nanoparticles can be produced by laser ablation of silver bulk located in a solution and the characteristics of the metal nanoparticles obtained depends on parameters such as laser wavelength, laser pulse time, ablation time, laser fluency and on the type of the liquid which can contain surfactants[25].
The chemical approaches are many and various. The most used of these approaches is the chemical reduction with the use of organic or inorganic agents.
Many reducing agents such as ascorbate, sodium citrate, elemental hydrogen sodium, borohydride (NaBH), polyol process, N, N-dimethylformamide (DMF), Tollens reagent, and poly (ethylene glycol)-block copolymers are used for the reduction of nanoparticles. The reducing agents allow the reduction of Ag^+ ions to metallic silver nanoparticles. The use of protective agents is fundamental to stabilize the nanoparticles during the preparation and protect them by avoiding agglomeration. The principal protective and stabilizing agent used are poly vinyl alcohol), poly (vinylpyrrolidone), poly (ethylene glycol), poly (methacrylic acid), and polymethylmethacrylate.

Microemulsion technique allows to obtain uniform and well dispersed nanoparticles. This synthesis consists in the preparation of a two-phased aqueous organic systems based on the initial separation of metal precursor and reducing agent in two separated phases. Metal particles are formed at the interface, but one of the principal disadvantages of these techniques is the use of toxic solvents.
The UV- initiated photoreduction is a simple process of nanoparticles reduction in presence of citrate, poly (vinylpyrrolidone), poly (acrylic acid), and collagen.
Silver nanoparticles were also synthetized by UV irradiation using poly vinyl alcohol as protecting and stabilizing agent and using silver nitrate as precursor.
Other photoinduced or photocatalytic methods can be also used as clean process for the production of silver nanoparticles allowing their reduction on several media or surfaces such as surfactant micelles, emulsion, cells, polymer films and glasses. The direct photoreduction of $AgNO_3$ was performed with different sources of light (UV, white, blue, cyan, green and orange) using sodium citrate and carboxymethylated chitosan as reducing and stabilizing agents.
Irradiation methods can be suitable for nanoparticles synthesis. For example laser or mercury lamp can be used as light sources for nanoparticles sensitization.
Microwaves can be applied in order to heat the reaction system and to reduce the reaction time, to reduce the energy consumption, to improve the product yields and to avoid the agglomeration of the nanoparticles.
Some of the most used chemical, photochemical and physic methods for the synthesis of silver nanoparticles are resumed in Table 4.2[27].

Table 4.2:some important chemical, photochemical and physic methods for the synthesis of silver nanoparticles[27].

Method	Silver precursor	Reducing agent	Stabilizing agent	Size (nm)
Chemical reduction	$AgNO_3$	DMF	-	< 25
Chemical reduction	$AgNO_3$	$NaHB_4$	Surfactin	3- 28
Chemical reduction	$AgNO_3$	Trisodium citrate (initial)- SFS (secondary)	Trisodium citrate	< 50
Chemical reduction	$AgNO_3$	Trisodium citrate	Trisodium citrate	30- 60
Chemical reduction	$AgNO_3$	Ascorbic acid	-	200- 650
Chemical reduction	$AgNO_3$	$NaHB_4$	DDA	≈7
Chemical reduction	$AgNO_3$	Paraffin	Oleylamine	10- 14
Chemical reduction (thermal)	$AgNO_3$	Dextrose	PVP	22± 4.7
Chemical reduction (thermal)	$AgNO_3$	Hydrazine	-	2- 10
Chemical reduction	$AgNO_3$	Glucose	Gluconic acid	40- 80

(oxidation of glucose)				
Chemical reduction (polyol process)	$AgNO_3$	Ethylene glycol	PVP	5- 25
Chemical reduction (polyol process)	$AgNO_3$	Ethylene glycol	PVP	50- 115
Electrochemical (polyol process)	$AgNO_3$	Electrolysis cathode: Ti, anode : Pt	PVP	≈11
Chemical reduction (Tollen)	$AgNO_3$	m-hydroxy benzaldeyde	SDS	15- 260
Physical synthesis	Ag wires	Electrical arch discharge, water	-	≈ 10
Physical synthesis	$AgNO_3$	Electrical arch discharge	Sodium citrate	14- 27
Chemical reduction (Microemulsion)	$AgNO_3$	Hydrazine hydrate	AOT	2- 5
Chemical reduction (Microemulsion)	$AgNO_3$	Hydrazine hydrate	AOT	< 1.6
Photochemical reduction (pulse radiolysis)	$AgClO_4$	Ethylene glycol	-	17-70
Photochemical reduction (microwave radiation)	$AgNO_3$	Ethylene glycol	PVP	5-10
Photochemical reduction (photoreduction)	$AgNO_3$	UV light	-	4- 10
Photochemical reduction (x-ray radiolysis)	Ag_2SO_4	X- ray	-	≈ 28
Photochemical reduction (x-ray radiolysis)	$AgNO_3$	CMCTS, UV	CMCTS	2- 8

Silver nanoparticles can also be produced by water solutions of a silver precursor and polymers and polysaccharides as stabilizing/reducing agents. The most used in literature are starch, glucose and heparin[11]. This is a Green approach because does not involves the use of a toxic solvent and the most used reducing and stabilizing agents are reported in Table 4.3.

Table 4.3: principal green reducing and stabilizing agents.

Reducing agents	
Formula/acronyms	**Compound**
$Na_3C_6H_5O_7$	Sodium citrate
$C_6H_{12}O_6$	Glucose/ fructose
$(C_6H_{10}O_5)_n$	Starch
$C_6H_8O_6$	Ascorbic acid
$C_7H_6O_5$	Gallic acid
Stabilizing agents	
Formula/acronyms	**Compound**
PVA	Poly vinyl alcohol
$(C_6H_{10}O_5)_n$	Starch

A new frontier of the green approach involves the use of natural plant extracts as reducing agents (Figure 4.2).

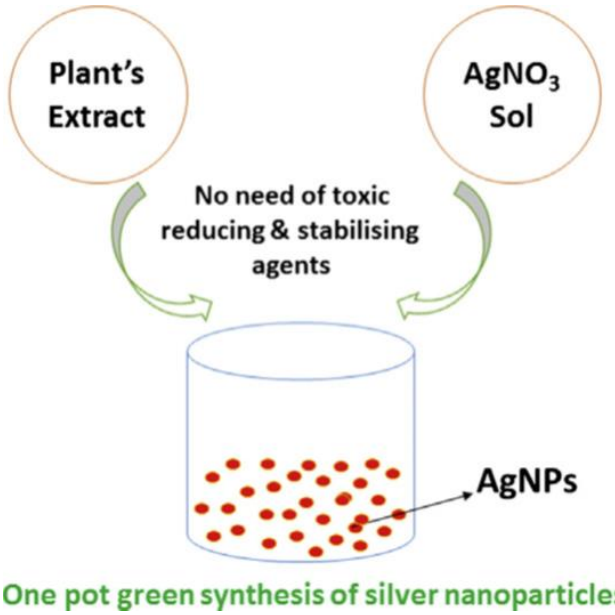

Figure 4.2: scheme of silver nanoparticles synthesis with plant's extract[28].

$AgNO_3$ reacts with plant's extract forming nanoparticles with the following reaction:

$Ag^+NO_3^-$ + plant's extract → Ag^0 NPs + other products [29]

The polyphenolic natural extracts used in chapter 2 and the essential oils of chapter 3 are suitable reducing agents for silver nanoparticles production.

4.4 Factors involved in silver nanoparticles activity

The antibacterial activity of silver nanoparticles depends on several parameters such as size, shape, surface chemistry and surface charge.

Size-dependent effects of silver nanoparticles have been treated in many articles that come to the same conclusion. For being effective against bacteria, the size of nanoparticles in a suspension should be under 50 nm and more in specific nanoparticles under 10-15 nm have increased stability and activity. This results could explained with the increase of the exposed surface areas that allows the nanoparticles to release more silver ions[9], [11], [30], [18]. The effect of the surface area acts also in the ROS generation, as reported by Carlson and al. [31], at the same concentration silver nanoparticles of 15 nm showed higher level of ROS in macrophages than silver nanoparticles of 50 nm.

However, Ivask et al. [32] tested the properties of different size of nanoparticles in the range of 1-100 nm against several bacteria, algae , yeast, mammalian cells and crustaceans normalizing the EC_{50} (Half maximal effective concentration, it refers to the concentration of Ag ions which induces a response halfway between the baseline and maximum) values of Ag ions that dissolved from the NPs (Dissolved Ag^{+} determined from the supernatant of nanoparticles suspension) to quantify the role of the released Ag ions in the toxicity or antibacterial effect of nanoparticles and the results are reported in Figure 4.3.

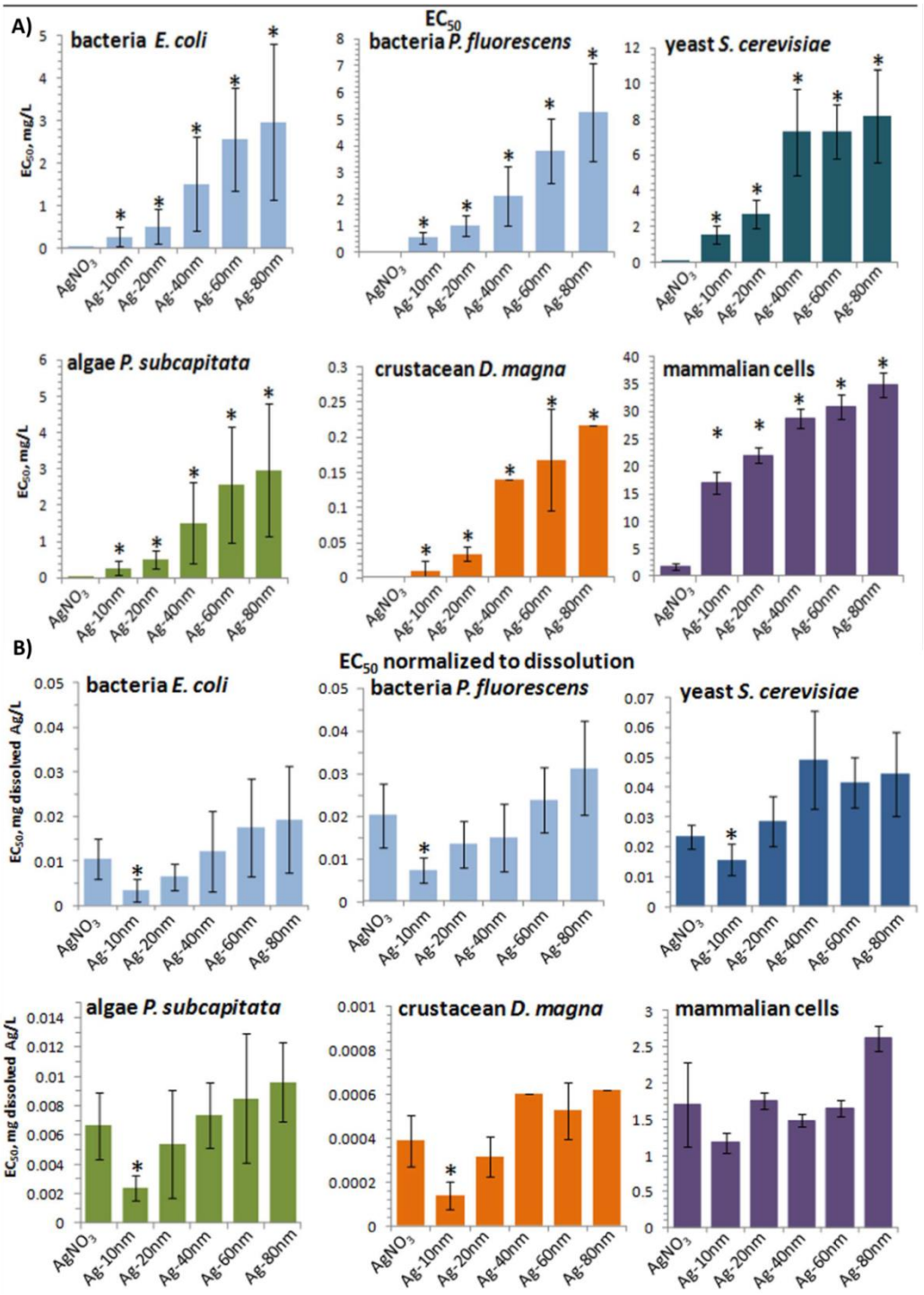

Figure 4.3: A) EC_{50} nominal values (mg/ml). * - significantly ($p<0.05$) different from EC_{50} value of $AgNO_3$, B) EC_{50} normalized to dissolution values of 10–80 nm Ag NPs and $AgNO_3$. EC_{50} was normalized for dissolved Ag .* - significantly ($p<0.05$) different from EC_{50} of $AgNO_3$[32].

The effect of silver is lower in mammalian cells and stronger against algae and crustacean and it has to be highlighted that the silver ion concentration active against bacteria is one magnitude lower than the one active against cells, confirming its oligodynamic behavior.
The toxicity of nanoparticles in the range between 20 and 80 nm can be explained as said before with the increase of the ion release due to the increase in the surface area, but for the nanoparticles of 10 nm the toxicity results higher than expected by the ion release. *Escherichia coli* was used to clarify the activity of these nanoparticles showing that a high bioavailability of nanoparticles with diameter equal or lower of 10 nm which are able to interact with bacteria not only dissolving in the proximity or on the surface, but also to entry inside the cells. Another aspect, influencing the effect of nanoparticles, is their shape that again influence their reactivity and the release of silver ions[33], [34]. Silver nanoparticles can be produced in many shapes as visible in Figure 4.4.

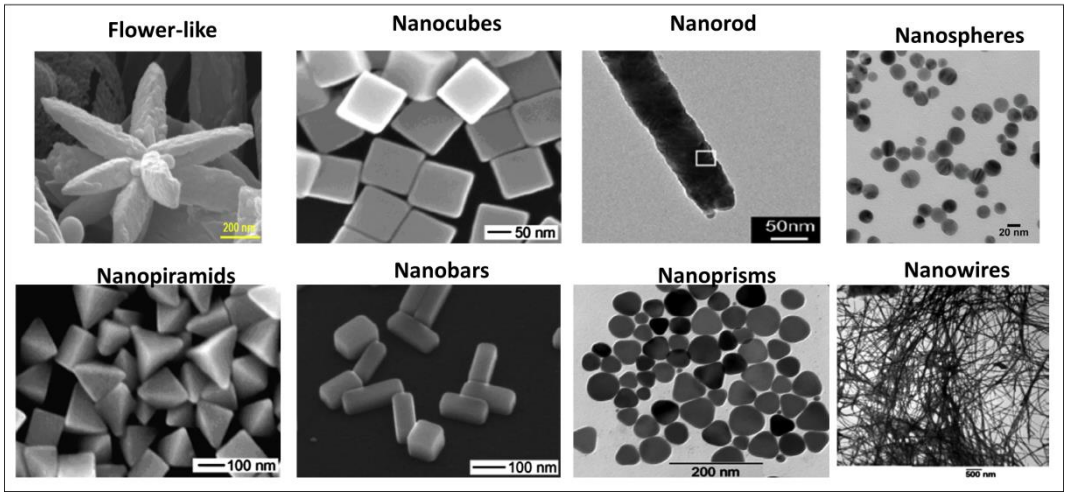

Figure 4.4: different shape of the silver nanoparticles [35], [36].

Pyramidal nanoparticles seem to be the most effective against bacteria and it could be explained with the higher percent of active facets in this kind of nanoparticles. This nanoparticles have {111} planes exposed while spherical nanoparticles, usually with a cubooctahedral or multiple-twinned decahedral or quasi-spherical morphology have mainly {100} facets with a small percentage of {111} facets. Rod- like structures have {100} facets on the side surfaces and {111} at the ends. The activity of the nanoparticles is enhanced by the presence of high-atom-density facets such as {111}, for this reason the pyramid-shape nanoparticles are more effective[37].

The surface chemistry and consequently the surface charge are critical factors for silver nanoparticles activity because the physical interaction of the nanoparticles with the surrounding environment and with the bacteria are strictly dependent by the surface charge[38]. Abbaszadegan et al. tested the antibacterial effects of three different kinds of silver nanoparticles, one negatively-charged, one neutral, and one positively-charged. The positively-charged nanoparticles showed the greatest effects against the higher number of microorganisms, the neutral nanoparticles has an intermediate effect and the negatively -charged have the lower effects. However, despite of their lower effect if compared with positively-charged and neutral nanoparticles, negatively-charged nanoparticles have anyway a strong effects[39].

The surface charges depend on the coating and on the way of synthetization.

Three types of spherical silver nanoparticles with different surface chemistry and charge were tested against *Escherichia coli*. One type was synthetized using citrate as stabilizing and coating material and have a negative z-potential, the second one using poly(vinylpyrrolidone (z potential= -10.7 mV) and the third with branched Polyethyleneimine (z potential= + 33.3 mV). This study shows again that the main effects for the negatively-charged nanoparticles is correlated with the amount of dissolved Ag^+ from the nanoparticles, while the positively-charged nanoparticles have the ability to interact directly with bacteria surface allowing a greater bioavailability of silver ions and are also able to interfere with the bacterial electron transport chain responsible for the ROS generation in the cell membrane[40].

It should also be kept in mind that the effects of the silver nanoparticles do not depend only on their physical and chemical characteristics but also on:

- The amount of oxidizer in the test conditions
- The composition of the medium with the presence of possible ligands
- The bacterial strain and the presence of biofilm
- The eventual recirculation of the medium
- Temperature
- pH
- Presence of light that can cause photoreduction of Ag^+ [16].

4.5 Silver release from nanoparticles

The release of silver from nanoparticles is a crucial aspect for their action.
The release of silver ions from the bulk of silver nanoparticles is due to oxidation reaction in aerobe environment and in proceeds with the following stoichiometric equations:

$2Ag_{(s)} + 1/2O_{2(aq)} + 2H^{+}_{(aq)} \leftrightarrow 2Ag^{+}_{(aq)} + H_2O$

As explained in the previous paragraph the rate and amount of Ag^+ dissolution does not depend only on silver nanoparticles concentration, but other important aspects influence the ion release. Temperature increase can accelerate the reaction and variations of the pH can modify the ion release because the presence of H^+ is involved in the dissolution reaction [41]. Kittler et al. observed for silver nanoparticles of 50 nm coated with PVP after 200 hours of release fluctuation in the ion release of the 5% at 5°C, 50% at 25°C and 90% at the 37°C [42]. The silver ion release was studied in solutions with different pH varying from pH 4 to pH 9 and the Ag^+ release increase 6 time when the pH goes down from 8 to 4[43], [44].
Also the formation of aggregates reduces the silver ion release because of the reduction of the surface exposed and in order to avoid the formation of these aggregates the use of a stabilizing agent it is fundamental. The primary particle size and the shape of nanoparticles which confer to the nanoparticles different thermodynamic properties are also crucial aspects for silver release as explained in the previous paragraph [45], [46]. The presence of salts in the release solution has also influence on the silver release. Kent et al. tested the dissolution process of silver nanoparticles in a phosphate buffer obtained by dissolving 1mM NaH_2PO_4 and 1 mM Na_2HPO_4 in deionized water and by adding different aliquots of 5M NaCl in order to achieve different concentration of NaCl. The rate of silver dissolution accelerate with the increase of NaCl in the solution because Cl^- could accelerates silver redox reactions complexing and removing Ag^+ prom the bulk of the nanoparticles [47].
However, the presence of Cl^- accelerates the rate of dissolution, but binding the silver ions it reduces their antibacterial effects. Also the presence of inorganic sulfide and organosulfur compounds reduces the effects of the released silver ions[45].
In Table 4.4, the main aspects influencing silver nanoparticles release and their antibacterial activity are resumed.

Table 4.4: main features influencing silver nanoparticles activity.

Features	Effects
Shape	Pyramidal nanoparticles have faster dissolution and higher antibacterial activities
Dimension	Nanoparticles with d< 10 nm have a larger surface areas and great antibacterial activity
Surface chemistry	The use of coating and stabilizer avoids aggregation of the nanoparticles increasing their antibacterial activity
Surface charge	Positively charged nanoparticles have a greater antibacterial behavior
pH	Acid pH increases the release of ions from nanoparticles
Temperature	Increasing of temperature (37°C) increases the silver release from nanoparticles

4.6 Side effects of silver nanoparticles

Silver in small concentration is established as non-toxic in normal use and probably one on the most relevant side effects is Argyria, disease which consists in an irreversible gray coloration of the skin [33]. However, it must be kept in mind that nanometric silver has toxic effects against higher organism even if in higher concentration. Exposition to high concentration of silver nanoparticles can have negative effects on respiratory system, gastrointestinal tract, skin and nervous system. If inhaled, particles smaller than 2.5 μm can go down to the alveoli. Silver nanoparticles used in healthcare and hygiene spray are less than 100 nm. In the pro-oxidative environment of alveoli, silver nanoparticles which have catalytic activity can facilitate the production of ROS radicals. However alveoli and lungs has several system devoted to eliminate solid particles such as mucocilliary escalator transport, particle dissolution with transfer into the blood and translocation to the lymphatic system. Skin problem can be correlated with Argyria, as said before, which require to be developed a long time abduction of a high amount of colloidal silver, and irritation and sensitization. Despite for Argyria, the reported side effects for ingested silver nanoparticles are few. From

the gastro intestinal tract, the nanoparticles can translocate to liver that seems to be the major reservoir of nanoparticles in human body, but probably the presence of enzyme, digested food, electrolyte and microflora can change and reduce the activity and the toxicity of nanoparticles before the transition. Regarding the nervous system, the toxicity of silver is not assessed, but some case of seizure were supposed to be related to silver exposition[48]. Some studies were performed with oral administration or peritoneal or subcutaneous injection of silver nanoparticles in rats and mice, investigating the effects on the nervous systems and the results are reported in Table 4.5.

Table 4.5:Neurotoxicity of silver nanoparticles in mice and rats[49].

Animals (No. of animals/group)	Test materials	Exposure			Observation/Autopsy	Findings
		Routes	Days	Doses		
FemaleWistar rats (45)	AgNPs (AD: 20 nm, Sigma-Aldrich Prod, No. 730793) in 0.02 mg/ml Na citrate solution*	Oral gavage	From GD 9 until end of gestation	25 mg/kg/day	After weaning	↓ Offspring body and relative brain weights; GPX activity and GSH levels in brain. ↑Microvascular structure, levels of MDA and Caspase 9, and Ag content in brain (analysed by ICP-MS). No effect on maternal body weight gain or gestation length.
Female SD rats (10)	C-AgNPs (see Charehsaz et al. [17]; in Table 1)	Oral gavage	GDs 7–20 (sperm – GD 0)	0.2, 2, or 20 mg/kg/day	PND 2	↑ Hippocampal sclerosis in pups of all treated-groups. No effect on gestational parameters in any group.
FemaleWistar rats (10)	AgNPs (Colloidal product containing 4000 ppm NS, AS: 30 nm, Nano Nasb Pars, Iran) in water*	Drinking water	Throughout gestation	1 or 10 ppm	Day of birth	↑ Expression of Procaspase-3 at 1 and 10 ppm (More pronounced effect in females than males). No information on general condition of dams or offspring.
Female NMRI mice (10)	AgNPs (AD: 32 nm, 99.9% pure, Neutrino Corp, Iran) in 0.1 M Na citrate solution*	sc	Once every 3 days during mating and gestation	5 or 50 µg/mouse/day	PNDs 28	↓ Fur development and relative spleen weight at 50 µg. ↑ Hyperactivity at 50 µg. No effect on maternal body weight or offspring sex ratio.
Female NMRI mice (10)	AgNPs (same as Rashno et al. [50])	sc	Once every 3 days from GD 3 until delivery (VP – GD 0)	0.2 or 2 mg/kg/day	PNDs 45–60	↓ Traverse distance at 2 mg and time spent at 0.2 and 2 mg in target quadrant of MWM in female offspring. ↑ Leaning number in OF in females at 2 mg. No information on general condition of dams or offspring.
Female NMRI mice (10)	AgNPs (S: 10 nm, 99.9% pure, Neutrino Corp, Iran)	sc	Once every 3 days from GD 0 until delivery	0.2 or 2 mg/kg/day	PND 45	↓ Mobility time in FST in males at 0.2 and 2 mg and in TST in females at 2 mg. ↑ Immobility time in FST in males at 0.2 and 2 mg and in TST in females at 2 mg. No information on general condition of dams or offspring.
Female SD rats (6)	AgNPs and PVP-AgNPs (see Wu et al. [21]; in Table 1)	ip	Every 2 days on GDs 10–18 (Copulation – GD 0)	20 mg/rat/day	PND 35(male offspring)	(In AgNP group) ↑ Escape latency in MWM. ↓GAP-43 mRNA and protein in hippocampus (lower than PVP-AgNP group). Enlarged intercellular space and decreased number of Nissl's bodies in hippocampus.

Some effects on the nervous systems were observed with high administration dose of several mg/ml/day for each rat. Cytotoxic effects were observed also for culture of human NSCs in direct contact with 5µm/ml concentration of silver nanoparticles or more [50].

In vitro test against several mammalian cell lines have highlighted cell damages as resumed in Table 4.6.

Table 4.6: toxic effects of nanosilver on mammalian cells[11]

Target cell/organism	Key aspects
Rat lung cells	Reduction in lung function and inflammatory lesions
Sprague-Dawley rats	Silver nanoparticles accumulation in olfactory bulb and subsequent translocation to the brain
Mouse stem cells	Cell leakage and reduction of mitochondrial function
Rat liver cells	Cell leakage and reduction of mitochondrial function
Human fibrosarcoma and human skin/carcinoma	Oxidative stress. Low doses produced apoptosis and higher dose necrosis
Mouse fibroblast	50 μg/mL induced apoptosis to 43.4% of cells
Human colon cancer	100 μg/mL produced necrosis to 40.2% of cells
Human glioblastoma	Silver nanoparticles were found cytotoxic, genotoxic and antiproliferative
Human fibroblast	Silver nanoparticles were found cytotoxic, genotoxic and antiproliferative

Silver nanoparticles seems to be toxic against several cell lines and organism such as zebrafish and Drosophila melanogaster[11].
However, it must be always remembered that the toxic concentration for mammalian cells and higher organisms are higher than the one used for antibacterial applications as reported in Table 4.7.

Table 4.7: toxicity and antimicrobial activity of silver ions and silver nanoparticles[20].

	Antimicrobial effect (MICs; mg/L)		Cytotoxicity and ecotoxicity (LC100; mg/L)			
	bacteria	yeasts	Human fibroblasts	*Monoraphidium sp.*	*Drosophila melanogaster*	*Paramecium caudatum*
Silver NPs	1-3*	1	60	60	60	30
Ionic silver	1	1	2	3	-	0.4

As visible the MCI found for bacteria and yeast is between 1-3 mg/l while is around 60 mg/l for human fibroblasts and Drosophila melanogaster[20], [44].
Silver nanoparticles after the transition in lungs, gastrointestinal system or through skin, are able to reach blood and also the sexual apparatus[14].
Barkhordari et al. tested the toxic effects of silver nanoparticles against mononuclear blood cells culturing the cells with 10 nm silver nanoparticles in

concentrations from 1 to 500 μg/ml for 6 and 24 h. This study evidenced a dose and time-depended toxicity of nanosilver on mononuclear blood cell with maximum toxicity observed with 500 μg/ml concentration after 24 h of exposure[51]. A study of the effects of silver nanoparticles on human sperm was performed by Wang et al. exposing sperm to different concentration of silver nanoparticles for 15, 30 and 60 minutes. This study confirms again the time and dose dependent toxic effects of silver nanoparticles highlighting the increasing ration of abnormal to normal sperm after 30 and 60 minutes of exposure to 200 and 400 μg/ml of nanosilver[51].
The different studies highlighted the time and dose dependent effects of silver nanoparticles and their possible cytotoxicity, but the exposure dosages are generally higher than the one needed for antibacterial applications.

4.7 In situ reduction of silver nanoparticles on titanium substrates

Several studies have reported the reduction silver nanoparticles on titanium surfaces by means of UV irradiation of silver nitrate solutions [52]–[55].
Zhao et al. [55] have fabricated titanium oxide nanotubes by anodization and loaded them with silver nanoparticles by means of photoreduction of $AgNO_3$ solution. They obtained nanoparticles with diameter lower than 10 nm uniformly distributed on the surface of the nanotubes. Piwonski et al.[52] functionalized a thin film of titania by photoreduction of silver nanoparticles. The nanoparticles grow directly on the titania surface immersed in an aqueous solution of $AgNO_3$. The amount of nanoparticles depends on the concentration of the silver nitrate solution while the dimension depends on the time of irradiation[56].
For antibacterial purposes, silver nanoparticles were also deposited onto titanium surfaces using the silanization method which allows the deposition of a small amount of nanoparticles with diameter ranging from 10 to hundreds of nm [57].
Silver nanoparticles with diameter between 4 and 19 nm were in situ reduced on titanium by means of a plasma immersion ion implantation process[58].
Silver nanoparticles were also used in combination with titania nanoparticles.
A TiO_2/Ag bilayers were prepared via colloid self-assembly process. Titania nanoparticles formed an internal support while the silver nanoparticles formed an external layer[59] and TiO_2/Ag nanoparticles were also synthetized by means of sol-gel technique[60] for antibacterial purpose. Always with the scope of

reducing bacterial contamination, Harrasser et al.[61] developed a silver nanoparticles enriched carbon like coating with a modified technique of ion implantation for titanium alloy in order to reduce infections in revision joint arthroplasty evidencing the reduction of several important bacterial strains.
In order to avoid post-surgery infections, titanium alloy substrate was also functionalized by Wang et al.[62] by means of plasma ion implantation treatment. Silver nanoparticles are of great interest also because their photocatalytic disinfection power which was exploited by van Grieken and al. using TiO_2 on suspension[63].

4.8 Commercial products with silver nanoparticles

Several products exploiting the properties of silver nanoparticles are just on the market. Between this products we can mention children' toys, textiles and clothing, coating for surfaces, housecleaning products, dietary supplements, soaps, masks, toothbrushes, toothpastes, hairbrushes and many more [64]. However, only a few numbers of biomedical devices are commercialized and the main sector is that of the wound dressing. Examples of these devices are [33] :

- *Anticoat-7* : polyethylene mesh coated with nanocrystalline silver
- *Aquacel-Ag hydrofiber* : carboxymethylcellulose dressing impregnated with silver nanoparticles
- *Actisorb Silver 220*: nanocrystalline silver is bound to charcoal dressing
- *Silverlon*: polymeric textile covered with nanosilver
- *Silverplug*: Silver based polymers with silver zeolite developed to fill up dental implant tunnel[65]

Regarding joint and prosthetic device in bone contact applications some patents are reported in literature, but it is difficult to obtain a clear resume of the situation of what device are just on the market worldwide.

4.9 Materials and Methods

4.9.1 Preparation of Ti6Al4V samples

Ti6Al4V samples were prepared as reported in chapter 2 paragraphs 2.5.4 and 2.5.5 and in chapter 3 paragraph 3.5.3 and the procedure is repeated below. The material used was Ti6Al4V (ASTM B348, Gr5, TitaniumConsulting and Trading). The samples were cut into slices with thickness of 2 mm from cylindrical bars (10 mm diameter) with an automatic cutter (Struers Accutom 5). After the cutting the samples were signed with a letter on one side and polished on the opposite one with abrasive SiC papers (up to 4000). The polished samples were washed in acetone for 5 minutes in an ultrasonic bath and then ultrasonically washed twice for 10 minutes in ultrapure water. After the washing the samples were dried at room temperature under laminar flow

4.9.2 In situ reduction of the silver nanoparticles

In order to made the titanium alloy samples bioactive and in situ to reduce the nanoparticles they were treated with a patented chemical treatment developed by the research group [13], [14]. This treatment consists in an acid etching with diluted hydrofluoric acid and a reoxydation in hydrogen peroxide. The samples were treated with diluted hydrofluoric acid in order to remove the native oxide layer, then the effects of the hydrofluoric acid was stopped by means of washing in two different solutions named H1 and H2 (the compositions of the solutions are not mentioned due to patent restriction) were used in order to found the suitable one for this application. In the end the samples were placed in a holder containing hydrogen peroxide until the formation of a nano-textured oxide layer. Three protocols (named T1, T2 and T3) were developed adding the silver precursor and the additives at different steps of the oxide growth.
These three protocols were performed with 2 different silver precursor concentrations.
The additives used were Gallic acid(GA, 97.5-102.5% (titration), G7384 Sigma Aldrich) e poly vinyl alcohol(PVA, average Mw 13,000-23,000, 98% hydrolyzed, 348406 Sigma Aldrich) in order to reduce and to stabilize a higher amount of nanoparticles avoiding the formation of aggregates. The silver precursor used was silver nitrate ($AgNO_3$, Silver Nitrate PA-ACS-ISO 131459, 1611, Panreac).

A solution of Gallic acid 1 mg/ ml in ultrapure water and a solution of PVA 1 mg/ ml in ultrapure water were prepared 1 hour before each samples series. As silver precursor a solution 1 M of silver nitrate in ultrapure water (5 ml of water + 0.849 g $AgNO_3$) was prepared. Additives and silver precursors were added at the beginning of the oxidation of the samples in the 10 ml of hydrogen peroxide solution (T1), at the half of the treatment (T2) or at 2/3 of the treatment at 60°C in the following order and amount:

- 1 ml of water solution (1 mg/ml) of gallic acid in order to obtain a final concentration of GA in H_2O_2 of at about 0.1 g/l, as reported in[68]
- 100 µl of water solution (1 mg/ml) of PVA, in order to obtain a final concentration of PVA in H_2O_2 of at about 0.01 g/l, as reported in [69]
- Silver precursor :

-50 µl of 1M $AgNO_3$ aqueous solution in order to obtain a final concentration of $AgNO_3$ in H_2O_2 of at about 0.005M, for the samples 0.005 M.

-10 µl of 1M $AgNO_3$ aqueous solution in order to obtain a final concentration of AgNO3 in H2O2 of at about 0.005M, for the samples 0.001 M.

After the in situ reduction of the nanoparticles, the samples where rinsed in ultrapure water and dried under laminar flow.

The procedure used is schematized in Figure 4. 5 and the nomenclature for each kind of samples are reported in Table 4.8

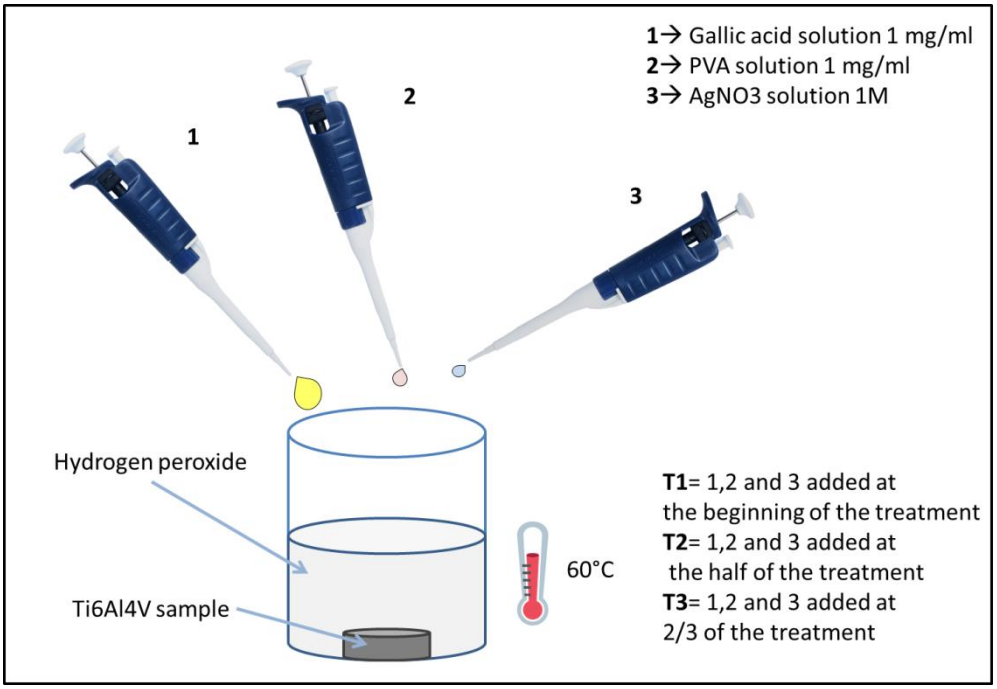

Figure 4.5: scheme of the procedure of silver nanoparticles in situ reduction.

Table 4.8: Nomenclature of the samples.

Name	Acid	Treatment step	Silver precursor concentration in hydrogen peroxide solution
CT(H1)_Ad+Ag(0.005M)_T1	H1	T1	0.005M
CT(H1)_Ad+Ag(0.005M)_T2	H1	T2	0.005M
CT(H1)_Ad+Ag(0.005M)_T3	H1	T3	0.005M
CT(H1)_Ad+Ag(0.001M)_T1	H1	T1	0.001M
CT(H1)_Ad+Ag(0.001M)_T2	H1	T2	0.001M
CT(H1)_Ad+Ag(0.001M)_T3	H1	T3	0.001M
CT(H2)_Ad+Ag(0.005M)_T1	H2	T1	0.005M
CT(H2)_Ad+Ag(0.005M)_T2	H2	T2	0.005M
CT(H2)_Ad+Ag(0.005M)_T3	H2	T3	0.005M
CT(H2)_Ad+Ag(0.001M)_T2	H2	T2	0.001M

The protocols of in situ reduction started with a high amount of silver precursor ($AgNO_3$ 0.005M) to facilitate the morphological characterization of nanoparticles and then the amount were tailored in order to adjust antibacterial behavior and cytocompatibility.

4.9.3 Surface characterization

Field Emission Scanning Electron Microscopy (FESEM - SUPRATM 40, Zeiss) equipped with Energy Dispersive Spectroscopy (EDS) was employed in order to investigate the presence, the shape, the morphology and the distribution of the silver nanoparticles on the surface of the samples.
The Surface chemical composition and the chemical state of the elements were investigated more in details by means of X-Ray Photoelectron Spectroscopy (XPS, PHI 5000 VERSA PROBE, PHYSICAL ELECTRONICS) in survey and high resolution mode of carbon, oxygen and silver. For these analysis each samples was mounted on a stab by means of a carbon-based tape.

4.9.4 Cross-section characterization

For the investigation of the distribution and of the shape of silver nanoparticles, Transmission Electron Microscopy (TEM) observations and STEM-EDS mapping were be performed with Titan G2 60-300 equipped with Chemistem on lamellas obtained in cross section from the samples (Figure 4.6). Lamellas were obtained from the cross section of the bulk samples by means of Focused Ion Beam (FIB) cut performed with NEON 40 EXB CrossBeam microscope. After the cut the lamellas were mounted on a copper cantilever for TEM observation.

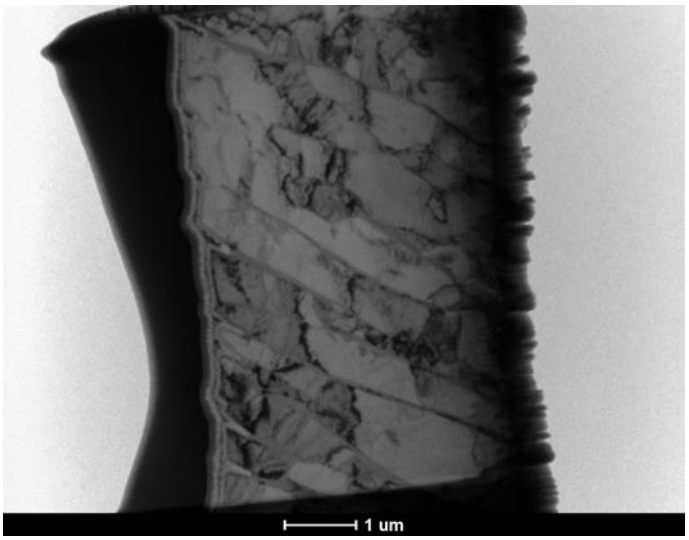

Figure 4.6: lamella obtained by means of FIB cutting on the gross section of the sample. The surface was protected by means of a layer of platinum.

These analyses were performed on samples:

- CT(H2)_Ad+Ag(0.005M)_T1
- CT(H2)_Ad+Ag(0.005M)_T2
- CT(H2)_Ad+Ag(0.005M)_T3

These analysis were performed at the International Centre of Electron Microscopy for Materials Science & Faculty of Metals Engineering and Industrial Computer Sciencen AGH University of Science and Technology, Al. Mickiewicza 30, PL-30 059, Krakow, thanks to the funds received from the European Union Seventh Framework Programme under Grant Agreement 312483 - ESTEEM2 (Integrated Infrastructure Initiative – I3).”

4.9.5 Silver release

The amount of silver released from the surface of modified samples was determined in ultrapure water by means of a photometer for silver analysis (HI 93737, Hanna Instruments). Each sample was soaked in 25 ml of ultrapure water at 37°C. After 3 hours, 1, 2, 7, 14 and 28 days the solution was changed with fresh one and analyzed for silver content.
The analytical kit is composed by four reagents (A, B, C, D) supplied with the instrument (Figure 4.7).

Figure 4.7: Photometric measurements kit.

When mixing the reagents with the solution to analyzed, the obtained solution turns orange. The color is more intense as the silver concentration is higher. One beaker was filled with 25 ml of ultrapure water (control) and one of 25 ml of the release solution (sample). At the control 1 ml of reagent A was added to the control and 1 ml of reagent B was added to the sample. After 2 minutes 1 ml of reagent C was added to both the beakers and again after 2 minutes 1 ml of reagent D was added to both the beakers. After 2 minutes one glass cuvette was fill with the control solution and one with the samples solution. The cuvettes were placed in the instruments and the measurements were performed. The release test was performed in triplicate for each sample.

4.5.6 Antibacterial tests

The antibacterial behavior of the treated samples was investigated by means of different analysis explained below.
The antibacterial evaluation tests performed on the samples with the in situ reduction of silver nanoparticles were just explained in chapter 3 paragraph 3.4.14. The procedure is again reported below.

Broth dilution method:

Bacteria adhesion tests were performed in order to quantify the amount of adherent and non-adherent bacteria. The tested bacteria is the same of the Kirby Bauer test *Staphylococcus aureus* ATCC 29213. In the adhesion tests, the samples were incubated in bacterial broths with inoculum of 10^4 CFU/ml for 24 h and then the evaluation of the adherent and non-adherent bacteria were performed. The tests consist in several steps explained below:

- The broth culture (mycorrhiza helper bacteria MHB) was prepared overnight at 37°C starting from pellet of microbank stored bacteria.
- N. 5 tubes were prepared. 5 ml of the broth were placed in the first test tube and dilution of 100 µl to 100µl was repeated until tube 5.
- Test tube n.5 was centrifuged at 4000 rpm for 10 minutes.
- The pellet was resuspended in 100µl of MHB.
- 5 ml of physiological solution 0.9% 0.5 Mc Farland were prepared (10^8 CFU/ml).
- The bacteria inoculum were prepared
    - 0.1ml of the 0.5 Mc Farland (10^8)+9.9 MHB→10^6
    - Final inoculum: 0.2ml of the 10^6 inoculum+19.8 MHB→10^4
- The samples were placed in a multiwell plate and covered with 5 ml of the final inoculum (10^4 CFU/ml), a CFU plate counting was also prepared with the final inoculum in order to control the concentration in agar nutrition.
- The samples and the control were incubated at 37°C for 24h.
- For the counting of non-adherent bacteria 0.5 ml of the broth culture of each sample were progressive diluted in sterile water and the relative CFU plating count on nutrient agar was performed.
- For the counting of adherent bacteria, the bacteria were removed from the surface of the samples. The samples were transferred into sterile bags with

1.5 ml of physiological solution 0.9% and sonicated at 43 Hz for 7 minutes in order to detach the bacteria from the surface.

- The samples were removed from the bags and the bags were placed in a vortex mixer.
- 0.5 ml of the physiological solution were taken from each bags progressive diluted with sterile water.
- For each samples were performed CFU plate counting obtaining the amount of the adherent bacteria.

This test was performed on the samples listed below:

- CT(H2)
- CT(H2)_Ad+Ag(0.005M)_T1
- CT(H2)_Ad+Ag(0.005M)_T2
- CT(H2)_Ad+Ag(0.005M)_T3

These analyses were performed at the Department of Public Health and Pediatrics of the University of Torino.

Evaluation of biofilm formation on modified surfaces:

Bacteria strain and growth conditions

A single colony of a multi-drug resistant (MDR) *Staphylococcus aureus* (reference strain ATCC 25923, purchased from the American Type Culture Collection, Manassas, USA) from an overnight culture onto selective Mannitol Salt Agar plate (Sigma-Aldrich) was resuspended in 9 mL of Luria Bertani broth (LB, Sigma-Aldrich) and incubated at 37°C for 18 h. After incubation, a new fresh LB tube diluted 1:10 was prepared. The new tube was incubated at 37°C for 3 hours in order to achieve the logarithmic growth phase. Finally, a fresh broth-culture was prepared prior each experiment by diluting bacteria in LB broth until optical density (o.d.) resulted as 0.005 at 600 nm, thus corresponding to a final concentration of $1*10^5$ cells /ml.

Biofilm formation

Sterile specimens were placed in a 24 multiwell plate (Nunclon Delta Surface, Thermo Scientific) and submerged in 1 ml of LB medium containing $1*10^5$ cells / ml prepared as previously described. The plate was incubated for 90 minutes at 37°C under agitation at 120 rpm (adhesion phase). Supernatants were then extracted to remove floating planktonic cells (separation phase) and specimens gently washed 3 times with PBS to remove non-adherent cells. Then, each

specimen was rinsed with 1 ml of fresh LB medium and plate incubated for 24, 48 and 72 hours at 37°C for biofilm culture.

Bacterial Cell Viability

To assess the growth capacity of the bacterial strains after 24, 48 and 72 h of direct contact compared to that of untreated controls, bacterial viability was evaluated by the validated quantitative colorimetric metabolic 2,3-bis (2-methoxy-4-nitro-5-sulphophenyl)-5-[(phenyl amino) carbonyl]-2H-tetrazolium hydroxide assay (XTT, Sigma-Aldrich). Briefly, 20 µL of XTT solution (3 mg/ml in acetone containing 0.1M menadione) were added to each well and plates were incubated at 37°C for 5 h in the dark. Then, 50 µL were collected from each well and centrifuged for 2 min at 480 g to remove any debris, and the optical density was evaluated using a spectrophotometer (SpectraCount, IBM) at 490 nm. Mirror-polished specimens were considered as control.

Live/Dead Assay

To determine the viability of bacteria a Live/Dead BacLight bacterial viability kit (Molecular Probes, Life Technologies Italia, Monza, Italy) was used. The kit includes two fluorescent nucleic acid stains: SYTO9 and propidium iodide. SYTO9 penetrates and stains both viable and nonviable bacteria, while propidium iodide enters only damaged/dead cells and quenches SYTO9 fluorescence.

For assessing viability, 1 mL of stock solution of each stain was added to 3 ml of PBS and, after mixing, the solution was distributed into the plates containing the materials specimens and incubated at RT for 15 min in the dark. Stained biofilms were examined by fluorescent microscope (Leica 6500, Leica Microsystems, Basel, Switzerland). Finally, the number of dead bacteria was calculated and expressed as % of total bacteria number by ImageJ (NIH, Bethesda, USA) software.

These analyses were performed on the samples:

- CT(H2)
- CT(H2)_Ad+Ag(0.005M)_T2
- CT(H2)_Ad+Ag(0.001M)_T2

These analysis were performed at the Department of Health Sciences, Università del Piemonte Orientale UPO, Via Solaroli 17, 28100 Novara, Italy

The bacterial broths of samples CT(H2)_Ad+Ag(0.005M)_T2 were analyzed after the bacteria cultures with Inductively coupled plasma mass spectrometry (ICP) in order to investigate the silver release in a complex medium and in presence of bacteria.

4.9.7 Cytocompatibility tests

Cytocompatibility tests were performed in order to evaluate the effects of released silver ions and silver nanoparticles on cells. The method used was explained in chapter 3 paragraph 3.4.14 and the procedure is again reported below. Samples cytocompatibility was evaluated towards human osteoblasts progenitor cells (hFOB 1.19) that were purchased from the American Type Culture Collection (ATCC, Manassas, USA, ATCC CRL-11372). hFOB were cultured in DMEM: Ham's F12 mixture (50:50, Sigma) supplemented with 10% fetal bovine serum, 1% antibiotics and 0.3 mg/ml neomycin (G418 salt, Sigma). Cells were cultured at 34°C, 5% CO_2 until 80–90% confluence, detached with trypsin–EDTA solution (Sigma) and used for experiments.

Sterile specimens were gently collected with surgical tweezers avoiding any surface impairment and seeded onto a new 24 well plate; cells (hFOB) were seeded in a defined number ($1*10^4$ cells/specimen) directly onto specimens' surface and cultivated using 1 ml of fresh medium for 24, 48 and 72 h at 37°C, 5% CO_2. Afterwards, at each selected time-point, cells viability was evaluated by the Alamar blue colorimetric assay (alamarBlue, Thermo Fisher) following manufacturer's instruction. Briefly, 100 µl of the ready-to-use Alamar solution was added to each well containing cells-seeded specimens and the plate was incubated 4 h at 37°C in the dark. Then, 100 µl of each supernatants were collected and transferred to a new black-bottom 96 wells plate; after gently shaking the plate, fluorescence intensity was detected at 600 nm with a spectrophotometer (Victor, IBM). Mirror-polished specimens were considered as control.

These analyses were performed on the samples listed below:

- CT(H2)
- CT(H2)_Ad+Ag(0.005M)_T2
- CT(H2)_Ad+Ag(0.001M)_T2

These analyses were performed at the Department of Health Sciences, Università del Piemonte Orientale UPO, Via Solaroli 17, 28100 Novara, Italy.

4.10 Results and discussion

4.10.1 Surface characterization

The surfaces of all the samples were investigated with FESEM observation and EDS analysis. The micrographs at two different magnifications are reported in Table 4.9. and 4.11, while the EDS results are reported in Table 4.10 and 4.12.

Table 4.9: FESEM micrographs of the CT(H1) samples with in situ reduction of silver nanoparticles. The first image for each sample is at 5.00 KX magnification and the second at 150.00 KX magnification.

CT(H1)_Ad+Ag(0.005M)_T1
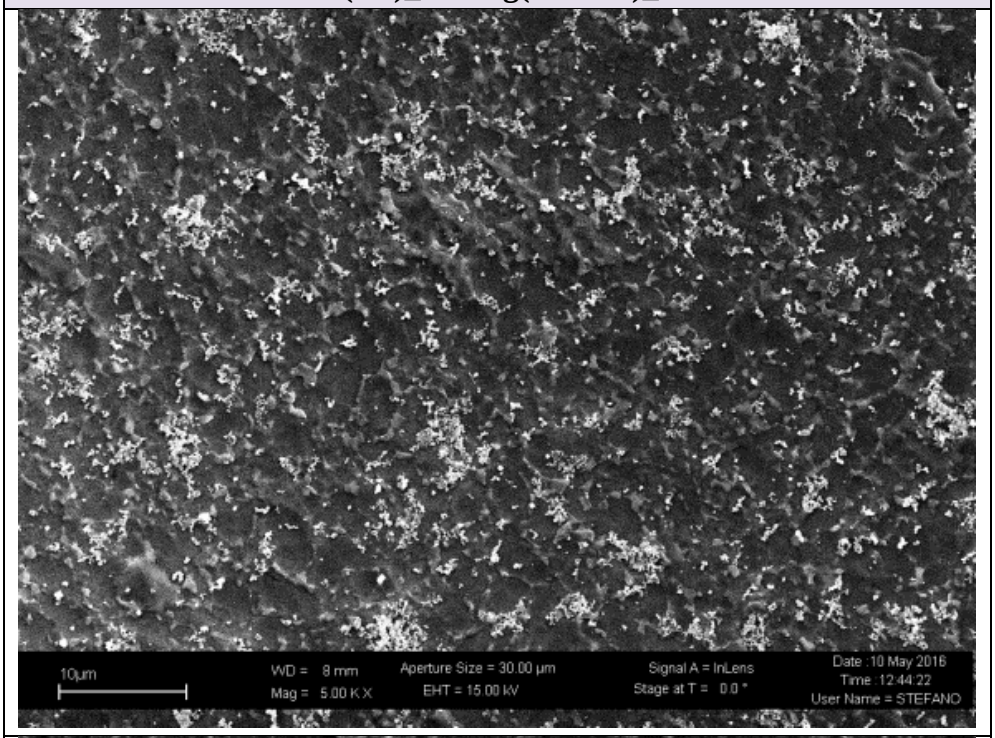
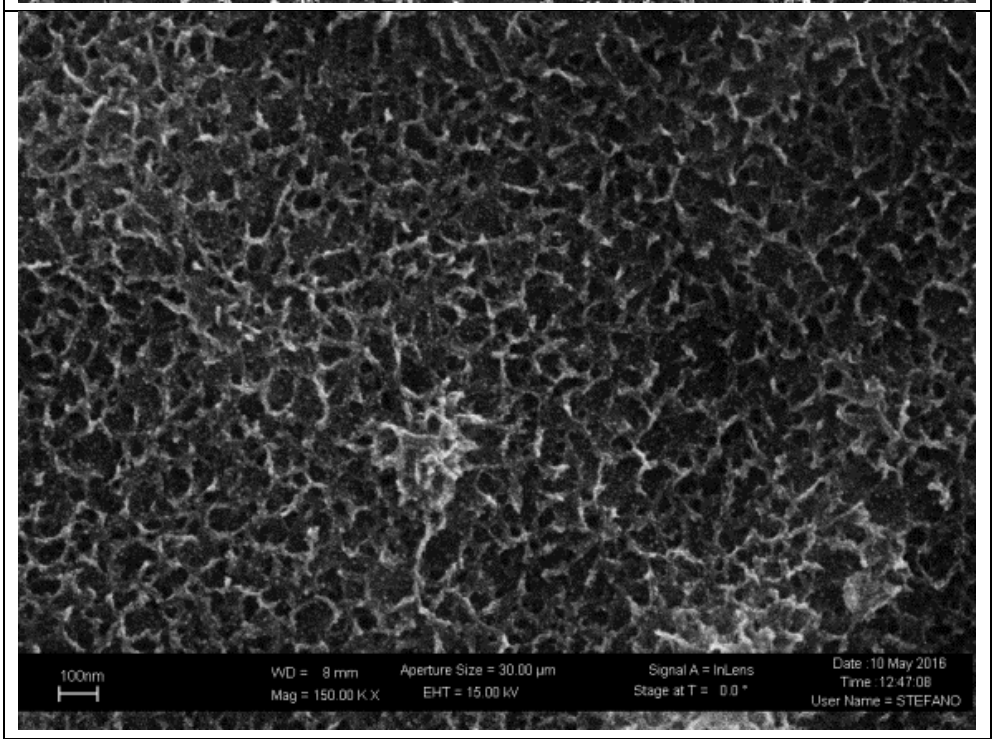

CT(H1)_Ad+Ag(0.005M)_T2

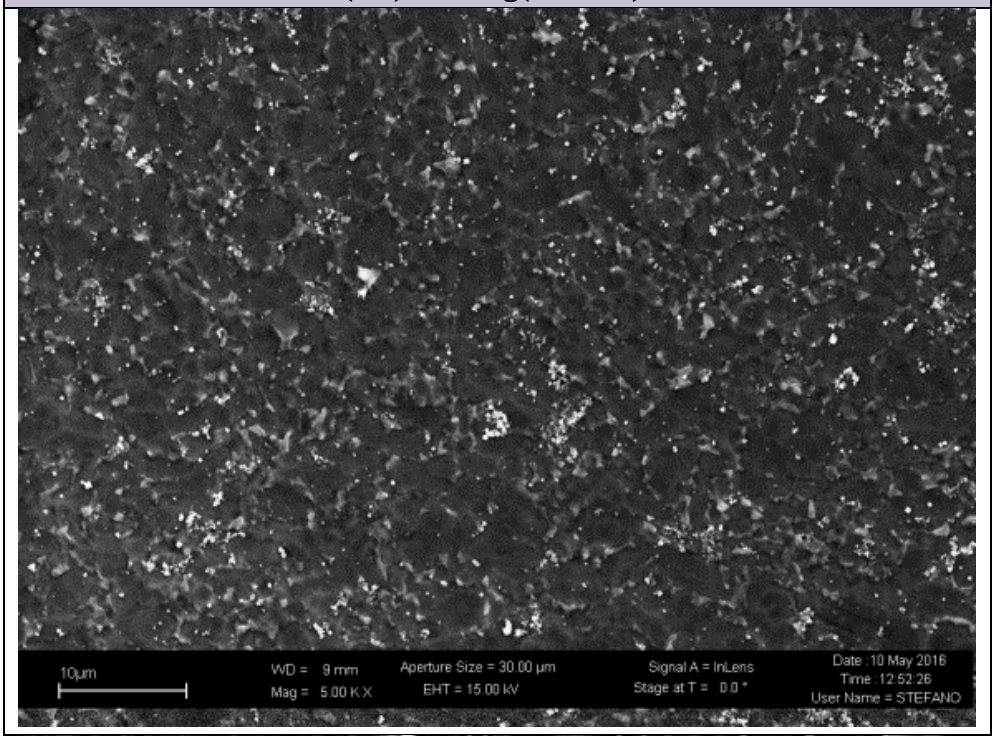

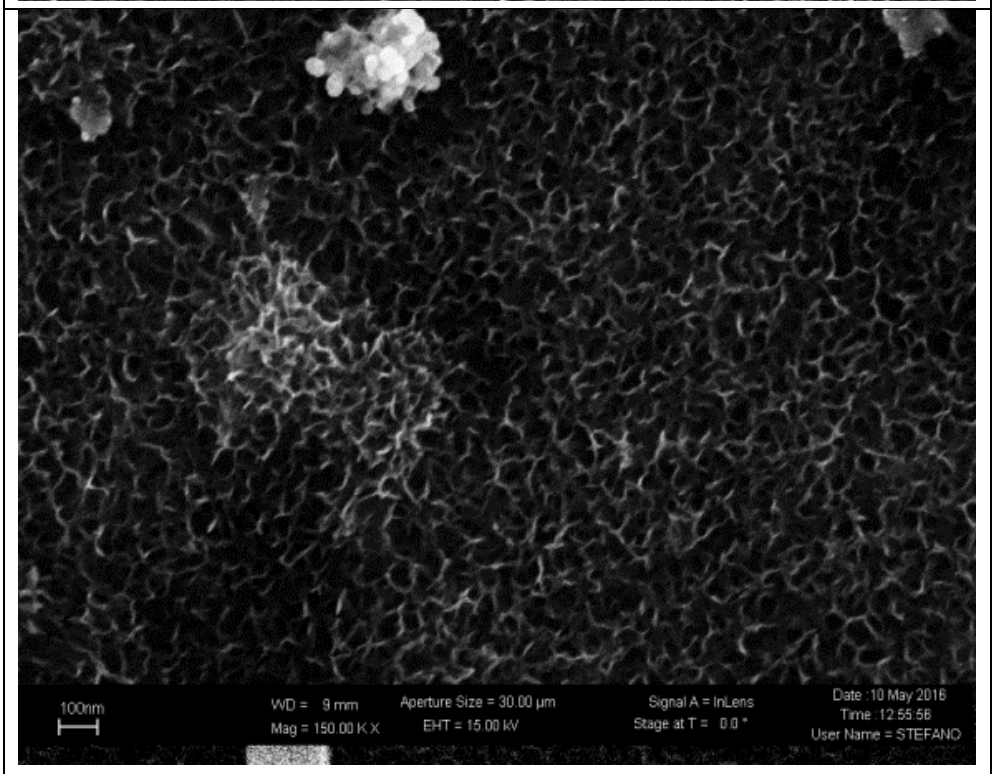

CT(H1)_Ad+Ag(0.005M)_T3

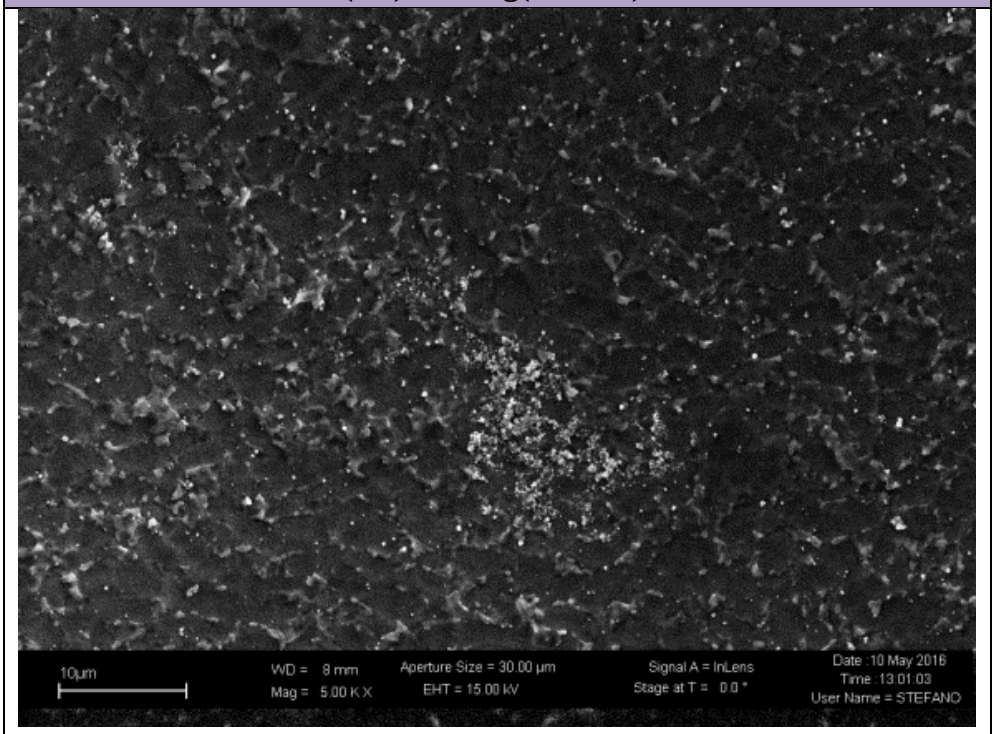

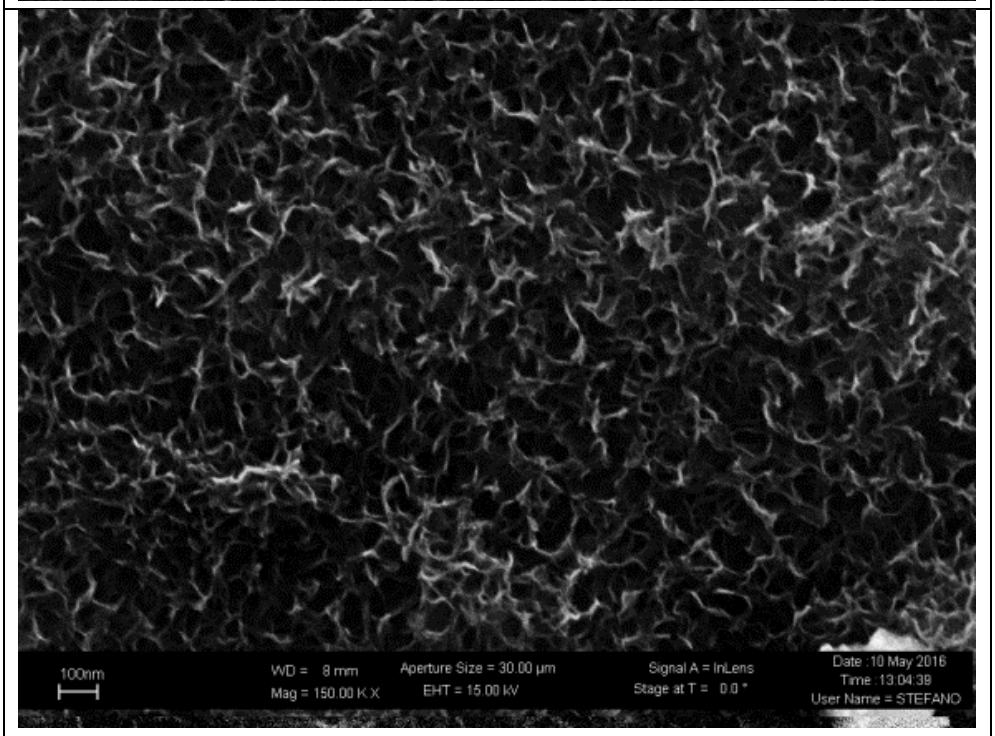

CT(H1)_Ad+Ag(0.001M)_T1

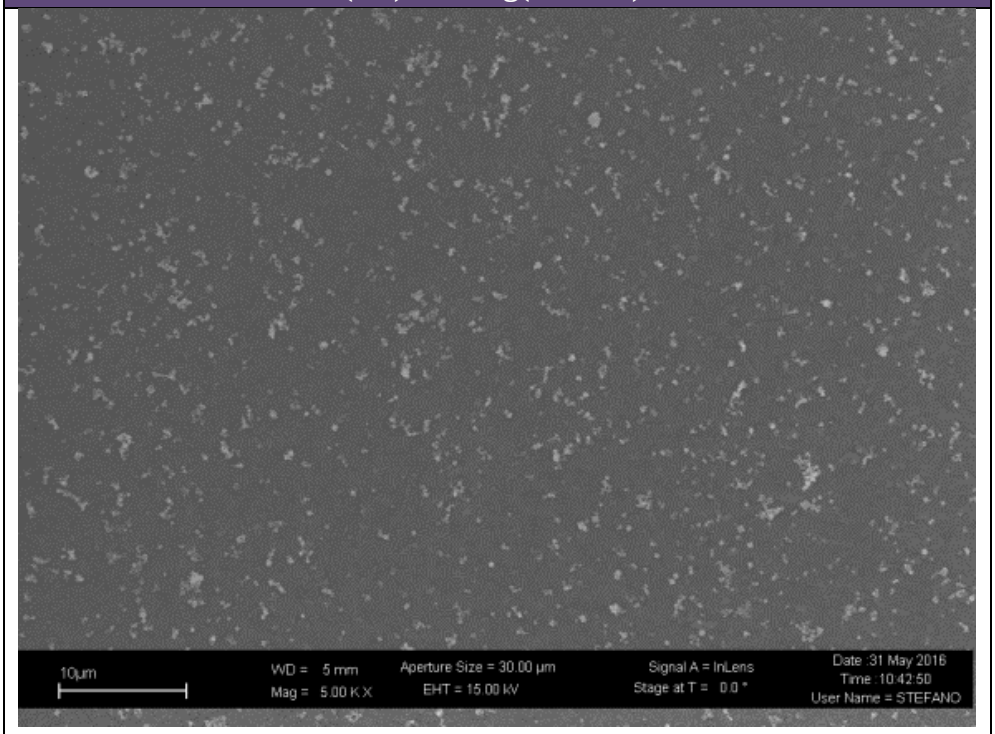

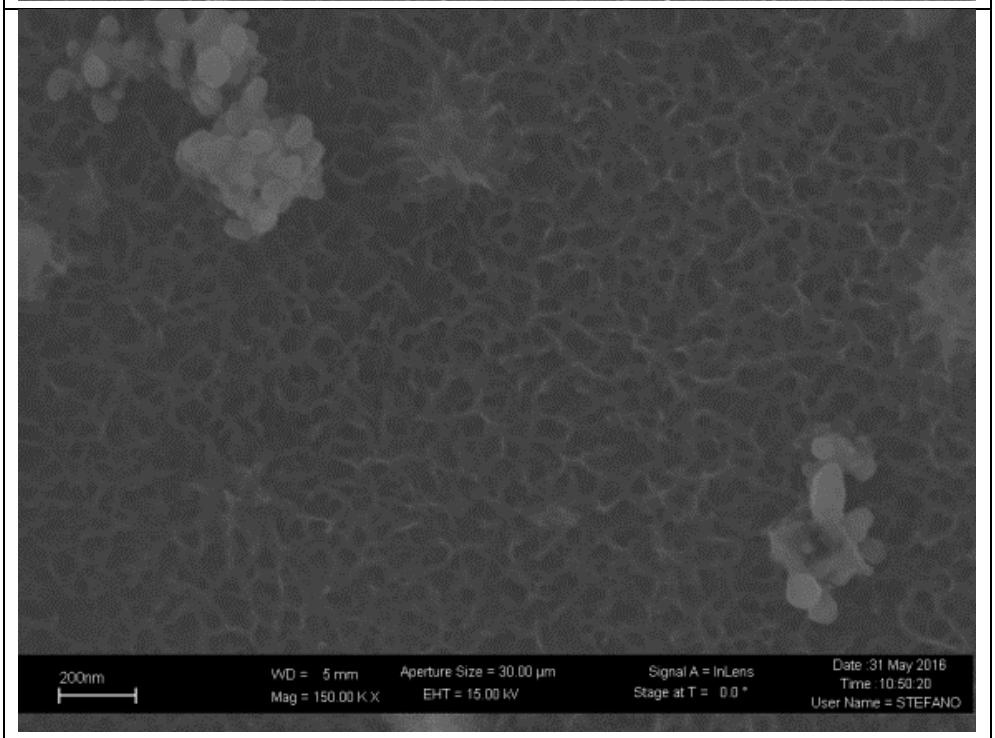

CT(H1)_Ad+Ag(0.001M)_T2

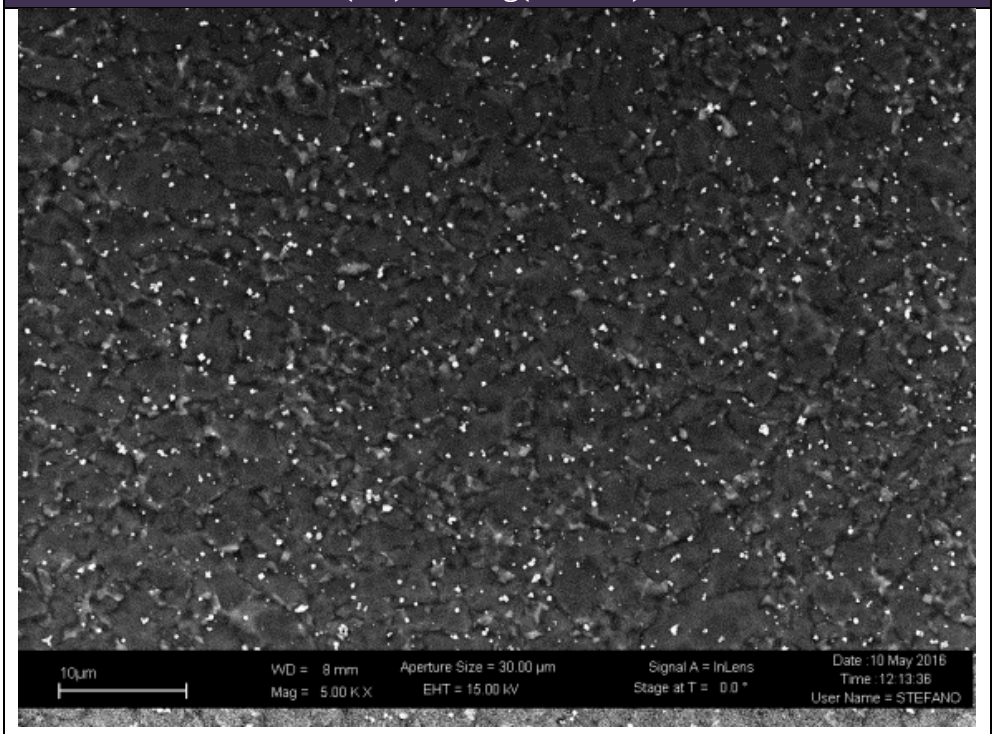

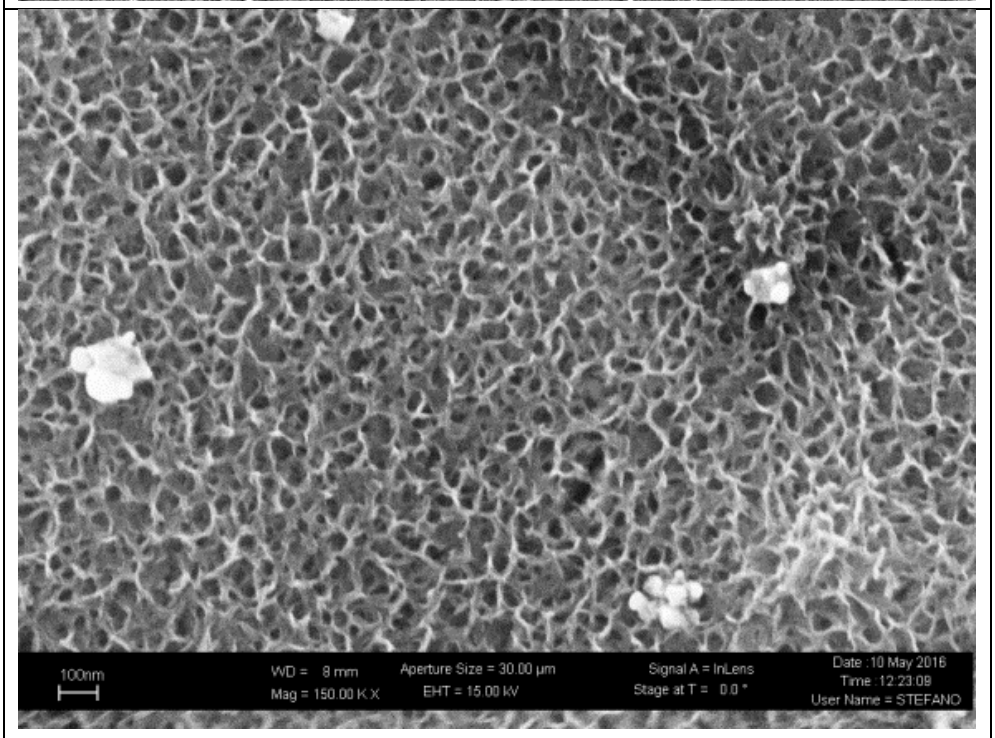

CT(H1)_Ad+Ag(0.001M)_T3
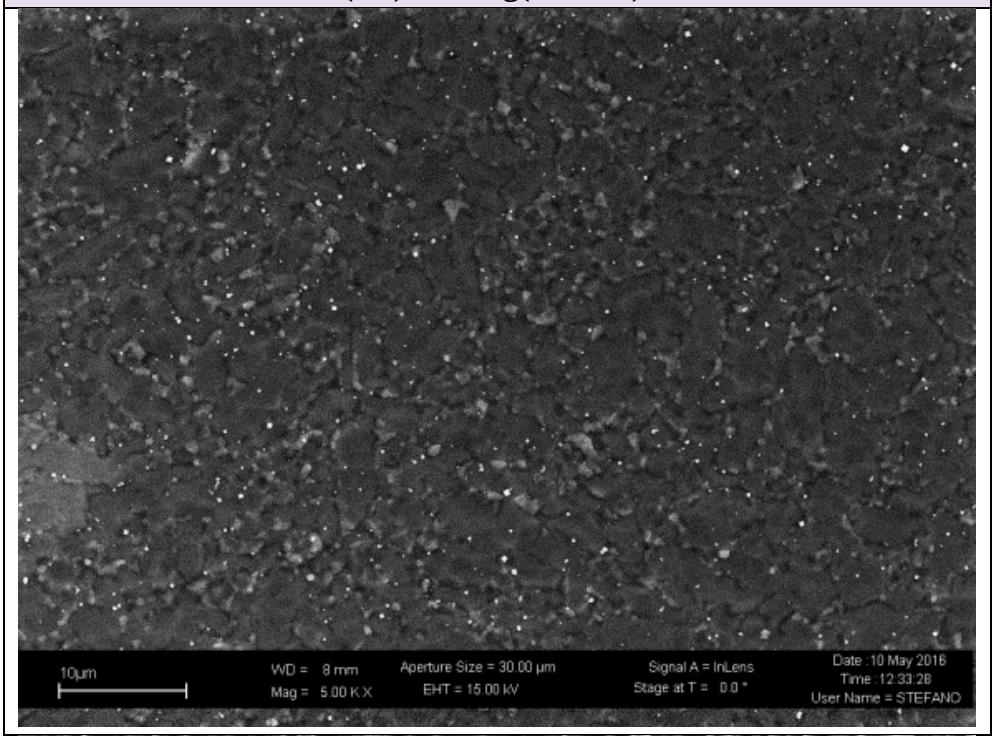
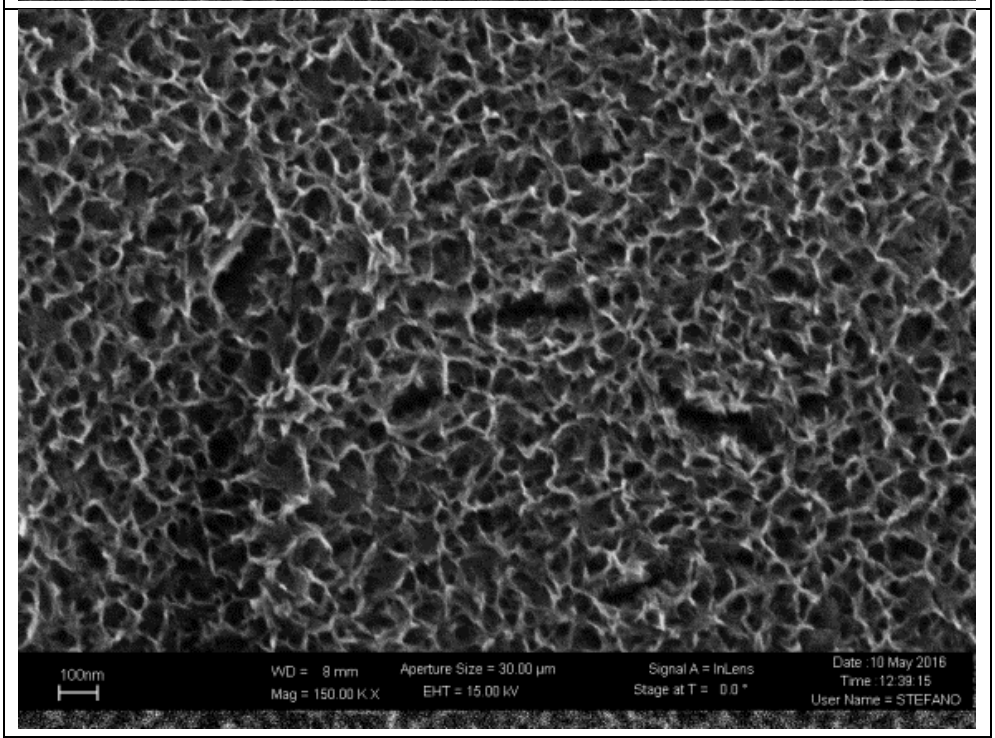

Table 4.10: EDS results of CT(H1) samples with the in situ reduction of silver nanoparticles area of 5400 μm^2).

Samples	CT(H1)_ Ad+Ag(0 .005M)_ T1	CT(H1)_ Ad+Ag(0 .005M)_ T2	CT(H1)_ Ad+Ag(0 .005M)_ T3	CT(H1)_ Ad+Ag(0 .001M)_ T1	CT(H1)_ Ad+Ag(0 .001M)_ T2	CT(H1)_ Ad+Ag(0 .001M)_ T3
Elements (at %)						
O	49.21	48.96	44.12	54.90	52.96	56.81
Al	4.95	4.87	6.36	4.03	4.14	4.04
Ti	44.59	45.27	48.98	40.29	41.27	37.79
Ag	1.24	0.89	0.54	0.77	0.59	0.4
V	-	-	-	-	1.03	0.96

The FESEM images show for each samples at 5.00 KX magnification the presence of silver particles smaller than 1 μm and the presence of silver salts (an images at higher magnification of the silver salt is reported as example in Figure 4.8) The formation of this silver salts is due to the use of the solution H1 during one step of the chemical treatment and to its reaction with the silver precursor $AgNO_3$.

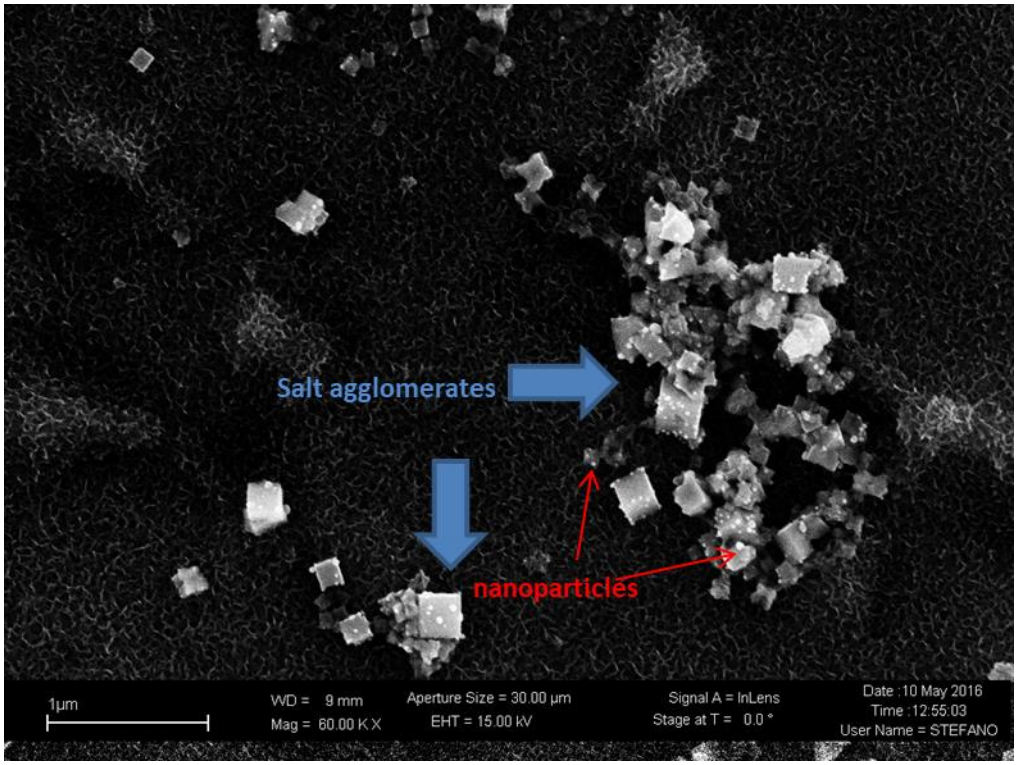

Figure 4.8: image at 60.00 KX magnification of the silver salt and nanoparticles on CT(H1) samples.

The samples treated with the protocol T1 show at 5.00 KX magnification a higher amount of salts and nanoparticles probably due to the longer time of sample explosion to the silver precursor.
At 150.00KX magnification, on the sample CT(H1)_AD+Ag(0.005M)_T1, well dispersed nanoparticles of diameter around 20-30 nm are present. On the sample CT(H1)_AD+Ag(0.005M)_T2 are visible few clusters of nanoparticles with dimension around 100 nm and on sample CT(H1)_AD+Ag(0.005M)_T3 the nanoparticles are not visible. The EDS analysis were performed on a surface of 5400 μm^2 of the samples avoiding zone where small clusters or evident contaminations are present, so the contribution from Ag salts is not included. Between the two concentration of silver precursor used (0.005M and 0.001 M), a small difference in the amount of silver relieved by this analysis was found, and it is possible to see in both cases a trend on silver content between the three different protocols with increasing silver in the sequence T3 <T2 <T1. This result could be correlated with the different time of permanence of the samples in contact with the silver nitrate solution: longer times allow a higher amount of salts to precipitate and a higher amount of silver nanoparticles to precipitate. The

evidence of silver in EDS also for samples CT(H1)_AD+Ag(0.005M)_T2 and CT(H1)_AD+Ag(0.005M)_T3 also in the zone where nanoclusters or salts are not present and the nanoparticles dispersed in the oxide layer are not visible could indicate the presence of very small nanoparticles with diameter < 10 nm or the presence of silver ion in the spoge-like nanostructure of the oxide layer.
For the samples CT(H1) treated with $AgNO_3$ 0.001M the results are the same obtained for the higher silver precursor concentration, but a lower concentration of silver on the surfaces is detected by EDS.

Table 4.11: FESEM micrographs of CT(H2) samples with silver nanoparticles in situ reduction. The first image for each sample is at 5.00 KX magnification and the second at 150.00 KX magnification.

CT(H2)_Ad+Ag(0.005M)_T1
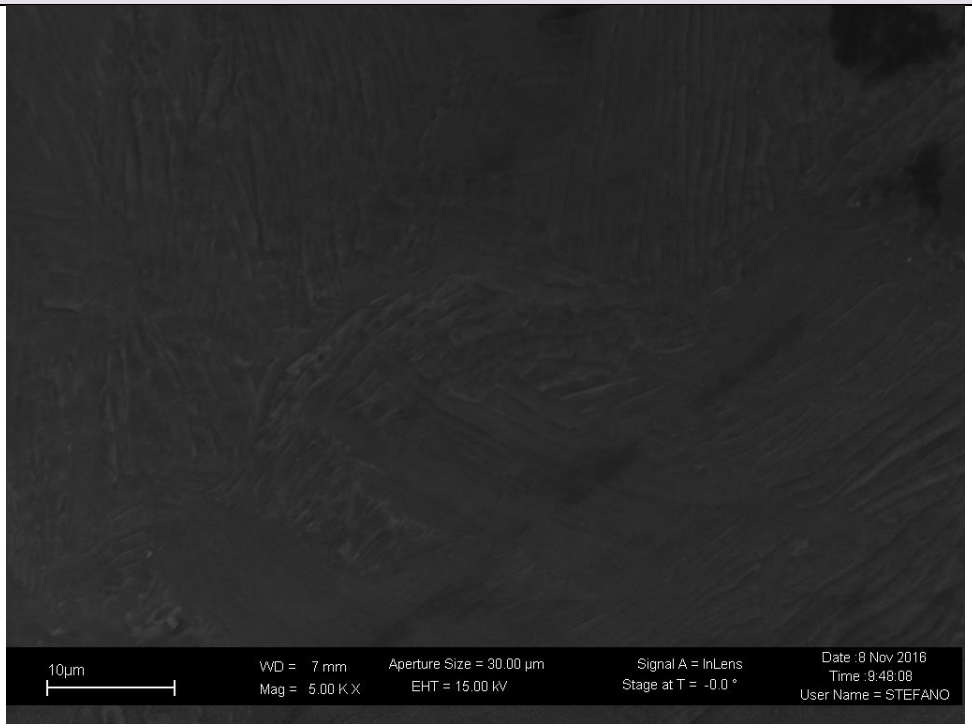
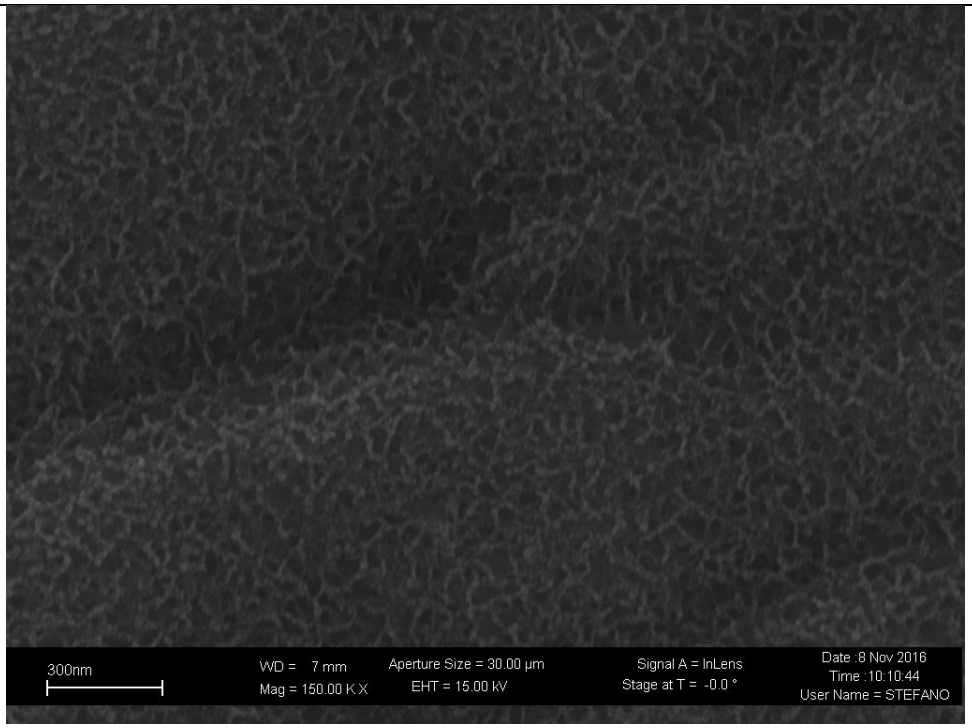

CT(H2)_Ad+Ag(0.005M)_T2

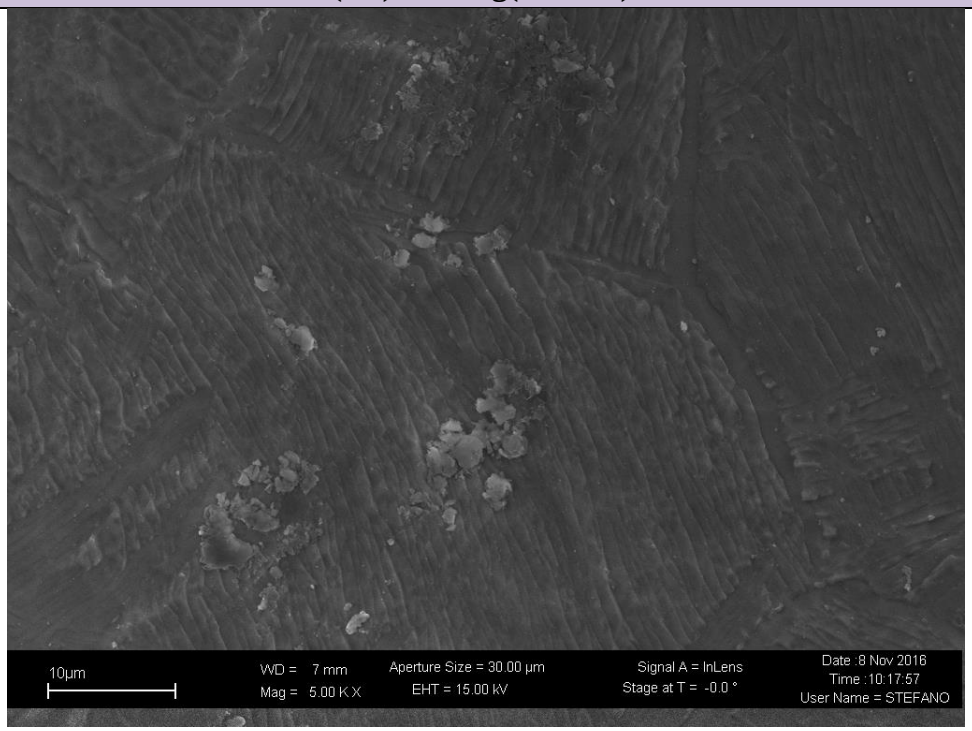

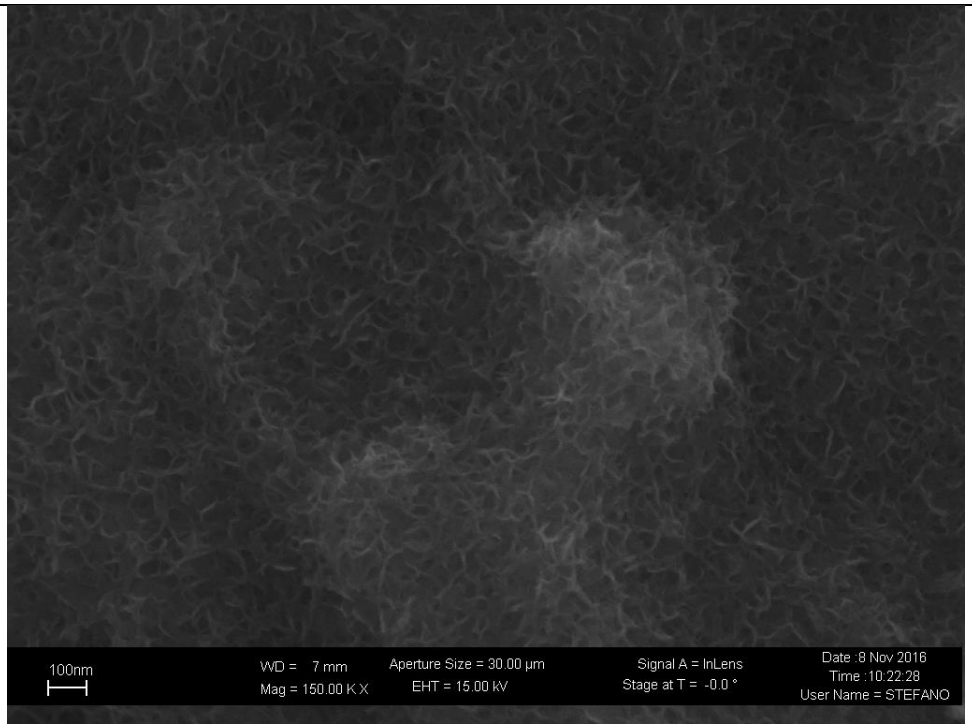

CT(H2)_Ad+Ag(0.005M)_T3

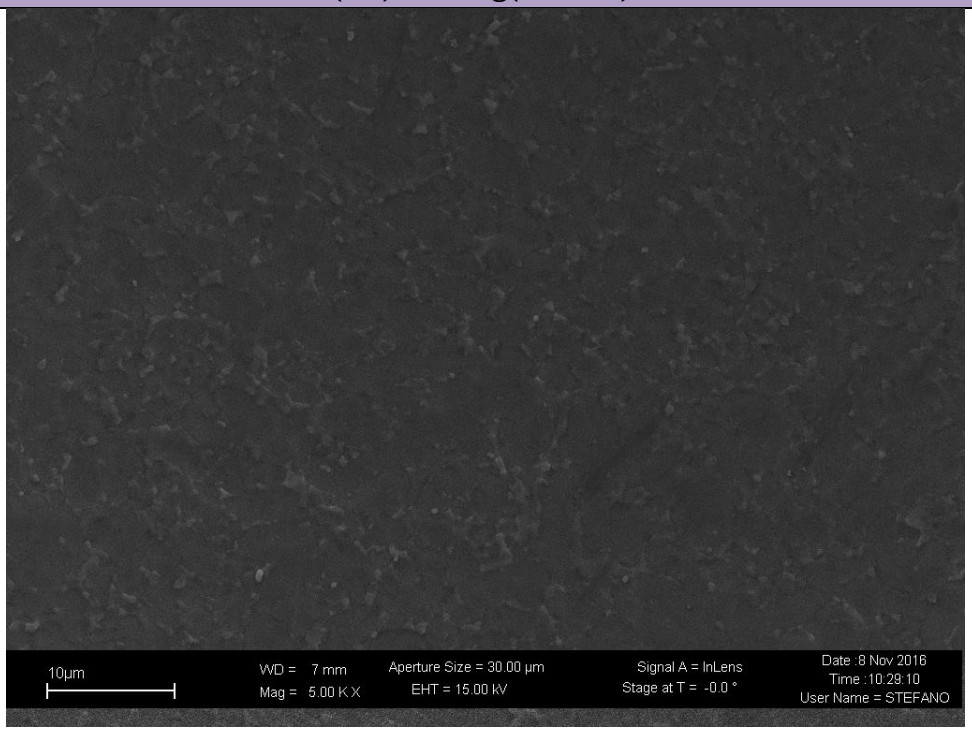

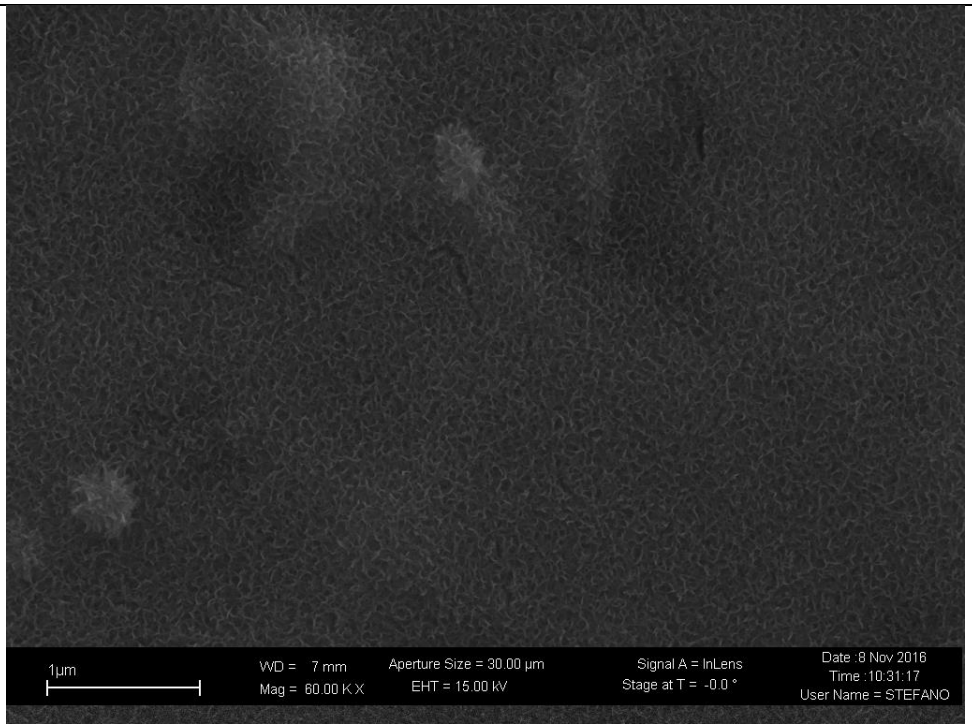

CT(H2)_Ad+Ag(0.001M)_T2

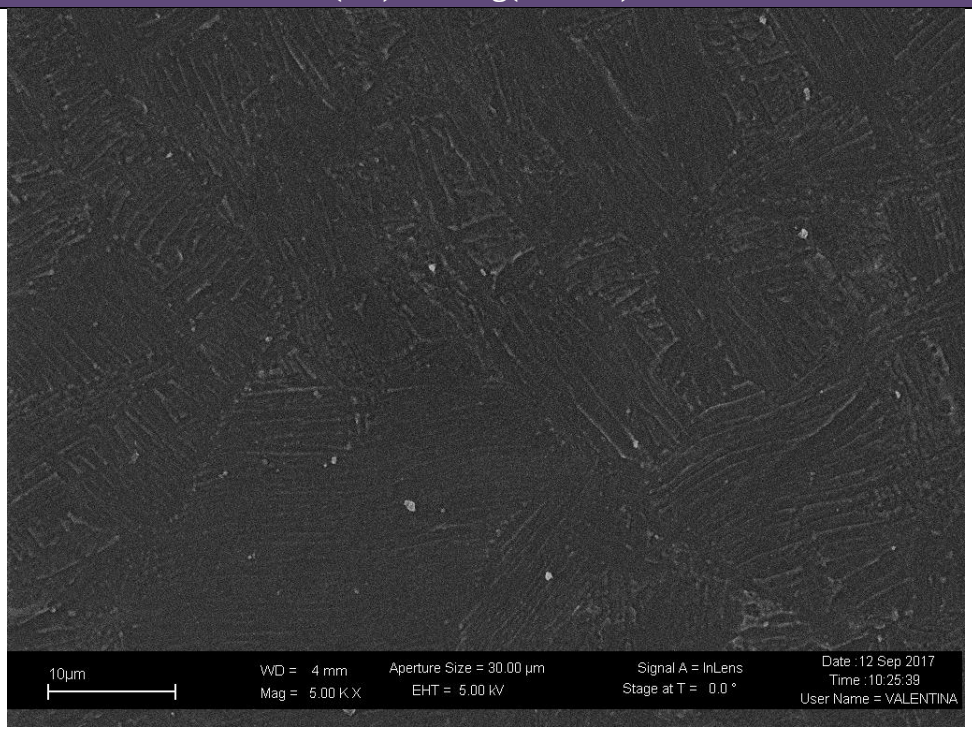

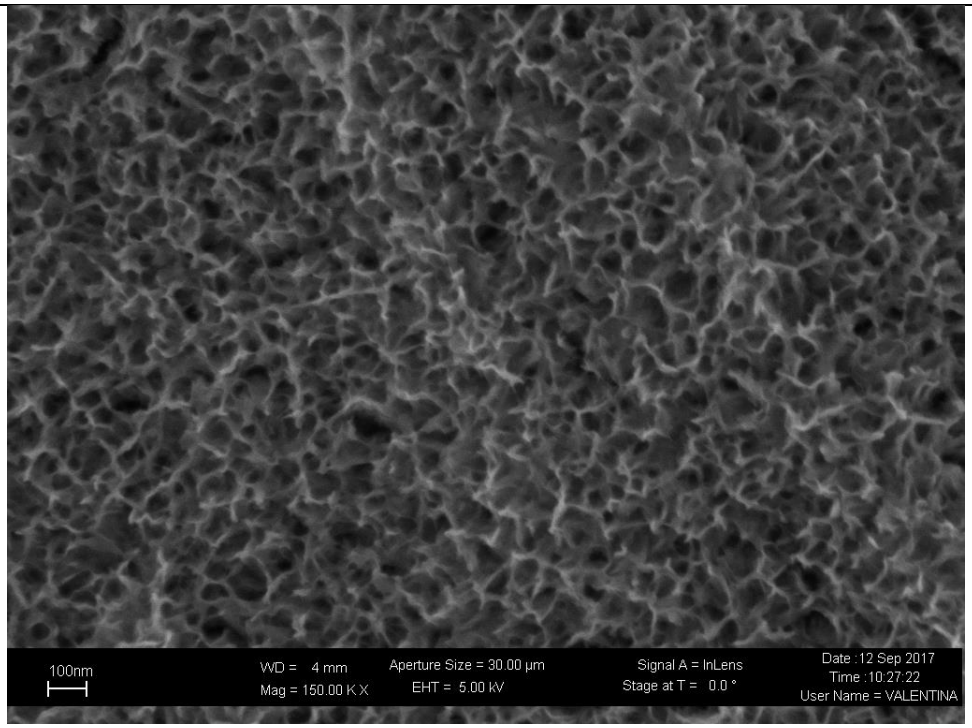

Table 4.12: EDS results of CT(H2) samples with the in situ reduction of silver nanoparticles.

Samples	**CT(H2)_Ad+ Ag(0.005M)_ T1**	**CT(H2)_Ad+ Ag(0.005M)_ T2**	**CT(H2)_Ad+ Ag(0.005M)_ T3**	**CT(H2)_Ad+ Ag(0.001M)_ T2**
Elements (at %)				
O	44.29	53.39	53.38	48.72
Al	5.39	4.74	3.94	4.93
Ti	47.98	39.87	40.67	44.83
Ag	0.75	0.86	0.92	0.33
V	1.59	1.13	1.10	1.20

In order to avoid the formation of the silver salts on the surface of the samples the solution H1 was replaced by the solution H2, during the chemical treatment and as it is visible on the images at 5.00 KX magnification of all the samples silver salts are no more detected. At this magnification, on samples CT(H2)_Ad+Ag(0.005M)_T2 some particle-like structure are visible, however they are titanium dioxide agglomerates and on samples CT(H2)_Ad+Ag(0.001M)_T2 few precipitates larger then 2-3 μm are visible which could be due to an organic contamination of the sample and the subsequent precipitation of larger silver clusters. At 150.00 KX the presence of the nanoparticles is barely visible for sample CT(H2)_Ad+Ag(0.005M)_T1 where nanoparticles of 20-30 nm are present, while it is not possible to see the nanoparticles at this magnification on all the other samples. The silver found by EDS analysis suggests for these samples the presence of nanoparticles with diameter <10 nm or of silver ions dispersed in the titanium oxide sponge-like structure. Looking at the EDS results of the samples with 0.005M $AgNO_3$, the trend of the silver amount seems to be different from the one of the samples treated with the acid H1, indeed the trend of the silver amount is T3> T2>T1, but the difference is less pronounced than in the previous case. It could be supposed that a higher amount of silver nanoparticles is obtained by avoiding the precipitation of silver salts which modifies the kinetic of silver nanoparticles reduction and by the addition of the additives and silver precursors later during the process. This higher amount of nanoparticles was detected by EDS. In this case, without the formation of the salts it is also much more visible a difference on the amount of silver detected between the samples CT(H1)_Ad+Ag(0.005M)_T2

and CT(H1)_Ad+Ag(0.001M)_T2 with the two different concentration of silver precursor.

The atomic percentage of the silver detected on the samples by EDS could vary by changing with the zone of the sample selected. For this reason for the analysis, the main conclusion that can be drawn is that the silver is well present on the surfaces of all the functionalized samples even when at higher magnifications the nanoparticles are not visible.

In order to understand if silver is in metallic or oxidized form and its amount on the external layer of the surface, XPS analysis was performed. This analysis was performed only on the samples with the higher concentration of silver precursor (0.005M $AgNO_3$). For the samples treated with the solution H2, which seems more promising because of the absence of silver salt precipitation, the XPS analysis was performed two times and the results are reported as media and standard deviation of the atomic percentage.

The atomic percentage of the elements detected with XPS analysis is reported in Table 4.13.

Table 4.13: Atomic percentage of the elements on the surface of the samples CT(H1) and CT(H2) with the in situ reduction of the silver nanoparticles. Samples CT(H1) reported as reference.

Samples	**CT(H1)**	**CT(H1)_Ad+Ag(0.005M)_T1**	**CT(H1)_Ad+Ag(0.005M)_T2**	**CT(H1)_Ad+Ag(0.005M)_T3**	**CT(H2)_Ad+Ag(0.005M)_T1**	**CT(H2)_Ad+Ag(0.005M)_T2**	**CT(H2)_Ad+Ag(0.005M)_T3**
Elements (at %)							
O	60.7	46.3	45.5	41.8	41.65±3.46	49.35±0.46	45.9±5.8
C	20.7	29.8	29.3	38.7	34.6±4.95	31.1±0.1	31.45±1.9
Ti	16.2	12.3	12.2	9.8	10.55±2.90	13.3±0.35	12.1±1.70
Ag	-	10.6	13	10.2	12.9±0.10	5.85±0.20	10.6±5.52
others	2.3	0.9	-	-	-	-	-

The main elements detected are oxygen, carbon, titanium silver and small percentage of other contaminants. The oxygen is present on all the samples and it is due to the presence of the titanium oxide layer and to the eventual contaminations with additives (gallic acid and poly vinyl alcohol). The content of carbon is correlated with the unavoidable surface contamination of the titanium samples[70], but could be again correlated with the presence of poly vinyl alcohol and gallic acid Looking at the Ag atomic concentration obtained from XPS analyses no specific trend with the time of silver introduction can be noticed, differently from what observed with EDS analyses. The difference in the trend of silver quantity detected with EDS and XPS analysis could be explained with a not uniform distribution of the nanoparticles on all the surfaces and by evidencing that these two analysis were performed only in small zones of each samples s as suggested by the high standard deviation of samples CT(H2)_Ad+Ag(0.005M)_T3. Furthermore, these two techniques have different depth of penetration and, using XPS, similar content of silver are measured

regardless of the samples treatment. High resolution spectra of carbon, oxygen and silver regions were performed in order to investigate the chemical bonds present on the surfaces and the oxidation state of silver.
The high resolution spectra of the carbon region are reported in Figure 4.9.

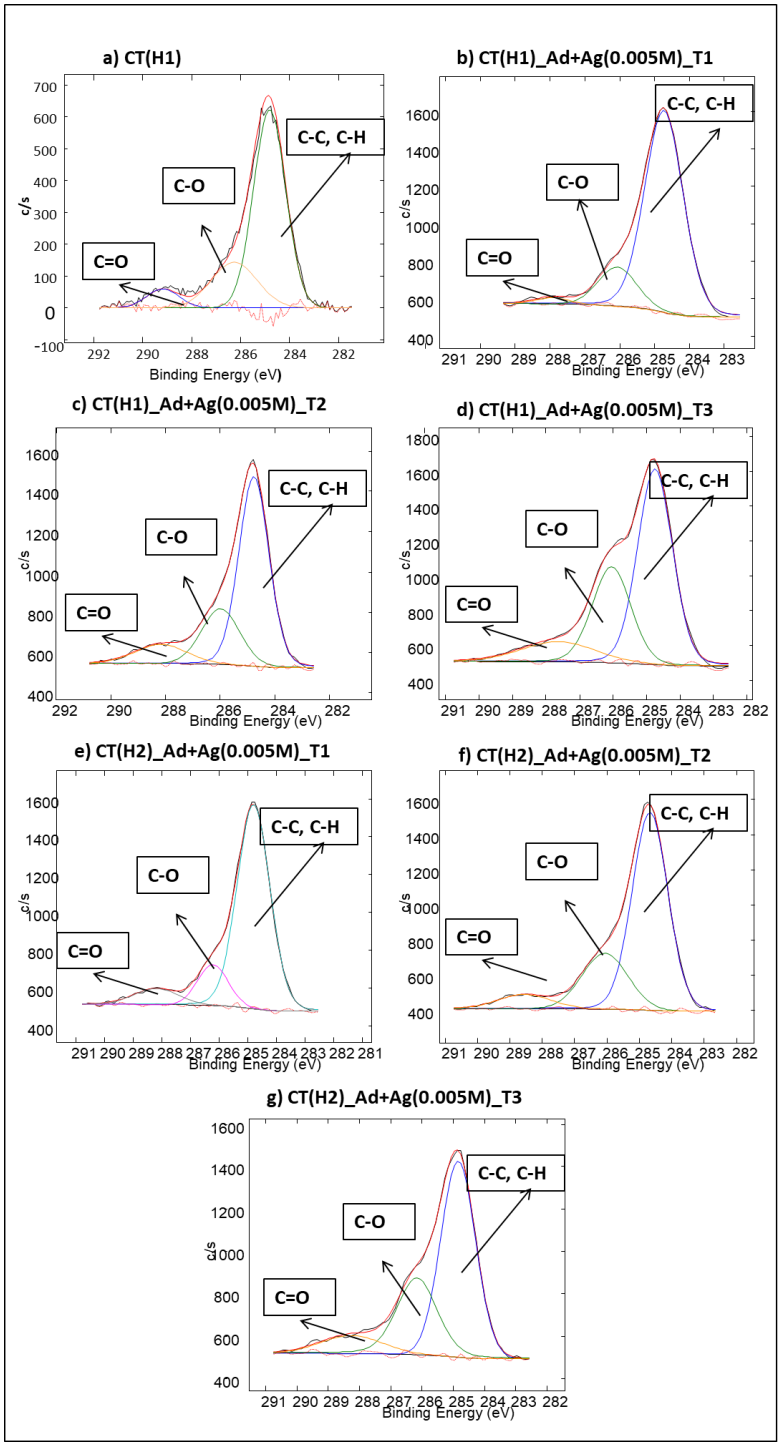

Figure 4.9: XPS detailed analysis of the carbon region of the samples a) CT(H1), b)CT(H1)_Ad+Ag(0.005M)_T1, c) CT(H1)_Ad+Ag(0.005M)_T2,d) CT(H1)_Ad+Ag(0.005M)_T3, e) CT(H2)_Ad+Ag(0.005M)_T1,f) CT(H2)_Ad+Ag(0.005M)_T2, g) CT(H2)_Ad+Ag(0.005M)_T3.

In Figure 4.9 the same three peaks around 284, 286 and 288 eV due respectively to C-C and C-H bonds[71], [72], C-O bonds[72] and C=O bonds[72] are present for all the samples. These peaks are due to the unavoidable carbon contamination of a reactive surface, but it could also be correlated with C-C, C-H, C-O and C=O bonds of gallic acid[73] and poly vinyl alcohol. The C-O signal increases moving from T1 to T3 suggesting a higher amount of organic species on the outermost surface layer when additives are introduced later.

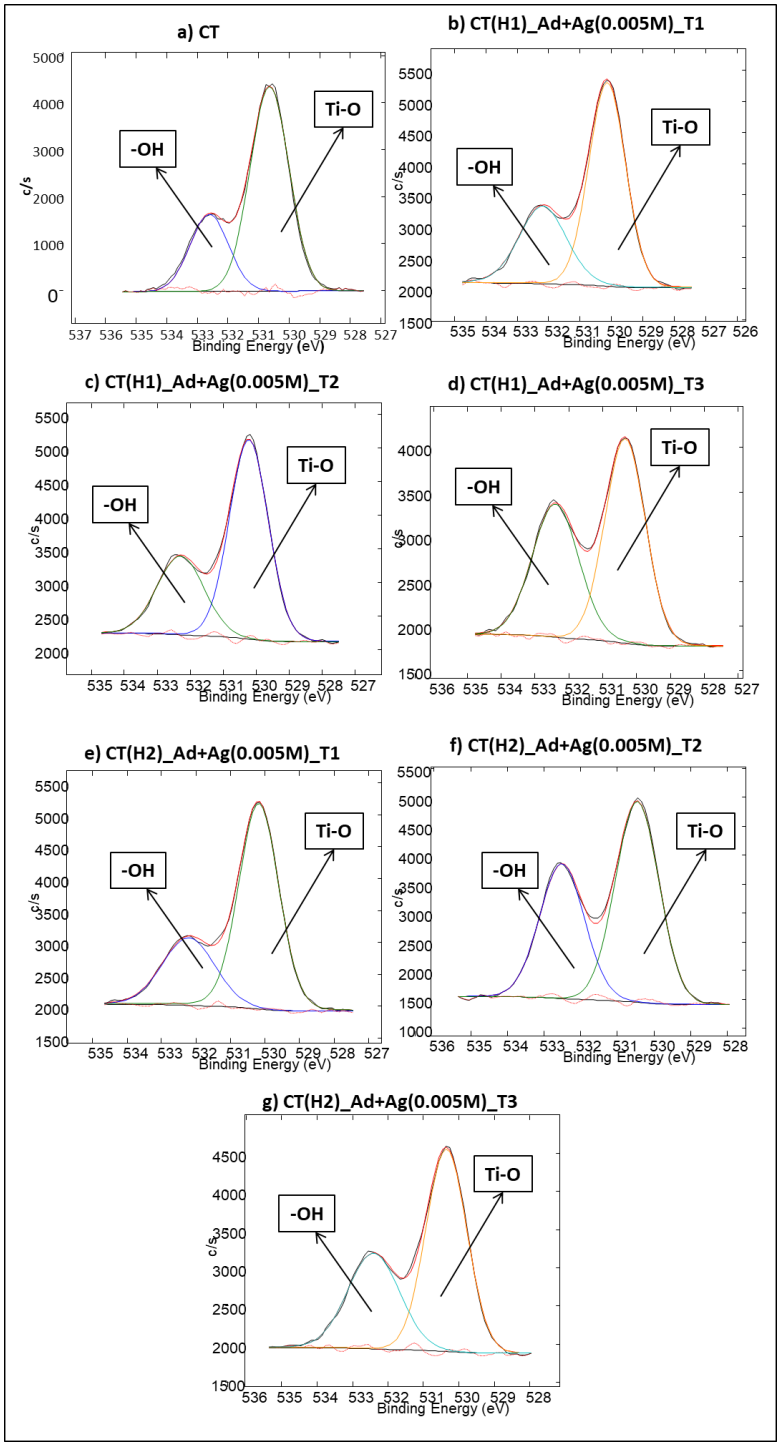

Figure 4.10: XPS detailed analysis of the oxygen region of the samples a) CT(H1), b)CT(H1)_Ad+Ag(0.005M)_T1, c) CT(H1)_Ad+Ag(0.005M)_T2, d) CT(H1)_Ad+Ag(0.005M)_T3, e) CT(H2)_Ad+Ag(0.005M)_T1, f) CT(H2)_Ad+Ag(0.005M)_T2, g) CT(H2)_Ad+Ag(0.005M)_T3.

In Figure 4.10, in the oxygen region, the same peaks are again visible for the spectra of all the samples. Two peaks around 530 and 532 eV are present and are respectively due to Ti-O bonds [74], [75] of the titanium oxide substrates and to –OH groups exposed by the patented chemical treatment[66], [74], [75].
Also in this case, the –OH groups exposed by gallic acids can contribute to the signal [73]. A moderate increase of the OH signals can be noticed from T1 to T3 (less evident for CT(H1) sample. As previously discussed for C-O signal this trend can be correlated with a higher presence of additives on the outermost surface when they are introduced later in the treatment.

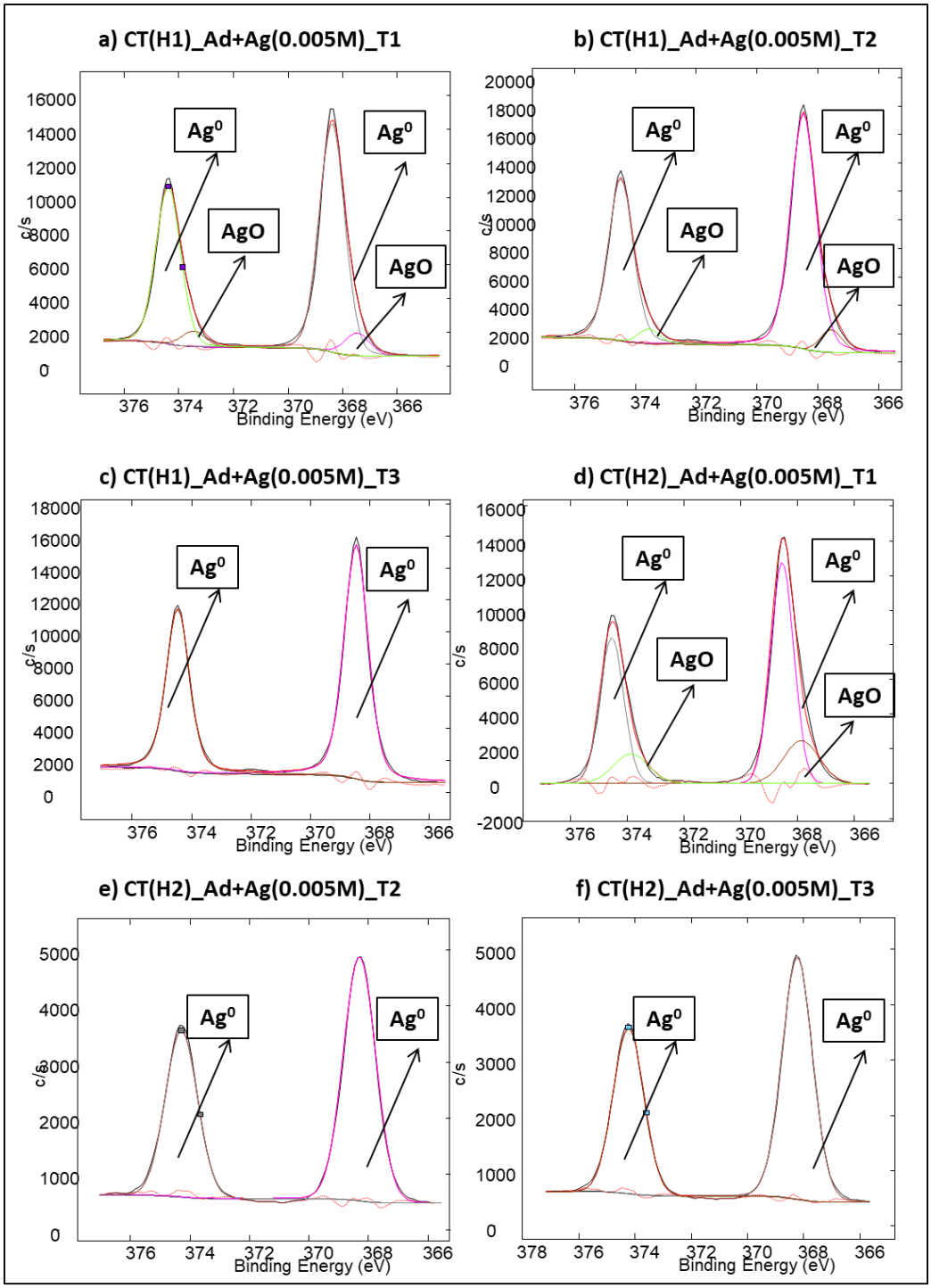

Figure 4.11: XPS detailed analysis of the silver region of the samples a)CT(H1)_Ad+Ag(0.005M)_T1, b) CT(H1)_Ad+Ag(0.005M)_T2, c) CT(H1)_Ad+Ag(0.005M)_T3, d) CT(H2)_Ad+Ag(0.005M)_T1, e) CT(H2)_Ad+Ag(0.005M)_T2, f) CT(H2)_Ad+Ag(0.005M)_T3.

In Figure 4.11 instead, in the spectra of the silver region, remarkable differences are visible. On the spectra of the samples CT(H1)_Ad+Ag(0.005M)_T1(Fig.4.11a), CT(H1)_Ad+Ag(0.005M)_T2(Fig.4.11b) and CT(H2)_Ad+Ag(0.005M)_T1(fig.4.13d) four peaks are present. The peaks at 368.38 and 374.38 eV of sample CT(H1)_Ad+Ag(0.005M)_T1, at 368.49 and 374.49 eV of sample CT(H1)_Ad+Ag(0.005M)_T2 and at 368.54 and 374.54 eV of sample CT(H2)_Ad+Ag(0.005M)_T1 are due to the presence of the metallic silver of the nanoparticles core [54], [76]. These two peaks have a little shift from the standard energy of metallic silver peaks which are at 368.2 and 374.2 eV and it is correlated by some authors with the presence of nanoparticles with diameter < 5 nm[77], [78]. The two peaks at 367.46 and 373.46 eV of sample CT(H1)_Ad+Ag(0.005M)_T1, at 367.49 and 373.49 eV of sample CT(H1)_Ad+Ag(0.005M)_T2 and at 367.86 and 373.86 eV of sample CT(H2)_Ad+Ag(0.005M)_T1 are due to the presence of silver oxide[79] which could cover the nanoparticles. For the samples CT(H1)_Ad+Ag(0.005M)_T3 (Fig. 4.13c), CT(H2)_Ad+Ag(0.005M)_T1 (Fig 4.11d) and CT(H2)_Ad+Ag(0.005M)_T3 (Fig 4.11f) are present only the two peaks due to metallic silver around 368.2 and 374.2 eV [54], [76] however for sample CT(H1)_Ad+Ag(0.005M)_T3 this peaks are shifted at 368.46 and 374.46 eV indicating probably the presence of nanoparticles smaller than 5 nm [77], [78].

The presence of the silver oxide coincide with a high amount of silver found by the survey analysis and could be due to the presence of ionic silver on the surface of the nanoparticles or in the sponge-like nanostructure of the titanium oxide layer. The presence of Ag^{+} could also depend on the rinsing procedure after the silver in situ reduction which could not remove the entire silver precursor.

The resume of peaks and relative attribution of the XPS analysis on samples CT(H1)_Ad+Ag(0.005M)_T1, CT(H1)_Ad+Ag(0.005M)_T2, CT(H1)_Ad+Ag(0.005M)_T3, CT(H2)_Ad+Ag(0.005M)_T1, CT(H2)_Ad+Ag(0.005M)_T2, and CT(H2)_Ad+Ag(0.005M)_T3 is reported in Table 4.14

Table 4.14: Carbon, oxygen and silver contributions and possible literature assignments.

CT(H1)_Ad+Ag(0.005M)_T1								
Region C			**Region O**			**Region Ag**		
Position	**Area %**	**Assignment**	**Position**	**Area %**	**Assignment**	**Position**	**Area %**	**Assignment**
284.72	81.65	C-C, C-H[71], [80]	530.13	66.23	Ti-O[74], [75]	367.46	5.34	AgO, Ag^{+}[79]
286.06	16	C-O[80]	532.18	33.77	Ti-OH[66], [74], [81]	368.38	53.54	Ag^{0}[54], [76]
287.91	2.35	C=O[80]				373.46	3.58	AgO, Ag^{+}[79]
						374.38	36.54	Ag^{0}[54], [76]
CT(H1)_Ad+Ag(0.005M)_T2								
Region C			**Region O**			**Region Ag**		
Position	**Area %**	**Assignment**	**Position**	**Area %**	**Assignment**	**Position**	**Area %**	**Assignment**
284.77	64.43	C-C, C-H[71], [80]	530.22	67.84	Ti-O[74], [75]	367.58	4.18	AgO, Ag^{+}[79]
285.99	24.25	C-O[80]	532.29	32.16	Ti-OH[66], [74], [81]	368.49	55.7	Ag^{0}[54], [76]
288.16	11.32	C=O[80]				373.58	2.8	AgO, Ag^{+}[79]
						374.49	37.32	Ag^{0}[54], [76]
CT(H1)_Ad+Ag(0.005M)_T3								
Region C			**Region O**			**Region Ag**		
Position	**Area %**	**Assignment**	**Position**	**Area %**	**Assignment**	**Position**	**Area %**	**Assignment**
284.7	56.67	C-C, C-	530.3	56.83	Ti-	368.4	59.88	Ag^{0}[54],

4		H[71], [80]	4		O[74], [75]	6		[76]
286.04	30.93	C-O[80]	532.39	43.17	Ti-OH[66], [74], [81]	374.46	40.12	Ag^0[54], [76]
287.64	12.41	C=O[80]						
CT(H2)_Ad+Ag(0.005M)_T1								
Region C			**Region O**			**Region Ag**		
Position	**Area %**	**Assignment**	**Position**	**Area %**	**Assignment**	**Position**	**Area %**	**Assignment**
284.8	78.05	C-C, C-H[71], [80]	530.18	70.59	Ti-O[74], [75]	367.86	13.71	AgO, Ag^+[79]
286.22	13.98	C-O[80]	532.21	29.41	Ti-OH[66], [74], [81]	368.54	46.17	Ag^0[54], [76]
288.18	7.97	C=O[80]				373.86	9.19	AgO, Ag^+[79]
						374.54	30.93	Ag^0[54], [76]
CT(H2)_Ad+Ag(0.005M)_T2								
Region C			**Region O**			**Region Ag**		
Position	**Area %**	**Assignment**	**Position**	**Area %**	**Assignment**	**Position**	**Area %**	**Assignment**
284.67	68.92	C-C, C-H[71], [80]	530.45	59.04	Ti-O[74], [75]	368.28	59.88	Ag^0[54], [76]
286.06	24.19	C-O[80]	532.51	40.96	Ti-OH[66], [74], [81]	374.28	40.12	Ag^0[54], [76]
288.55	6.89	C=O[80]						

CT(H2)_Ad+Ag(0.005M)_T3								
Region C			**Region O**			**Region Ag**		
Position	**Area %**	**Assignment**	**Position**	**Area %**	**Assignment**	**Position**	**Area %**	**Assignment**
284.84	60.18	C-C, C-H[71], [80]	530.35	62.45	Ti-O[74], [75]	368.22	59.88	Ag^0[54], [76]
286.17	29.8	C-O[80]	532.41	37.55	Ti-OH[66], [74], [81]	374.22	40.12	Ag^0[54], [76]
288.25	10.02	C=O[80]						

4.10.2 Cross-section characterization

In order to investigate the distribution of the silver nanoparticles in the thickness of the titanium oxide layer and to observe the smaller nanoparticles which are not visible in FESEM analysis, TEM observation with STEM-EDS maps were performed on the cross-section of the samples CT(H2)_Ad+Ag(0.005M)_T1, CT(H2)_Ad+Ag(0.005M)_T2 and CT(H2)_Ad+Ag(0.005M)_T3.
In Figure 4.12 the images of the lamellas of the three kinds of samples are reported.

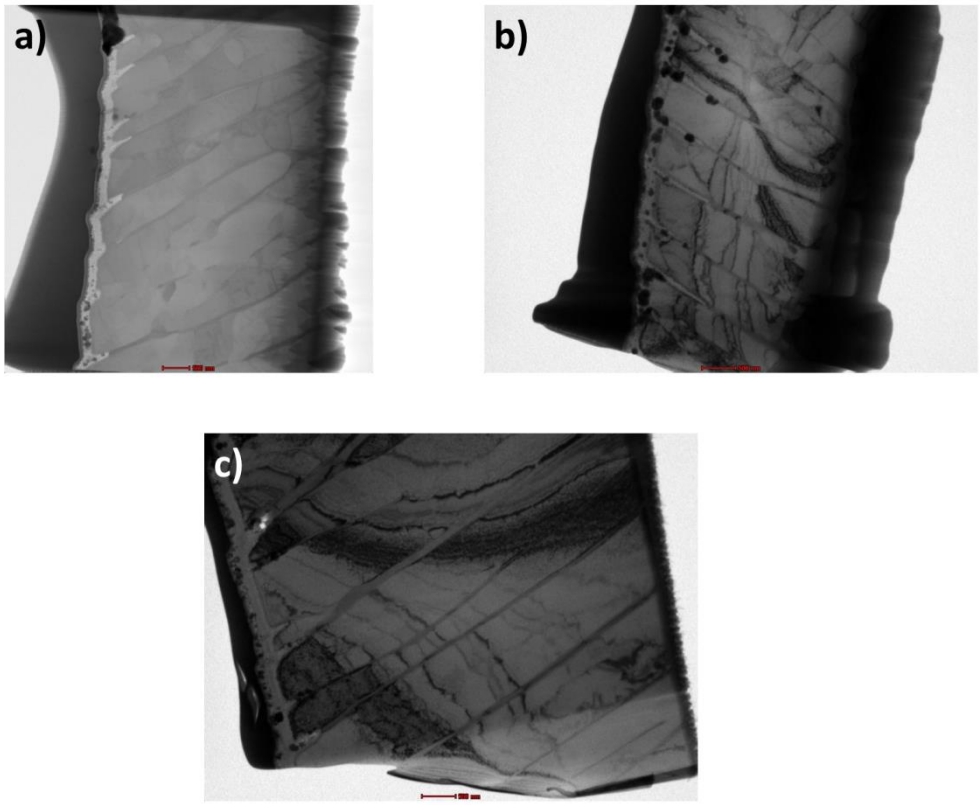

Figure 4.12: TEM images of samples a) CT(H2)_Ad+Ag(0.005M)_T1 14KX magnification, b) CT(H2)_Ad+Ag(0.005M)_T2 13KX magnification, c) CT(H2)_Ad+Ag(0.005M)_T1 13KX magnification. From left to right, for each samples, the protective platinum layer, the titanium oxide layer with the silver nanoparticles, and the Ti6Al4V bulk structure are visible.

In Figure 4.12 the microstructure of the titanium alloy is visible with elongated crystals in the direction of the extrusion of the bar from which the samples were cut. The attack with hydrofluoric acid digs the grain boundaries alloying the following growth of titanium oxide in the superficial space between the grains. In Figure 4.13 images at 40KX of the samples are reported.

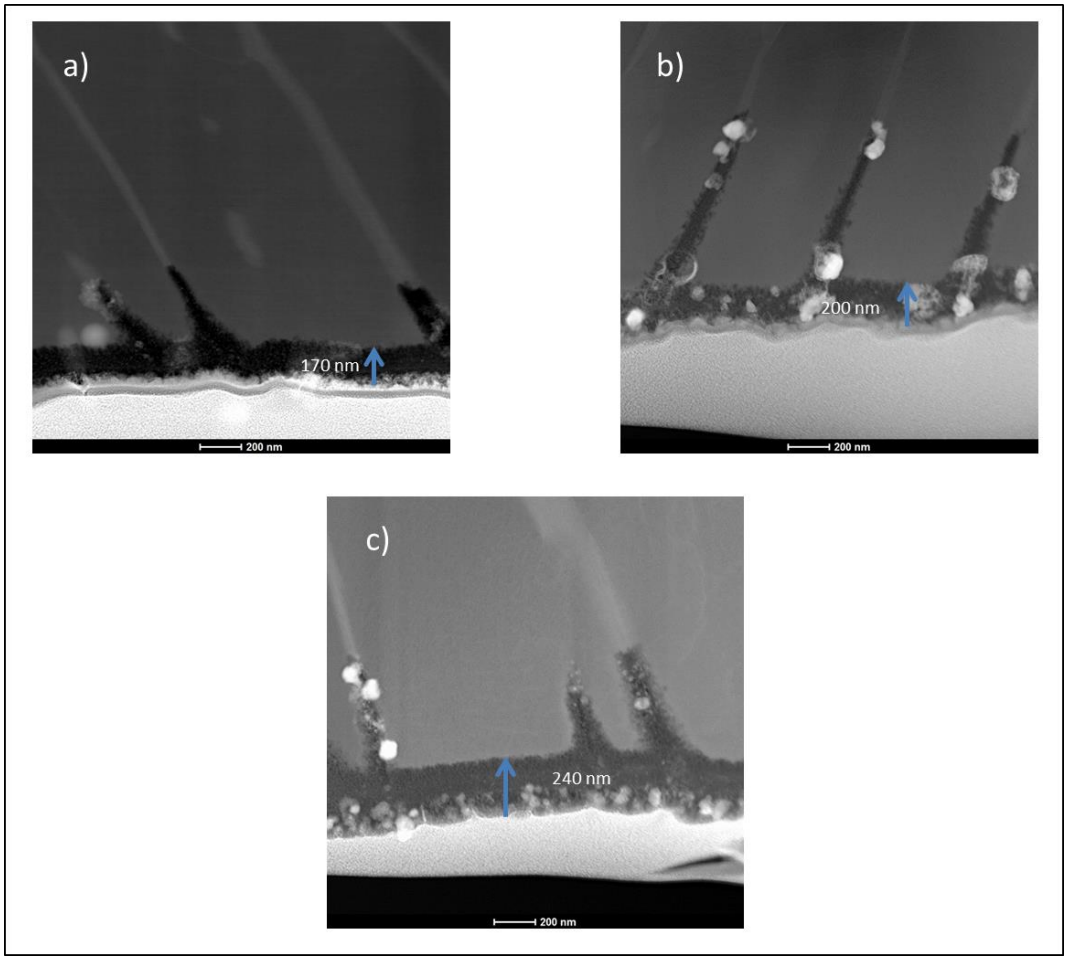

Figure 4.13: TEM images of samples a) CT(H2)_Ad+Ag(0.005M)_T1, b) CT(H2)_Ad+Ag(0.005M)_T2, c) CT(H2)_Ad+Ag(0.005M)_T1. 40 KX magnification.

At this magnification the difference in the thickness of the oxide layer is visible. For the sample CT(H2)_Ad+Ag(0.005M)_T1 the thickness of the oxide layer is around 170 nm, for the sample CT(H2)_Ad+Ag(0.005M)_T2 is around 200 nm and for the sample CT(H2)_Ad+Ag(0.005M)_T3 is around 240 nm. This difference in the oxide thickness is correlated with the timing of silver precursor addition. The sooner the silver precursor where added during the growth of the oxide layer, the thinner is the final layer. It has already been observed [82] that the introduction of silver into the hydrogen peroxide solution reduces the final thickness of the oxide layer. This phenomenon can be explained considering that in presence of silver both silver reduction and titanium oxidation occur at the material surface and in these conditions the growing rate of the titanium oxide layer can be slowed down. In these images, it is also possible to see the presence

of nanoparticles around 50 nm along the thickness of the oxide layer and in contact even with the nude titanium alloy substrate even on the samples in which the silver precursor where added after an initial growth of the oxide layer (Fig 4.13 b, c). It means that the micro and nano structure of the oxide layer let pass silver atoms allowing the formation of the silver nanoparticles also inside the oxide layer itself. An accumulation of silver nanoparticles on the titanium oxide developed on the superficial grain boundaries is well visible.
More detailed images at higher magnification of these samples are reported in Figure 4.14.

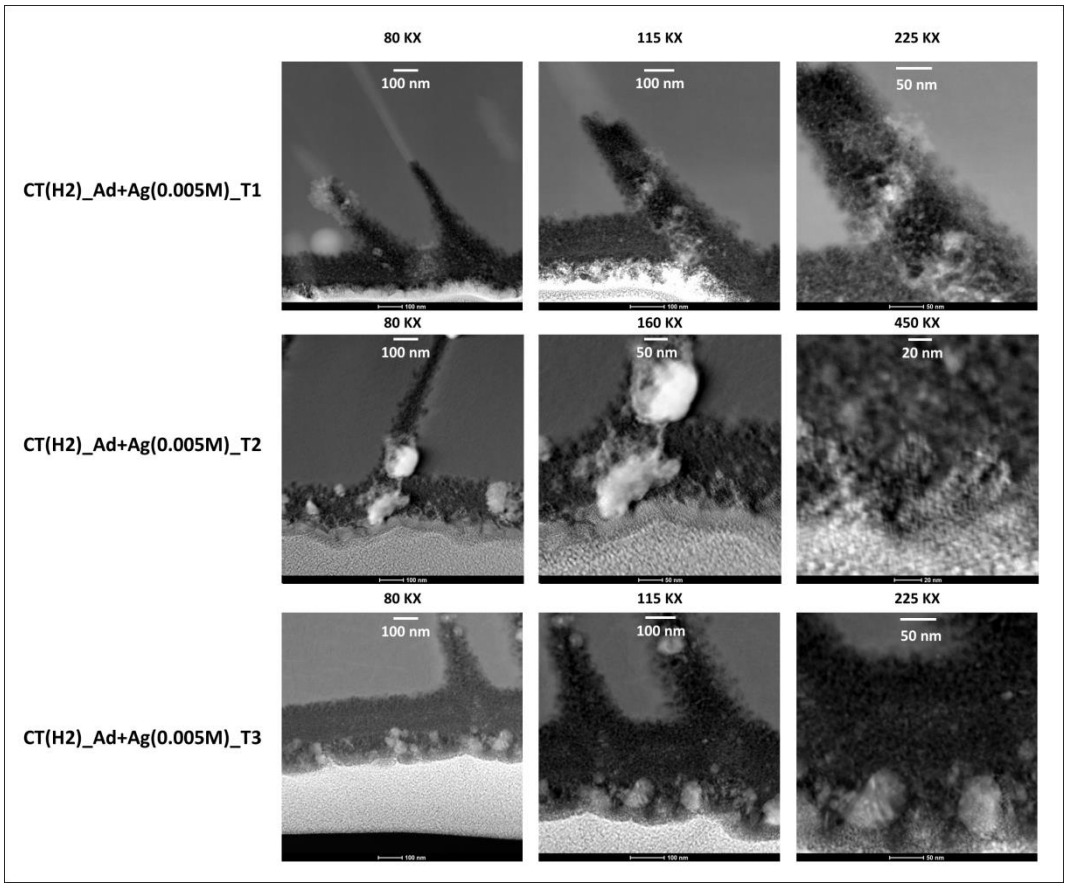

Figure 4.14: TEM images of samples CT(H2)_Ad+Ag(0.005M)_T1, CT(H2)_Ad+Ag(0.005M)_T2, CT(H2)_Ad+Ag(0.005M)_T1. 40 KX magnification.

In Figure 4.14, the presence of nanoparticles of few nanometers and of bigger nanoparticles around 50 nm is visible for all the samples. For sample CT(H2)_Ad+Ag(0.005M)_T1, the nanoparticles seems to be small and well distributed in the oxide layer. For sample CT(H2)_Ad+Ag(0.005M)_T2, the

nanoparticles seems to be preferentially in the middle of the oxide layer and between the grain boundaries, while for samples CT(H2)_Ad+Ag(0.005M)_T3 the nanoparticles are preferentially on the surface of the oxide layer and some particles are between the grain boundaries. In order to better understand the silver distribution of the silver nanoparticles in the oxide layer, STEM-EDS and linescan analyses were performed and are reported in Figure 4.15 and 4.16.

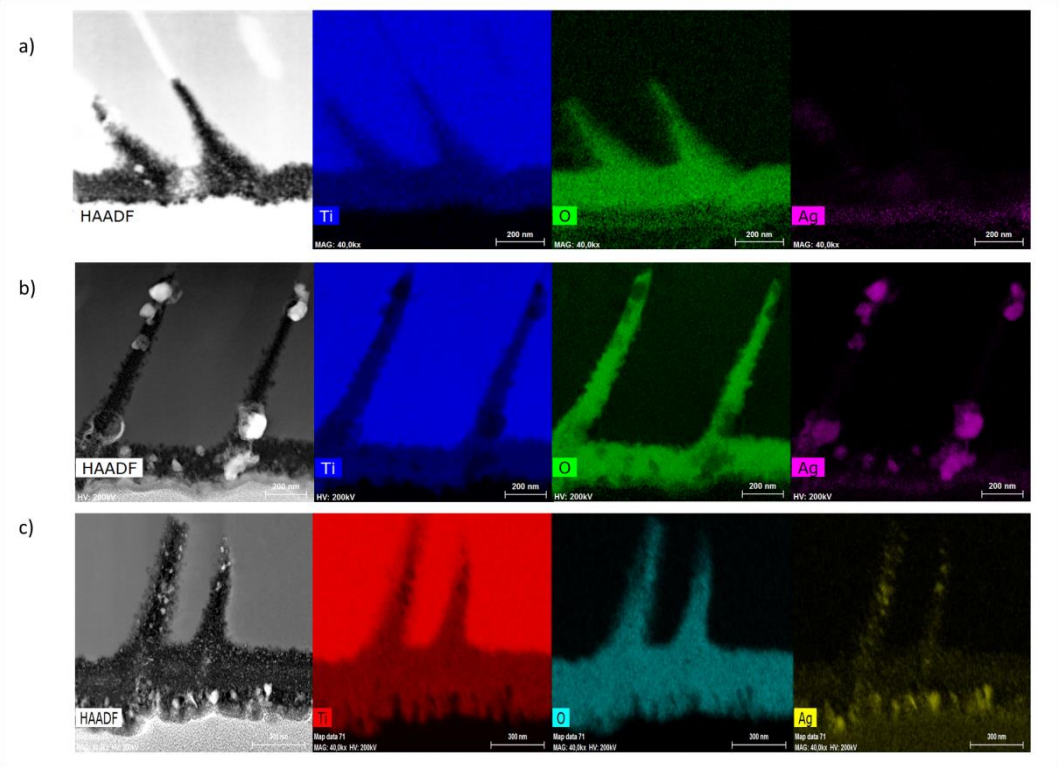

Figure 4.15: STEM_EDS maps of samples a)CT(H2)_Ad+Ag(0.005M)_T1, b) CT(H2)_Ad+Ag(0.005M)_T2, c) CT(H2)_Ad+Ag(0.005M)_T1. 40 KX magnification.

The STEM-EDS maps confirm the conclusion drowns from the images, For sample CT(H2)_Ad+Ag(0.005M)_T1, the nanoparticles are well dispersed in the oxide layer (Fig 4.15a), for samples CT(H2)_Ad+Ag(0.005M)_T2, there are nanoparticles and bigger agglomerates in the middle of the oxide layer, but also in the oxide between the grain boundaries and for samples CT(H2)_Ad+Ag(0.005M)_T3 the nanoparticles are bigger than the ones of samples CT(H2)_Ad+Ag(0.005M)_T1, but smaller than the agglomerates of sample CT(H2)_Ad+Ag(0.005M)_T2 and are mainly distributed on the surface of the oxide layer and in a minor amount in the grain boundaries.

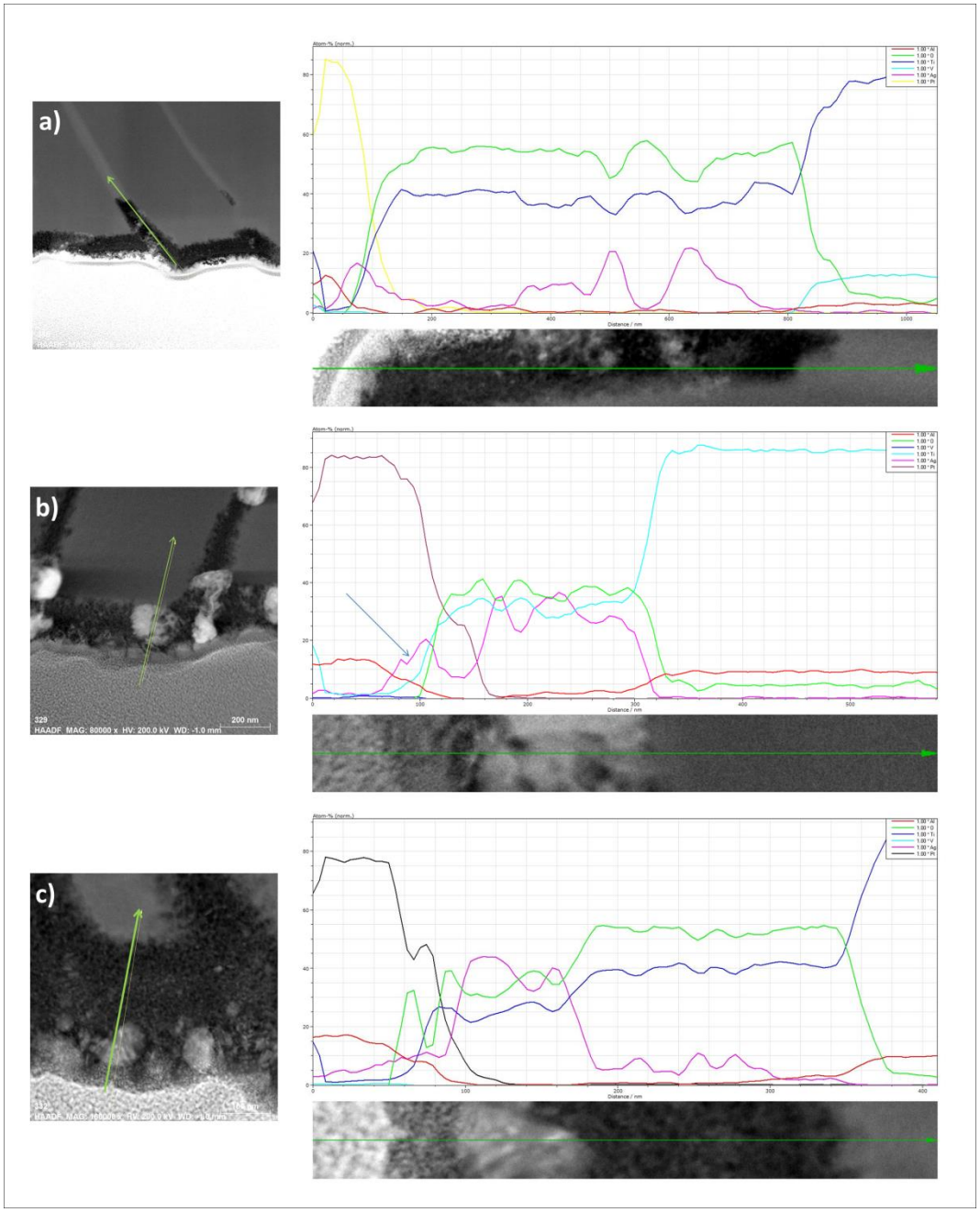

Figure 4.16: linescan of samples CT(H2)_Ad+Ag(0.005M)_T1, CT(H2)_Ad+Ag(0.005M)_T2, CT(H2)_Ad+Ag(0.005M)_T1. 40 KX magnification. Purple line= silver atomic%, blue line=titanium atomic %, red line= aluminum atomic %, green line= oxygen atomic %, light blue line= vanadium atomic %, yellow line= platinum atomic percentage.

The linescans of the samples (with the atomic percentage of the elements) reported in Figure 4.16, confirm again the previous results. For samples CT(H2)_Ad+Ag(0.005M)_T1 (Fig. 4.16a), silver is quasi-homogeneously disperses, with two peaks in correspondence with bigger silver nanoparticles. For samples CT(H2)_Ad+Ag(0.005M)_T2 (Fig. 4.16b) silver is well present in the entire layer with aggregates in the middle and at the grain boundaries. In the end, for sample CT(H2)_Ad+Ag(0.005M)_T3 (Fig 4.16c), the higher amount of nanoparticles is on the surface of the oxide layer.
These analyses suggest that the different protocols with different timing of adding of the silver precursor and the additives allows to obtain different distribution of the nanoparticles and that even after the growth, the sponge-like structure of the chemically treated titanium oxide allows the transit of silver and the formation of silver nanoparticles inside it.

4.10.3 Silver release

The silver release was performed in ultrapure water after 3 hours, 1, 2, 7, 14 and 28 days for the samples:

- CT(H1)_Ad+Ag(0.005M)_T1
- CT(H1)_Ad+Ag(0.005M)_T2
- CT(H1)_Ad+Ag(0.005M)_T3
- CT(H1)_Ad+Ag(0.001M)_T1
- CT(H1)_Ad+Ag(0.001M)_T2
- CT(H1)_Ad+Ag(0.001M)_T3
- CT(H2)_Ad+Ag(0.005M)_T1
- CT(H2)_Ad+Ag(0.005M)_T2
- CT(H2)_Ad+Ag(0.005M)_T3

A preliminary results was also obtained at 24 h for the sample CT(H2)_Ad+Ag(0.001M)_T2.
In Figure 4.17, the silver release over time of samples treated with solution H1 is reported.

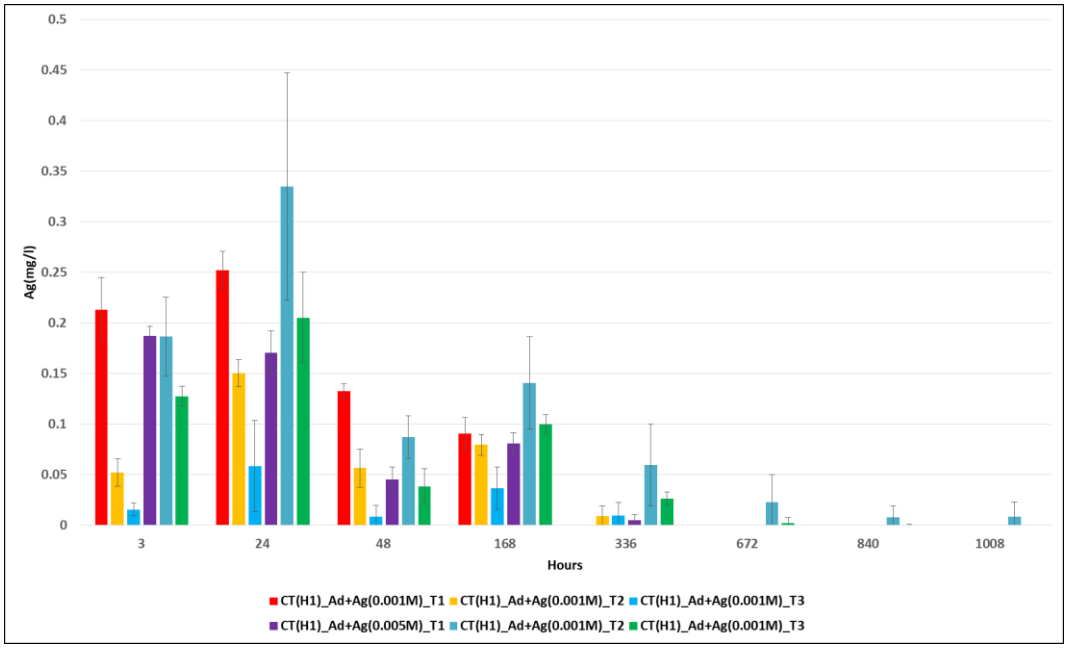

Figure 4.17: silver release over time of samples CT treated with acid H1 with the in situ reduction of silver nanoparticles.

Except for the samples with the T1 protocols, the samples treated with the higher amount of silver have a higher release after 24h.
For the samples with the silver precursor concentration 0.001M, the release lasts up to 7 days for the samples with the protocol T1 and up to 14 days for the protocols T2 and T3.
For the samples with the silver precursor concentration 0.005M the release lasts up to 14 days for samples T1, up to 42 days for samples T2 and 35 days for samples T3. The addition of the additives and the silver precursor after a first growth of the oxide layer, such as protocols T2 and T3 seems to lead to sustain release for longer period of time when increasing the silver precursor content.
The higher standard deviation can be correlated with the release of the silver salt due to the use of the solution H1.
The graph of the cumulative silver release is reported in Figure 4.18 in order to understand if the amount of silver released is compatible with the antibacterial purpose of the treatment and if it could avoid cytotoxic effects.

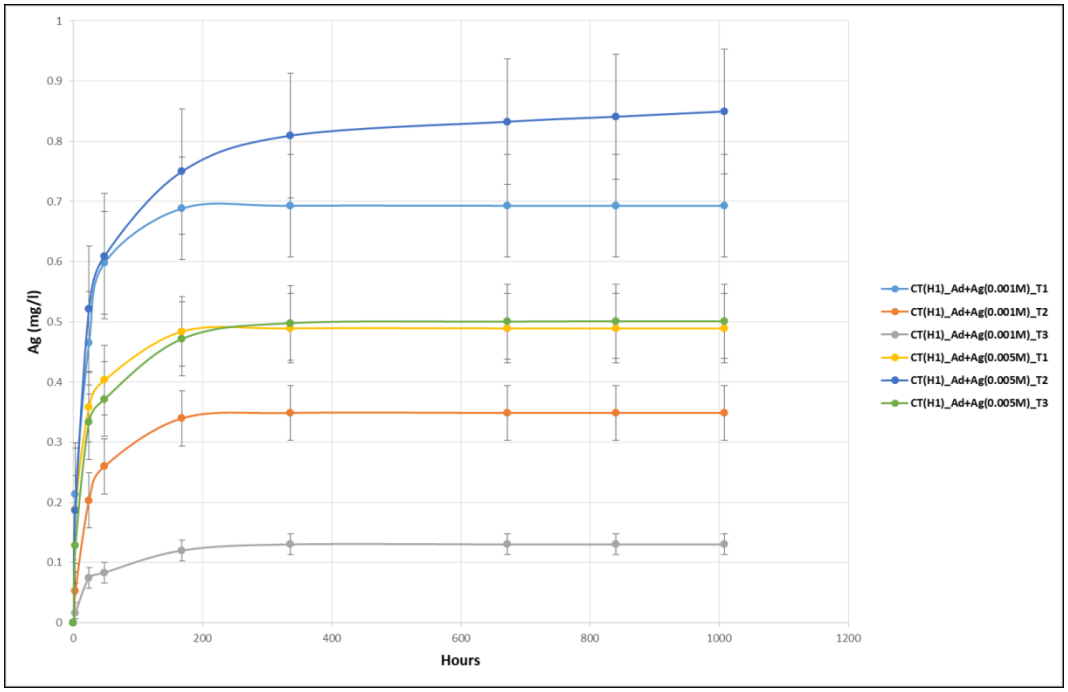

Figure 4.18: silver cumulative release of samples CT treated with acid H1 with the in situ reduction of silver nanoparticles.

In Figure 4.18, it is possible to see that the samples CT(H1)_Ad+Ag(0.005M)_T2, which exhibit the longest ion release, also has the higher amount of released silver (around 0.84 mg/l), which is closer of the amount 1 mg/l of the MIC of many bacteria, but significantly lower than the LC_{100} (concentration at which 100% of the cells die) of fibroblast which is 60 mg/ml [10], [20], [21]. For the other samples, the cumulative release is lower and distant from the MIC of the principal bacteria. In order to avoid the effects due to the deposition of silver salt, the samples with the higher concentration of silver precursor were prepared using solution H2 instead of solution H1 and the release was tested again and the result over time is reported in Figure 4.19.

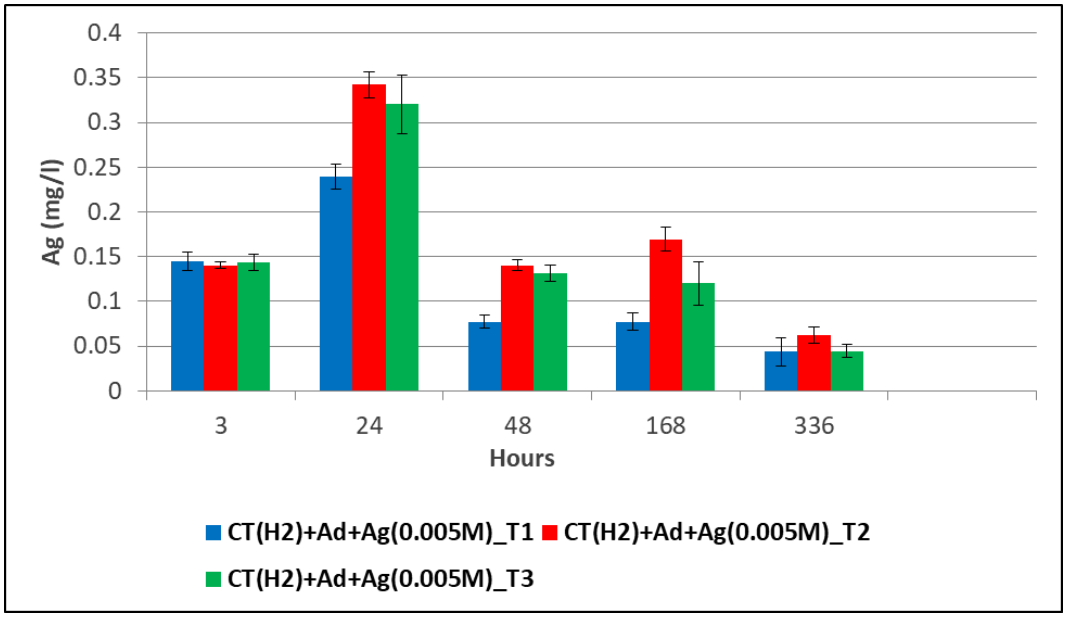

Figure 4.19: silver release over time of samples CT treated with acid H2 with the in situ reduction of silver nanoparticles.

Such as for the samples treated with the solution H1, the maximum of the release is at 24 h and it is higher for the samples treated with the protocol T2. For all these samples, the silver release lasts up to 14 days which is a shorted time if compared with what observed before, but the standard deviation of each sample is significantly lower indicating greater reproducibility and uniformity of the samples. The graph of the cumulative silver release is reported in Figure 4.20 in order to understand also for these samples if the amount of silver released is compatible with the antibacterial purpose of the treatment and if it could avoid cytotoxic effects.

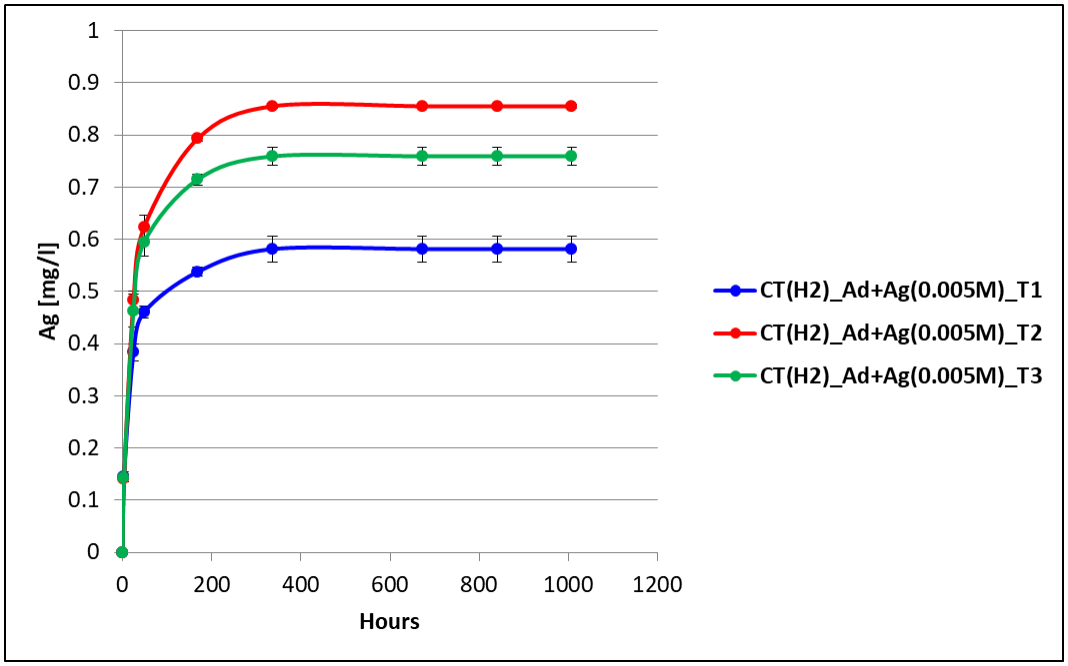

Figure 4.20: silver cumulative release of samples CT treated with acid H2 with the in situ reduction of silver nanoparticles.

The cumulative release is again higher for the samples treated with the protocol T2 and it is 0.85 mg/l, similar to what observed before for the samples treated with the protocol T2 with solution H1. Because of the absence of silver salts, the distribution of the silver nanoparticles in all the thickness of the oxide layer, the release lasting until 14 days with an amount of silver suitable for antibacterial purpose and the reproducibility, the samples CT(H2)_Ad+Ag(0.005M)_T2 seems to be the more promising for the bone contact applications purpose of this work.
The silver release was also performed only at 24 h for the samples CT(H2)_Ad+Ag(0.001M)_T2 obtaining a values of 0.05±0.03 mg/ml.
In order to clarify the results, the principal characteristics of the samples are resumed in Table 4.15.

Table 4.15: resume of the results obtained for the different samples.

Samples	**$AgNO_3$ concentration**	**Protocol**	**Silver salt**	**Silver release (days)**	**Release at 24 h (mg/l)**	**Cumulative silver release (mg/l)**
CT(H1)_Ad+Ag(0.005M)_T1	0.005M	T1	yes	14	0.17±0.02	0.49±0.05
CT(H1)_Ad+Ag(0.005M)_T2	0.005M	T2	yes	42	0.33±0.11	0.84±0.06
CT(H1)_Ad+Ag(0.005M)_T3	0.005M	T3	yes	35	0.20±0.04	0.50±0.10
CT(H1)_Ad+Ag(0.001M)_T1	0.001M	T1	yes	7	0.25±0.02	0.69±0.04
CT(H1)_Ad+Ag(0.001M)_T2	0.001M	T2	yes	14	0.15±0.01	0.35±0.02
CT(H1)_Ad+Ag(0.001M)_T3	0.001M	T3	yes	14	0.06±0.05	0.13±0,11
CT(H2)_Ad+Ag(0.005M)_T1	0.005M	T1	no	14	0.24±0.01	0.58±0.03
CT(H2)_Ad+Ag(0.005M)_T2	0.005M	T2	no	14	0.34±0.01	0.85±0.01
CT(H2)_Ad+Ag(0.005M)_T3	0.005M	T3	no	14	0.32±0.03	0.76±0.02
CT(H2)_Ad+Ag(0.001M)_T2	0.001M	T2	no	unknown	0.05±0.03	unknown

4.10.4 Antibacterial tests

Broth dilution method:

The CFU plate counting of the bacterial (*Staphylococcus aureus*) adhesion test performed on the samples CT(H2) with the in situ silver nanoparticles reduction is reported in Figure 4.21 and 4.22 and CT(H2) samples without the silver nanoparticles reduction were used as control series.

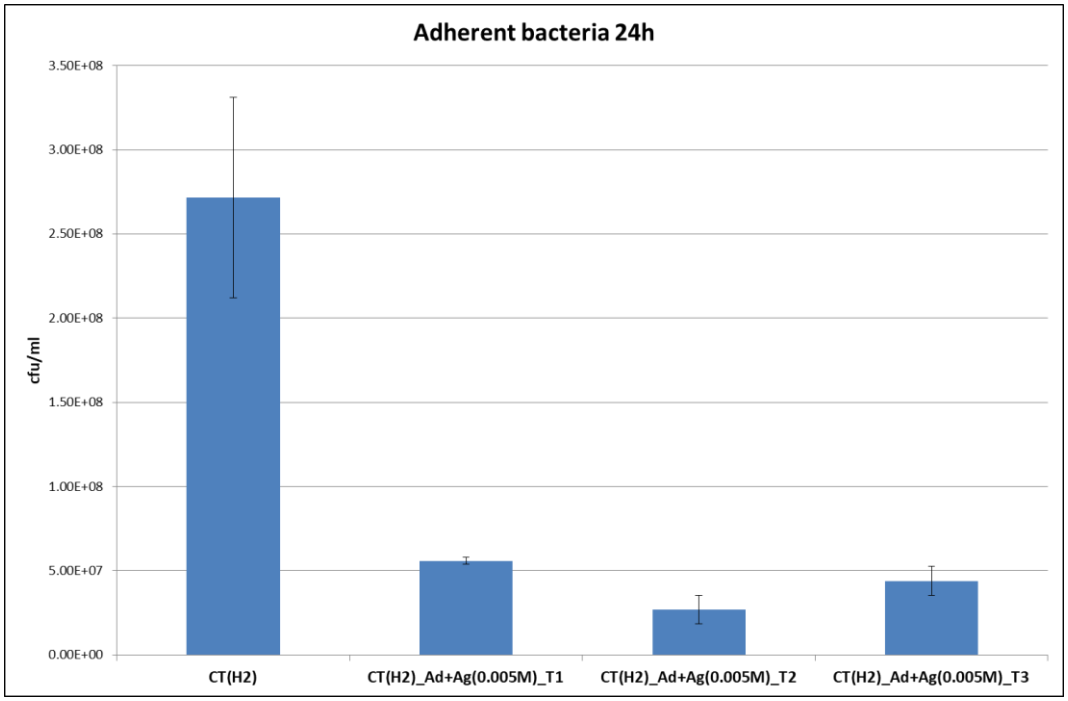

Figure 4.21: amount of adherent bacteria on examined samples.

The medium amount of the adherent bacteria present on the control samples CT(H2) after 24h of incubation is $2.4*10^8 \pm 5.9*10^7$ CFU/ml. For the samples with the in situ reduction of silver nanoparticles the count of the adherent bacteria decreases of one order of magnitude, indeed the count is $5.6*10^7 \pm 1.1*10^6$ CFU/ml for samples CT(H2)_Ad+Ag(0.005M)_T1, $2.7*10^7 \pm 8.3*10^6$ CFU/ml for samples CT(H2)_Ad+Ag(0.005M)_T2 and $4.4*10^7 \pm 8.6*10^6$ CFU/ml for samples CT(H2)_Ad+Ag(0.005M)_T3. The presence of silver reduces the amount of bacteria adherent to the surface of the samples, but the reduction is lower than what expected.

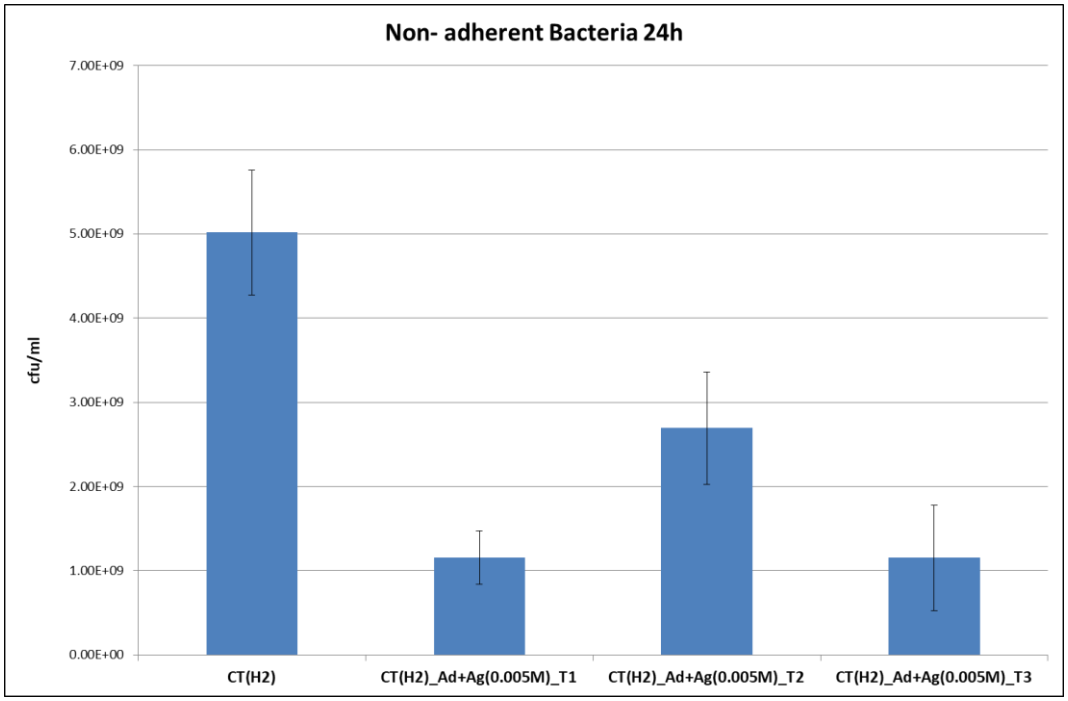

Figure 4.22: amount of non-adherent bacteria on examined samples.

Also in the non- adherent bacteria, as reported in the graph in Figure 4.22, it is possible to see a reduction in the number of bacteria for the samples functionalized with the silver nanoparticles. However, this reduction is less than one order of magnitude and is smaller than what expected. Considering that the aim of this research is to avoid biofilm formation on titanium implants and this kind of test seems to be not completely reliable, we decide to pursue with test more focused on the surface behavior.

Evaluation of biofilm formation on modified surfaces:

On the basis of the previous release results and on the analysis on the cross section, the antibacterial properties were evaluated for two kinds of samples:

- CT(H2)_Ad+Ag(0.005M)_T2
- CT(H2)_Ad+Ag(0.001M)_T2

The activity of the samples with the higher amount of silver, CT(H2)_Ad+Ag(0.005M)_T2, are reported in Figure 4.23 for what concerns the floating planktonic cells and in Figure 4.24 for what concern biofilm formation.

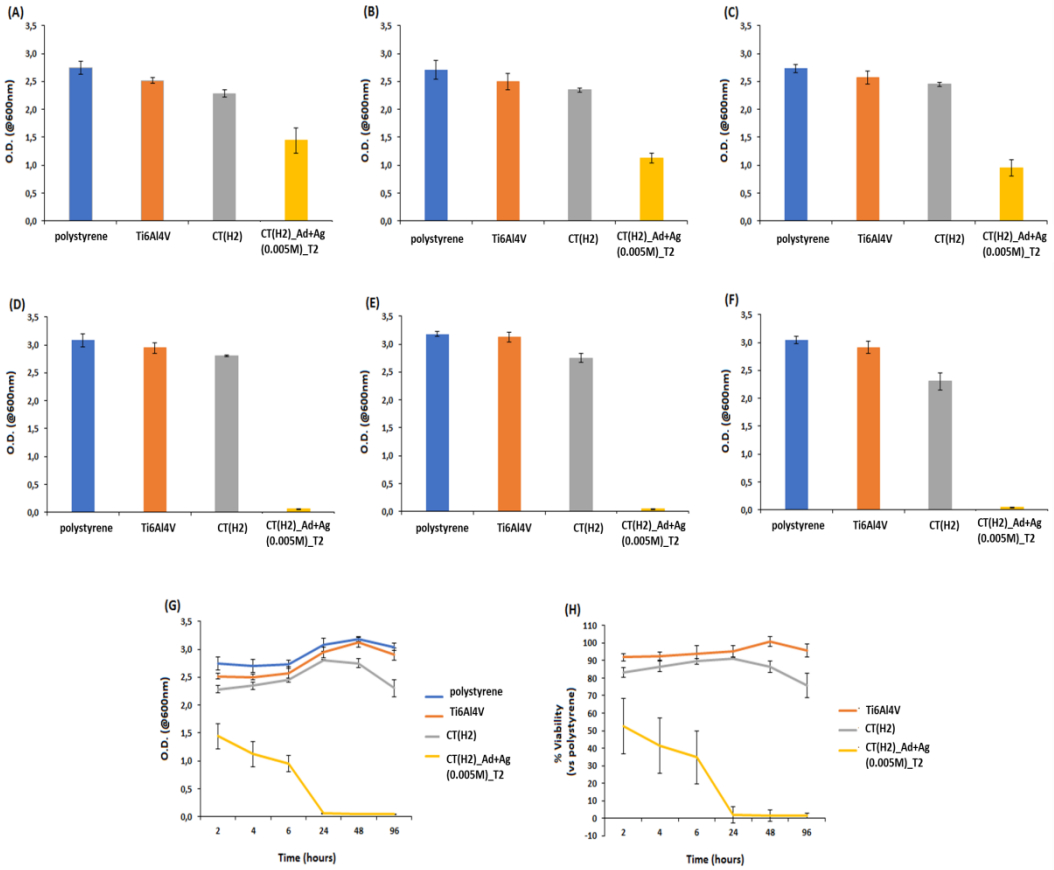

Figure 4.23: S. aureus planktonic cells viability after 2 (A), 4 (B), 6 (C), 24 (D), 48 (E), 96 (F) hours. Only Ag-doped specimens (CT(H2)_Ad+Ag(0.005M)_T2) were effective in reducing bacteria viability. Particular, no live bacteria were detected after 24 hours infection. Results are summarized as O.D. in function of time (G) and % viability towards untreated controls (H). Bars represent means and standard deviations.

In general, the samples with the silver nanoparticles in situ reduction showed a strong antibacterial activity towards both floating planktonic cells (Figure 4.23) and adhered biofilm counterparts (Figure 4.24).

According to the obtained results, CT(H2)_Ad+Ag(0.005M)_T2 samples are able to release an effective amount of Ag ions to determine floating bacteria killing within 24 hours (Fig,. 4.23); in fact, bacteria viability is early markedly decreased at 2 (A), 4 (B) and 6 (C) hours infection, but after 24 hours (D) no viability is further detected. Accordingly, following 48 (E) and 96 (F) time points confirmed that all floating planktonic cells are killed by the Ag ions released from CT(H2)_Ad+Ag(0.005M)_T2 samples. Only a small reduction is obtained on the

bare CT(H2) samples if compared with the polished Ti6Al4V samples and with the polystyrene control.

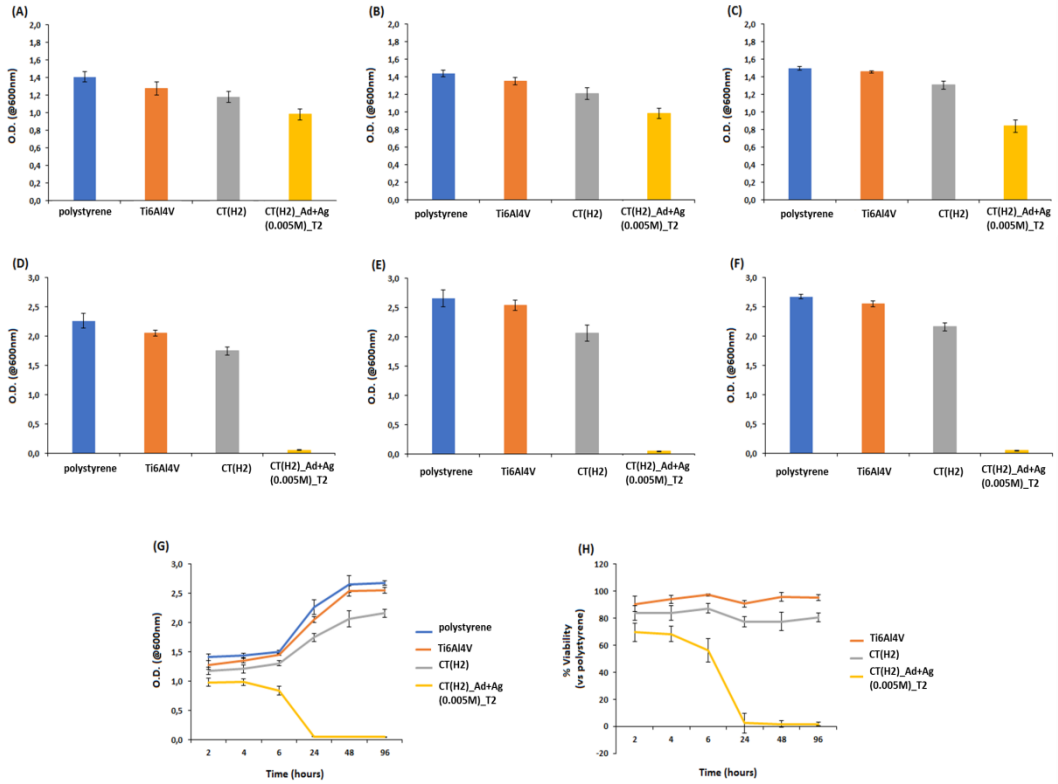

Figure 4.24: S. aureus biofilm cells viability after 2 (A), 4 (B), 6 (C), 24 (D), 48 (E), 96 (F) hours. Only samples with silver nanoparticles (CT(H2)_Ad+Ag(0.005M)_T2) were effective in reducing bacteria viability. Particular, no live bacteria were detected after 24 hours infection. Results are summarized as O.D. in function of time (G) and % viability towards untreated controls (H). Bars represent means and standard deviations.

Similar results are obtained by evaluating samples' activity towards *S. aureus* biofilm (Figure 4.24). Only samples with silver nanoparticles (CT(H2)_Ad+Ag(0.005M)_T2) are effective in reducing biofilm viability even at early time-points 2 (A), 4 (B) and 6 (C) hours. No living bacteria are noticed after 24 (D), 48 (E), and 96 (F) hours. Accordingly, O.D. values are significantly reduced during experimental time (G) as well as bacteria % viability (expressed as function of untreated controls) is reduced until reach < 1% after 24 hours.
Finally, fluorescence Live/Dead assay performed onto 96 hours biofilm specimens (Figure 4.25) confirms the presence of live bacteria onto untreated TI6Al4V mirror polished surfaces (upper panel, stained in green) while only few random

dead ones are noticed onto CT(H2)_Ad+Ag(0.005M)_T2 surfaces (lower panel, stained in red).

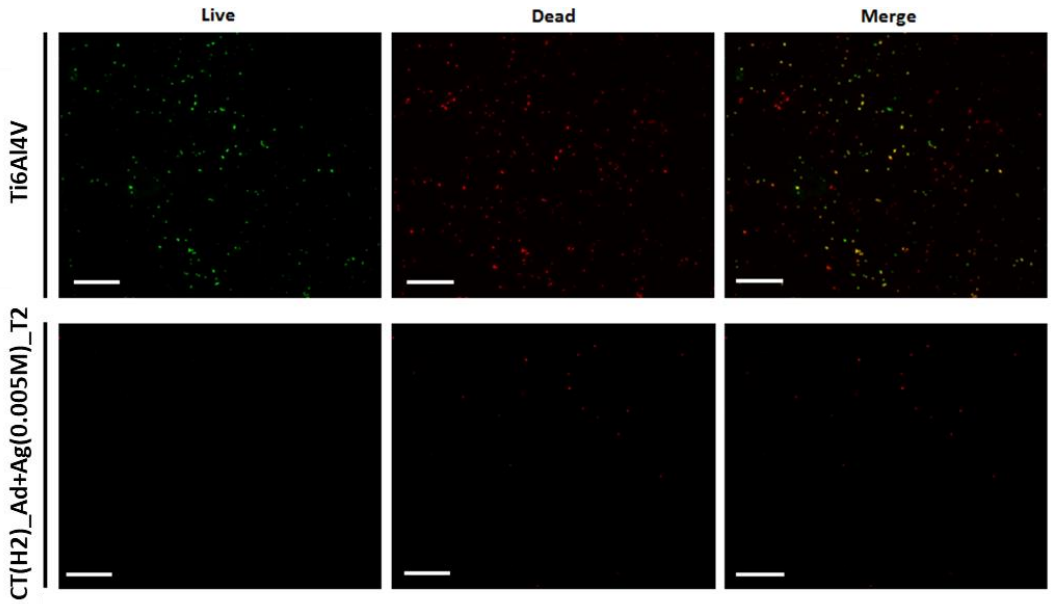

Figure 4.25: Live/Dead assay onto 96 hours *S. aureus* biofilm. Untreated Ti6Al4V mirror polished surfaces showed the presence of homogeneous living bacteria (upper panel, in green) while CT(H2)_Ad+Ag(0.005M)_T2 surfaces presented only few random dead bacteria (lower panel, in red). Magnification 20x, bar scale = 25 um.

On the bacterial broth used for this analysis, inductively coupled plasma mass spectrometry (ICP) investigations were also performed in order to observe the silver release in the bacterial broth and the results are reported in Figure 4.26.

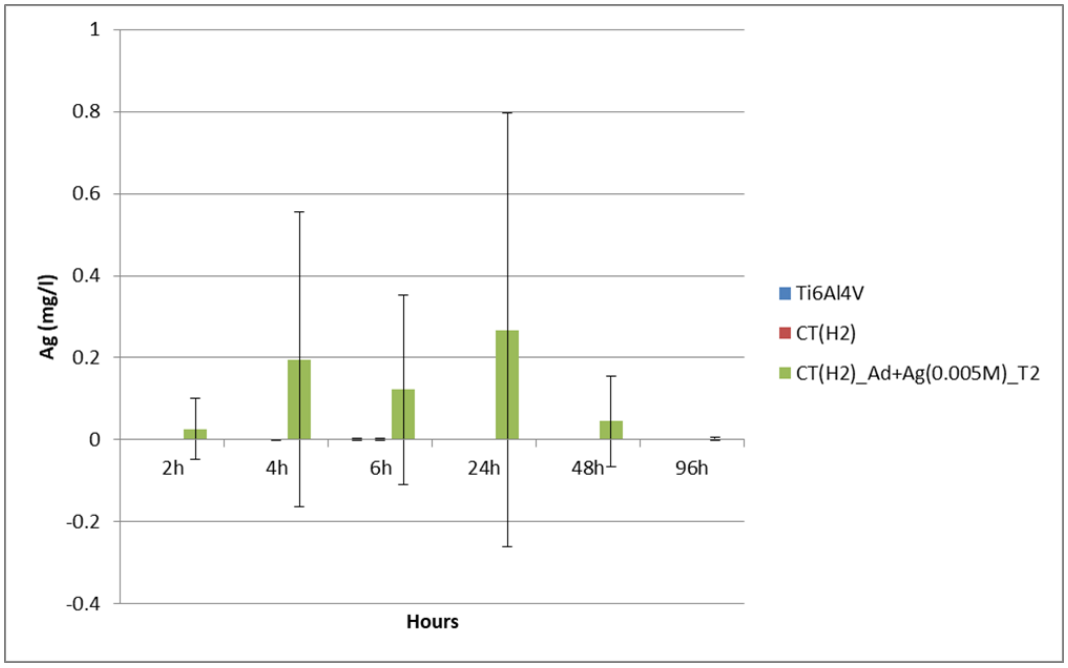

Figure 4.26: silver release in bacterial broth.

In the bacterial broth the samples seem to release silver until 48 hours with a maximum at 24h. The mean values are lower than the ones observed for the release in double distilled water, but the standard deviation is really high. On the basis of the strong effects observed on bacteria, the low mean values and the high standard deviations could be correlated with the reaction of the silver with broth proteins which can make silver randomly not detected by the analysis and by the internalization of the silver by bacteria which have been removed from the solution before the ICP analysis.

These results on bacteria shows strong effects of samples CT(H2)_Ad+Ag(0.005M)_T2 against *Staphylococcus aureus*. On the basis of these important results that eliminate the bacterial contamination from the surfaces, samples with a smaller concentration of silver were tested. The activity of the samples with the smaller amount of silver, CT(H2)_Ad+Ag(0.001M)_T2, is reported in Figure 4.27 for what concern the floating planktonic cells and in Figure 4.27 for what concern biofilm.

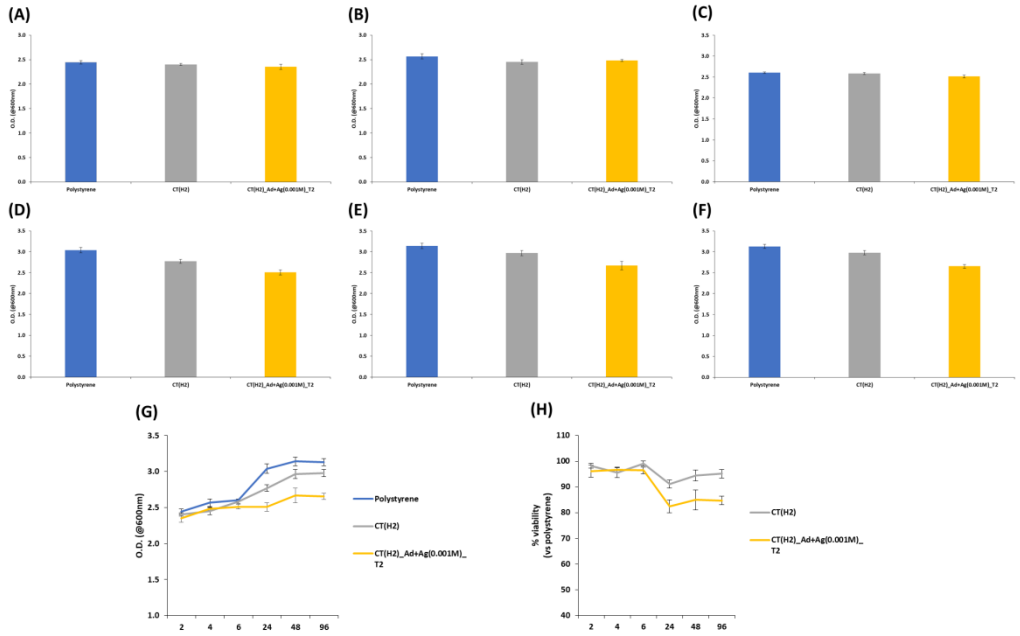

Figure 4.27: S. aureus planktonic cells viability after 2 (A), 4 (B), 6 (C), 24 (D), 48 (E), 96 (F) hours. Only specimens (CT(H2)_Ad+Ag(0.001M)_T2) were effective in reducing bacteria viability. Results are summarized as O.D. in function of time (G) and % viability towards untreated controls (H). Bars represent means and standard deviations.

Despite from what observed for the samples with the silver concentration 0.005M, the samples with silver 0.001M show a weak antibacterial activity towards floating planktonic cells (Figure 4.27), but a strong activity on adhered biofilm counterparts (Figure 4.28).
According to the silver release at 24 hours, samples CT(H2)_Ad+Ag(0.001M)_T2 are able to release a small amount of Ag ions able to kill, after 24 h, only 10% of the floating bacteria; in fact, bacteria viability is not markedly decreased at 2 (A), 4 (B), 6 (C), 24 hours (D), 48 hours (E) and (F) 96 hours.

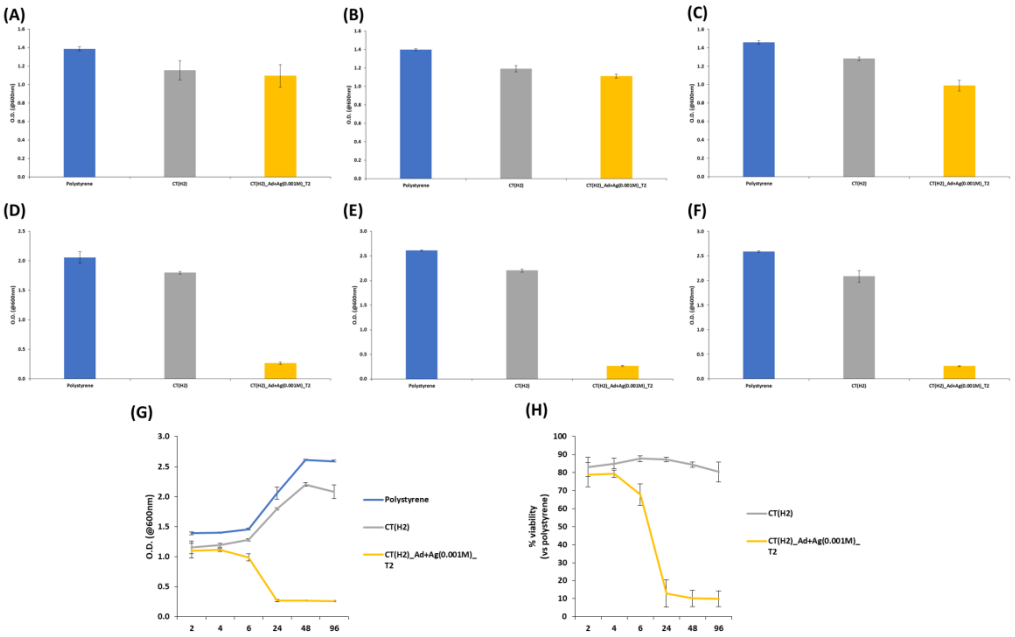

Figure 4.28: S. aureus biofilm cells viability after 2 (A), 4 (B), 6 (C), 24 (D), 48 (E), 96 (F) hours. Only samples (CT(H2)_Ad+Ag(0.001M)_T2) were effective in reducing bacteria viability. Results are summarized as O.D. in function of time (G) and % viability towards untreated controls (H). Bars represent means and standard deviations.

Despite of the results on floating planktonic bacteria, the effects of samples CT(H2)_Ad+Ag(0.001M)_T2 on biofilm is evident in Figure 4.28.
CT(H2)_Ad+Ag(0.001M)_T2 were effective in reducing biofilm viability even at early time-points 2 (A), 4 (B) and 6 (C) hours. Only 10% living bacteria were noticed after 24 (D), 48 (E), and 96 (F) hours. Accordingly, O.D. values were significantly reduced during experimental time (G) as well as bacteria % viability (expressed as function of untreated controls) was reduced until reach < 10% after 24 hours.
On the basis of these results the samples with the higher amount of silver are bactericide while the samples with the lower amount of silver have poor bactericide activity but, a good bacteriostatic property.

4.10.5 Cytocompatibility tests

Toxicity of the samples CT(H2)_Ad+Ag(0.005M)_T2 is evaluated towards human osteoblasts progenitor (hFOB) after 24(A), 48 (B) and 72(C) hours of direct seeding on . The results are reported in Figure 4.29.
In general, the silver functionalization introduced a marked toxic effect that was evident after 24 h (A); then, cells viability decrease continued after 48 (B) and 72 (C) hours as summarized in (D). Accordingly, cells viability was reduced of >80 % after 72 h of direct contact (E).

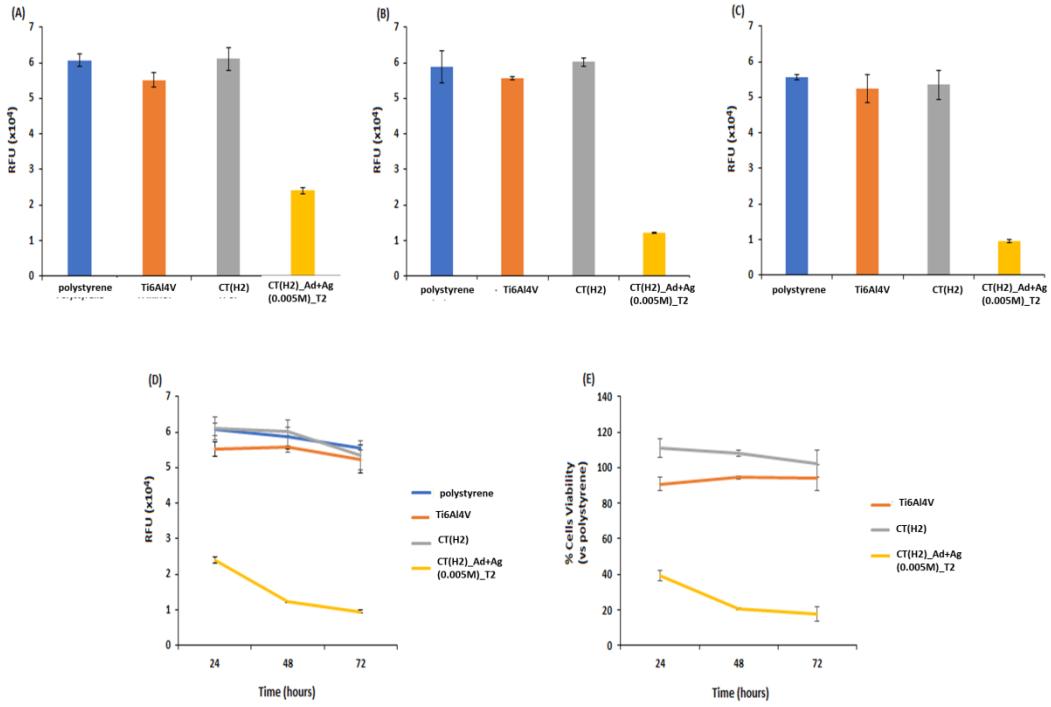

Figure 4.29: Osteoblasts progenitor hFOB cells viability. The presence of Ag induced toxicity; in fact, cells viability was markedly reduced in contact with CT(H2)_Ad+Ag(0.005M)_T2 specimens while no toxic effects were notice for the bare CT(H2) ones. Bars represent means and standard deviations.

These results evidenced strong cytotoxic effects of the samples that were not expected by observing the amount of silver released. These effects could be correlated with the direct contacts of cells with the silver nanoparticles onto the substrates. The same test was performed for the samples

CT(H2)_Ad+Ag(0.001M)_T2 with the lower amount of silver and are reported in Figure 4.30.

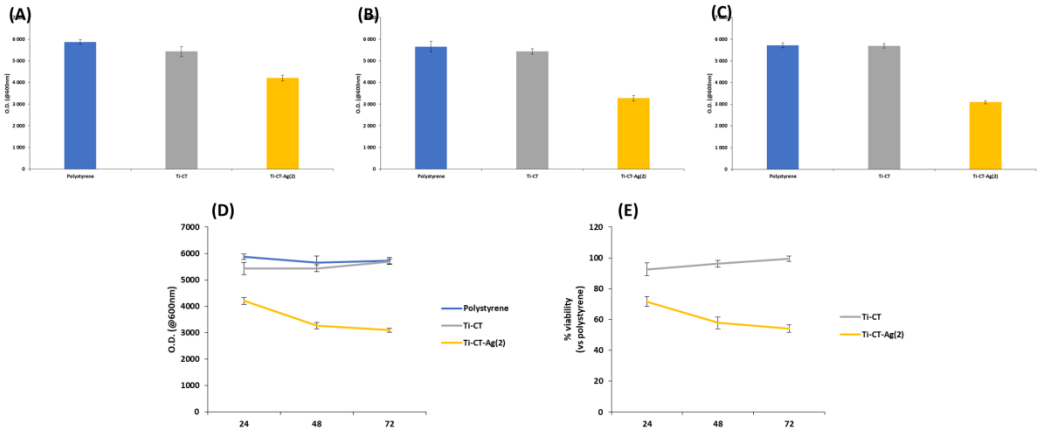

Figure 4.30: Osteoblasts progenitor hFOB cells viability. The presence of Ag doping determined toxicity; in fact, cells viability was reduced in contact with CT(H2)_Ad+Ag(0.001M)_T2 samples while no toxic effects were notice for the bare CT(H2) ones. Bars represent means and standard deviations.

The silver functionalization with the lower amount of silver introduced again a marked toxic effect that was evident after 24 hours (A); then, cells viability decrease continued after 48 (B) and 72 (C) hours as summarized in (D). Accordingly, cells viability was reduced of >54 % after 72 hours of direct contact (E). The cytotoxic effect is lower than the previous observed for the samples CT(H2)_Ad+Ag(0.005M)_T2, but it is still relevant and higher than what expected. However, the good behavior against biofilm and the reduction of the cytotoxic effects of the samples with the lower amount of silver are interesting results in the perspective to obtain bacteriostatic material tailoring again the silver content of the samples.

4.11 Conclusions

The work exposed in this chapter was devoted to the in situ reduction of silver nanoparticles on the surface of the titanium alloy Ti6Al4V during the growth of a micro e nano structured layer of titanium oxide bioactive and suitable for bone contact applications. The use of two different solutions, H1 and H2, during the patented chemical treatment and the development of three different protocols which involve the addition of additive and silver precursor at different steps of the patented chemical treatment were investigated using two different concentration of the silver precursor $AgNO_3$ (0.005M and 0.001M). The reaction between the silver precursor and the solution H1 leads to the formation of silver salts which implies a lack of reproducibility of the samples and a reduction of the silver active against bacteria. With the solution H2 the problem of the silver salts deposition was overcome by obtaining more reproducible samples with nanoparticles exposed on the surfaces with diameter between 50 and 5 nm, as confirmed by FESEM and XPS analysis. The samples CT(H2)_Ad+Ag(0.005M)_T1, CT(H2)_Ad+Ag(0.005M)_T2 and CT(H2)_Ad+Ag(0.005M)_T3 were also analyzed with TEM and STEM-EDS analysis on the cross section in order to investigate the distribution of the nanoparticles in the oxide layer developed with the 3 different protocols. The images on the cross section showed a more uniform distribution of the nanoparticles in almost all the thickness of the oxide for the protocol T2. On the basis of these results and of the silver release tests in water samples CT(H2)_Ad+Ag(0.005M)_T2 and CT(H2)_Ad+Ag(0.001M)_T2 were chosen for antibacterial and cellular tests. Samples CT(H2)_Ad+Ag(0.005M)_T2 with a release in water of 0.83 mg/l showed the ability to reduce to <1% the count of planktonic bacteria and is also totally effective against biofilm, however these samples results also highly cytotoxic, much more that what expected observing the silver release in water. For this reason the same tests were performed on samples CT(H2)_Ad+Ag(0.001M)_T2. The effects of these samples on planktonic bacteria are lower than the one observed for the previous samples, but the effects on biofilm remain strong and the cytotoxicity drops to around 50%. The results on these samples suggest the possibility of treat the titanium alloy in order to obtain a bioactive surface, suitable for bone contact applications and with in situ reduction of nanoparticles in order to confer bacteriostatic properties to the surface after a further tailoring of the silver precursor amount used for the functionalization. More investigations are needed with particular attention to the silver release tests. The high affinity of silver to react with many compounds and its possible release of silver not only in the ionic for, but also as nanoparticles or

clusters could made the detection with photometrical methods or by ICP not completely exhaustive and a more accurate measure of the silver released by samples can be obtained digesting the release solution before the analysis. Tailoring the amount of the silver precursor reducing it to 0.0005M could allow to avoid cytotoxic effects maintaining the activity against biofilm formation which can plays a crucial role in avoiding the early formation of chronic infections.

References:

[1] J. Prathapachandran and N. Suresh, "Management of peri-implantitis," *Dent. Res. J. (Isfahan).*, vol. 9, no. 5, pp. 516–521, 2017.

[2] A. D. Pye, D. E. A. Lockhart, M. P. Dawson, C. A. Murray, and A. J. Smith, "A review of dental implants and infection," *J. Hosp. Infect.*, vol. 72, no. 2, pp. 104–110, 2009.

[3] D. Peres, I. Neves, F. Vieira, and I. Devesa, "Prosthesis infections after orthopedic joint replacement: the possible role of bacterial biofilms," *Acta Med. Port.*, vol. 5, no. e14, pp. 67–72, 2013.

[4] J. M. Schierholz and J. Beuth, "Implant infections: A haven for opportunistic bacteria," *J. Hosp. Infect.*, vol. 49, no. 2, pp. 87–93, 2001.

[5] C. R. Arciola, D. Campoccia, G. D. Ehrlich, and L. Montanaro, "Biofilm-based Healthcare-associated Infections," *Adv. Exp. Med. Biol.*, vol. 830, pp. 29–46, 2015.

[6] L. Le Guéhennec, A. Soueidan, P. Layrolle, and Y. Amouriq, "Surface treatments of titanium dental implants for rapid osseointegration," *Dent. Mater.*, vol. 23, no. 7, pp. 844–854, 2007.

[7] J. L. T. Albrektsson, P. -I. Branemark, H. -A. Hansson, "Osseointegrated titanium implants: Requirements for ensuring a long-lasting, direct bone-to-implant anchorage in man," *Acta Orthop. Scand.*, vol. 52, pp. 155–170, 1981.

[8] J. Gallo, M. Holinka, and C. S. Moucha, *Antibacterial surface treatment for orthopaedic implants*, vol. 15, no. 8. 2014.

[9] M. Raza, Z. Kanwal, A. Rauf, A. Sabri, S. Riaz, and S. Naseem, "Size- and Shape-Dependent Antibacterial Studies of Silver Nanoparticles Synthesized by Wet Chemical Routes," *Nanomaterials*, vol. 6, no. 4, p. 74, 2016.

[10] G. Ren, D. Hu, E. W. C. Cheng, M. A. Vargas-reus, P. Reip, and R. P. Allaker, "Characterisation of copper oxide nanoparticles for antimicrobial applications," *Int. J. Antimicrob. Agents*, vol. 33, pp. 587–590, 2009.

[11] C. Marambio-Jones and E. M. V. Hoek, "A review of the antibacterial effects of silver nanomaterials and potential implications for human health and the environment," *J. Nanoparticle Res.*, vol. 12, no. 5, pp. 1531–1551, 2010.

[12] W. von H. Werner Kühni, "1. A Brief Hstory of Silver," in *Colloidal Silver: The Natural Antibiotic*, 2016, pp. 3–9.
[13] J. L. Clement and P. S. Jarrett, "Antibacterial Silver," *Met. Based. Drugs*, vol. 1, no. 5–6, pp. 467–482, 1994.
[14] S. Prabhu and E. K. Poulose, "Silver nanoparticles: mechanism of antimicrobial action, synthesis, medical applications, and toxicity effects," *Int. Nano Lett.*, vol. 2, no. 1, p. 32, 2012.
[15] A. Manke, L. Wang, and Y. Rojanasakul, "Mechanisms of Nanoparticle-Induced Oxidative Stress and Toxicity," *Biomed Res. Int.*, vol. 2013, pp. 1–15, 2013.
[16] B. Le Ouay and F. Stellacci, "Antibacterial activity of silver nanoparticles : A surface science insight," *Nano Today*, vol. 10, no. 3, pp. 339–354, 2015.
[17] N. Durán, M. Durán, M. B. De Jesus, A. B. Seabra, W. J. Fávaro, and G. Nakazato, "Silver nanoparticles : A new view on mechanistic aspects on antimicrobial activity," *Nanomedicine Nanotechnology, Biol. Med.*, vol. 12, no. 3, pp. 789–799, 2016.
[18] T. C. Dakal, A. Kumar, R. S. Majumdar, and V. Yadav, "Mechanistic Basis of Antimicrobial Actions of Silver Nanoparticles," *Front. Microbiol.*, vol. 7, no. November, pp. 1–17, 2016.
[19] S. Ferraris and S. Spriano, "Antibacterial titanium surfaces for medical implants," *Mater. Sci. Eng. C*, vol. 61, pp. 965–978, 2016.
[20] Y. A. Krutyakov, "Antibacterial activity and toxicity of silver – nanosilver versus ionic silver Antibacterial activity and toxicity of silver - nanosilver versus ionic silver," *J. Phys.*, vol. 304, pp. 12–29, 2011.
[21] J. P. Ruparelia, A. Kumar, and S. P. Duttagupta, "Strain specificity in antimicrobial activity of silver and copper nanoparticles," *Acta Biomater.*, vol. 4, no. 3, pp. 707–716, 2008.
[22] C. P. Randall, A. Gupta, N. Jackson, D. Busse, and A. J. O. Neill, "Silver resistance in Gram-negative bacteria : a dissection of endogenous and exogenous mechanisms," *J. Antimicrob. Chemother.*, vol. 70, no. January, pp. 1037–1046, 2015.
[23] K. I. Radtsig MA, Koksharova OA, "Antibacterial effects of silver ions: effect on gram-negative bacteria growth and biofilm formation," *Mol. Genet. Microbiol. Virol.*, vol. 4, pp. 27–31, 2009.
[24] J. Joutsensaari, P. Ahonen, U. Tapper, E. I. Kauppinen, J. Laurila, and V. Kuokkala, "Generation of nanophase fullerene particles via aerosol routes," *Synth. Met.*, vol. 77, pp. 85–88, 1996.
[25] K. M. M. A. El-nour, A. Al-warthan, and R. A. A. Ammar, "Synthesis and applications of silver nanoparticles," *Arab. J. Chem.*, vol. 3, pp. 135–140, 2010.
[26] J. Hee, H. Cheol, H. Soo, J. Ho, and S. Soo, "Metal nanoparticle generation using a small ceramic heater with a local heating area," *J. Aerosol Sci.*, vol. 37, pp. 1662–1670, 2006.
[27] S. Iravani, H. Korbekandi, S. V Mirmohammadi, and B. Zolfaghari,

"Synthesis of silver nanoparticles : chemical , physical and biological methods," *Res. Pharm. Sci.*, vol. 9, no. 6, pp. 385–406, 2017.
[28] S. Ahmed, M. Ahmad, B. L. Swami, and S. Ikram, "A review on plants extract mediated synthesis of silver nanoparticles for antimicrobial applications : A green expertise," *J. Adv. Res.*, vol. 7, no. 1, pp. 17–28, 2016.
[29] P. Kuppusamy, M. M. Yusoff, and G. P. Maniam, "Biosynthesis of metallic nanoparticles using plant derivatives and their new avenues in pharmacological applications – An updated report," *Saudi Pharm. J.*, vol. 24, no. 4, pp. 473–484, 2016.
[30] M. Rai, K. Kon, A. Ingle, N. Duran, S. Galdiero, and M. Galdiero, "Broad-spectrum bioactivities of silver nanoparticles: The emerging trends and future prospects," *Appl. Microbiol. Biotechnol.*, vol. 98, no. 5, pp. 1951–1961, 2014.
[31] C. Carlson, S. M. Hussain, a M. Schrand, K. L. Hess, R. L. Jones, and J. J. Schlager, "Unique Cellular Interaction of Silver Nanoparticles : Size-Dependent Generation of Reactive Oxygen Species Unique Cellular Interaction of Silver Nanoparticles : Size-Dependent Generation of Reactive," *J. Phys. Chem. B*, vol. 112, pp. 13608–13619, 2008.
[32] A. Ivask *et al.*, "Size-dependent toxicity of silver nanoparticles to bacteria, yeast, algae, crustaceans and mammalian cells in vitro," *PLoS One*, vol. 9, no. 7, pp. 1–14, 2014.
[33] R. Bhattacharya and P. Mukherjee, "Biological properties of 'naked' metal nanoparticles," *Adv. Drug Deliv. Rev.*, vol. 60, no. 11, pp. 1289–1306, 2008.
[34] M. R. Nateghi and H. Hajimirzababa, "Effect of silver nanoparticles morphologies on antimicrobial properties of cotton fabrics," *J. Text. Inst.*, vol. 105, no. 8, pp. 806–813, 2014.
[35] B. Khodashenas and H. R. Ghorbani, "Synthesis of silver nanoparticles with different shapes," *Arab. J. Chem.*, 2015.
[36] "https://www.sigmaaldrich.com/catalog/product/ALDRICH/730793?lang=it&region=IT (28/11/2017, 11:22 am)."
[37] S. Pal, Y. K. Tak, and J. M. Song, "Does the antibacterial activity of silver nanoparticles depend on the shape of the nanoparticle? A study of the gram-negative bacterium Escherichia coli," *Appl. Environ. Microbiol.*, vol. 73, no. 6, pp. 1712–1720, 2015.
[38] A. M. El Badawy, R. G. Silva, B. Morris, K. G. Scheckel, M. T. Suidan, and T. M. Tolaymat, "Surface charge-dependent toxicity of silver nanoparticles.," *Environ. Sci. Technol.*, vol. 45, no. 1, pp. 283–287, 2011.
[39] A. Abbaszadegan *et al.*, "The effect of charge at the surface of silver nanoparticles on antimicrobial activity against gram-positive and gram-negative bacteria: A preliminary study," *J. Nanomater.*, vol. 2015, pp. 1–8, 2015.

[40] A. Ivask *et al.*, "Toxicity mechanisms in Escherichia coli vary for silver nanoparticles and differ from ionic silver," *ACS Nano*, vol. 8, no. 1, pp. 374–386, 2014.
[41] W. Zhang, Y. Yao, N. Sullivan, and Y. Chen, "Modeling the Primary Size Effects of Citrate-Coated Silver Nanoparticles on Their Ion Release Kinetics," *Environ. Sci. Technol.*, vol. 45, pp. 4422–4428, 2011.
[42] M. E. S. Kittler, C. Greulich, J. Diendorf, M. K oller, "Toxicity of Silver Nanoparticles Increases during Storage Because of Slow Dissolution under Release of Silver Ions," *Chem. Mater.*, vol. 22, no. 15, pp. 4548–4554, 2010.
[43] N. Innovation and R. Island, "Ion Release Kinetics and Particle Persistence in Aqueous Nano-Silver Colloids," *Environ. Sci. Technol.*, vol. 44, pp. 2169–2175, 2010.
[44] C. Ho, S. K. Yau, C. Lok, and M. So, "Oxidative Dissolution of Silver Nanoparticles by Biologically Relevant Oxidants : A Kinetic and Mechanistic Study," *Chem. Asian J.*, vol. 5, pp. 285–293, 2010.
[45] J. Liu, D. A. Sonshine, S. Shervani, and R. H. Hurt, "Controlled Release of Biologically Active Silver from Nanosilver Surfaces," *ACS Nano*, vol. 4, no. 11, pp. 6903–6913, 2010.
[46] G. A. S. A. S. E. PRATSINIS, "Antibacterial Activity of Nanosilver Ions and Particles," *Environ. Sci. Technol.*, vol. 44, pp. 5649–5654, 2010.
[47] R. D. Kent and P. J. Vikesland, "Controlled Evaluation of Silver Nanoparticle Dissolution Using Atomic Force Microscopy," *Environ. Sci. Technol.*, vol. 46, pp. 6977–6984, 2012.
[48] X. Chen and H. J. Schluesener, "Nanosilver : A nanoproduct in medical application," *Toxicol. Lett.*, vol. 176, pp. 1–12, 2008.
[49] M. Ema, H. Okuda, M. Gamo, and K. Honda, "A review of reproductive and developmental toxicity of silver nanoparticles in laboratory animals," *Reprod. Toxicol.*, vol. 67, pp. 149–154, 2017.
[50] F. Liu *et al.*, "Effects of silver nanoparticles on human and rat embryonic neural stem cells," *Front. Neurosci.*, vol. 9, no. April, pp. 1–9, 2015.
[51] A. Barkhordari, S. Barzegar, H. Hekmatimoghaddam, A. Jebali, S. R. Moghadam, and N. Khanjani, "The Toxic Effects of Silver Nanoparticles on Blood Mononuclear Cells," *theijoem*, vol. 5, pp. 164–168, 2014.
[52] I. Piwoński *et al.*, "The effect of the deposition parameters on size, distribution and antimicrobial properties of photoinduced silver nanoparticles on titania coatings," *Appl. Surf. Sci.*, vol. 257, no. 16, pp. 7076–7082, 2011.
[53] S. Ferraris and S. Spriano, "Antibacterial titanium surfaces for medical implants," *Mater. Sci. Eng. C*, vol. 61, pp. 965–978, 2016.
[54] L. Zhao *et al.*, "Antibacterial nano-structured titania coating incorporated with silver nanoparticles," *Biomaterials*, vol. 32, no. 24, pp. 5706–5716, 2011.
[55] C. Zhao, B. Feng, Y. Li, J. Tan, X. Lu, and J. Weng, "Preparation and

antibacterial activity of titanium nanotubes loaded with Ag nanoparticles in the dark and under the UV light," *Appl. Surf. Sci.*, vol. 280, pp. 8–14, 2013.
[56] C. Y. Flores *et al.*, "Spontaneous adsorption of silver nanoparticles on Ti/TiO2 surfaces. Antibacterial effect on Pseudomonas aeruginosa," *J. Colloid Interface Sci.*, vol. 350, no. 2, pp. 402–408, 2010.
[57] L. Juan, Z. Zhimin, M. Anchun, L. Lei, and Z. Jingchao, "Deposition of silver nanoparticles on titanium surface for antibacterial effect," *Int. J. Nanomedicine*, vol. 5, no. 1, pp. 261–267, 2010.
[58] H. Cao *et al.*, "Osteogenesis Catalyzed by Titanium-Supported Silver Nanoparticles," *ACS Appl. Mater. Interfaces*, vol. 9, no. 6, pp. 5149–5157, 2017.
[59] J. Maciejewska, O. Magdalena, and Z. Adamczyk, "Titanium dioxide / silver nanoparticle bilayers prepared in self-assembly processes," *Ann. Univertitatis Mariae Curie-Sklodowska*, vol. LXXI, pp. 29–46, 2016.
[60] W. I. Abdel-Fatah, M. M. Gobara, S. F. M. Mustafa, G. W. Ali, and O. W. Guirguis, "Role of silver nanoparticles in imparting antimicrobial activity of titanium dioxide," *Mater. Lett.*, vol. 179, pp. 190–193, 2016.
[61] N. Harrasser *et al.*, "Antibacterial efficacy of titanium-containing alloy with silver-nanoparticles enriched diamond-like carbon coatings," *AMB Express*, vol. 5, no. 1, p. 77, 2015.
[62] J. Wang *et al.*, "Silver-nanoparticles-modified biomaterial surface resistant to staphylococcus: New insight into the antimicrobial action of silver," *Sci. Rep.*, vol. 6, no. March, pp. 1–16, 2016.
[63] R. van Grieken, J. Marugán, C. Sordo, P. Martínez, and C. Pablos, "Photocatalytic inactivation of bacteria in water using suspended and immobilized silver-TiO2," *Appl. Catal. B Environ.*, vol. 93, no. 1–2, pp. 112–118, 2009.
[64] N. S. Tulve *et al.*, "Characterization of silver nanoparticles in selected consumer products and its relevance for predicting children's potential exposures," *Int. J. Hyg. Environ. Health*, vol. 218, no. 3, pp. 345–357, 2015.
[65] "http://www.silverplug.it/what-is-silverplug/ (17/12/2017, 05:07 pm)."
[66] S. Ferraris *et al.*, "Surface modification of Ti-6Al-4V alloy for biomineralization and specific biological response: Part I, inorganic modification," *J. Mater. Sci. Mater. Med.*, vol. 22, no. 3, pp. 533–545, 2011.
[67] "S.Spriano et al., European Patent 2214732."
[68] G. A. Martinez-Castanon, N. Niño-Martínez, F. Martínez-Gutierrez, J. R. Martínez-Mendoza, and F. Ruiz, "Synthesis and antibacterial activity of silver nanoparticles with different sizes," *J. Nanoparticle Res.*, vol. 10, no. 8, pp. 1343–1348, 2008.
[69] A. A. El-Kheshen and S. F. G. El-Rab, "Effect of reducing and protecting agents on size of silver nanoparticles and their anti-bacterial activity," *Der Pharma Chem.*, vol. 4, no. 1, pp. 53–65, 2012.

[70] M. Textor, C. Sittig, V. Frauchiger, and S. Tosatti, *Properties and Biological Significance of Natural Oxide Films on Titanium and Its Alloys*. 2001.
[71] M. Morra *et al.*, "Surface Chemistry Effects of Topographic Modification of Titanium Dental Implant Surfaces : 1. Surface Analysis," *Int. J. Oral Maxillofac. Implant. 41*, vol. 18, no. 1, pp. 40–45, 2003.
[72] "http://www.xpsfitting.com/2011/03/c-1s-carbonates.html (31 August 2017, 2:46 pm)."
[73] X. Zhang, S. Ferraris, E. Prenesti, and E. Verné, "Surface functionalization of bioactive glasses with natural molecules of biological significance, part I: Gallic acid as model molecule," *Appl. Surf. Sci.*, vol. 287, pp. 329–340, 2013.
[74] S. Rtimi, J. Nesic, C. Pulgarin, R. Sanjines, M. Bensimon, and J. Kiwi, "Effect of surface pretreatment of TiO2 films on interfacial processes leading to bacterial inactivation in the dark and under light irradiation," *Interface Focus*, vol. 5, no. 1, pp. 20140046–20140046, 2014.
[75] "http://xpssimplified.com/elements/oxygen.php (07/12/ 2017, 10:25 am)."
[76] B. Yu, K. M. Leung, Q. Guo, W. M. Lau, and J. Yang, "Synthesis of Ag – TiO 2 composite nano thin film for antimicrobial application," *Nanotechnology*, vol. 22, pp. 1–9, 2011.
[77] A. M. Ferraria, A. P. Carapeto, and A. M. Botelho Do Rego, "X-ray photoelectron spectroscopy: Silver salts revisited," *Vacuum*, vol. 86, no. 12, pp. 1988–1991, 2012.
[78] V. S. Calderon, R. E. Galindo, N. Benito, C. Palacio, A. Cavaleiro, and S. Carvalho, "Ag+ release inhibition from ZrCN-Ag coatings by surface agglomeration mechanism: Structural characterization," *J. Phys. D. Appl. Phys.*, vol. 46, no. 32, pp. 1–10, 2013.
[79] E. Albiter, M. A. Valenzuela, S. Alfaro, and G. Valverde-aguilar, "Photocatalytic deposition of Ag nanoparticles on TiO 2 : Metal precursor effect on the structural and photoactivity properties," *J. Saudi Chem. Soc.*, vol. 19, pp. 563–573, 2015.
[80] "http://www.xpssimplified.com/elements/carbon.php (15/11/2017, 10:46 am)."
[81] H. J. Song, S. H. Park, S. H. Jeong, and Y. J. Park, "Surface characteristics and bioactivity of oxide films formed by anodic spark oxidation on titanium in different electrolytes," *J. Mater. Process. Technol.*, vol. 209, no. 2, pp. 864–870, 2009.
[82] S. Ferraris, A. Venturello, M. Miola, A. Cochis, L. Rimondini, and S. Spriano, "Antibacterial and bioactive nanostructured titanium surfaces for bone integration," *Appl. Surf. Sci.*, vol. 311, pp. 279–291, 2014.

General outcomes and conclusions

Resuming the conclusions, the protocols of functionalization of silica based bioactive glass and bioactive titanium alloy with GA, TPH, GPH and PPH were successfully designed and tailored. The surfaces have different reactivity, indeed the bioactive glass, which is rich of calcium and is able to rise the pH of the solutions deprotonating polyphenols in order to obtain a higher reactivity of the molecules does not need a buffered medium with calcium addition, contrary the bioactive titanium. For this second kind of substrate the use of a buffered medium with calcium is fundamental in order to graft the biomolecules to the surface by means of bridging calcium ions. The polyphenols show antioxidant, osteoinductive and antinflammatory activity with selective actions on healthy and tumoral cells, they protect healthy cells from ROS and induce apoptosis in tumoral cells. Further studies of the role of calcium in the grafting of the biomolecules to the bioactive surfaces are still ongoing. Future works concerning the functionalization of bioactive glass and bioactive titanium alloy with polyphenols will be aimed to study the long term stability of these biomolecules after grafting and the best way of sterilization. The functionalization with polyphenols can be applied to glass powder used as bone filler and to the surface of bioactive glass scaffolds. The functionalization of titanium alloy surface with polyphenols instead, can be applied to improve prosthetic osteointegration. Surface functionalization or coating of chemically treated titanium alloy by using Mentha essential oil was investigated for the first time and suitable methods of analysis were researched. Comparative analysis with fluorescent microscope, FTIR and gaschromatograph allow to understand the distribution and the composition of the oil fraction which is able to be linked to the substrate. For the samples functionalized, only two molecules, beta-cubebene and trans-caryophyllene are grafted to the surface, which are minority compounds of the oil. In the case of the coated surfaces, the coating contains menthol, hydroxyl-menthofuran, menthyl-acetate and beta-cubebene. The substrates functionalized or coated by Mentha oil showed a reduction of *Staphylococcus aureus* adhesion highlighting the possible use of these biomolecules as antibacterial agent. Further investigations involving the study of the single molecules beta-cubebene and trans-caryophyllene in order to understand their mechanism of grafting and to find

a possible way of improve the antibacterial action reducing the cytotoxicity are ongoing. For future works it is also possible to think to the use of essential oils naturally rich in these biomolecules. A possible promising application for Mentha essential oil derived biomolecules is the coating or functionalization of materials and biomaterials not for implant, but always with antibacterial requirements such as surgery room surfaces, braces, towels, incubators, and many more.

The protocols developed for the in situ reduction of silver nanoparticles using GA as reducing agent allowed to obtain well dispersed and small sized nanoparticles distributed along the all thickness of the titanium oxide layer. The samples showed a long lasting release up to 14 days and a great activity against biofilm, however, they also show cytotoxic effects against cells. In both cases, it is challenging to find a proper balance between antibacterial effect and cytocompatibility and the study of a protocol suitable for find this balance is still ongoing reducing the concentration of the silver precursor. Further study will be aimed to enhance the cytocompatibility maintaining anti-biofilm properties and also in this case, such as for functionalization with essential oil is possible to think to not for implant applications. In conclusion, the use of plant derived natural molecules for the functionalization of surface for bone contact application or their using order to reduce metallic nanoparticles is a promising way to obtain multifunctional surfaces with large-scale applicability and containing costs.